universität wien

DISSERTATION

Titel der Dissertation

Substrate Selectivity Profiling of the Human Monoamine Transporters

Verfasst von

Amir Seddik, B.Sc., M.Sc.

angestrebter akademischer Grad

Doktor der Naturwissenschaften (Dr. rer. nat.)

Wien, 2015

Studienkennzahl lt. Studienblatt:	A 796 610 449
Dissertationsgebiet lt. Studienblatt:	Pharmazie, DK: Molecular Drug Targets
Betreut von:	Univ.-Prof. Mag. Dr. Gerhard F. Ecker

Acknowledgement

Hereby I would like to express my sincere gratitude to Prof. Gerhard F. Ecker, who has integrated me into the scientific community by letting me join his research group. I am thankful for his training during all these years, which has formed me into a very independent researcher. I thank him for his time and support and I admire his ambitions and interest for integrating students on European and international level. It has been an honor to work at the pharmaceutical department of the University of Vienna in this beautiful city. Gerhard, thank you for the great time.

My gratitude goes out to Michael Freissmuth and my co-supervisor Harald H. Sitte with whom we had very successful collaborations and I thank them for giving me the opportunity to learn the experimental methods.

I acknowledge the support from the MolTag program, to which I have applied for in the first place. The consortium has proven that collaboration between groups of different expertise is educative and beneficial to publish in world-class journals. I thank Steffen Hering, Gerhard Ecker, Marko Mihovilovic, Margot Ernst, Doris Stenitzer and Sophia Khom for devoting their time to the management of the project. I thank the scientific advisory board for the critical feedback during the retreats.

My gratitude goes out to Thomas Stockner; the molecular dynamics simulations on the transporter systems would not have been possible without him.

Many thanks go out to Nico Vermeulen and Daan Geerke in Amsterdam, for their hospitality during my internship. Foremost I am grateful to Daan for his patience and interest in my work, while giving me the opportunity to learn about the fundamentals of biomolecular simulation.

I would like to thank Chris Oostenbrink for organizing the exciting ABC seminars and giving me the honor to present there, and thank Thierry Langer for the stimulating feedback on my presentation.

Especially I will miss the warm-hearted Pharmacoinformatics colleagues: I thank Barbara Zdrazil for supervising and introducing me into the field of computational drug-design. Many thanks go out to so many people that I have worked together with and that were around: Lars, Nathan, Thomas Haschka, Marta, Melanie, Chonticha, René, Andreas, Freya, Daniela Digles, Yogesh, Ishrat, Andrea, Daria, Floriane, Doris, Eva, Eleni, Michael, Taymara, Alina, Theresa, Dennis, Alexandra, Bernhard, Sankalp, Priska, Lydia, Eugenia, Noor, Katharina Prokes, Katharina Bulyha, Marian, Victoria, Natesh, Petra, Anika, Katharina Krammler and Daniela Past. Thank you for the great time I had and for always being there for me. I wish everyone the best of luck in their career.

Certainly I will miss the educational and fun time I had in Amsterdam, thanks to Luigi, Ruben, Marc, Koen and Rosa, who I wish great luck with their further projects.

Of course I will miss the members of the Währingerstrasse, who devote their life to science and with whom I enjoyed the fruitful discussions, Walter, Sonja, Kusumika, Marion, Oliver, Felix, Ali, Tina, Thomas Steinkellner and many others I thank for the supervision and the great time in the wet-lab. I have learned a lot in a short amount of time thanks to them.

My love goes out to my father who unfortunately passed away during my Master's. I thank my mother, Selma and my family for always being there when I visited the Netherlands. My love goes out to Laura who has survived living with a PhD student.

INDEX

List of Abbreviations

4-MEC	4-Methyl-*N*-ethylcathinone
4-MePPP	4'-Methyl-α-pyrrolidinopropiophenone
5-HT	5-hydroxytryptamine
5-HTR	5-hydroxytryptamine receptor
Aa	Aquifex aeolicus
ADHD	Attention-Deficit Hyperactivity Disorder
APC	Amino-acid/Polyamine/Organocation
Arg	Arginine
Asp	Aspartate
BAT	Biogenic Amine Transporter
BBB	Blood-Brain-Barrier
BLAST	Basic Local Alignment Search Tool
$CDCl_3$	Deuterated Chloroform
Cl^-	Chloride
COPII	Coat Protein II
COS	CV-1 Origin SV40
DA	Dopamine
DAT	Dopamine Transporter
DMEM	Dulbecco's Modified Eagle's medium
DMF	Dimethylformamide
DMSO	Dimethyl Sulphoxide
DNA	Deoxyribonucleic Acid
dNTP	Deoxyribonucleophosphate
DOPE	Discrete Optimized Protein Energy
Dpn	Diplococcus pneumoniae
EBI	European Bioinformatics Institute
EL	Extracellular loop
GA	Genetic Algorithm
GAT	Gamma-amino-butyric acid Transporter
GB	Generalized Born
Glu	Glutamate
GlyT	Glycine Transporter
GOLD	Genetic Optimization for Ligand Docking
GRIND	Grid Independent Descriptors
HB	Hydrogen Bond
HCl	Hydrogen Chloride
HEK	Human Embryonic Kidney
HeLa	Henrietta Lacks
HEPES	2-[4-(2-OH-Et)piperazin-1-yl]ethanesulfonic acid
IFD	Induced-Fit Docking
IMAP	2-(methylaminol-l-(4-iodophenyl)propan-l-one
KCl	Potassium Chloride
keV	kilo electron volt
LeuT	Leucine Transporter
LB	Lysogeny Broth
LC-MS	Liquid Chromatography/Mass
LINCS	Linear Constraint Solver
LJ	Lennard-Jones
Lys	Lysine
MAT	Monoamine Transporter
MCAT	Methcathinone
MD	Molecular Dynamics
MDMA	3,4-methylenedioxymethamphetamine
MEPH	Mephedrone
MLR	Multiple Linear Regression
MM	Molecular mechanics
MOE	Molecular Operating Environment
MPP^+	Methylpyridinium
MR	Molar refractivity
MSA	Multiple Sequence Alignment
Na^+	Sodium ion
NaOH	Sodium Hydroxide
NCBI	National Center for Biotechnology Information
NE	Norepinephrine
NET	Norepinephrine Transporter
NMR	Nuclear Magnetic Resonance
NSS	Neurotransmitter/Sodium Symporter
OG	Octyl glucoside
OPLS	Optimized Potentials for Liquid Simulations
PEA	Phenylethylamine
PB	Poisson-Boltzmann
PCR	Polymerase-chain reaction
PDB	Protein Data Bank
PDL	poly-*d*-lysine
PET	Positron Emission Tomography
PLP	Piecewise Linear Potential
PLS	Partial-Least Squares
PME	Particle Mesh Ewald summation
POPC	1-palmitoyl-2-oleoyl-sn-glycero-3-phosphocholine
POVME	Pocket Volume Measurer
PP	Phenylpiperazine
QM	Quantum mechanics
QQ	Electrostatics
QSAR	Quantitative Structure-Activity Relationship
RCSB	Research Collaboratory for Structural Bioinformatics
RMSD	Root-mean-square Deviation
SA	Surface area
SAR	Structure-Activity Relationship
SDS	Sodium Dodecyl sulfate
SERT	Serotonin Transporter
SFF	(*S*)-fenfluramine
SLC	Solute Carrier
SMILES	Simplified Molecular-input line-Entry System
SNRI	Selective Norepinephrine Reuptake Inhibitor
SSRI	Selective Serotonin Reuptake Inhibitor
SPC	Single point charge
SVL	Scientific Vector Language
TCA	Tricyclic Antidepressant
TI	Thermodynamic Integration
Tris	tris(hydroxymethyl)aminomethane
vdW	Van der Waals
VMD	Visual Molecular Dynamics
VSA	van der Waals Surface Area
WT	Wild-type

Abstract

The serotonin, dopamine and norepinephrine transporter proteins (SERT, DAT, NET, respectively) are collectively named as the monoamine transporters (MATs) and are involved in a variety of psychiatric disorders such as depression, anxiety, addiction and attention-deficit hyperactivity disorder. The high sequence identity and functional similarity to each other, despite their involvement in different behaviors and disorders, have made them a central topic in life sciences research during the last decades. Small molecules that bind to the MATs can be divided into inhibitors and substrates, whose selectivity for the latter has been thoroughly studied during this thesis, using computational and biochemical methods.

The binding modes of endogenous substrates such as dopamine, norepinephrine and serotonin have been suggested previously, but the binding and selectivity of exogenous compounds not extensively. Cathinones are amphetamine derivates gaining increased popularity in the party scene and are also transported by the MATs, depending on their physicochemical properties. Their uptake inhibitory activity on the MATs was exploited in order to better understand the selectivity phenomenon.

Molecular docking of a set of these cathinones into an outward-facing homology model of SERT validated their binding mode in the substrate binding site and indicated that their chemical scaffold overlap. Additionally, their binding activity was rationalized based on the interaction between the chemical substituents and protein residues that surround them. Further validation was obtained by Hansch analysis, a type of quantitative structure-activity relationship (QSAR) study whereby chemical moieties are described by their electron-withdrawing, lipophilic, steric and polarizable nature. This ligand-based approach indicated that a polarizable or lipophilic *para*-substituent increases SERT affinity, whereas a bulky nitrogen substituent would be unfavorable.

The DAT-over-SERT selectivity was however not grasped by docking and the ligand-based approach. Different datasets indicated that a lack of substituents on the aromatic ring rendered the compounds DAT-over-SERT selective. Therefore, a molecular dynamics (MD) and thermodynamic integration (TI) study was conducted, which indicated the substrate binding site to be the major recognition site for these compounds. The DAT-over-SERT selectivity was ascribed to more favorable aromatic stacking and attractive electrostatic interactions. The stacking interactions were more favorable in DAT presumably, due to a less bulky Val152 compared to Ile172 in SERT that would disrupt such an interaction. The hypotheses were validated by uptake inhibitory assays on transporter mutants. The more favorable electrostatic interactions in DAT were caused by a slightly tighter DAT binding pocket with a smaller number of waters on average entering the binding site, as compared to SERT.

Abstract

Die Serotonin, Dopamin und Noradrenalin Transporter (bzw. SERT, DAT, NET) werden zusammen als die Monoamin Transporter (MAT) Proteine bezeichnet und sind an einer Vielzahl von psychiatrischen Störungen wie Depression, Angst, Sucht und Aufmerksamkeitsdefizit-/Hyperaktivitätsstörung (ADHS) beteiligt. Die hohe Sequenzidentität und funktionelle Ähnlichkeit der MAT zu einander - trotz Beteiligung an unterschiedlichen menschlichen Verhalten und Störungen - haben sie zu einem zentralen Thema in der Forschung der Lebenswissenschaften der letzten Jahrzehnte gemacht. Die Selektivität der MAT Substrate, die im Gegensatz zu Inhibitoren transportiert werden, wurde im Rahmen dieser Arbeit mittels Computer-Kalkulationen und biochemischen Methoden gründlich studiert.

Die Bindungsmodi von endogenen Substraten, wie Dopamin, Norepinephrin und Serotonin wurden bereits zuvor elklärt, die Bindung und Selektivität von exogenen Verbindungen jedoch nicht extensiv. Kathinone sind Amphetaminderivate mit steigender erholsamen Konzum, die ebenfalls je nach ihren physikochemischen Eigenschaften transportiert werden. Ihre aufnahmehemmende Aktivität auf die MAT wurde genutzt, um das Selektivitätsphänomen genauer zu erklären.

Das molekulare *Docken* von einem Set dieser Kathinone in einem Homologie-Model des SERTs in der nach außen weisenden Konformation, hat ihren Bindungsmodus in der Substrat Bindungstasche validiert und lässt darauf schliessen, dass ihre chemischen Gerüste überlappen. Zusätzlich wurde die Bindungsaktivität mit Hilfe der Interaktionen zwischen den chemischen Substituenten und den Aminosäuren im Protein, die sie umgeben, erläutert. Eine weitere Validierung wurde durch Hansch-Analyse - eine Form der Quantitativen Struktur-Wirkungs-Beziehung (QSAR) - erhalten. Hierbei werden chemische Substituenten als elektronenziehende, lipophile, sterische oder polarisierbare Eigenschaften beschrieben. Dieser Ligand-basierte Ansatz hat gezeigt, dass ein polarisierbarer oder lipophiler *para*-Substituent für SERT Affinität wichtig wäre.

Die höhere Selektivität von DAT gegenüber SERT konnte jedoch nicht durch *Docken* und Liganden-basierte Studien erläutert werden. Datensätze zeigten, dass das Fehlen von Substituenten am aromatischen Ring die Selektivität der Verbindungen zugunsten von DAT im Vergleich zu SERT erhöht. Daher wurden Moleküldynamik (MD) und Thermodynamische Integration (TI) Studien durchgeführt, die zeigten, dass die Substrat Bindungstasche der meist bestimmende Bindungsplatz dieser Verbindungen wäre. Die höhere Selektivität von DAT verglichen mit SERT wurde durch eine günstigere aromatische Stapelung, sowie auch durch attraktivere elektrostatische Interaktionen erklärt. Die Stapel-Interaktionen zeigen sich in DAT günstiger, vermutlich aufgrund einer weniger sperrigen Val152, im Vergleich zu Ile172 in SERT - der eine solche Interaktion unterbrechen würde - zurückzuführen ist. Die Hypothesen wurden mittels Aufnahmehemmungsassays an mutanten der Transporterproteinen validiert. Die günstigeren elektrostatischen Interaktionen in DAT waren -im Gegensatz zu SERT- durch eine leicht straffere Bindungstasche mit einer im Durchschnitt kleineren Anzahl an Wassermolekülen zu erklären.

I

Background

Motivation

Mental health problems are a social burden and can hamper work productivity, impact well-being and lead to suicidal ideation. Around 1.4 billion people worldwide are currently affected by a mental disorder, while the suicide rate is about 800,000 people per year. Moreover, mental disabilities are an important risk factor to the infection with HIV, the development of cardiovascular diseases and substance addiction. In many countries there still exists a taboo on mental disorders which leads to social exclusion of the patients and prevents them from appropriate healthcare access. Additionally, another 230 million people have at least once used an illicit substance in their life.[1]

Scientific research is able to offer a helping hand to these problems. The first psychotherapeutical treatments date back already from prehistory and later during the time of the ancient Greeks and the Chinese dynasties around 600 BC. But the use of marketed psychotropic medication started only recently, in the 1950s with the antipsychotic drug chlorpromazine. These drugs were very unselective and caused many side effects and withdrawal symptoms.[2, 3]

Depression, anxiety, Parkinson's disease[4], obsessive-compulsive disorder (OCD), eating disorders, addiction and attention-deficit hyperactivity disorder (ADHD) are related to an impaired function or abnormal expression of one or more of the monoamine transporters proteins (MATs). Although cognitive behavioral therapy is increasingly shown to be beneficial against some of these disorders[5], therapeutic drugs are effective in most cases as well.[6, 7] However, the neurochemistry behind the MATs is not completely understood yet and therefore there is still space for improvement.

Recreational drugs such as cocaine, amphetamine and ecstasy also act on the MATs and can lead to psychological dependence, mood swings and neurodegenerative and cardiovascular symptoms. They may therefore pose a major burden to society and hence the study of these compounds offers the possibility to improve their regulation and to treat their negative symptoms once the drug is (over)-used.

Selectivity plays a central role in the drug discovery and development process in the pharmaceutical industry. Active hit compounds are tweaked to make them bind stronger and weaker to targets and off-targets, respectively. This process increases the efficacy and selectivity of the drug and ideally leads to fewer side-effects.

The purpose of this thesis was to assess the selectivity with regard to transported compounds that are not commonly applied as therapeutic drugs, but of which their assessment can steer their development. A better understanding of protein-ligand interactions and neurotransmitter sodium symporter function is gained. The structure and activity of selective substrates have been very useful for this purpose, such as the SERT-over-DAT selective (*S*)-fenfluramine (section II.A) and the DAT/NET-over-DAT selective (*S*)-methcathinone (section II.C).

A Biological Background

a Monoamine Transporter Function and Classification

The human monoamine transporters (MATs) are also known as the biogenic amine transporters (BATs) and represent the serotonin, dopamine and norepinephrine transporter (SERT, DAT and NET, respectively). They reside in the cell membrane and re-uptake chemical messenger molecules back into the synapse.[8] This transport process is driven by the electrochemical gradient of sodium, which can also be co-transported with a chloride ion, in combination with the counter transport of a potassium ion.[9-12] The MATs therefore control a great deal of the interneuronal communication and hence are an important target of therapeutic and euphorigenic drugs (see Figure 1). These modulatory drugs, such as Selective Serotonin Re-uptake inhibitors (SSRIs) and Ritalin®, act on these transporters, by blocking the re-uptake process, leading to an increase in extracellular neurotransmitter concentration.

The MATs are biosynthesized in the nerve cell body after decoding of genes found on different chromosomes (see Table 1). Trafficking proteins of the SEC24 family export the MATs from the endoplasmic reticulum to the nerve endings via anterograde transporter through the axons.[13] Expression to the cell surface is triggered by *N*-glycosylation of the extracellular loop 2 (EL2).[14, 15]

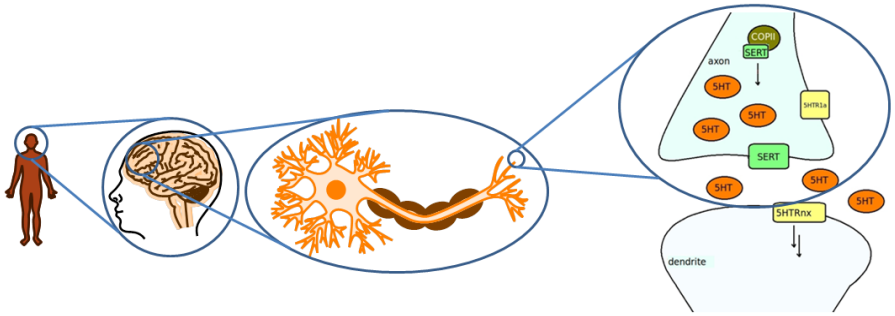

Figure 1 *The serotonin transporter is located in the presynaptic membrane of axonal termini of the raphe nuclei in the brain*

Table 1 *Monoamine transporter loci, properties and physical location*

Protein	Endogenous substrate	Symbol	Gene locus[16]	Protein length (residues)	Principal location
SERT	serotonin	SLC6A4	17q11.2	630[17]	Raphe nuclei, blood platelets
DAT	dopamine, norepinephrine, tyramine	SLC6A3	5p13.3	620[18]	Ventral mesencephalon[19]
NET	norepinephrine, dopamine, tyramine	SLC6A2	16q12.2	617[20]	Locus coeruleus[21]

The monoamine transporters (MATs) have been sequenced in the 1990s and are part of the Neurotransmitter:Sodium Symporter (NSS) family, which are in turn are part of the amino-acid/polyamine/organocation (APC) superfamily, classified within the solute carrier (SLC) transporter proteins (see Figure 2). Inside a presynaptic neuron, the substrates are also transported into vesicles by the vesicular monoamine transporters (VMATs), but these are part of a different superfamily than the MATs and share scarce sequence and structural similarity.

Amino Acid-Polyamine-Organocation (APC) superfamily
- APC subfamily
- Betaine/Carnitine/Choline Transporter (BCCT)
- Amino Acid/Auxin Permease (AAAP)
- Solute:Sodium Symporter (SSS)
- Alanine or Glycine:Cation Symporter (AGCS)
- Cation-Chloride Co-transporter (CCC)
- Nucleobase:Cation Symporter-1 (NCS1)
- Hydroxy/Aromatic Amino Acid Permease (HAAAP)
- Neurotransmitter:Sodium Symporter (NSS)
  - Monoamine transporters
    - **NE neurotransmitter transporter**
    - **DA neurotransmitter transporter**
    - **5-HT transporter**
    - Inebriated neurotransmitter transporter
  - Amino acid transporters
    - GABA transporter (GAT) 1
    - Taurine/β-Alanine transporter
    - Creatine transporter
    - Glycine transporter (GlyT) 1
    - GlyT 2
    - GAT-3
    - GAT-4
    - Betaine/GABA transporter (BGT1)
    - GAT-2
    - **Leucine transporter**
  - Orphan neurotransmitter transporter

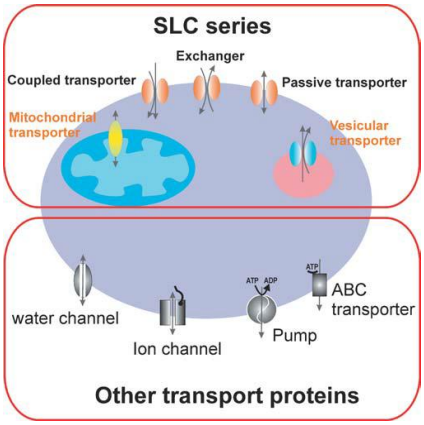

Figure 2 *Left: classification of the monoamine transporters and the homologous leucine transporter.*[15] *Right: the different types of transporter proteins (picture taken from Hediger et al, 2004).*

b Monoamine Transporter Structure

Protein structures can be resolved by means of X-Ray crystallography, but for the human MATs this is problematic since they are difficult to over-express as compared to their prokaryotic counterparts.[22, 23] The homologous bacterial leucine transporter from *Auquifex Aeolicus* ($LeuT_{Aa}$) has therefore been the principal protein used to model the human SERT, DAT and NET, due to its relative ease of crystallization.[24] LeuT was resolved in three different conformational states: the outward-open, occluded and inward-open state. Due to its similarity to the human transporters, it is assumed that these states are also present our species. Two different binding sites in the vestibule were identified based on the electron density observed, i.e. the substrate binding site (S1) and a secondary site located 11 Å more outward (S2).

The outward-open state is achieved by binding to an inhibitor, as shown in the LeuT in complex with tryptophan and a variety of SSRIs such as clomipramine, and in the *Drosophila* DAT (dDAT) in complex with nortryptiline. The same conformation of the protein was observed for 'SERT'-ized LeuT (LeuBAT) in complex with SSRIs and the DAT/NET-selective inhibitor mazindol. The LeuT structures and a previous docking study[25] indicated that inhibitors bind preferably in the S2 site, but the LeuBAT and dDAT structures showed that they rather bind in the S1 site.

The alternating access model suggests that a substrate is only transported upon binding of another substrate in the S2 site simultaneously.[26] Structural studies showed that the occluded conformation in LeuT was only observed in complex with the substrate leucine or alanine, hence it seems that LeuT substrates do not bind to S2. This is therefore heavily being debated between experimental groups[27] (see Table 2). The inward-facing conformation of LeuT was only induced by applying mutations and by antibody binding, whereby the TM1a subunit on the intracellular side is bent significantly, as compared to the occluded and outward facing

structures. Molecular dynamics studies have however shown that this subunit would not be stable in the membrane. [28]

Table 2 *Crystal structures homologous to monoamine transporters with location of the co-crystallized ligands*

	Leucine Transporter (LeuT)	**LeuBAT**	**dDAT**
S1 site ligands	Leucine, Alanine, Glycine, Methionine, 4-F-phenylalanine	sertraline, fluoxetine, duloxetine, clomipramine, fluvoxamine, paroxetine, desvenlaxafaxine, mazindol	nortryptiline
S2 site ligands	imipramine, clomipramine, desipramine, octyl glucoside, sertraline, fluoxetine	desvenlaxafaxine	-
Conformations	inward, occluded, outward	outward	outward
Resolution	1.65 - 3.0 Å	~2.9 Å	2.95 Å
Sequence identity to hMATs	~20%	~22%	~50%
Sequence similarity in S1	~60%	~90%	~75%

The MATs consist each of twelve transmembrane helices organized as a pseudo-symmetric fold whereby the transport cycle is controlled by the concerted movement of two bundles: the trans-membrane (TM) helices 1, 2, 5-8 and 3, 4, 9-12.[29] The termini are located intracellularly, whereby studies have shown that the *N*-terminus is involved in amphetamine induced reverse transport of substrate by activation of protein kinase C and subsequent phosphorylation of a serine or threonine side chain.[30] The *C*-terminus in DAT is a small α-helix that functions as a latch.[31] Additionally, the transporters have two extracellular loops (EL2 and EL4) that are involved in substrate recognition. The DAT contains a zinc binding site in the EL2 whereupon binding of this ion, the transport activity is inhibited.[32, 33]

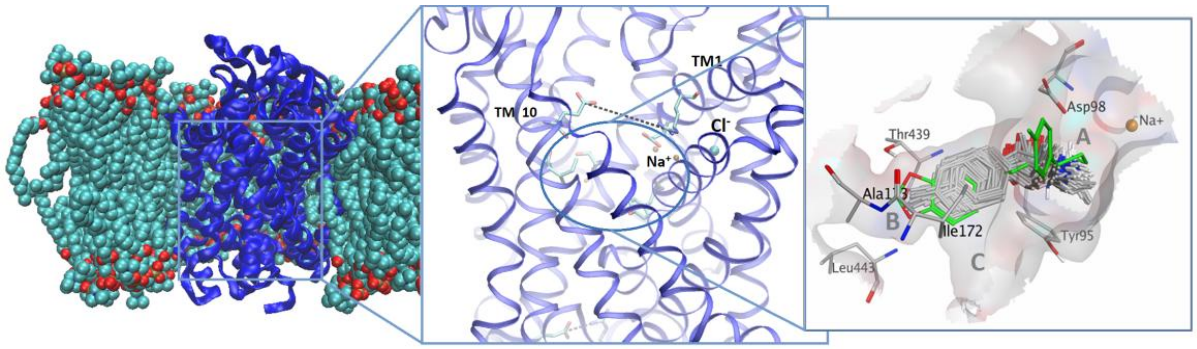

Figure 3 *Homology model of the dopamine transporter in the occluded conformation in a POPC membrane (left). The transporters all have an intra- and extracellular salt-bridge gate composed of an arginine and glutamate or aspartate side chain (middle). The right figure shows an example of the S1 site in the outward-open model with the high affinity SERT inhibitor paroxetine (green) and docking poses of the substrate mephedrone (grey). The substrate and inhibitor partially overlap with their cationic nitrogen and aromatic moiety.*

All MATs contain two sodium binding sites Na1 and Na2 and one chloride binding site coordinated by charged protein groups. The Na1 site has a higher affinity than Na2 and is closer to the hypothesized chloride binding site.[34] The backbone carbonyl oxygen atoms and threonine and serine side chains stabilize the Na1 site. The

Na2 site is comprised of an alanine and serine backbone and two asparagine and aspartate side chains and has millimolar affinity for the sodium ion that is transported. The S1 site consists of different subpockets: A: the cationic group of the ligand forms a salt-bridge with the central aspartate side chain and stacks with the π electrons of the lower lying aromatic side chain. The subpocket B generally accommodates the aromatic moiety of the ligand, whereas in subpocket C no electron density was found in crystal structures (see Figure 3). The S1 site of SERT, DAT and NET slightly differ in their amino acids composition, which may account for their substrate selectivity. Most overlap is seen between DAT and NET, while the least is noticed between SERT and DAT (see Figure 4).

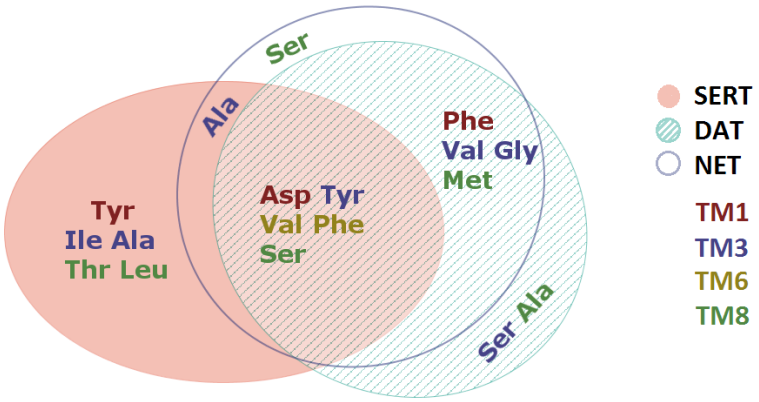

Figure 4 *Area proportional Euler diagram showing the overlap of eleven amino acid residues of the substrate binding site (S1) of SERT, DAT and NET, based on a structural alignment. The residues are colored based on the transmembrane helix (TM) they belong to.*

The conformation of the MATs is heavily dependent on membrane constituents as well, as it was shown for DAT that an outward facing conformation is stabilized with an increased cholesterol concentration.[35] Moreover, for SERT it was shown that it oligomerizes to up to at least pentamers, independently of its surface density or cholesterol concentration.[36]

c Pharmacochemistry of Monoamine Transporter Substrates

The exogenous MAT substrates mostly include psychotropic party drugs such as 3,4-methylenedioxymethamphetamine (MDMA, ecstasy) and other amphetamines. As soon as the drug is circulating through the bloodstream, subsequent blood-brain-barrier (BBB) passage may cause the drug to interact with different membrane proteins. Major proteins include the G-Protein Coupled Receptors (GPCRs) such as the dopamine, serotonin and adrenergic receptors that activate or block intracellular pathways and lead to the drug's effects. But transporters play an equally important role. Binding of these drugs typically leads to an inhibition and subsequently higher extracellular neurotransmitter concentration. Uptake studies have shown that amphetamines are also actively taken up by MATs into the cell where they can enter neurotransmitter storage vesicles and induce a reverse transport of their cognate neurotransmitter.[37, 38] How these processes lead to the reported euphoric effects is however not completely understood yet.

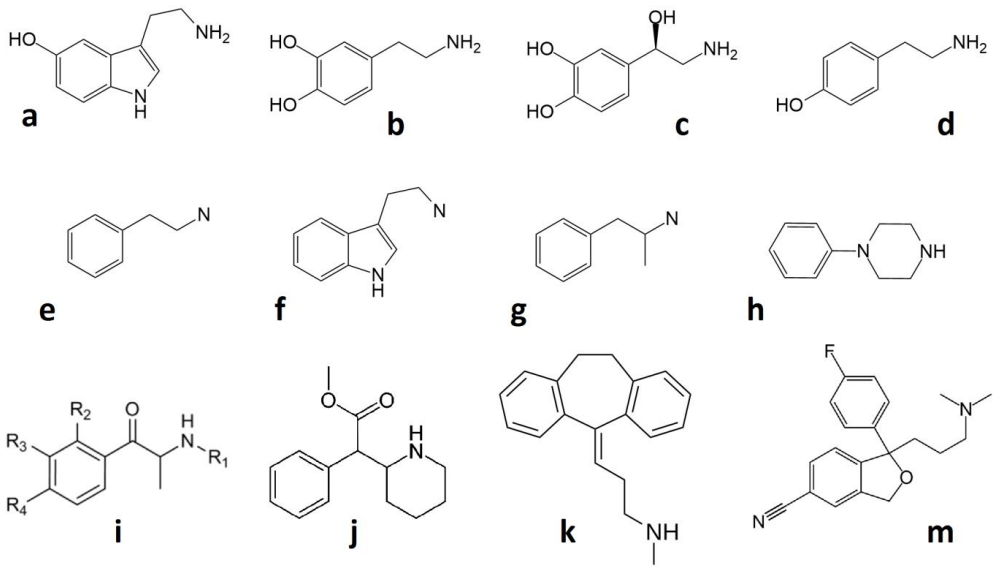

Figure 5 a-d *Endogenous monoamine transporter substrates serotonin, dopamine, norepinephrine and tyramine.* **e-i** *Chemical scaffolds of monoamine transporter substrates extracted from literature: phenylethylamine, tryptamine, amphetamine, phenylpiperazine and cathinone* **j-m** *Examples of MAT inhibitors: the DAT inhibitor methylphenidate, the tricyclic antidepressant nortryptiline and the SSRI citalopram.*

MAT substrates all have an aromatic and a positively ionizable feature in common, which are therefore the required pharmacophoric features for binding (see Figure 5). The size seems to be a clear structural difference between inhibitors and substrates: inhibitors are generally larger and usually bear at least two aromatic moieties and a longer linker to the center of the cationic charge. So-called 'partial' substrates have recently been described which display an inhibitory as well as partial release effect, as compared to full substrates. These compounds bear a slightly larger aromatic feature, i.e. a naphthalene ring.[7]

Uptake inhibitory studies of MAT ligands are commonly performed to assess their binding affinity and selectivity. Table 3 shows the different datasets extracted from literature and their structural class. It is evident that not many substrate activities have been measured for an extensive ligand-based study. Such a study can therefore only deliver qualitative assessments of which substituents are contributing to affinity and/or selectivity.

Table 3 *Substrate binding affinity data obtained from literature*

Class	Targets	Cell type	# of compounds	Type	Source
Phenylethylamines	rSERT, rDAT, rNET	Synaptosomes	18	K_i	Baumann *et al* [39] *(see section II.A)*
Phenylethylamines	hSERT	HeLa	18	K_i	Barker *et al* [40, 41]
Tryptamines	hSERT	HEK-293	11	K_i	Celik *et al* [42]
Amphetamines	hSERT, hDAT, hNET	HEK-293	15	IC_{50}	Simmler *et al* [43]
Phenylpiperazines	hSERT, hDAT, hNET	HEK-293	25, 8, 8, resp.	K_i	Severinsen *et al* [44]
Cathinones	hSERT, hNET hDAT	HEK-293 COS	13	IC_{50}	Cozzi *et al (see section II.B)*

Amphetamines, such as methamphetamine ('ice') and MDMA are psychostimulants infamous for causing damage to the body and hence may cause a burden to society.[45] Despite their structural similarity to dopamine and norepinephrine, they are far more lipophilic due to their lack of hydroxyl groups and hence easily cross the

BBB. There exist strong differences in how these compounds exert their effect: methamphetamine is more addictive than amphetamine and has a stronger effect on DAT,[46] whereas MDMA has a strong entactogenic effect.

Phenylpiperazines (PPs) are a related class of compounds with a slightly larger distance between the two pharmacophoric features than in amphetamines. The highly toxic and permanently charged 1-methyl-4-phenylpyridinium (MPP+) is a common PP used as radioligand in uptake inhibitory studies on DAT. Also a new type of antidepressant, vortioxetine, contains the PP scaffold.

B Methods in Computational Drug design

The use of computers to study biomolecular processes is a relatively recent event and is increasing with the development of faster computers. Still, many algorithms are simplifications of real-world definitions in order to speed up calculations. Therefore a trade-off between efficiency and accuracy is always present.

a Homology Modelling

Homology modeling, also known as comparative modelling, is a widely used technique wherein the 3D structure of a protein is predicted on atomic scale based on a resolved template structure with which it shares reasonable sequence identity. It is assumed that a similar sequence leads to a similar structure. In practice, the sequence identity should be at least 20%, but the many possible side chain conformations, secondary structures and folds have to be considered. Reliable structural models are created with sequence identities typically exceeding 70%.

Several techniques exist to resolve an experimental structure, such as nuclear magnetic resonance (NMR) and X-ray diffraction. The latter method offers generally the highest resolution and many structures are available as coordinate file on the Research Collaboratory for Structural Bioinformatics (RCSB) Protein Data Bank (PDB). Resolving an experimental structure is not always possible, e.g. a protein might be too large for NMR analysis, or it may be too difficult to overexpress, purify or crystallize. Membrane proteins are especially hard to crystallize.

A multiple sequence alignment (MSA) is helpful for the creation of a homology model. Template structures can be searched on the PDB using a gene or sequence query via the BLAST® tool which scans the NCBI database for similarity. Sequences can be added to the MSA by searching structurally similar proteins using the Structural Similarity Tool of the RCSB, which screens the PDB and provides an output with the root mean square deviation (RMSD) and the sequence identity. Additionally, homologous sequences from the family can be added to the MSA using BLAST®. After the selection of appropriate sequences, the MSA can be performed with e.g. ClustalX,[47] which is both a web-based and downloadable alignment program.

The homology models can be constructed using alignment and forcefield algorithms, such as in Modeller.[48] This tool requires three input files: an alignment of the template and the target sequence, the template PDB structure and a script containing the commands and file paths. Since the algorithm is based on a probability density function, multiple models can be created to compare or cluster the output and make a proper selection. Additionally, one has the option to apply distance restraints from e.g. NMR studies and secondary structure constraints.

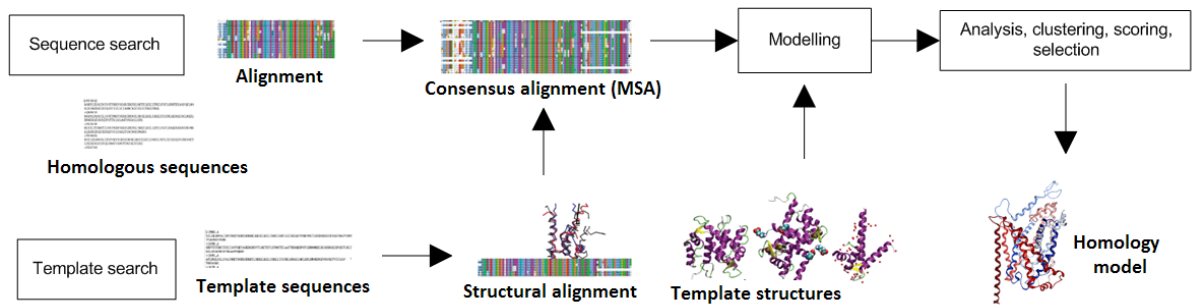

Figure 6 *Homology modelling workflow, adapted from biskit.pasteur.fr*

A final model is selected from a pool of generated models, based on energy functions, Ramachandran plots, agreement with mutational data and solvent accessibility studies and energy functions. The Discrete Optimized Protein Energy (DOPE) function assesses the model quality using a statistical potential function. Third-party tools such as PROCHECK[49] calculate Ramachandran plots, while the QMEAN server[50] can be used to obtain a *Z*-score, which indicates the deviation from experimental structures[50] (see Figure 6).

Homology models may give more insight into the architecture and function of the protein, are generated very quickly and are shown to be successful in drug design[51] and for understanding selectivity phenomena as shown in this work. For monoamine transporter models such as SERT and DAT, $LeuT_{Aa}$ is the most commonly used template structure.

b Docking

Molecular docking is a computational technique that generates conformations and orientations of a ligand in a protein pocket, leading to a 'pose' or binding hypothesis. The method originated in the USA in the 1980s with the software named DOCK[52], but subsequent research institutes followed and online services such as the ZDOCK server became available.[53] At present times, docking software is typically run on a local computer. Docking programs vary in their algorithm: the search method for obtaining a 'pose', the sampling of ligand and protein flexibility and the type of scoring function.

AutoDock Vina is a fast, free and flexible docking tool[54] where runs can be performed from a command line. Although it supports flexible side chains, it does not allow for setting distance restraints. Schrodinger's Glide[55] program makes a grid out of a rigid protein model and randomly generates many ligand poses, of which the conformation is optimized based on energies derived from a forcefield. A more rigorous form of docking is Schrodinger's induced-fit docking[56] (IFD), wherein protein flexibility can be accounted for: the binding site is defined and selected side chains are truncated. The selection of the side chains is either done manually or based on their temperature factor. The ligand is docked using Glide and the side chains are rebuilt around the ligand using the Prime[57] tool, while calculating the optimal energies. Two variants of IFD exist: the single and extended precision.

Genetic Optimization of Ligand Docking (GOLD)[58] is a commonly used commercial package wherein the user defines the pocket by a radius and a center by coordinates or by a reference ligand from a co-crystal structure. Hydrophobic and hydrogen bond (HB) fitting points on both the protein and the ligand are created. Optionally, side chain movements can be accounted for, either by angles defined in a rotamer database[59] or by a brute force exploration of all possible angles, typically in 10 degree bins. Since water can play an important role in protein-ligand binding, the option for predicting their location and orientation is also available. The option for

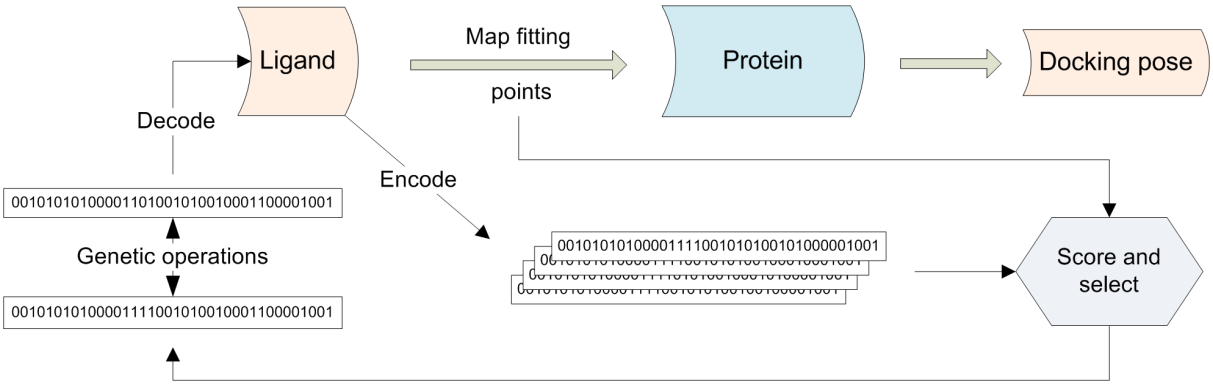

Figure 7 *Genetic algorithm implemented in the docking software GOLD*

fixing the distance between two atoms using a harmonic potential is also available, within the protein and between protein and ligand atoms. This is especially useful when experimental data is available, which dramatically reduces the pose space. A genetic algorithm is employed whereby the ligand torsional angles are converted into bit strings ('chromosome'). A scoring function is applied and two random poses are selected and weighted by their score. Of those two chromosomes, genetic operations are performed that typically include mutation, crossover and migration 'deepening' at a certain rate. The cycle repeats until the desired number of poses is reached (see Figure 7).

Monoamine transporter ligands are commonly built as the more active (*S*)-enantiomer,[60] whereas protonation states can be visualized on chemicalize.org[31] or calculated with a tool such as Protonate3D in Molecular Operating Environment[61] (MOE) or Epik[62] in Schrodinger. This commonly leads to a cationic nitrogen atom. The protein models can be obtained from homology modelling or molecular dynamics (MD) simulations and the choice of the protein conformation, i.e. outward-open, occluded or inward-open, is made based on experimental data known of the ligand. For example, a substrate has to cross the occluded state, whereas an inhibitor commonly binds in the outward-open state.

The docking poses can either be generated using a bias into specific subpockets or without any bias when more poses are required to e.g. obtain a probability distribution of the binding mode. For the former protocol, a common substructure is used for setting restraints, whereby a ligand atom can be forced to be within a certain distance to a protein atom. The poses can be clustered based on the placement into specific subpockets. For the latter protocol, a faster scoring function is recommended and a probability distribution of protein-ligand interactions of interest can be described as an interatomic distance. Visualization can be in the form of e.g. heatmaps using packages such as Matplotlib[63] and Plotly[64]. See Appendix **A1** for an example. The user may also consider to energy minimize the ligand and residues within a certain radius for re-scoring purposes.

The advantage of docking is its efficiency as compared to explicit simulation methods. The method gains insight into different binding possibilities, it can be used for the fast screening of large compound databases and as a tool for defining a starting complex for MD simulations. The method does however not sample backbone movements which might contribute to binding as well.

b 1 Scoring functions

Scoring functions can be divided into three classes:

- Empirical: this is the most commonly used type because it is faster than using a forcefield, while being more reliable than a knowledge-based function. Empirical scoring functions consist of energetic terms with coefficients determined by multiple linear regression (MLR) trained on experimental protein-ligand complexes. Popular training databases include the Astex dataset of 305 protein-ligand complexes and various versions of the PDBbind, i.e. v2007, v2012 and v2013.
- Force-field based: these scoring functions calculate explicit pair-wise interactions between atoms of the protein and the ligand within a certain cut-off. They are based on a forcefield used in MD simulations.
- Knowledge based: these are also known as statistical potential functions and exploit the probability of finding protein and ligand atoms within a certain distance to each other to obtain a 'potential of mean force'.[65] They do not have any physical meaning[66] but tend to correlate with free energy differences.[67]

Scoring functions can also be applied after docking (`re-scoring') and offer the possibility to obtain a consensus from multiple scoring functions in order to prioritize a binding hypothesis.[68] The GOLD software has several scoring functions, such as GoldScore, ChemScore, ChemPLP and the Astex Statistical Potential (ASP). GoldScore is forcefield based, performs well but is relatively slow compared to ChemPLP. ChemPLP is a piecewise linear potential function that uses the 'Ants' algorithm.[69] ChemScore is mostly to be used in the case of metal complexes since it contains terms for that.[70]

The empirical scoring function X-Score can easily be scripted and requires about 2 seconds of computation time per protein-ligand complex. The function is known to perform well is most cases and is validated against a set of 800 protein-ligand complexes. Besides van der Waals and electrostatic terms, it approximates the ligand entropic contribution by taking its number of rotatable bonds into account.[71]

Scoring functions are infamously known for performing poor, i.e. having a low predictability. This is due their simplistic nature; recent studies have shown that machine-learning methods to training a function outperforms MLR trained scoring functions.[72] Moreover, a scoring function only assesses a score based on one snapshot of a protein-ligand complex. This is very unreliable considering the fact that binding affinity is related to a Boltzmann weighted average of different states of a complex. Additionally, most scoring functions ignore the contribution of desolvation and entropy of the binding pocket and interactions with water. On the other hand, scoring functions are very fast and in some cases very useful for the screening of large compound libraries.

b 2 Agglomerative Hierarchical Clustering

Docking poses can be clustered hierarchically based on a root mean square distance matrix of the ligand poses' heavy atoms in Euclidean space. The abundance of poses within a certain range, typically 2 Å, may indicate the binding mode to have a higher probability being the biologically active one. Co-crystal structures with ligands that have a chemical scaffold in common can be placed in the same fashion in a protein as well.[73] Therefore, cluster analysis can be a powerful method to group poses of different ligands with the same scaffold together. The scaffold has then first to be extracted from the poses by defining e.g. a SMILES string and writing them as coordinates to a database.

With agglomerative hierarchical clustering, each pose is a cluster on its own (see Figure 8). Different methods exist to link these clusters together: in the complete linkage method, a dendrogram is formed by combining those clusters that have the shortest distance to each other, wherein two elements are the farthest neighbor. This avoids clusters being combined falsely due to outliers within a cluster, which can occur in the single-linkage method. A dendrogram is produced which the user can cut at a desired height; which represents the RMSD between the clusters in the case of docking poses. The user may also qualitatively determine the number of clusters from visualizing the poses and then select the cut-off. Cluster analysis can be performed with the MS Excel add-in XLStat[74] or by scripting.

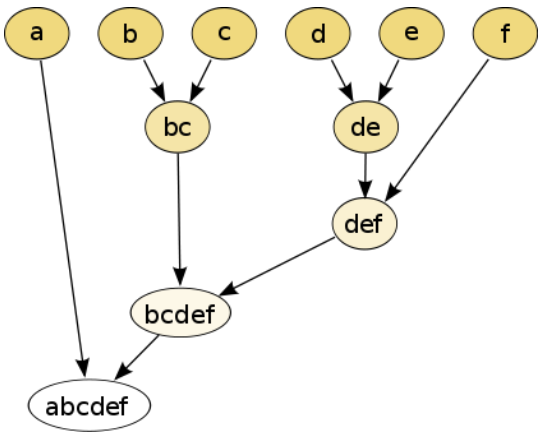

Figure 8 *Depiction of Agglomerative Hierarchal Clustering*

c Molecular Dynamics

Biomolecular simulations were first performed in the 1970s by notable physicists, such as the Viennese born Martin Karplus and Dutchman Herman Berendsen. Karplus contributed to the Chemistry at HARvard Molecular Mechanics (CHARMM) forcefield which is commonly used today. Berendsen is known for its temperature and pressure coupling schemes which are also frequently applied in biomolecular simulations.

Molecular dynamics is a structure-based sampling technique that is much more rigorous than docking since it explicitly calculates the pair-wise interactions of the molecules in time. Many molecular mechanical approximations are made, based on quantum mechanical (QM) effects. Besides, there is a finite time step which has to be shorter than the time of the fastest oscillation in the system, which is the hydrogen bond. The forcefield is divided into bonded and the non-bonded terms and represents the forces acting on each atom due to the surrounding atoms. The bonded terms are purely intramolecular and consist of stretching, bending and dihedral terms. The distance between two covalently bonded atoms can be represented by a harmonic oscillation or, preferably, constrained by additional algorithms such as SHAKE[75] and LINCS[76], which correct for the interatomic distance every several time steps. Bending terms are used to account for the attraction or repulsion that *i* and *i*+2 bonded atoms have to each other, while dihedral terms simplify the same for interactions between atoms *i* and *i*+3. These empirical approximations greatly reduce computational time.

The non-bonded terms define how both atoms *i* with *i*+4 and beyond, paired and intermolecular atoms interact with each other. The Optimized Potentials for Liquid Simulations (OPLS), pairs the 1-4 atoms and introduces a fudging factor to reduce their interactions, which can lead to better agreement with QM results. The non-bonded terms consist of the Coulombic and the Lennard-Jones (LJ) potential, the latter being a representation of the van der Waals interactions which defines the Pauli exclusion volume of the atom by a certain radius σ and an attractive 'well' defined by ε. Since the LJ potential is typically r^{-6} and r^{-12} dependent, it approaches 0 very quickly with increasing interatomic distance. The Coulombic potential is however present at longer range, due to its $1/r$ dependence (see Figure 9).

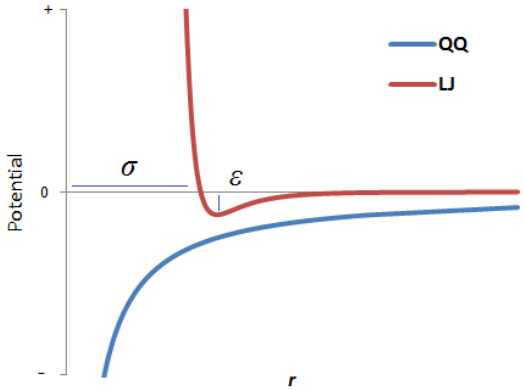

Figure 9 *Potential energy curves and functional forms used in the forcefield for the electrostatic (QQ) and van der Waals (LJ) components of the pair-wise atomic interactions.*

$$V_{LJ}(r) = 4\,\epsilon\left(\frac{\sigma^{12}}{r^{12}} - \frac{\sigma^{6}}{r^{6}}\right) \qquad V_{QQ}(r) = -\frac{q_1 q_2}{4\pi\epsilon_0\, r}$$

ε is the well-depth, σ represents the atom's radius, ε_0 the electric constant, q_1 and q_2 opposite charges and r the interatomic distance.

Computation of the non-bonded terms requires most of the computational time and therefore cut-offs are introduced. A cut-off radius of 1 nm is e.g. used in the OPLS forcefield. Interactions beyond that are commonly approximated by Particle Mesh Ewald summation (PME)[77]. Protein systems are typically simulated in a box using periodic boundary conditions to mimic crystal structure conditions and to prevent unwanted effects from the presence of a wall.

The system is parametrized by a topology and a starting structure can be energy minimized to remove any overlapping van der Waals cores. Then each atom is given a random velocity v based on a Maxwell-Boltzmann distribution at the desired reference temperature *T*. This is related by:

$$\frac{1}{2}\sum_{i=1}^{N} mv^2 = \frac{3}{2}k_B T \quad (1)$$

with k_B the Boltzmann constant, *m* the particle mass and *N* the total number of atoms in the system

The Newton equations of motion are solved by an integrator such as the leap-frog or Verlet[78] algorithm. Potential energies are calculated by integrating the force over the interatomic distance and summing up all the pairwise interactions within the cut-off region.

The advantage of using MD is that is strives to mimic the structure of interest as realistic as possible. Additionally, precise energy values can be obtained and many conformations are produced that can be useful for docking studies or explaining protein-ligand interactions in the dimension of time. However, a classical MD simulation does not sample conformational space as efficiently as Monte Carlo or Markov Chain methods, since, depending on the starting structure, trajectories may be trapped in a multidimensional energy minimum.

e Free Energy Calculations

The calculation of accurate binding free energy ΔG_{bind} is becoming of greater importance in guiding of synthesis projects in the pharmaceutical industry.[79-81] During a protein-ligand binding event, several microscopic processes occur:

1. Ligand desolvation leading to a loss in hydration enthalpy: $\Delta H\uparrow$
2. Pocket desolvation leading to more favorable water entropy: $T\Delta S\uparrow$
3. Protein-ligand binding leading to entropy reduction but usually a much more favorable enthalpy: $T\Delta S\downarrow\ \Delta H\downarrow\downarrow$

The sum of the change in the energies associated with these events equals the binding free energy:

$$\Delta G_{\text{bind}} = \Delta H - T\Delta S \quad (2)$$

It is however not trivial to calculate these terms separately, especially the entropic contribution. But since free energy is a state function, a computationally more feasible 'alchemical' path from state A to state B can be designed and it does not matter how the path is calculated. For the calculation of the relative binding free energy between two ligands, a thermodynamic cycle can be constructed, which shows that the difference in free energy of the complexes and of the ligand in solution equals the relative binding free energy of the two ligands for that protein. Similarly, the difference in binding free energy between two different proteins in presence and absence of a ligand equals the relative free energy between the two proteins for that ligand (see Figure 10).

Figure 10 *Thermodynamic cycles for relative binding free energy calculations between two ligands (left) and between two proteins (right). The difference between ΔG_4 and ΔG_3 equals the difference between ΔG_2 and ΔG_1.*

Thermodynamic Integration (TI) is a technique developed by Kirkwood in the 1930s and is the most commonly used binding free energy calculation method, due to its relative simplicity and exploitability by parallel computing.[82] A perturbation of e.g. a chemical moiety or atom is typically divided into several λ-dependent steps ('windows') in order to gradually account for the physical change and to assure phase space overlap. The change can be the atom centered partial charge, the Van der Waals radius σ, its well depth ϵ and the bonded terms described by the forcefield. The mass of the particle is normally kept constant, even if this leads to an 'empty' dummy atom, since this quantity has only influence on the kinetic energy but not on the potential energy of interest. The TI method is derived from statistical mechanics:
The distribution of states of a system consisting of *N* particles contained within a volume *V*, has a total energy *E*, coordinates **r** and momenta **p** and is described by the partition function as:

$$Z(N,V,T) = c \iint e^{-\frac{E(\mathbf{r},\mathbf{p})}{k_B T}} \mathrm{d}\mathbf{r}\, \mathrm{d}\mathbf{p} \tag{3}$$

With *c* being a constant that corrects for the indistinguishability of the particles

The free energy *A* is related to the partition function as follows:

$$\Delta A\,(N, V, T) = -\, k_B T \ln Z\,(N,V,T) \tag{4}$$

The TI theory states that the free energy *A* can be made a function of the coupling parameter λ and that the derivative of *A* with respect to λ is exactly the same as the ensemble average of the derivative of the total energy *E* of the system with respect to λ (see Appendix **A2** for a derivation) [82]:

$$\frac{\partial A\,(\lambda)}{\partial \lambda} = \left\langle \frac{\partial E\,(\lambda)}{\partial \lambda} \right\rangle \tag{5}$$

During the perturbation, the potential energy *V* is a mixed one of the starting state *A* and end state *B:*

$$V\,(r) = (1 - \lambda)\; V_A\,(r) + \lambda\; V_B\,(r) \tag{6}$$

with *r* the interatomic distance

The potentials are commonly made a function of λ as well, to introduce softness of the van der Waals core in the intermediate windows. This prevents fluctuations at λ values close to 0 and 1 when a particle suddenly appears or disappears. The pairwise LJ interactions are then calculated as follows:

$$V_{LJ}\,(\lambda, r) = (1-\lambda)\; 4\; \epsilon_A \left(\frac{{\sigma_A}^{12}}{(\alpha\lambda + r^6)^2} - \frac{{\sigma_A}^{6}}{\alpha\lambda + r^6}\right) + \lambda\; 4\; \epsilon_B \left(\frac{{\sigma_B}^{12}}{(\alpha(1-\lambda) + r^6)^2} - \frac{{\sigma_B}^{6}}{\alpha(1-\lambda) + r^6}\right) \tag{7}$$

with α the dimensionless softness factor commonly set to 0.5

In order to prevent too strong attraction of oppositely charged atoms when decoupling an atom or moiety, the charges can be turned off before changing the van der Waals core, and *vice versa*.

The derivative of the total energy with respect to λ, is calculated typically every 10 or 100 time steps by the code and has the following form:

$$\frac{\delta E(\lambda)}{\delta \lambda} = (1\text{-}\lambda)\,\frac{\delta E_{\mathrm{A}}(\lambda)}{\delta \lambda} - E_{\mathrm{A}}(\lambda) + \lambda\,\frac{\delta E_{\mathrm{B}}(\lambda)}{\delta \lambda} + E_{\mathrm{B}}(\lambda) \tag{8}$$

This means that when λ equals 0 or 1, the potential of the pairwise interactions in one endstate is also influenced by the potential of the other endstate.

From the obtained $\delta E/\delta\lambda$ values, block averaging is performed on a stably converged trajectory to obtain the ensemble average $\langle \delta E/\delta\lambda \rangle$. The error is calculated similarly from the variance between the averages of the *m* blocks:

$$Error = \sqrt{\sum_{m=2}^{m} \frac{\mathrm{Var}(\frac{dE}{d\lambda})}{m(m-1)}} \tag{9}$$[83]

Sampling is considered sufficient as soon as the error reaches a plateau with increasing block size.[83] The difference in free energy between state *A* and *B* is obtained by numerical integration, such as by the trapezoidal rule, of a smooth line connecting these ensemble averages of the separate windows:

$$\Delta A_{\text{A-B}} = \int_{\lambda=0}^{1} \langle \frac{\partial E}{\partial \lambda} \rangle \, d\lambda \tag{10}$$

The relative binding free energy between two ligands is then calculated as:

$$\Delta\Delta G_{\text{bind}} = \Delta A_{\text{A-B,complex}} - \Delta A_{\text{A-B,water}} \tag{11}$$

Free energy calculations have the advantage to obtain very accurate predictions of the binding free energy of a protein-ligand binding event, although they are very rigorous and may require several weeks in order to obtain a single value. Besides that, the value cannot be perfectly accurate because of the sampling problem: a simulation has to be performed in the limit of infinite time to obtain the correct distribution of states and mimic experimental conditions. On the other hand, experimental results can also differ significantly between different labs, while measured values may have substantial standard deviations due to different cell types, the influence of regulatory proteins interfering with the target protein of interest and physical conditions such as changes in light and temperature.

f Quantitative Structure-Activity Relationship (QSAR) Methods

QSAR is a ligand-based method to identify physicochemical properties that contribute to activity and/or to predict the activity of novel compounds. A dataset of ligands and their activities can be prepared by extraction from literature sources or by the curation of databases, such as ChEMBL[84] and OpenPHACTS[85]. Ligands have to be measured in the same assay and have the same activity type (K_i/IC_{50}) to make reliable models. This also includes the type of species, cells, tissue and the temperature.

The physicochemical properties of the ligands are represented by descriptors. 1D and 2D descriptors include e.g. the number of carbon atoms or topological polar surface area (TPSA), respectively. Classical 3D-QSAR can

be performed when assuming that all ligands bind in the same fashion. In that case an alignment of the ligands has to be made based on their atom types or pharmacophoric features.

Hammett descriptors are a series of descriptors (constants) that quantify the electron withdrawing or donating effect of an aromatic substituent (**σ**). Corwin Hansch was one of the first medicinal chemists to use these constants for the determination of partition coefficients (*log P*). These constants were calculated from the ratio between the equilibrium constants of substituted and unsubstituted benzoic acids, *K* and K_0, respectively:

$$log\ K\ /\ K_0 = \boldsymbol{\sigma\rho} \tag{12}$$

ρ is the reaction constant and usually set to unity

Sigma constants can also be derived from *ab initio* calculations since they were found to linearly correlate with the core-electron binding energy of the aromatic carbon attached to the substituent.[86]

Descriptors that represent the steric factor E_s, molar refractivity *MR* and lipophilicity **π** have also been derived similarly. Simplified QSAR methods were later introduced by Fujita-Ban and Free-Wilson where a certain chemical moiety or physical property of a ligand, such as enantiomerism, is defined as a binary value describing its presence or absence. These methods can be combined with Hammett's **σ** and **π** constants.

The selection of descriptors is important for making the model interpretable and to prevent over fitting the data. This can be performed is a variety of ways, such as by creating a correlation matrix and discarding intercorrelated descriptors or by using of a wrapper method such as forward or backward selection. The backward selection is performed by fitting all the descriptors to the model and then removing descriptors sequentially that have the lowest importance. The use of a genetic algorithm that selects an optimized combination of descriptors can also be used.

Classical QSAR models are made by multiple linear regression of calculated descriptor values of a training set, whereas classification models are commonly made by machine learning methods such as *k*-nearest neighbor, random forests or support vector machines, which vary in their predictivity and interpretability. Different tools are available to perform QSAR, such as Weka, XLStat or MOE.

The validation of a model is indispensible and different methods exist, such as cross validation and bootstrapping. Leave-one-out cross validation is a powerful and easy method to assess the predictivity of the obtained model, whereby a new correlation coefficient Q^2 using *n* compounds with activity Y_i, can be calculated as follows:

$$Q^2 = 1 - \sum_{i=1}^{n}(Y_i - \hat{Y}_i^{(-i)})^2 / \sum_{i=1}^{n}(Y_i - \bar{Y})^2 \tag{13}$$

with $\hat{Y}_i^{(-i)}$ being the estimate of Y_i after leaving out the *i*th compound

A Q^2 of 0.6 is considered to be the lower limit for a QSAR model to be predictive.[87] Validation can also be performed by *Y*-scrambling whereby the order of the dependent variables is randomized, which should lead to a poor model.

The advantage of QSAR is its efficiency and reliability within the chemical and activity space. A chemist can however be limited to using the same chemical class without reliable extrapolation. With the classical QSAR methods, it has to be assumed that all compounds bind in the same binding site with the same orientation. This can be problematic, since protein pockets can be very flexible and prone to induced-fit effects, whereas several studies have shown that multiple binding modes of one ligand may occur in crystal structures.[88, 89] The use of alignment independent tools such as GRIND[90] may alleviate this problem.

C Experimental Methods

a Site-directed mutagenesis

Mutant proteins are useful for understanding protein-ligand interactions and protein function. The creation of their DNA is performed in several steps: primers are designed that are complementary to the region of interest on the wild-type protein DNA and include a mutation. The typical length of a primer is between 25 and 45 bases with a melting temperature of at least 78 °C and a minimum guanine/cytosine (GC) content of 40%. Vendor kits such as Agilent® offer online tools to calculate a proper GC content.[91] The wild-type DNA that is contained within a plasmid, also contains DNA for enzymes that degrade an antibiotic such as kanamycin or ampicillin for use as background. The primers are both in forward and reverse direction for the nonsense and sense strand of the DNA, respectively. A kit generally also contains DNA polymerase for the elongation with the deoxyribonucleotides (dNTPs) that are added as well.

The polymerase-chain reaction (PCR) is used to perform cycles of denaturing, primer annealing and primer elongation. After digestion of the parental DNA using a restriction endonuclease that recognizes methylated DNA, the plasmid is multiplied by transformation: competent bacteria are mixed with the DNA and a short heatshock is given so that the bacteria take up the plasmid. Then the bacteria are grown on agar containing the antibiotic for which the plasmid has resistance genes. Colonies are picked the following day and grown in lysogeny broth (LB) medium containing the same antibiotic. A turbid mixture indicates growth and mini-prep is performed to isolate the DNA from the bacteria: the bacteria are lysed, the DNA is absorbed on a cationic filter and eluted using a buffer solution (see Figure 11).

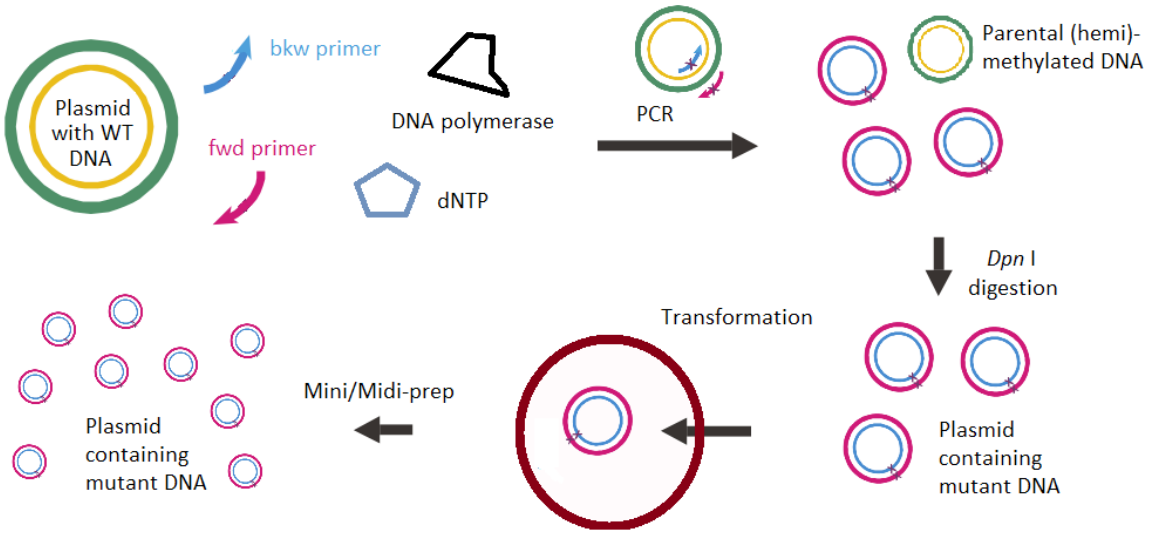

Figure 11 *Process of site-directed mutagenesis*

Quantification can be performed using a nanophotometer set at wavelengths that DNA absorbs. A 280nm/260nm ratio of 1.8 indicates high purity, whereas a DNA concentration of around 1 µg/µL is desired. The DNA sequencing is usually outsourced and results should indicate whether the creation of the DNA of interest has been achieved. The DNA solution is re-transformed and isolated by midi-prep, which is similar as mini-prep, but on a higher scale.

b Transient transfection

Transient transfection of a DNA plasmid is the process of integrating DNA into test cells. Different kits are available that vary in efficiency and price. Lipofectamine® is an efficient transfection agent that contains lipids with a cationic head group. These encapsulate the DNA to form liposomes that attach to the negatively charged membrane surface of eukaryotic cells. The genetic material can enter the cell and then has a probability to enter the nuclear envelope. For optimal transfection, lipofectamine requires the use of a minimal amount of medium, starved from antibiotic and serum. The following day, transfection is checked by observing fluorescence at the emission wavelength of the biological marker. Successful fluorescence is confirmed based on the presence of a homogeneous glow.

The advantage of transient transfection is its flexibility, relative ease of application and price. One only needs to have a prepared plasmid and to split cells, whereas the cells may express the protein of interest the following day. The drawback of the method is its relatively weak expression (ca. 50%) compared to a stably transfected cell line.

c Uptake inhibitory measurements

Uptake inhibitory measurements are the method of choice to determine the inhibitory activity by a compound of interest on a transmembrane transporter. By binding to the transporter, the measured compound blocks the uptake of a radioligand into the cell (see Figure 12, left). The transfected cells are seeded on a plate, coated with poly-D-lysine (PDL) to make sure that the cells attach to the surface. The experiment is normally performed with a confluence of at least 80%. The cells are first pre-incubated with defined concentrations of the compound to be tested. After pre-incubation, a solution with the same concentration of compound is added, that also contains a radioligand. A blank and inhibitor solution is measured too, for determining the maximum and unspecific uptake, respectively (see Figure 12, above). Unspecific uptake may occur for example through the cell membrane.

The reaction is halted by cooling the cells down with cold buffer solution and the cells are lysed with a detergent solution. The solutions are then measured after mixing them with a scintillation cocktail, which contains a solvent, a surfactant and a scintillator additive. The neurotransmitter radioligands contain tritium, which has a half-life of ca. 12 years and emits β^- particles upon decay to helium: ${}^3_1\mathrm{H} \rightarrow {}^3_2\mathrm{He} + \beta^- + \bar{\nu}$. The radiation is of such low energy (ca. 5.7 keV) that exposure to the compounds is practically harmless to the researcher. The counts can be plotted with a software such as SigmaPlot[92] to obtain the concentration at half-maximal uptake (IC_{50}) by sigmoidal regression. According to the Cheng-Prusoff equation, the IC_{50} or inhibition constant (K_i) can be related to the affinity, only if compared to the activity of other compounds that bind on the same site in the same protein.

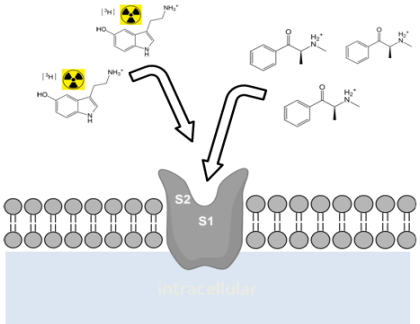

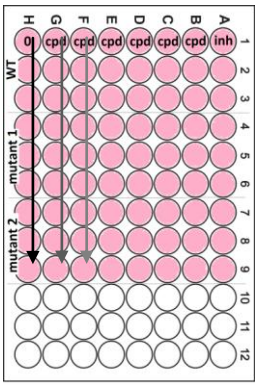

Figure 12 ***Left****: Depiction of an uptake inhibitory assay on SERT showing tritiated serotonin and (S)-methcathinone molecules.* ***Above****: Example of a 96-well plate used in an uptake inhibitory assay. The filled wells (pink) represent the medium with the cells attached on the surface. The top row indicates the solution added to each column.*

Bibliography

1. *World Health Organization*, 2015.
2. Ban, T.A., Fifty years chlorpromazine: a historical perspective*, Neuropsychiatr Dis Treat*, 2007. **3**(4): p. 495-500.
3. Jacobsen, E., The early history of psychotherapeutic drugs*, Psychopharmacology (Berl)*, 1986. **89**(2): p. 138-144.
4. Seeman, P. and H.B. Niznik, Dopamine receptors and transporters in Parkinson's disease and schizophrenia*, FASEB J*, 1990. **4**(10): p. 2737-44.
5. Therapy deficit*, Nature*, 2012. **489**(7417): p. 473-4.
6. Rothman, R.B., et al., Studies of the biogenic amine transporters. 13. Identification of "agonist" and "antagonist" allosteric modulators of amphetamine-induced dopamine release*, J Pharmacol Exp Ther*, 2009. **329**(2): p. 718-28.
7. Rothman, R.B., et al., Studies of the biogenic amine transporters. 14. Identification of low-efficacy "partial" substrates for the biogenic amine transporters*, J Pharmacol Exp Ther*, 2012. **341**(1): p. 251-62.
8. Hertting, G. and J. Axelrod, Fate of tritiated noradrenaline at the sympathetic nerve-endings*, Nature*, 1961. **192**: p. 172-3.
9. Henry, L.K., et al., A Conserved Asparagine Residue in Transmembrane Segment 1 (TM1) of Serotonin Transporter Dictates Chloride-coupled Neurotransmitter Transport*, Journal of Biological Chemistry*, 2011. **286**(35): p. 30823-30836.
10. Lingjærde, O., Uptake of Serotonin in Blood Platelets in vitro. I: The Effects of Chloride*, Acta Physiologica Scandinavica*, 1971. **81**(1): p. 75-83.
11. Quick, M.W., Regulating the Conducting States of a Mammalian Serotonin Transporter*, Neuron*. **40**(3): p. 537-549.
12. Adams, S.V. and L.J. DeFelice, Flux coupling in the human serotonin transporter*, Biophysical Journal*, 2002. **83**(6): p. 3268-3282.
13. Sucic, S., et al., The serotonin transporter is an exclusive client of the coat protein complex II (COPII) component SEC24C*, J Biol Chem*, 2011. **286**(18): p. 16482-90.
14. Li, L.B., et al., The role of N-glycosylation in function and surface trafficking of the human dopamine transporter*, J Biol Chem*, 2004. **279**(20): p. 21012-20.
15. Tate, C.G. and R.D. Blakely, The effect of N-linked glycosylation on activity of the Na(+)- and Cl(-)-dependent serotonin transporter expressed using recombinant baculovirus in insect cells*, Journal of Biological Chemistry*, 1994. **269**(42): p. 26303-26310.
16. ncbi.nlm.nih.gov.
17. Ramamoorthy, S., et al., Antidepressant- and cocaine-sensitive human serotonin transporter: molecular cloning, expression, and chromosomal localization*, Proc Natl Acad Sci U S A*, 1993. **90**(6): p. 2542-6.
18. Giros, B., et al., Cloning, pharmacological characterization, and chromosome assignment of the human dopamine transporter*, Molecular Pharmacology*, 1992. **42**(3): p. 383-390.
19. Ciliax, B.J., et al., Immunocytochemical localization of the dopamine transporter in human brain*, The Journal of Comparative Neurology*, 1999. **409**(1): p. 38-56.
20. Pacholczyk, T., R.D. Blakely, and S.G. Amara, Expression cloning of a cocaine-and antidepressant-sensitive human noradrenaline transporter*, Nature*, 1991. **350**(6316): p. 350-354.
21. Hoffman, B.J., et al., Localization and dynamic regulation of biogenic amine transporters in the mammalian central nervous system*, Front Neuroendocrinol*, 1998. **19**(3): p. 187-231.
22. Lemieux, M.J., A perspective on the structural studies of inner membrane electrochemical potential-driven transporters*, Biochim Biophys Acta*, 2008. **1778**(9): p. 1805-13.
23. Carpenter, E.P., et al., Overcoming the challenges of membrane protein crystallography*, Current Opinion in Structural Biology*, 2008. **18**(5): p. 581-586.
24. Penmatsa, A. and E. Gouaux, How LeuT shapes our understanding of the mechanisms of sodium-coupled neurotransmitter transporters*, J Physiol*, 2014. **592**(Pt 5): p. 863-9.
25. Sarker, S., et al., The high-affinity binding site for tricyclic antidepressants resides in the outer vestibule of the serotonin transporter*, Mol Pharmacol*, 2010. **78**(6): p. 1026-35.
26. Kazmier, K., et al., Conformational dynamics of ligand-dependent alternating access in LeuT*, Nat Struct Mol Biol*, 2014. **21**(5): p. 472-479.
27. Zhao, Y., et al., Substrate-modulated gating dynamics in a Na+-coupled neurotransmitter transporter homologue*, Nature*, 2011. **474**(7349): p. 109-13.
28. Grouleff, J., et al., Properties of an Inward-Facing State of LeuT: Conformational Stability and Substrate Release*, Biophys J*, 2015. **108**(6): p. 1390-9.
29. Yamashita, A., et al., Crystal structure of a bacterial homologue of Na+/Cl--dependent neurotransmitter transporters*, Nature*, 2005. **437**(7056): p. 215-23.
30. Sucic, S., et al., The N Terminus of Monoamine Transporters Is a Lever Required for the Action of Amphetamines*, The Journal of Biological Chemistry*, 2010. **285**(14): p. 10924-10938.
31. Penmatsa, A., K.H. Wang, and E. Gouaux, X-ray structure of dopamine transporter elucidates antidepressant mechanism*, Nature*, 2013.
32. Stockner, T., et al., Mutational analysis of the high-affinity zinc binding site validates a refined human dopamine transporter homology model*, PLoS Comput Biol*, 2013. **9**(2): p. e1002909.

33. Norregaard, L., et al., Delineation of an endogenous zinc-binding site in the human dopamine transporter, *EMBO J*, 1998. **17**(15): p. 4266-73.
34. Zomot, E., et al., Mechanism of chloride interaction with neurotransmitter:sodium symporters, *Nature*, 2007. **449**(7163): p. 726-30.
35. Hong, W.C. and S.G. Amara, Membrane Cholesterol Modulates the Outward Facing Conformation of the Dopamine Transporter and Alters Cocaine Binding, *Journal of Biological Chemistry*, 2010. **285**(42): p. 32616-32626.
36. Anderluh, A., et al., Single molecule analysis reveals coexistence of stable serotonin transporter monomers and oligomers in the live cell plasma membrane, *J Biol Chem*, 2014. **289**(7): p. 4387-94.
37. Fog, J.U., et al., Calmodulin kinase II interacts with the dopamine transporter C terminus to regulate amphetamine-induced reverse transport, *Neuron*, 2006. **51**(4): p. 417-29.
38. Buchmayer, F., et al., Amphetamine actions at the serotonin transporter rely on the availability of phosphatidylinositol-4,5-bisphosphate, *Proc Natl Acad Sci U S A*, 2013. **110**(28): p. 11642-7.
39. Rothman, R.B. and M.H. Baumann, Monoamine transporters and psychostimulant drugs, *Eur J Pharmacol*, 2003. **479**(1-3): p. 23-40.
40. Rodriguez, G.J., et al., Distinct recognition of substrates by the human and Drosophila serotonin transporters, *J Pharmacol Exp Ther*, 2003. **306**(1): p. 338-46.
41. Roman, D.L., et al., Distinct molecular recognition of psychostimulants by human and Drosophila serotonin transporters, *J Pharmacol Exp Ther*, 2004. **308**(2): p. 679-87.
42. Celik, L., et al., Binding of serotonin to the human serotonin transporter. Molecular modeling and experimental validation, *J Am Chem Soc*, 2008. **130**(12): p. 3853-65.
43. Simmler, L.D., et al., Pharmacological characterization of designer cathinones in vitro, *Br J Pharmacol*, 2013. **168**(2): p. 458-70.
44. Severinsen, K., et al., Binding of the amphetamine-like 1-phenyl-piperazine to monoamine transporters, *ACS Chem Neurosci*, 2012. **3**(9): p. 693-705.
45. Teixeira-Gomes, A., et al., The neurotoxicity of amphetamines during the adolescent period, *International Journal of Developmental Neuroscience*, 2015. **41**(0): p. 44-62.
46. Goodwin, J.S., et al., Amphetamine and Methamphetamine Differentially Affect Dopamine Transporters in Vitro and in Vivo, *Journal of Biological Chemistry*, 2009. **284**(5): p. 2978-2989.
47. Thompson, J.D., T.J. Gibson, and D.G. Higgins, Multiple sequence alignment using ClustalW and ClustalX, *Curr Protoc Bioinformatics*, 2002. **Chapter 2**: p. Unit 2 3.
48. Sali, A., et al., Evaluation of comparative protein modeling by MODELLER, *Proteins*, 1995. **23**(3): p. 318-26.
49. Laskowski, R.A., et al., PROCHECK: a program to check the stereochemical quality of protein structures, *Journal of Applied Crystallography*, 1993. **26**(2): p. 283-291.
50. Benkert, P., S.C. Tosatto, and D. Schomburg, QMEAN: A comprehensive scoring function for model quality assessment, *Proteins*, 2008. **71**(1): p. 261-77.
51. Hillisch, A., L.F. Pineda, and R. Hilgenfeld, Utility of homology models in the drug discovery process, *Drug Discov Today*, 2004. **9**(15): p. 659-69.
52. Kuntz, I.D., et al., A geometric approach to macromolecule-ligand interactions, *J Mol Biol*, 1982. **161**(2): p. 269-88.
53. Chen, R., L. Li, and Z. Weng, ZDOCK: an initial-stage protein-docking algorithm, *Proteins*, 2003. **52**(1): p. 80-7.
54. Goodsell, D.S., G.M. Morris, and A.J. Olson, Automated docking of flexible ligands: applications of AutoDock, *J Mol Recognit*, 1996. **9**(1): p. 1-5.
55. Friesner, R.A., et al., Glide: a new approach for rapid, accurate docking and scoring. 1. Method and assessment of docking accuracy, *J Med Chem*, 2004. **47**(7): p. 1739-49.
56. Sherman, W., et al., Novel procedure for modeling ligand/receptor induced fit effects, *J Med Chem*, 2006. **49**(2): p. 534-53.
57. Jacobson, M.P., et al., On the Role of the Crystal Environment in Determining Protein Side-chain Conformations, *Journal of Molecular Biology*, 2002. **320**(3): p. 597-608.
58. Jones, G., et al., Development and validation of a genetic algorithm for flexible docking, *J Mol Biol*, 1997. **267**(3): p. 727-48.
59. Lovell, S.C., et al., The penultimate rotamer library, *Proteins*, 2000. **40**(3): p. 389-408.
60. Seddik, A., et al., Probing the Selectivity of Monoamine Transporter Substrates by Means of Molecular Modeling, *Mol Inform*, 2013. **32**(5-6): p. 409-413.
61. Molecular Operating Environment (MOE), C.C.G.I., 1010 Sherbooke St. West, Suite #910, Montreal, QC, Canada, H3A 2R7, 2015.
62. Shelley, J., et al., Epik: a software program for pK a prediction and protonation state generation for drug-like molecules, *Journal of Computer-Aided Molecular Design*, 2007. **21**(12): p. 681-691.
63. Hunter, J.D., Matplotlib: A 2D Graphics Environment, *Computing in Science and Engg.*, 2007. **9**(3): p. 90-95.
64. *https://plot.ly*.
65. Sippl, M.J., Calculation of conformational ensembles from potentials of mean force. An approach to the knowledge-based prediction of local structures in globular proteins, *J Mol Biol*, 1990. **213**(4): p. 859-83.
66. Thomas, P.D. and K.A. Dill, Statistical Potentials Extracted From Protein Structures: How Accurate Are They?, *J Mol Biol*, 1996. **257**(2): p. 457-469.

67. Hamelryck, T., et al., Potentials of Mean Force for Protein Structure Prediction Vindicated, Formalized and Generalized, *PLoS ONE*, 2010. **5**(11): p. e13714.
68. Jabeen, I., et al., Probing the stereoselectivity of P-glycoprotein-synthesis, biological activity and ligand docking studies of a set of enantiopure benzopyrano[3,4-b][1,4]oxazines, *Chem Commun (Camb)*, 2011. **47**(9): p. 2586-8.
69. Korb, O., T. Stutzle, and T.E. Exner, Empirical scoring functions for advanced protein-ligand docking with PLANTS, *J Chem Inf Model*, 2009. **49**(1): p. 84-96.
70. Eldridge, M.D., et al., Empirical scoring functions: I. The development of a fast empirical scoring function to estimate the binding affinity of ligands in receptor complexes, *J Comput Aided Mol Des*, 1997. **11**(5): p. 425-45.
71. Cheng, T., et al., Comparative assessment of scoring functions on a diverse test set, *J Chem Inf Model*, 2009. **49**(4): p. 1079-93.
72. Li, H., et al., Substituting random forest for multiple linear regression improves binding affinity prediction of scoring functions: Cyscore as a case study, *BMC Bioinformatics*, 2014. **15**: p. 291.
73. Wang, H., et al., Structural basis for action by diverse antidepressants on biogenic amine transporters, *Nature*, 2013. **503**(7474): p. 141-5.
74. Addinsoft Inc., N.Y., NY. USA.
75. Ryckaert, J.-P., G. Ciccotti, and H.J.C. Berendsen, Numerical integration of the cartesian equations of motion of a system with constraints: molecular dynamics of n-alkanes, *Journal of Computational Physics*, 1977. **23**(3): p. 327-341.
76. Hess, B., et al., LINCS: A linear constraint solver for molecular simulations, *J Comput Chem*, 1997. **18**(12): p. 1463-1472.
77. Ewald, P.P., Die Berechnung optischer und elektrostatischer Gitterpotentiale, *Annalen der Physik*, 1921. **369**(3): p. 253-287.
78. Verlet, L., Computer Experiments on Classical Fluids .I. Thermodynamical Properties of Lennard-Jones Molecules, *Physical Review*, 1967. **159**(1): p. 98-&.
79. Christ, C.D. and T. Fox, Accuracy assessment and automation of free energy calculations for drug design, *J Chem Inf Model*, 2014. **54**(1): p. 108-20.
80. Fox, S.J., et al., Free energies of binding from large-scale first-principles quantum mechanical calculations: application to ligand hydration energies, *J Phys Chem B*, 2013. **117**(32): p. 9478-85.
81. Chipot, C., Free energy calculations applied to membrane proteins, *Methods Mol Biol*, 2008. **443**: p. 121-44.
82. Kirkwood, J.G., Statistical mechanics of fluid mixtures, *Journal of Chemical Physics*, 1935. **3**(5): p. 300-313.
83. Hess, B., Determining the shear viscosity of model liquids from molecular dynamics simulations, *Journal of Chemical Physics*, 2002. **116**(1): p. 209-217.
84. Bento, A.P., et al., The ChEMBL bioactivity database: an update, *Nucleic Acids Res*, 2014. **42**(D1): p. D1083-D1090.
85. Ratnam, J., et al., The Application of the Open Pharmacological Concepts Triple Store (Open PHACTS) to Support Drug Discovery Research, *PLoS ONE*, 2014. **9**(12): p. e115460.
86. Takahata, Y. and D.P. Chong, Estimation of Hammett sigma constants of substituted benzenes through accurate density-functional calculation of core-electron binding energy shifts, *International Journal of Quantum Chemistry*, 2005. **103**(5): p. 509-515.
87. Golbraikh, A. and A. Tropsha, Beware of q2!, *Journal of Molecular Graphics and Modelling*, 2002. **20**(4): p. 269-276.
88. Dahms, S.O., et al., Interaction of the amyloid precursor protein-like protein 1 (APLP1) E2 domain with heparan sulfate involves two distinct binding modes, *Acta Crystallographica Section D*, 2015. **71**(3): p. 494-504.
89. Bell, C.H., et al., A Dual Binding Mode for RhoGTPases in Plexin Signalling, *PLoS Biol*, 2011. **9**(8): p. e1001134.
90. Pastor, M., et al., GRid-INdependent descriptors (GRIND): a novel class of alignment-independent three-dimensional molecular descriptors, *J Med Chem*, 2000. **43**(17): p. 3233-43.
91. Agilent, QuikChange II XL Site-Directed Mutagenesis Kit, *Instruction Manual*.
92. *SigmaPlot (Systat Software, San Jose, CA)*.

II

Results and Discussion

A

Probing the Selectivity of Monoamine Transporter Substrates by Means of Molecular Modeling

Amir Seddik, Marion Holy, René Weissensteiner, Barbara Zdrazil, Harald H. Sitte, Gerhard F. Ecker

Published in *Molecular Informatics*, 32, 409-413, **2013**

In the following communication, a kick-off summary is given about currently known phenylethylamine substrates of the serotonin and dopamine transporter. Hypotheses for SERT-over-DAT selectivity are drawn based on their chemical properties and by docking of the selective probe compound (*S*)-fenfluramine.

molecular informatics

Special Issue EuroQSAR

DOI: 10.1002/minf.201300013

Probing the Selectivity of Monoamine Transporter Substrates by Means of Molecular Modeling

Amir Seddik,[a] Marion Holy,[b] René Weissensteiner,[a] Barbara Zdrazil,[a] Harald H. Sitte,[b] and Gerhard F. Ecker*[a]

Keywords: Serotonin transporter (SERT) · Dopamine transporter (DAT) · Substrate selectivity · Fenfluramine · Docking · Common scaffold clustering

The structurally similar serotonin and dopamine transporter (resp. SERT and DAT) play an important role in neuronal transmission. Although the concept of their function, i.e. the re-uptake of neurotransmitters from the synaptic cleft, has been extensively studied,[1–4] the exact mechanism for their substrate selectivity is still unknown. Phenylethylamines (PEAs) are ligands of SERT and DAT and many induce reverse transport (efflux) of the protein's natural substrate (the neurotransmitters 5-hydroxytryptamine and dopamine) in varying degrees and with different kinetics.[2,5–7] Thus, studying the interplay of bioactivity values and certain structural features of selected PEAs can lead to new insights about monoamine transporter selectivity. The broadest SAR data currently available for PEAs and their interaction with SERT and DAT has been measured in rat synaptosomes by Baumann and colleagues.[8,9]

Thus, we used this data set to figure out important features which contribute towards selectivity and to guide the selection of a probe compound for subsequent structure-based studies. Consequently, pEC_{50} values of 28 compounds for SERT and DAT (Table 1) were plotted against each other, providing a clear picture of the PEA's selectivity profile (Figure 1). Out of this, a couple of detailed SARs can be drawn:

I. Chirality of the α-methylene atom of amphetamines does not influence SERT/DAT selectivity.
II. The (*S*)-enantiomer is the most active in both transporters.
III. DAT selective substrates seem smaller in size and therefore, their conformational flexibility in the binding pocket is expected to be relatively high and interactions with the target less defined.
IV. *N*-Methyl substitution slightly increases activity in SERT (compare compounds **4**, **8**, **20** and **21**), and is somewhat unchanged in DAT (compare compounds **16**, **17**, **18** and **19**). The only exception is for the naphtylisopropylamine (NIPA, **23**) which is not selective for both transporters and shows a slight decrease in SERT activity (**24**).
V. *N*-Ethyl substitution is generally more favorable in SERT as compared to methyl substitution or no substitution, while it decreases activity in DAT (see compounds **19**, **22** and **25**).
VI. *para*-Chlorine, *meta*-CF_3 or *meta*-methyl substitution dramatically increases SERT affinity (compare **9**, **11**, **12**, **4**, **17**).
VII. β-Hydroxyl substitution (R_4, Table 1) decreases affinity in both SERT and DAT (compare **1**, **3**, **5**, **7**).
VIII. *para*-Methyl substitution increases SERT affinity and slightly decreases DAT affinity (compare **4**, **10**, **26**, **27**).

The highest SERT/DAT selectivity is shown by (*S*)-fenfluramine (SFF) and because of its relatively large size, docking studies with this ligand are expected to result in a more restricted amount of poses as compared to the smaller analogs. Subsequently, we used SFF as a probe compound in order to study the molecular basis of the high affinity and selectivity of this compound towards SERT by means of a structure-based approach. Conveniently, sequence identity between the human and rat transporters is very high (92% with SERT; 93% with DAT), and local alignment of the primary substrate binding site (S1[4]) shows even 100% sequence identity between both species.[10] Thus, in order to build upon our already established protein homology models for human SERT[11], we switched to human proteins for subsequent studies.

To show that data derived from rat transporters indeed can be transferred to the human transporters, we confirmed the high selectivity of SFF for SERT employing an uptake inhibition assay on HEK cells expressing human

[a] *A. Seddik, R. Weissensteiner, B. Zdrazil, G. F. Ecker*
University of Vienna, Department of Medicinal Chemistry, Pharmacoinformatics Research Group
Vienna, Austria
**e-mail: gerhard.f.ecker@univie.ac.at*

[b] *M. Holy, H. H. Sitte*
Medical University Vienna, Center for Physiology and Pharmacology, Institute of Pharmacology
Vienna, Austria

Table 1. Monoamine transporter substrate structure-activity relationships.

Cpd	Name	R_1	R_2	R_3	R_4	R_5	R_6	pEC_{50} rDAT	pEC_{50} rSERT
	Phenylethylamines 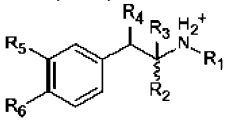								
1	Dopamine	H	H	H	H	OH	OH	7.1	5.0
2	Tyramine	H	H	H	H	H	OH	6.9	5.6
3	Norepinephrine	H	H	H	*(S)*-OH	OH	OH	6.1	5.0
4	(*S*)-Amphetamine	H	Me	H	H	H	H	7.6	5.6
5	(*R*)-Ephedrine	Me	Me	H	(*S*)-OH	OH	OH	5.9	5.0
6	HMA [a]	H	Me	H	H	H	OH	5.5	6.1
7	(*R*)-Methamphetamine	Me	Me	H	H	H	H	6.4	5.3
8	(*S*)-Methamphetamine							7.6	6.1
9	*m*-Methylamphetamine [a]	H	Me	H	H	Me	H	7.5	6.7
10	*p*-Methylamphetamine [a]	H	Me	H	H	H	Me	7.5	6.7
11	Phentermine	H	Me	Me	H	H	H	6.6	5.5
12	Chlorphentermine	H	Me	Me	H	H	Cl	5.6	7.5
13	*m*-Fluoroamphetamine [a]	H	Me	H	H	F	H	7.6	5.7
14	*p*-Fluoroamphetamine [a]	H	Me	H	H	H	F	7.3	6.0
15	HMMA [a]	Me	Me	H	H	MeO	OH	5.5	6.2
16	(*R*)-Norfenfluramine	H	Me	H	H	CF_3	H	5.0	6.5
17	(*S*)-Norfenfluramine							6.0	7.2
18	(*R*)-Fenfluramine	Et	Me	H	H	CF_3	H	5.0	6.8
19	(*S*)-Fenfluramine							5.0	7.3
		R_1	**3,4-Methylenedioxyamphetamines** 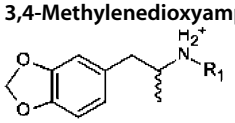						
20	MDA [a]	H						7.0	7.0
21	(*S*)-MDMA	Me						7.3	7.3
22	(*S*)-MDEA	Et						6.3	7.3
		R_1	**Naphtylisopropylamines** 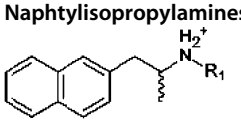						
23	NIPA [a]	H						7.8	8.4
24	(*S*)-*N*-Methyl-NIPA	Me						8.0	7.9
25	(*S*)-*N*-Ethyl-NIPA	Et						7.3	7.9
			Cathinones 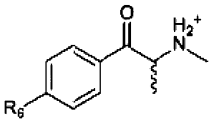				R_6		
26	Methcathinone [a]						H	7.7	5.4
27	Mephedrone [a]						Me	7.3	6.9
			Other 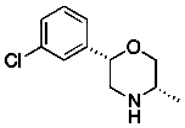						
28	PAL-738							7.2	7.6

[a] Chiral amphetimes without designated configuration represent the racemic mixture; H: hydrogen, Me: methyl, Et: ethyl, OH: hydroxy, MeO: methoxy, CF_3: trifluoromethyl

SERT and DAT (IC_{50} = 5.89 μM in SERT and 118 μM in DAT, see Figure 2).

Docking of a set of diverse high-affinity SERT substrates (see Methods) into a homology model of hSERT followed by common scaffold clustering revealed a binding mode for SFF which is in accordance to previously published studies.[12,13] In addition, SFF was docked into an analogously constructed homology model of hDAT. Results showed that this ligand fits nicely into the S1 site, meaning that steric hindrance caused by the trifluoromethyl or *N*-ethyl group could not serve as an explanation for its low DAT affinity (see Figure 3). In addition, scoring functions could not show a preference of SFF for SERT or DAT (see Table 2) and hence are not able to capture the activity determining factors. Since SFF's trifluoromethyl moiety seems to be driving the selectivity, we further analysed the pocket between the

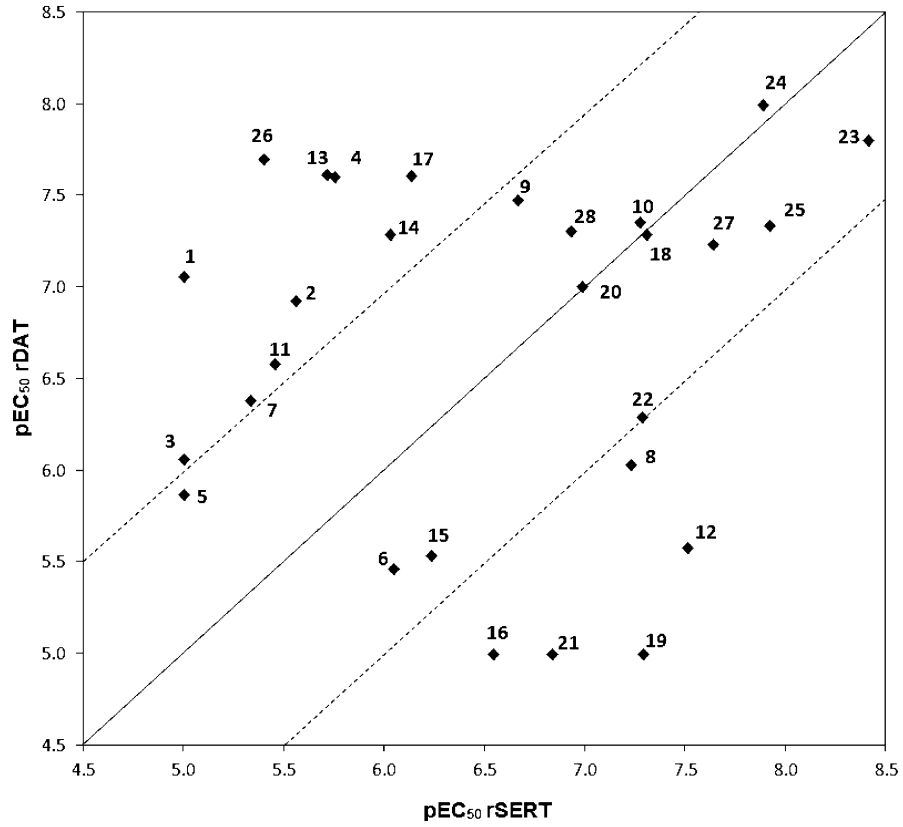

Figure 1. Selectivity plot with numbers corresponding to Table 1. Compounds with similar SERT/DAT affinity are located around the middle diagonal line, while compounds in the upper left corner and lower right corner are DAT and SERT-selective, respectively.

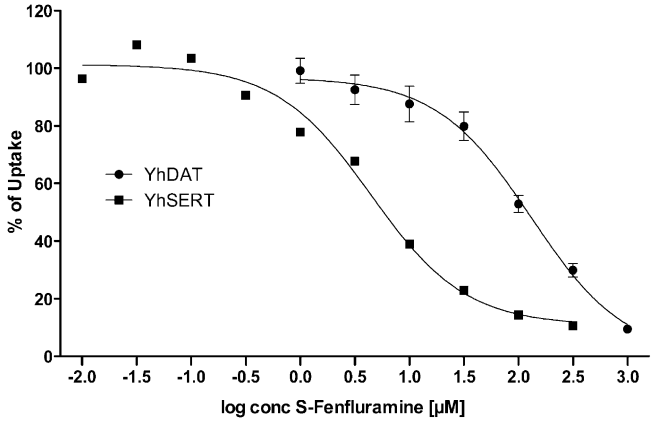

Figure 2. Uptake inhibition by (*S*)-fenfluramine in HEK293 cells stably expressing YFP-tagged DAT and SERT. Uptake was inhibited by increasing concentrations of fenfluramine as indicated. The concentration of tritiated substrates was 0.15 µM in the case of [^{3}H]5HT while 0.1 µM was used for [^{3}H]DA. Data are shown as means ± SEM of three (DAT) or four (SERT) independent experiments carried out in triplicate.

TM3 and TM8 helical domains where this moiety is located: local alignment of SERT and DAT showed that five of the seven residues within this pocket are different. In general, the SERT pocket has more lipophilic side chains in its binding site, except for Thr439 in SERT which is more hydrophilic than the corresponding Ala423 in DAT (see Table 3).

Table 2. Average scoring values after docking and evaluation of *(S)*-fenfluramine in the substrate binding site of homology models of SERT and DAT.

	SERT	DAT
X-score ($-K_D$ in kcal/mol)	6.5 ± 0.1	6.4 ± 0.1
DSX	−85 ± 9	−85 ± 12
London dG	−12.4 ± 1.5	−12.7 ± 0.7
N poses	14	9

This indicates a potential role of the CF_3 group and Thr439 for SERT selectivity. Furthermore, as shown in Table 1, (*S*)-amphetamine and (*S*)-norfenfluramine only have a trifluoromethyl moiety dissimilar, and their K_i values for rSERT are 3830 nM and 214 nM, respectively.[5,8] Since the ratio of these values should be similar to the K_D ratio (and since K_i is comparable to K_D[14]), the binding free energy formula can be applied:

$$\Delta G = -RT \ln K_D = -RT \ln (3830/214) = -1.72 \text{ kcal/mol}$$

with $T = 298.15$ K[5]
and

$R = 1.997 \quad 10^{-3}$ kcal/mol K

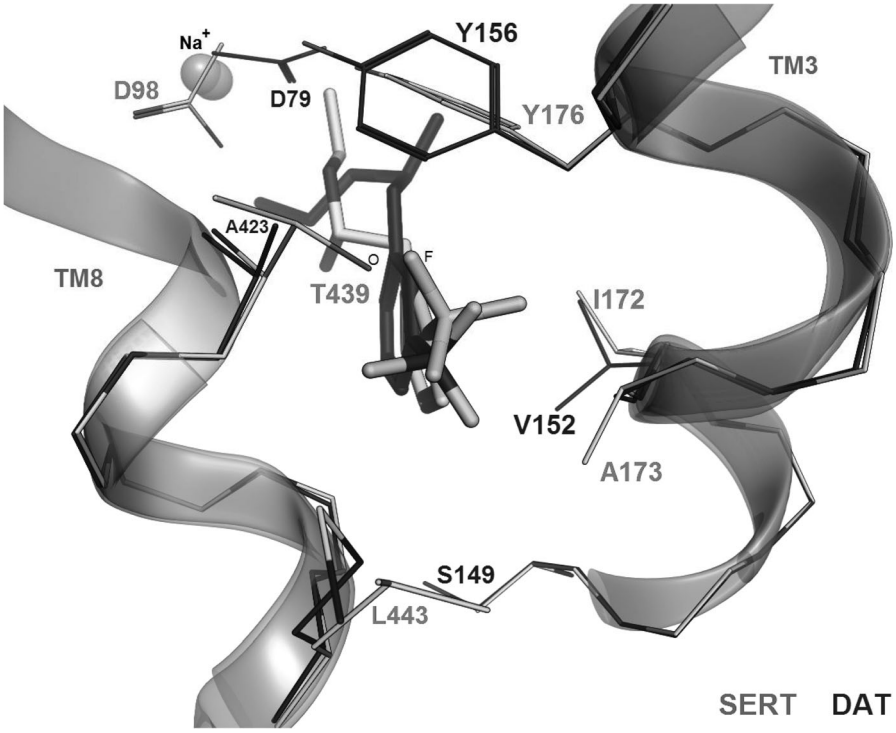

Figure 3. Overlay of the selected fenfluramine (SFF) poses in the substrate binding site of hSERT and hDAT with a T439(O)-F(SFF) distance of 3.5 Å.

Table 3. Local alignment of the helical domains TM3 and TM8 of hSERT and hDAT showing more lipophilic side chains in SERT, except that for Thr439.

SERT	A169	I172	A173	Y176	T439	G442	L443
DAT	S149	V152	G153	Y156	A423	G426	M427

Hence, from a ligand-based point of view, a more favorable binding energy of about 1.72 kcal/mol is calculated for (*S*)-norfenfluramine. Considering the inhibitory values of (*S*)-fenfluramine from our human DAT and SERT uptake inhibition assay, we obtain a binding free energy difference of about 1.75 kcal/mol:[15]

$$\Delta G = -RT \ln (118/5.89) = -1.75 \text{ kcal/mol}$$

with $T = 293.15$ K

Both calculated energy values are close to each other, strengthening the evidence that the trifluoromethyl group is responsible for SERT/DAT selectivity and high SERT affinity. Moreover, these values are relatively close to the ΔG value of a sp^3-fluorine hydrogen bond (−2.38 kcal/mol).[16] It is thus tempting to speculate that an interaction of Thr439 with the CF_3 group triggers both affinity and selectivity of SFF in SERT. In addition, lipophilic dispersion forces with the SERT specific side chains (Ala169, Ile172, Ala173) that surround the trifluoromethyl moiety might contribute. Further evidence for the potential role of the lipophilicity of this pocket can be deduced from the increase in activity of the more lipophilic *meta*-methyl-substituted compound **9** and a decrease in activity of the hydrophilic *meta*-hydroxy-substituted dopamine (**1**) and norepinephrine (**3**) in this protein. Finally, when comparing phentermine and chlorphentermine, the halide increases the SERT affinity 13 900/338 = 41 times,[5] which corresponds to more favorable energy of about 2.21 kcal/mol. Whether this can be ascribed to an interaction between the chlorine and Thr439, or simply to lipophilic contributions, is a point of discussion.

With this study we have shown that combining ligand- and structure based studies are a powerful tool to probe substrate selectivity of monoamine transporters leading to preliminary evidence for the potential role of halogen atoms and Thr439 in SERT. Synthesis of additional PEAs combined with biochemical studies in both wild type and T439A mutants are obvious further steps towards this direction.

Experimental

Materials and Methods. Dulbecco's modified Eagle's medium (DMEM) and trypsin were purchased from PAA Laboratories GmbH (Pasching, Austria). Fetal calf serum was purchased from Invitrogen. [^{3}H]5HT ([^{3}H]5-hydroxytryptamine; serotonin; 28.3Ci/mmol) and [^{3}H]DA (dopamine; 35 Ci/mmol) were purchased from PerkinElmer, Boston, MA, USA. Serotonin (5HT), dopamine (DA) and SFF were purchased from Sigma.

Uptake Inhibition Assays. The generation of HEK293 cell lines expressing Yellow Fluorescent Protein (YFP)-tagged hSERT and hDAT is described earlier (Sucic et al. [15]). HEK293 cells stably expressing either SERT or DAT were seeded onto poly-D-lysine-coated 48-well plates (0.5×10^5 cells/well), 24 hours prior to the experiment. For inhibition experiments, the specific activity of the tritiated substrate was kept constant: [^{3}H]DA: 0.1 μM, [^{3}H]5HT: 0.15 μM. Assay conditions were as outlined;[15] in brief: the cells were washed thrice with Krebs-Ringer-HEPES buffer (KHB; composition: 25 mM HEPES.NaOH, pH 7.4, 120 mM NaCl, 5 mM KCl, 1.2 mM $CaCl_2$, and 1.2 mm $MgSO_4$ supplemented with 5 mM D-glucose). Then, the diluted reference and sample compounds were added and incubated for 5 minutes to allow for equilibration with the transporters. Subsequently, the tritiated substrates were added and the reaction was stopped after 5 minutes. Cells were lysed with SDS 1% and counted in a beta-counter (Packard instruments). All determinations have been performed in triplicate.

Homology Modeling. Models of the human SERT and DAT were created as described by Sarker et al.[11] using $LeuT_{Aa}$ in the occluded conformation (PDB id 2A65, 1.65 Å)[17] as template. The highest DOPE scored structure was energy minimized in the AMBER99 forcefield and underwent a quality check using the QMEAN server. The binding site was defined using the Site Finder tool of Molecular Operating Environment.

Docking. Nine structurally diverse PEAs with high SERT affinity (**10**, **12, 19, 21, 22, 25, 27, 28, 29**) were docked into the S1 of SERT using CCDC GOLD 5.0.1. In case of an amphetamine, only the (*S*) enantiomer was docked. SFF was docked into the DAT S1 alone because its low affinity could cause a distinct conformation in the binding site. One hundred poses per ligand were generated and the ligand and residue's side chains within a 6Å radius were set as freely flexible (10 degree bins). Poses not comprising a required ionic interaction with the D79 (DAT) and D98 (SERT) side chain[18] were discarded, leading to 45 SFF-SERT and 65 SFF-DAT complexes. The ligand and surrounding atoms within a 8 Å radius were energy minimized in the Merck Molecular Forcefield (MMFF94x). Common scaffold clustering was applied on the SERT complexes, whereby the PEA scaffold was extracted from each complex and an RMSD matrix based on its heavy atoms was calculated.[19] Agglomerative hierarchical clustering, using XLStat (complete linkage, cutoff level 3), led to 13 clusters. Those clusters not containing all ligands were discarded, leading to 7 clusters comprising 41 SFF poses. From the top 10 scored poses of X-Score[20] and DSX scoring function,[21] one consensus pose was found and from the 14 complexes of the cluster containing this pose, the average rescoring values were calculated. For the DAT poses, 11 clusters were obtained of which two had a similar ligand orientation (the aromatic ring in the same position) as in the consensus SERT pose. From these two clusters (9 poses), the average scores were calculated (Table 2).

Acknowledgements

We acknowledge financial support provided by the *Austrian Science Fund* (*FWF*), Grants F03502, F3506 and W1232.

References

[1] N. R. Goldberg, T. Beuming, O. S. Soyer, R. A. Goldstein, H. Weinstein, J. A. Javitch, *Eur. J. Pharmacol.* **2003**, *479(1–3)*, 3–12.
[2] B. Hilber, P. Scholze, M. M. Dorostkar, W. Sandtner, M. Holy, S. Boehm, E. A. Singer, H. H. Sitte, *Neuropharmacology* **2005**, *49(6)*, 811–819.
[3] S. Seidel, E. A. Singer, H. Just, H. Farhan, P. Scholze, O. Kudlacek, M. Holy, K. Koppatz, P. Krivanek, M. Freissmuth, H. H. Sitte, *Mol. Pharmacol.* **2005**, *67(1)*, 140–151.
[4] L. Shi, M. Quick, Y. Zhao, H. Weinstein, J. A. Javitch, *Mol. Cell* **2008**, *30(6)*, 667–677.
[5] R. B. Rothman, M. H. Baumann, C. M. Dersch, D. V. Romero, K. C. Rice, F. I. Carroll, J. S. Partilla, *Synapse* **2001**, *39(1)*, 32–41.
[6] R. B. Rothman, J. S. Partilla, M. H. Baumann, C. Lightfoot-Siordia, B. E. Blough, *J. Pharmacol. Exp. Ther.* **2012**, *341(1)*, 251–262.
[7] H. H. Sitte, M. Freissmuth, *J. Neurochem.* **2010**, *112(2)*, 340–355.
[8] R. B. Rothman, M. H. Baumann, *Eur. J. Pharmacol.* **2003**, *479(1–3)*, 23–40.
[9] N. V. Cozzi, S. D. Brandt, P. F. Daley, J. S. Partilla, R. B. Rothman, A. Tulzer, H. H. Sitte, M. H. Baumann, *Eur. J. Pharmacol.* **2013**, *699*, 180–187.
[10] T. Beuming, L. Shi, J. A. Javitch, H. Weinstein, *Mol. Pharmacol.* **2006**, *70(5)*, 1630–1642.
[11] S. Sarker, R. Weissensteiner, I. Steiner, H. H. Sitte, G. F. Ecker, M. Freissmuth, S. Sucic, *Mol. Pharmacol* **2010**, *78(6)*, 1026–1035.
[12] H. Bisgaard, M. A. Larsen, S. Mazier, T. Beuming, A. H. Newman, H. Weinstein, L. Shi, C. J. Loland, U. Gether, *Neuropharmacology* **2011**, *60(1)*, 182–190.
[13] X. Huang, C. G. Zhan, *Biophys. J.* **2007**, *93(10)*, 3627–3639.
[14] H. Gu, S. C. Wall, G. Rudnick, *J. Biol. Chem.* **1994**, *269(10)*, 7124–7130.
[15] S. Sucic, S. Dallinger, B. Zdrazil, R. Weissensteiner, T. N. Jorgensen, M. Holy, O. Kudlacek, S. Seidel, J. H. Cha, U. Gether, A. H. Newman, G. F. Ecker, M. Freissmuth, H. H. Sitte, *J. Biol. Chem.* **2010**, *285(14)*, 10924–10938.
[16] *Organofluorine Chemistry : Principles and Commercial Applications* (Eds: R. E. Banks, B. E. Smart, J. C. Tatlow), *Topics in Applied Chemistry*, Plenum Press, New York, **1994**.
[17] A. Yamashita, S. K. Singh, T. Kawate, Y. Jin, E. Gouaux, *Nature* **2005**, *437(7056)*, 215–223.
[18] S. Kitayama, S. Shimada, H. Xu, L. Markham, D. M. Donovan, G. R. Uhl, *Proc. Natl. Acad. Sci. USA* **1992**, *89(16)*, 7782–7785.
[19] L. Richter, C. de Graaf, W. Sieghart, Z. Varagic, M. Morzinger, I. J. de Esch, G. F. Ecker, M. Ernst, *Nat. Chem. Biol.* **2012**, *8(5)*, 455–464.
[20] R. Wang, Y. Lu, S. Wang, *J. Med. Chem.* **2003**, *46(12)*, 2287–2303.
[21] G. Neudert, G. Klebe, *J. Chem. Inf. Model.* **2011**, *51(10)*, 2731–2745.

Received: January 25, 2013
Accepted: March 28, 2013
Published online: June 12, 2013

B

Combined Hansch analysis and docking of cathinone analogs indicate differences in interaction patterns between monoamine transporters

Manuscript to be submitted

In the following manuscript, I conducted a ligand-based analysis on a set of cathinone ligands and supported these results by docking studies. The results indicated a polarizable or lipophilic *para*-substituent to be beneficial for SERT affinity, whereas a bulky substituent on the cationic nitrogen atom would be unfavorable.

Combined Hansch analysis and docking of cathinone analogs indicate differences in interaction patterns between monoamine transporters

*Amir Seddik (1), Nicholas Cozzi (2), Harald H.Sitte (3), Gerhard F. Ecker * (1).*

(1) University of Vienna, Department of Pharmaceutical Chemistry, Althanstrasse 14, 1090, Vienna, Austria;

(2) Department of Cell And Regenerative Biology, 2695 Medical Sciences Center, University of Wisconsin, 1300 University Ave, Madison, Wisconsin 53706, United States

(3) Institute of Pharmacology, Center of Physiology and Pharmacology, Medical University of Vienna, Waehringerstrasse 13a, 1090, Vienna, Austria

ABSTRACT

The sodium coupled neurotransmitter symporters (NSS) are major contributors to physiological processes, such as mood, sleep, and addiction, and hence are important targets for psychotherapeutical drugs. Cathinones are an emerging class of drugs of abuse that bind to a subfamily of the NSS, namely the monoamine transporters (MATs). In this study, Hansch analysis is used to analyze the physicochemical contribution of a variety of substituents on these ligands' aromatic rings to MAT inhibitory activity. Using crystal structure information of protein-ligand complexes with chemically related inhibitors, an experimental data guided docking protocol was applied. The results indicate a stronger contribution of dispersive interactions in SERT vs DAT and NET, and more entropic and/or induced fit effects in DAT and NET. This combined ligand- and structure based method proved to be useful for the molecular understanding of transporter subtype selectivity.

INTRODUCTION

The family of NSS transporters are a major class of transmembrane proteins and are comprised of many subfamilies including the gamma-aminobutyric acid and monoamine transporters (GATs1-4, MATs, respectively). These subfamilies are implicated in many psychiatric disorders, such as depression, attention-deficit hyperactivity disorder (ADHD), epilepsy, anxiety, obsessive-compulsive disorder (OCD), Parkinson's disease and addiction.

The human MATs, which comprise the serotonin, dopamine and norepinephrine transporter (SERT, DAT, NET, respectively) regulate the extracellular concentration of their cognate substrates serotonin, dopamine and norepinephrine,[1] hence their involvement in major CNS disorders prompted extensive research on the transport cycle of various ligands,[2] their proposed binding sites[3] and the development of inhibitors such as the selective serotonin reuptake inhibitors (SSRIs), that are used to treat some of the symptoms mentioned above.[4]

In the last decades, several ligand based studies have been performed on MATs; notably Christensen *et al* described the importance of an electron withdrawing group at the *para* position of benztropine analogs for DAT affinity.[5] This is informative for substrates since mutational and molecular dynamics studies have shown that the binding site of dopamine and these inhibitors overlap[6, 7]. Wellsow *et al* showed by Comparative Molecular Field and Similarity Indices Analysis, using the highly SERT selective (*S*)-citalopram as reference compound, the importance of an electron withdrawing group on the aromatic moiety[8] that is placed in the B subsite, part of the substrate binding site (S1) in SERT upon binding[9, 10]. A comparison was made to NET inhibitors showing that large substituents should be avoided on this aromatic moiety for NET affinity.

The binding and activity of small biogenic compounds such as amphetamines has received less attention though. The recently crystallized dopamine transporter ($dDAT_{cryst}$) and the "SERT-ized" bacterial leucine transporters (LeuBATs) offered a wealth of new information and further validated that inhibitors fit in the S1 site. Generally, all inhibitors and substrates share two important pharmacophoric features, i.e. a positive charge induced by a basic nitrogen atom and an aromatic moiety (Figure 1, right).

Cathinones are a subclass of amphetamines and currently popular illicit drugs sold as bath salts to evade the detection by authorities.[11, 12] In this study we aim to dissect the basis of MAT selectivity for different cathinone analogs using a combination of Hansch analysis and docking on an *in-house* dataset.

METHODS

Hansch analysis.

Ligand structures (figure 1) were drawn with the Builder tool of Molecular Operating Environment (MOE).[13] From the non-methylenedioxy bridged ligands, Hammett sigma, lipophilicity, Taft size and molar refractivity (MR) parameters for the *meta*- and *para*-substituents were taken from ref.[14] [15, 16] [17]. Lipophilicity, van der Waals volume and MR values for the substitutions on the cationic nitrogen were obtained by subtracting the LogP(o/w), vdw_vol and MR values calculated by MOE, of two whole molecules. The LogP(o/w) algorithm of MOE leads to slightly different values than the Hammett π values for the aromatic ring, but we decided to keep the latter values for the aromatic ring, since they are published and comparable with previous studies that employ these descriptors. Moreover, coefficients of derived QSAR formulas are able to correct for these slight differences. One compound in the dataset, 2-TFMAP, was outside the applicability domain because it was the only one with an *ortho* substituent and was therefore excluded from the dataset. This led to a total of 13 compounds to be analyzed. QSAR models were derived by backward selection of normalized coefficient values while using the pIC_{50} values as dependent variable. The partial least-squares (PLS) algorithm of MOE was applied to fit the final model and evaluation was performed using a leave-one-out cross validation (Q^2). The same procedure was applied for an amphetamine dataset extracted from Baumann *et al* (see Supporting Information).

Protein Model Preparation.

The sequence of the recently crystallized *Drosophila* dopamine transporter in the outward facing conformation in complex with nortryptiline, $dDAT_{cryst}$ (PDB id 4M48),[18] was aligned to the human MAT sequences (ncbi.nlm.nih.gov) using ClustalX.[19] Non-structural waters were removed and 250 homology models of

hSERT, hDAT and hNET in complex with nortryptiline were created using Modeller 9.11.[20] The models with the highest 'Discrete Optimization of Protein Energy' (DOPE) score showed no disallowed dihedrals near the central binding site and were selected.

Mazindol has the highest DAT and NET affinity of all the co-crystallized ligands in LeuBAT,[21] while paroxetine has the highest SERT affinity.[22, 23] Therefore higher affinity MAT complexes were created by superposition based on the pocket C_α atoms of Δ13-LeuBAT in complex with paroxetine (pdb 4MM4) and mazindol (pdb 4MME)[24] with the SERT and DAT/NET model, respectively. These complexes were protonated at pH 7 using the Protonate3D tool in MOE followed by an energy minimization within 5 Å of the ligand using a distance dependent dielectric constant of 2 to 80 in the OPLS all-atom forcefield.[25]

Restrained Docking.

Ligand structures were built in protonated form since their interactions in the binding pocket are primarily driven by a salt bridge with a conserved aspartate residue (Asp98/79/75) and a cation-π interaction with the Tyr95/Phe76/Phe72 side chain (SERT/DAT/NET, resp.).[7, 26, 27] Also, the (*S*) enantiomer was employed because it is the most active in this class of compounds.[28] The transporter-inhibitor complexes were loaded in the docking software Genetic Optimization for Ligand Docking (GOLD) 5.2,[29] which uses a genetic algorithm to obtain poses non-deterministically. Waters were removed and the binding site was defined as the center of mass of the inhibitor. The poses were scored with GoldScore and rescored with ChemPLP, which are based on different algorithms The cathinone substructure was used for setting restraints: to account for the established cationic interactions, the nitrogen atom of the ligand was forced to be within a range of 2-4 Å to the Tyr95/Phe76/Phe72 backbone carbonyl oxygen atom by a distance restraint with a default spring constant. This led to docking poses with the cationic nitrogen atom to be approximately in the same position as the inhibitor's positive partial charge density in the LeuBAT crystal structures (subpocket A).

Two additional subsites B and C in the S1 pocket were defined for separate docking runs: for the B-site, two additional distance restraints were set on the cathinone aromatic *para*-carbon to be within a distance of 3-5 Å to both the Ser438 backbone carbonyl carbon and the Ile172/Val152/Val148 C_β atom (see Figure 2).

For docking in the C-site, restraints on the same cathinone carbon were set with the Ile172/Val152/Val148 C_β and the Tyr95/Phe76/Phe72 side chain *meta*-carbon that points toward the central binding site, both within 4-5 Å using a higher *k* of 20 AUs to prevent the ligands to be displaced from this smaller sized pocket. See Table 1 for alignment of SERT, DAT and NET pockets and figure 2 for the surface maps.

The restraints forced the aromatic moiety of the cathinones to be placed analogously to the inhibitor's ones. This gives an advantage to reliably compare the docking scores within a particular binding mode, since docking scores are very sensitive to changes in distance between interacting atoms. Binding modes of seventeen cathinones (Figure 1) with known activity values were generated 25 times while keeping the protein rigid to preserve the crystal structure topology. Poses with a root-mean square deviation (RMSD) > 2Å of the aromatic carbons of all the docked cathinones to a representative pose that resembled the inhibitor pose most were discarded. The average scores were ranked and compared with the pIC_{50} rank using Spearman's rank correlation (see Supporting Information for details).

RESULTS AND DISCUSSION

Inhibition of uptake in SERT, DAT and NET.

The bar graph (figure 1) shows that DAT and NET are rather promiscuous towards cathinones, except for the very low affinity of DAT for trifluoromethyl substituted cathinones as shown previously.[30] SERT seems, however, quite selective toward cathinones: the ring-unsubstituted and *N*-bulk-substituted derivatives bind weaker, while a *para* iodine atom appears to be most favorable. Furthermore, the trifluoromethyl group on the *ortho* position decreased affinity in all MATs, probably due to reduced aromaticity of the ring[31] whereas the central binding sites contain four aromatic side chains (Phe72/Phe76/Tyr95, Tyr152/156/176, Phe316/320/355 and Phe322/326/341 in NET/DAT/SERT, respectively) responsible for important stacking interactions.[32-34] The high selectivity for unsubstituted cathinones for DAT and NET over SERT is in line with the ligand based study of Wellsow *et al*.[8]

QSAR model for SERT affinity.

Based on the cathinone uptake inhibitory activities, QSAR models for SERT were derived. The molar refractivity (MR) descriptors clarify the importance of polarizable groups at the *meta* and/or *para* position as can be observed from figure 1, where halogen substituents increase activity at SERT. This is also in agreement with the docking poses that show the *para* substituent to be in the vicinity of a threonine, alanine and isoleucine (B pocket). Model (3) was the most predictive model and additionally indicated an unfavorable contribution of a lipophilic *meta* substituent. The docking poses show that the *meta* substituent is in the vicinity of the hydrophilic tyrosine hydroxyl group.

$$\text{SERT-}pIC_{50} = 4.5 + 0.13\ MR_p + 0.13\ MR_m - 0.01\ N\text{-vdw} \quad (1)$$

N=13, RMSE: 0.31, R^2: 0.79, XRMSE: 0.41, Q^2: 0.64

MR: molar refractivity contribution of chemical substituent, *N*-vdW: van der Waals volume of *N*-substituent

The *para*-MR descriptor could be replaced with π_p, leading to slightly better fit quality:

$$\text{SERT-}pIC_{50} = 4.6 + 1.24\ \boldsymbol{\pi}_p + 0.14\ MR_m - 0.01\ N\text{-vdw} \quad (2)$$

N=13, RMSE: 0.30, R^2: 0.80, XRMSE: 0.39, Q^2: 0.66

The MR descriptor could be combined, leading to a better model:

$$\text{SERT-}pIC_{50} = 4.0 + 0.13\ MR_{ring} - 0.9\ \textit{meta-}\boldsymbol{\pi} - 0.01\ N\text{-vdw} \quad (3)$$

N=13, RMSE: 0.22, R^2: 0.89, XRMSE: 0.32, Q^2: 0.78

Replacing MR(arom) with the “apol” values of the substituents leads to an unreliable model (q2=0.30). Replacing *meta-pi* with *pi* of all ring substituents: (q2=0.22), replacing *meta-pi* with *para-pi* was less predictive: q2=0.62.

The *para*-substituent descriptor for lipophilicity or polarizability had the highest contributions to activity. Replacing MR_m with MR of the whole molecule or with a steric parameter (Taft size) was not predictive in both

(1) and (2). Based on our docking, this moiety indeed showed favorable interactions with proximal side chains in SERT: notably the B site around the cathinone's *para* position is prone to hydrophobic interactions (see *Restrained Docking* section) and as previously shown in the LeuT-based SERT homology model.[28] This is supported by the study where employing a lipophilic *para* group in amphetamines positively correlated to modulation of serotonin receptors.[35]

During training of model (1) and (2), 3-hydroxymethcathinone was an outlier and predicted as about ten times less active than its measured affinity. The docking pose of this ligand (see *Restrained Docking* section) indicated that a hydrogen bond to a nearby carbonyl oxygen upon thermal motion is very probable (figure 2), whereas the ligand binds unselectively to SERT, DAT and NET. Hydrogen bonding of MAT substrates was also shown in molecular dynamics studies whereby serotonin interacted with the hSERT Ala169 backbone,[34] 3-hydroxyphenylpiperazine with the hSERT Gly442/Ser438 backbone[34, 36] and the dopamine hydroxyl groups with the hDAT Ala423/Gly426 backbone.[7] A hydrogen bond may increase the enthalpic contribution with about 4.7 kcal/mol, depending on the donor-acceptor distance and D-H-A angle[37], whereas the ratio in SERT IC_{50} between 3-OH-MAP and MCAT is about 13. According to the Cheng-Prusoff equation, this ratio should be equal to the K_i ratio with the same radioligand concentration ([S]):

$$K_{i,A}/K_{i,B} = IC_{50,A}/IC_{50,B}\,(1+[S]_B/K_D)/(1+[S]_A/K_D) = IC_{50,A}/IC_{50,B}$$

with K_D being the dissociation constant of the radioligand for SERT.

With a difference in binding free energy of 1.5 kcal/mol at 298K, using $\Delta\Delta G = RT\ln(IC_{50,A}/IC_{50,B})$, a hydrogen bond would well cover the 13x higher activity of 3-OH-MAP as compared to MCAT in SERT and compensate for its repulsive hydrophilicity in this protein pocket. Therefore 3-OH-MCAT is predicted to have a lower activity than measured since the QSAR models do not capture hydrogen bonding.

The descriptors used in these models were however well correlated to the efflux activity of non-*beta*-keto amphetamines obtained from Baumann *et al*.[38] A well fitted model (4) was obtained, suggesting that during transport, amphetamines and cathinones share their position of the aromatic ring in SERT with the same orientation of the *meta* substituent.

$$\text{SERT-pEC}_{50} = 5.40\ (\pm 0.05) + 0.30\ (\pm 0.02)\ MR_m + 2.46\ (\pm 0.12)\ \pi_p \qquad (4)$$

$$N=11,\ R^2\text{: } 0.91,\ \text{RMSE: } 0.19,\ \text{XRMSE: } 0.26,\ Q^2\text{: } 0.83$$

Using MR for the whole ring was not predictive (R2=0.55), neither was using π for the whole ring (q2=0.42) or with *meta*-π (R2=0.24). This suggests a very local effect of the *meta* and *para* substituent in the binding pocket.

Restrained Docking.

The LeuBAT X-ray crystal structures have shown that the binding modes of a set of different inhibitors, including SSRI, SNRIs and tricyclics[24] were very similar: the positive partial charge density overlapped and so did the aromatic moieties of the ligands. Therefore, cathinones were docked analogously and the ranking performance of two different scoring functions (GoldScore and ChemPLP) was assessed based on the corresponding ligand activities.

Homology models of the human MATs were derived from *Drosophila* DAT, a protein with a considerably higher sequence identity than the commonly used bacterial leucine transporter. The use of homology models in the outward facing conformation ensured the binding of all cathinones in the central binding site, since not all of them are transported as indicated by efflux experiments[38]. The pose of high affinity inhibitors in LeuBAT superposed into SERT showed placements of the aromatic methylenedioxy moiety of paroxetine in a previously reported B pocket,[28, 39] and accepted a hydrogen bond from Thr439. The *p*-chlorophenyl moiety of the DAT/NET-over-SERT selective mazindol was placed halfway between the B- and C-pocket and *T*-stacked with Phe76 in DAT and Phe72 in NET. Based on these findings, the cathinones were docked in these two subsites using restraining potentials. This resulted in the *meta* substituents pointing to the C site when docked in the B pocket.

The scores of the (*S*)-cathinone poses in the hSERT model that satisfied the imposed restraints, showed a statistically significant ranking performance for both scoring functions (GoldScore: $\rho = 0.72$, ChemPLP: $\rho = 0.62$) in subsite B (see Table 2 and figure 4). As postulated in our parallel study on the differences between 4-MEC and 4-MePPP binding, 4-MePPP might due to its bulkiness have a shifted binding mode which leads to incomparable scores. This might be the cause for it being an outlier in the correlation. Most ligands docked in the subsite C did not satisfy the restraints, since this pocket was much narrower leading to less favorable placement. The relevance of a C-pocket is also questionable for substrates since this pocket is absent in the occluded conformation of LeuT and its homology models.[28, 40, 41] Ligands placed in both sub pockets in DAT and NET had very insignificant ranking performance of scoring functions. Only in the SERT model correlations were obtained with a probability lower than 0.5% that the ranking occurred by chance.

GoldScore and ChemPLP[42] are scoring functions based on direct interaction with the protein, suggesting that cathinone binding in the S1 site in SERT is mostly determined by enthalpy. At the same time, since scoring functions are poorly parametrized for stacking interactions[43] and since no score correlation was found in DAT and NET in the rigid structure, the affinity for cathinones in these two targets are either driven by stacking and/or less loss of entropy during binding and/or a higher flexibility of DAT and NET.

CONCLUDING REMARKS.

Several QSAR models from cathinone and amphetamine datasets were obtained for SERT; the QSAR models describe the importance of lipophilicity or polarizability on the *para* position. No QSAR model for DAT and NET were obtained, because the variance of the training set values of the majority of the values was too low, whereas the *n*-TFMAP compounds are too inactive (DAT).

A major finding in this study is the correlation between the inhibitory activity of the cathinones in SERT and the scoring values obtained for the restrained docking. This strongly indicates that the S1 pocket of this protein is at least responsible for substrate recognition and that *Drosophila* DAT in the outward facing conformation is an excellent template for rigid docking studies on SERT homology models based on it.

Based on these ligand- and structure-based results, SERT affinity seems to be induced by the dispersive interactions between the ligand's *para*-substituent and the residues lining the B pocket. Hence, these models can be used for the further design of selective tool compounds for studying these targets.

Since the B subpocket of NET and DAT would be slightly larger than that of SERT based on sequence alignment and comparison of the molecular surface maps (Figure 2), the fact that unsubstituted amphetamines are DAT- and NET-selective and the notion that no correlation was found in the optimized homology model of DAT and NET with the scoring functions employed, has several implications:

1. DAT and NET are more flexible proteins than SERT
2. Cathinones in DAT and NET retain more degrees of freedom in the central binding site upon binding than in SERT
3. Affinity in DAT and NET is influences by recognition sites other than the S1.

We are currently conducting molecular dynamics studies to test these hypotheses.

Although speculative, novel compounds can be 'grown' into the C pocket, which is absent in the occluded conformation of the protein (based on the LeuT structures and on a previously reported DAT homology model[44]). Such novel inhibitors could lock the transporter in an outward-open conformation. Our results have shown that the combination of Hansch analysis and docking is powerful and forms a basis for the fine-tuning of inhibitors currently known, assisting in the development of more selective drugs.

FIGURES

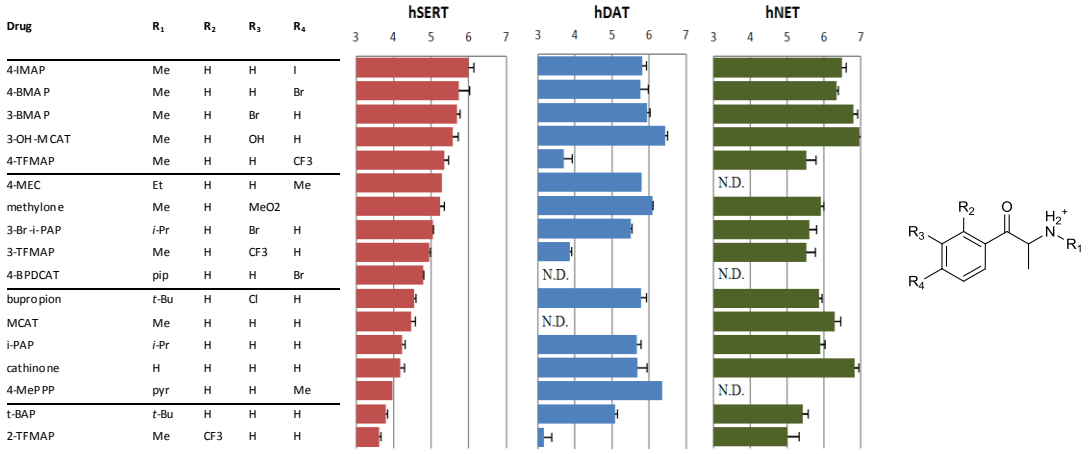

Figure 1. Bar graph of *–log* IC_{50} values of tested cathinones. MCAT: *N*-methylcathinone, bupropion: 3-chloro-*N*-tertbutylcathinone, *n*-BMAP: *n*-bromo-methcathinone, 4-IMAP: 4-iodo-methcathinone, *i*-PAP: *N*-isopropylcathinone, *t*-BAP: *N*-tertbutylcathinone, 3-OH-MCAT: 3-hydroxymethcathinone, *n*-TFMAP: *n*-trifluoromethylmethcathinone, 4-BPDCAT: 4-bromo-*N*-piperidylcathinone. Absence of a bar refers to a value not determined. SERT uptake was measured in human platelets, except 4-methyl-N-ethylcathinone (4-MEC) and 4-methyl-α-pyrrolidinopropiophenone (4-MePPP) were measured in HEK-293 cells. DAT was measured in COS cells, except for the *n*-TFMAPs which were measured in HEK293 cells. The compounds measured on NET were performed in C6 glioma cells.

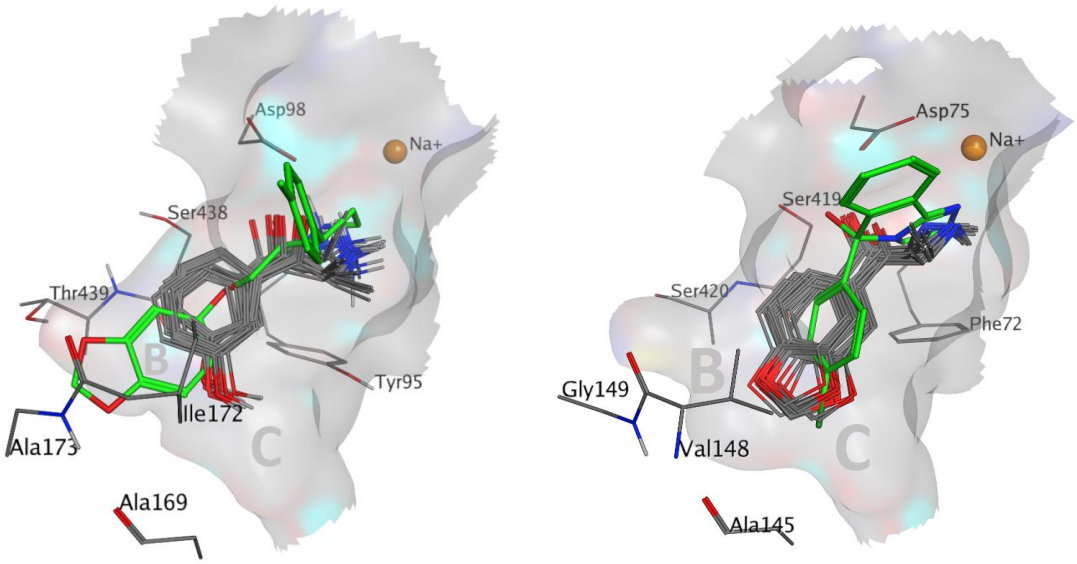

Figure 2. Binding pockets of homology models of human SERT (left) and NET (right) in the outward-occluded conformation. Paroxetine and mazindol are shown in green and represent the conformation found in LeuBAT (pdb 4MM4 and 4MME, respectively). The docking poses of 3-OH-MAP and methylone after common scaffold

clustering are shown, as well as the proximity of the 3-OH-MAP hydroxyl group to the Ala169 backbone carbonyl oxygen.

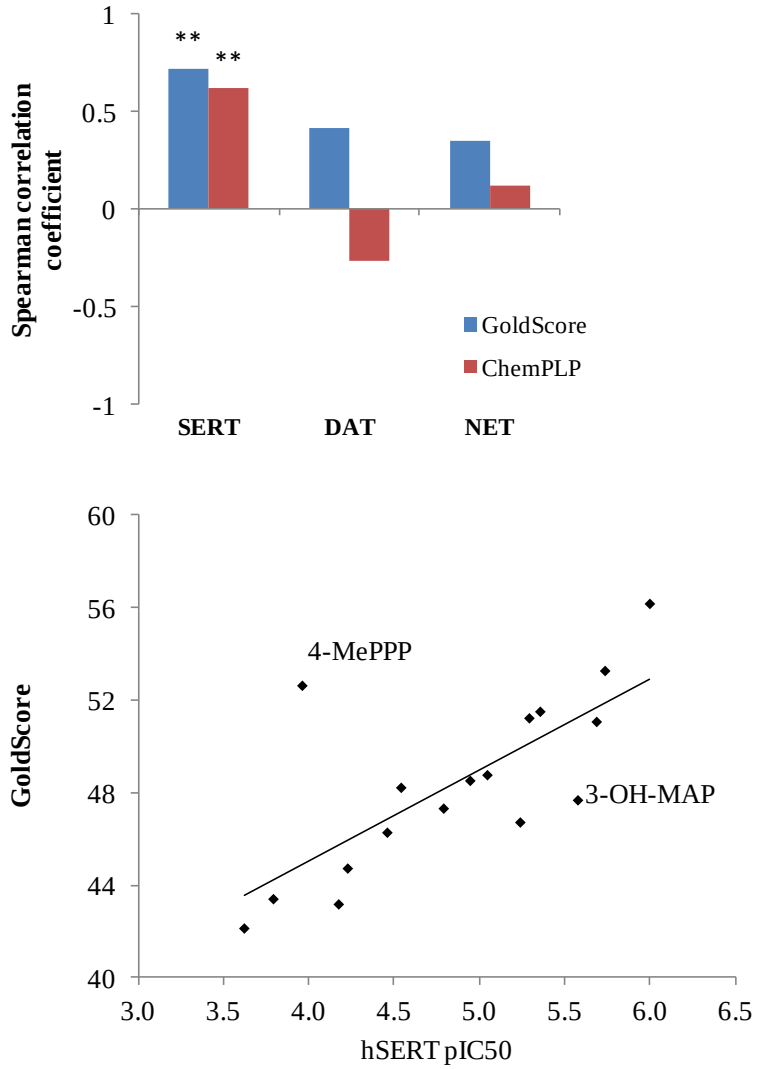

Figure 4. Above: Score-affinity Spearman's rank correlation coefficients (ρ) of (*S*)-cathinones docked in B-subsite of dDAT-based monoamine transporter homology models. **p<0.005. **Below**: GoldScore-SERT activity correlation of (*S*)-cathinones docked in SERT B-subsite (R^2 = 0.54). The R^2 = 0.81 upon removal of the 4-MePPP outlier.

Table 1. Structural alignment of monoamine transporter pockets

subsite B, between TM3 and TM8							
SERT	A169	I172	A173	T439	L443	T439	
DAT	S149	V152	G153	A423	M427	A423	
NET	A145	V148	G149	S420	M423	S420	
subsite C							
SERT	Y95	I168	A169	I172	F341	V343	T497
DAT	F75	I148	S149	V152	F326	V228	A480
NET	F72	I144	A145	V148	F323	V325	I481

Table 2. Spearman rank correlations of docking poses in subsites (B, C) part of the central binding site of dDAT-based monoamine transporter homology models

(*S*)-cathinones	**SERT**	**DAT**	**NET**
subsite B			
GoldScore	** 0.72	0.57	0.35
ChemPLP	** 0.62	-0.27	0.12
subsite C			
GoldScore	0.29	-1	0.09
ChemPLP	0.71	-1	-0.80
(*R*)-cathinones, subsite B			
GoldScore	0.33	* 0.53	-0.01
ChemPLP	** 0.68	-0.11	-0.34

**$p < 0.005$, * $p < 0.05$, remaining values: $p > 0.1$

ASSOCIATED CONTENT

Supporting Information

The Supporting Information contains a table with the amphetamine dataset extracted from Baumann *et al*[45, 46] with assigned Hammett descriptor values. In addition an example is given of the score ranking of docked cathinones in the SERT B-pocket.

AUTHOR INFORMATION

Corresponding Author

*E-mail: gerhard.f.ecker@univie.ac.at (G.F.E.)

Author Contributions

We wish to thank Dr. Daan P. Geerke (Vrije Universiteit Amsterdam) for helpful discussions and his interest in our work.

Funding Sources

We acknowledge financial support provided by the Austrian Science Fund, grants F03502 and W1232.

ABBREVIATIONS

MAT, monoamine transporter; SERT, serotonin transporter; DAT, dopamine transporter; NET, norepinephrine transporter

REFERENCES

1. Goldberg, N.R., et al., *Probing conformational changes in neurotransmitter transporters: a structural context.* Eur J Pharmacol, 2003. **479**(1-3): p. 3-12.
2. Jorgensen, A.M. and S. Topiol, *Driving forces for ligand migration in the leucine transporter.* Chem Biol Drug Des, 2008. **72**(4): p. 265-72.
3. Lim, H.H. and C. Miller, *It takes two to transport, or is it one?* Nat Struct Mol Biol, 2012. **19**(2): p. 129-30.
4. Hyttel, J., *Neurochemical characterization of a new potent and selective serotonin uptake inhibitor: Lu 10-171.* Psychopharmacology (Berl), 1977. **51**(3): p. 225-33.
5. Christensen, H.S., et al., *QSAR studies and pharmacophore identification for arylsubstituted cycloalkenecarboxylic acid methyl esters with affinity for the human dopamine transporter.* Bioorg Med Chem, 2007. **15**(15): p. 5262-74.
6. Bisgaard, H., et al., *The binding sites for benztropines and dopamine in the dopamine transporter overlap.* Neuropharmacology, 2011. **60**(1): p. 182-90.
7. Beuming, T., et al., *The binding sites for cocaine and dopamine in the dopamine transporter overlap.* Nat Neurosci, 2008. **11**(7): p. 780-9.
8. Wellsow, J., K.A. Kovar, and H.J. Machulla, *Molecular modeling of potential new and selective PET radiotracers for the serotonin transporter. Positron Emission Tomography.* J Pharm Pharm Sci, 2002. **5**(3): p. 245-57.
9. Andersen, J., et al., *Mutational mapping and modeling of the binding site for (S)-citalopram in the human serotonin transporter.* J Biol Chem, 2010. **285**(3): p. 2051-63.
10. Koldso, H., et al., *The two enantiomers of citalopram bind to the human serotonin transporter in reversed orientations.* J Am Chem Soc, 2010. **132**(4): p. 1311-22.
11. Capriola, M., *Synthetic cathinone abuse.* Clin Pharmacol, 2013. **5**: p. 109-15.
12. Hilber, B., et al., *Serotonin-transporter mediated efflux: a pharmacological analysis of amphetamines and non-amphetamines.* Neuropharmacology, 2005. **49**(6): p. 811-9.
13. Molecular Operating Environment (MOE), C.C.G.I., 1010 Sherbooke St. West, Suite #910, Montreal, QC, Canada, H3A 2R7, 2013.
14. Skagerberg, B., et al., *Principal properties of aromatic substituents.* Prog Clin Biol Res, 1989. **291**: p. 127-30.
15. Hansch, C. and A. Leo, *Substituent constants for correlation analysis in chemistry and biology*. A Wiley-Interscience publication. 1979, New York: Chichester : Wiley. vii, 339p.
16. Takahata, Y. and D.P. Chong, *Estimation of Hammett sigma constants of substituted benzenes through accurate density-functional calculation of core-electron binding energy shifts.* International Journal of Quantum Chemistry, 2005. **103**(5): p. 509-515.
17. Hansch, C. and A. Leo, *Substituent constants for correlation analysis in chemistry and biology*. 1979, New York (Chichester (etc.)): Wiley. ix ,339p.
18. Penmatsa, A., K.H. Wang, and E. Gouaux, *X-ray structure of dopamine transporter elucidates antidepressant mechanism.* Nature, 2013.
19. Thompson, J.D., T.J. Gibson, and D.G. Higgins, *Multiple sequence alignment using ClustalW and ClustalX.* Curr Protoc Bioinformatics, 2002. **Chapter 2**: p. Unit 2 3.
20. Eswar, N., et al., *Protein structure modeling with MODELLER.* Methods Mol Biol, 2008. **426**: p. 145-59.
21. Houlihan, W.J., et al., *Mazindol analogues as potential inhibitors of the cocaine binding site at the dopamine transporter.* J Med Chem, 2002. **45**(19): p. 4097-4109.
22. Mattson, R.J., et al., *Conformationally restricted homotryptamines. 2. Indole cyclopropylmethylamines as selective serotonin reuptake inhibitors.* J Med Chem, 2005. **48**(19): p. 6023-34.

23. Tatsumi, M., et al., *Pharmacological profile of antidepressants and related compounds at human monoamine transporters.* Eur J Pharmacol, 1997. **340**(2-3): p. 249-58.
24. Wang, H., et al., *Structural basis for action by diverse antidepressants on biogenic amine transporters.* Nature, 2013.
25. Jorgensen, W.L., D.S. Maxwell, and J. TiradoRives, *Development and testing of the OPLS all-atom force field on conformational energetics and properties of organic liquids.* J Am Chem Soc, 1996. **118**(45): p. 11225-11236.
26. Wang, H., et al., *Structural basis for action by diverse antidepressants on biogenic amine transporters.* Nature, 2013. **503**(7474): p. 141-5.
27. Zhou, Z., et al., *Antidepressant specificity of serotonin transporter suggested by three LeuT-SSRI structures.* Nat Struct Mol Biol, 2009. **16**(6): p. 652-7.
28. Seddik, A., et al., *Probing the Selectivity of Monoamine Transporter Substrates by Means of Molecular Modeling.* Mol Inform, 2013. **32**(5-6): p. 409-413.
29. Jones, G., P. Willett, and R.C. Glen, *Molecular recognition of receptor sites using a genetic algorithm with a description of desolvation.* J Mol Biol, 1995. **245**(1): p. 43-53.
30. Cozzi, N.V., et al., *Pharmacological examination of trifluoromethyl ring-substituted methcathinone analogs.* Eur J Pharmacol, 2013. **699**(1-3): p. 180-7.
31. Dearden, J.C. and J.H. Ohara, *Partition-Coefficients of Some Alkyl Derivatives of 4-Acetamidophenol.* European Journal of Medicinal Chemistry, 1978. **13**(5): p. 415-419.
32. Kitayama, S., et al., *Dopamine transporter site-directed mutations differentially alter substrate transport and cocaine binding.* Proc Natl Acad Sci U S A, 1992. **89**(16): p. 7782-5.
33. Wang, W.F., et al., *Dissociation of high-affinity cocaine analog binding and dopamine uptake inhibition at the dopamine transporter.* Molecular Pharmacology, 2003. **64**(2): p. 430-439.
34. Celik, L., et al., *Binding of serotonin to the human serotonin transporter. Molecular modeling and experimental validation.* J Am Chem Soc, 2008. **130**(12): p. 3853-65.
35. Domelsmith, L.N., et al., *Photo-Electron Spectra of Psychotropic-Drugs .6. Relationships between Physical-Properties and Pharmacological Actions of Amphetamine Analogs.* J Med Chem, 1981. **24**(12): p. 1414-1421.
36. Koldso, H., et al., *Comparative Modeling of the Human Monoamine Transporters: Similarities in Substrate Binding.* Acs Chemical Neuroscience, 2013. **4**(2): p. 295-309.
37. Pimentel, G.C. and Mcclella.Al, *Hydrogen Bonding.* Annual Review of Physical Chemistry, 1971. **22**: p. 347-&.
38. Rothman, R.B. and M.H. Baumann, *Monoamine transporters and psychostimulant drugs.* Eur J Pharmacol, 2003. **479**(1-3): p. 23-40.
39. Ravna, A.W., I. Sylte, and S.G. Dahl, *Molecular mechanism of citalopram and cocaine interactions with neurotransmitter transporters.* Journal of Pharmacology and Experimental Therapeutics, 2003. **307**(1): p. 34-41.
40. Sarker, S., et al., *The high-affinity binding site for tricyclic antidepressants resides in the outer vestibule of the serotonin transporter.* Mol Pharmacol, 2010. **78**(6): p. 1026-35.
41. Yamashita, A., et al., *Crystal structure of a bacterial homologue of Na+/Cl--dependent neurotransmitter transporters.* Nature, 2005. **437**(7056): p. 215-23.
42. Korb, O., T. Stutzle, and T.E. Exner, *Empirical scoring functions for advanced protein-ligand docking with PLANTS.* J Chem Inf Model, 2009. **49**(1): p. 84-96.
43. Luhmer, M., et al., *The Importance of Quadrupolar Interactions in Molecular Recognition Processes Involving a Phenyl Group.* Bulletin De La Societe Chimique De France, 1994. **131**(5): p. 603-606.
44. Stockner, T., et al., *Mutational analysis of the high-affinity zinc binding site validates a refined human dopamine transporter homology model.* PLoS Comput Biol, 2013. **9**(2): p. e1002909.
45. Rothman, R.B., et al., *Studies of the biogenic amine transporters. 14. Identification of low-efficacy "partial" substrates for the biogenic amine transporters.* J Pharmacol Exp Ther, 2012. **341**(1): p. 251-62.
46. Baumann, M.H., et al., *The designer methcathinone analogs, mephedrone and methylone, are substrates for monoamine transporters in brain tissue.* Neuropsychopharmacology, 2012. **37**(5): p. 1192-203.

Supporting information

SUPPLEMENTARY TABLES

Table S1. Amphetamine dataset extracted from Baumann *et al*[45, 46]:

Substrate	SERT pEC50	NET pEC50	*m*-sigma	*m*-MR	*p*-pi
p-MeS-methamphetamine	7.12	*N.D.*	0	1.03	0.61
fenfluramine	7.10	6.13	0.43	5.02	0
HMA	6.05	6.16	0.12	7.87	-0.67
HMMA	6.23	6.20	0.12	7.87	-0.67
norfenfluramine	6.98	6.77	0.43	5.02	0
p-fluoroamphetamine	6.03	7.55	0	1.03	0.14
p-Me-amphetamine	7.30	7.65	0	1.03	0.56
m-Me-amphetamine	6.66	7.74	-0.07	5.65	0
methamphetamine	5.82	7.78	0	1.03	0
m-F-amphetamine	5.71	7.79	0.337	0.92	0
amphetamine	5.43	8.02	0	1.03	0

Sigma, MR and pi values from ref.[15]

Table S2. Restrained Docking of (*S*)-cathinones in SERT

ligand	affinity rank	GoldScore	GoldScore rank	ChemPLP score	ChemPLP rank
4-IMAP	1	56.15	1	57.01	3
4-BMAP	2	53.25	2	56.00	4
3-BMAP	3	51.05	6	55.05	7
3OH-MAP	4	47.66	10	52.46	9
4-TFMAP	5	51.49	4	49.35	14
4-MEC	6	51.20	5	55.68	5
methylone	7	46.70	12	59.40	1
3-Br-i-PAP	8	48.75	7	55.07	6
3-TFMAP	9	48.50	8	58.41	2
4-BPDCAT	10	47.30	11	41.70	17
bupropion	11	48.20	9	52.87	8
MCAT	12	46.26	13	50.93	11
i-PAP	13	44.71	14	51.54	10
cathinone	14	43.16	16	47.89	15
4-MePPP*	15	52.61	3	50.28	12
t-BAP	16	43.39	15	49.60	13
2-TFMAP	17	42.12	17	43.81	16

Spearman's rank correlation coefficient $\rho = 1 - \frac{6 \sum d_i^2}{n(n^2 - 1)}$

C

Stacking interactions confer selectivity in the Dopamine Transporter for unsubstituted Amphetamine-like Cathinones

Draft manuscript

In the following study, the dopamine transporter (DAT)-over-serotonin transporter (SERT) selectivity for small cathinone ligands was studied by using molecular dynamics simulations and thermodynamic integration. Selectivity seemed caused by differences in stacking and attractive electrostatic interactions. The stacking hypothesis was confirmed by uptake inhibitory assays on the serotonin transporter

Stacking interactions confer selectivity in the Dopamine Transporter for unsubstituted Amphetamine-like Cathinones

Amir Seddik [1], Daan Geerke [2], Thomas Stockner [3], Marion Holy [3], Oliver Kudlacek [3], Harald H. Sitte [3], Gerhard F. Ecker [1]

[1] University of Vienna, Department of Pharmaceutical Chemistry, Division of Drug Design & Medicinal Chemistry, Althanstrasse 14, 1090 Vienna, Austria

[2] AIMMS Division of Molecular Toxicology, Department of Chemistry and Pharmaceutical Sciences, Faculty of Sciences, VU University Amsterdam, De Boelelaan 1083, 1081 HV Amsterdam, the Netherlands

[3] Medical University of Vienna, Center for Physiology and Pharmacology, Institute of Pharmacology, Vienna, Austria

ABSTRACT

The absence of substituents on the aromatic ring of amphetamines renders the ligand a selective substrate for the dopamine transporter (DAT) over the serotonin transporter (SERT). Docking studies on amphetamine-like cathinones were unable to explain this phenomenon and therefore MD simulations of an already established DAT model in the occluded conformation were performed, in addition to different mutants with SERT residues in the substrate binding site (S1). Results indicated that cathinones may have two binding modes of which one is more favorable, whereas free energy calculations indicated the S1 to be primary recognition site for these ligands. By employing *in silico* and *in vitro* SERT-like mutations, it was shown that stacking interactions with Phe320 may cause unsubstituted amphetamines to bind more favorably to DAT, due to a smaller Val152, compared to the bulkier Ile172 in SERT. Additionally, stronger attractive electrostatic interactions in DAT were present due to a slightly tighter pocket, as compared to in 'SERT'. Uptake inhibitory measurements showed an increase in binding affinity in SERT-I172V as hypothesized from the computational methods. Our results pave the way for further development of more selective drugs acting on SERT and DAT.

Introduction

The dopamine and serotonin transporter are part of the neurotransmitter:sodium symporter (NSS) subfamily and play a vital role in behaviors and mental illnesses such as depression[1], anxiety[2], obsessive-compulsive disorder[3] and attention-deficit hyperactivity disorder[4,5]. They exert their action by re-uptaking neurotransmitter back into the synaptic cleft using the electrochemical gradient of sodium. The molecular determinants for their selectivity is increasingly being debated but is not completely understood yet.[6-9] The SERT-over-DAT selectivity of monoamine transporter substrates is being described in a parallel manuscript and indicate polarizable and lipophilic *para*-substituents to be the driving force, due to more favorable binding in the B-subpocket of the substrate binding site.[6] However, causes for DAT-over-SERT selectivity is not fully understood and it was shown that amphetamines lacking substituents on their aromatic ring tend to be DAT-over-SERT selective.[9,10]

In this study, we performed a combined computational and experimental approach to pin down the basis for DAT-over-SERT selectivity by exploiting their binding activity to cathinones, a class of street drugs with increasing popularity. Molecular dynamics (MD) simulations were performed starting from an already equilibrated DAT system[11], while mutating residues in the primary binding pocket (S1) toward SERT to assess the contributing residues for DAT/SERT selectivity, if any. The systems were simulated in complex with the DAT-over-SERT selective substrate (*S*)-methcathinone (MCAT) and the non-selective 4-iodomethcathinone

(IMAP). Key interactions were analyzed and to indicate whether the S1 site is the main recognition site, relative binding free energies between two enantiomeric ligands MCAT and mephedrone (MEPH) were calculated using the thermodynamic integration (TI) method. We support our computational results by uptake inhibitory assays using these enantiomers.

RESULTS AND DISCUSSION

Cathinones seem to bind with their carbonyl group toward transmembrane helix 6 in DAT and SERT

The larger of the two ligands employed in this study, IMAP, was docked in the substrate binding site of the DAT model previously stabilized[11]. Two different poses were obtained whereby the ligand carbonyl group was either directed extracellularly or toward transmembrane helix 6 (TM6) (Figure 1, left). The simulations in the wild-type DAT and the mutants were stable and based on direct protein-ligand interactions, the simulations of pose 2 were energetically more favorable (Figure 1, right). Additionally, pose 2 simulations had stable hydrogen bonding between the cationic nitrogen of the ligand and the Phe320 backbone. This interaction was also observed in occluded LeuT co-crystal structures, with the homologous Phe253 backbone[12] and in previous MD studies of DAT and SERT in complex with phenylethylamine substrates[13-15]. Therefore the pose 2 simulations were used for assessing the differences between SERT and DAT binding.

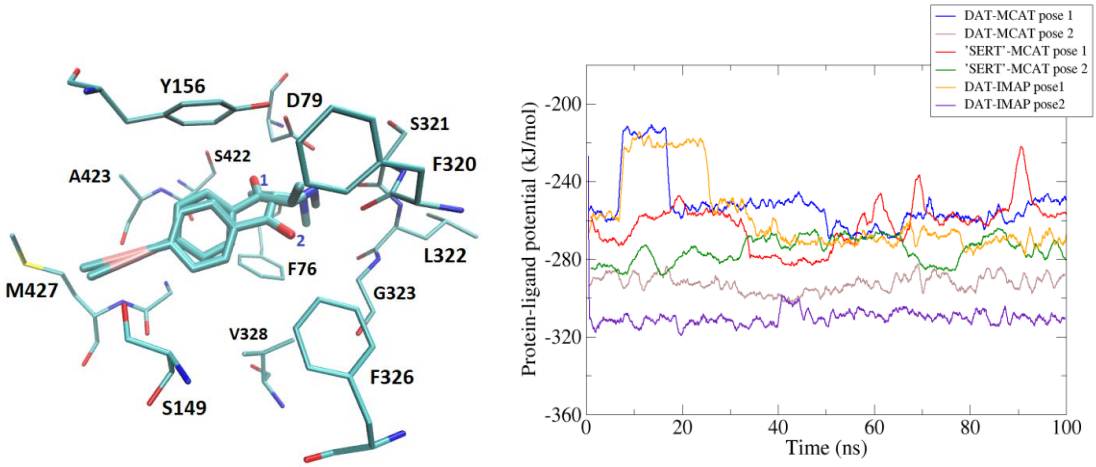

Figure 1 Left: *Two binding modes of 4-iodomethcathinone (IMAP) in the S1 site of the dopamine transporter obtained by docking. The turquoise 'atom' on the iodine atom represents the sigma hole.* **Right**: *Simulations with pose 2 had generally more favorable protein-ligand interactions potentials. The time series represent a 2 ns running average.*

MEPH inhibits SERT uptake more than MCAT

Uptake inhibitory experiments have shown that MEPH and MCAT are most active as their (*S*) enantiomer. Assuming the absence of another binding site along the access path of the transporter, or if the dissociation constant for another site is the same for both ligands, the binding free energy difference of these ligands for SERT is ca. 2.17 kcal/mol:

$$\frac{K_{D,MEPH}}{K_{D,MCAT}} \approx \frac{K_{i,MEPH}}{K_{i,MCAT}} = \frac{IC_{50,MEPH}}{IC_{50,MCAT}} \frac{(1+\frac{[5HT]}{K_{D,5HT}})}{(1+\frac{[5HT]}{K_{D,5HT}})} = \frac{IC_{50,MEPH}}{IC_{50,MCAT}}$$

$$\Delta\Delta G_{\mathrm{MEPH}\rightarrow\mathrm{MCAT}} \approx -RT\ln\frac{IC_{50,MEPH}}{IC_{50,MCAT}} = +2.17\ \mathrm{kcal/mol}$$

The selectivity of SERT for MEPH over MCAT might reside in the substrate binding site

Since experiments have shown that MEPH binds stronger than MCAT to SERT, a thermodynamic integration (TI) calculation was performed in the DAT system with a SERT-like S1 pocket. TI is, due to its relative simplicity, a commonly used free energy calculation method with increasing use due to faster computers, was shown to be successful for the calculation of relative binding free energies between bornyl and thiolactomycin derivatives in globular complexes [16] and potassium channels[17]. The partition function contains the Hamiltonian ($\mathcal{H}$) which can easily be obtained by sampling the system of interest. Calculation of the derivative of the van der Waals and electrostatic potentials with respect to a coupling parameter λ at regular intervals, followed by block averaging and integration yields the free energy (Δ*A)* between two thermodynamic states *A* and *B*:

$$\Delta A_{A-B} = \int_{\lambda=0}^{1} \langle\frac{\partial\mathcal{H}}{\partial\lambda}\rangle d\lambda$$

The simultaneous decoupling of the *para*-methyl group and the coupling of the *para*-hydrogen of MEPH in the complex, yielded smooth curves by employing a distance of 0.05 λ between the simulation windows in the 'soft' states (λ 0.2-0.8). See Figure 2 for the thermodynamic cycle and Supplemental Figure 1 for the integrands. The TI perturbation in the backward direction was performed by first modifying the Lennard-Jones (LJ) potentials before the electrostatic (QQ) potentials to prevent numerical instabilities due to the growing charges of methyl group. Therefore, the derivative curves from the protein-ligand complex calculations were slightly deviating, but the hysteresis was relatively low (<1 kcal/mol). Hence we suggest that the SERT S1 site is responsible for the difference in binding affinity between these two ligands and that differential access can be excluded for this class of ligands.

$\Delta\Delta G_{cald.}$ =	+1.83	± 0.21	kcal/mol
$\Delta\Delta G_{exp.}$ =	**+2.17**		kcal/mol

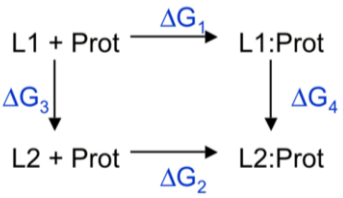

Figure 2 *Thermodynamic cycle employed for the calculation of the relative binding free energy between MEPH and MCAT*

DAT selectivity for ring-unsubstituted amphetamines seems partly caused by more favorable interactions with a Phe320 in DAT as compared to Phe355 in SERT, due to a Val/Ile switch in the central binding site

The distance between the aromatic ring of MCAT and Phe320 was ca. 1 Å less in DAT as compared to in 'SERT'. At the same time, the stacking distance between the non-selective IMAP and Phe320 were the same in DAT and 'SERT' (6.5 Å), indicating that the stacking contributes to selectivity (see Figure 4a and 4b). According to previous quantum mechanical studies on *π-π* stacking of benzene rings, this difference would account for a maximum of 4 kJ/mol more favorable enthalpy and hence would not be the major driving force for

selectivity.[18] Although stacking interactions are not explicitly represented in the MD simulations, the Lennard-Jones (LJ) interactions were in good agreement: the interaction energy between DAT and MCAT was ca. 5 kJ/mol more favorable as compared to 'SERT'-MCAT. This difference was pinned down to the LJ interactions between the ligand and the Phe320 side chain (see Figure 4c).

Based on uptake inhibitory assays on (*S*)-MCAT, the selectivity is around 50x for DAT over SERT, corresponding to ca. 9.8 kJ/mol difference in binding free energy (see next section). In order to pin down residues responsible for this, the mutant DAT-V152I and 'SERT'-I152V, blocked and reversed the stacking interaction, respectively (see Figure 4b). The uptake inhibitory activity of MCAT in the SERT-I172V mutant (homologous to 'SERT'-I152V in the simulation) was indeed increased significantly (see Figure 4d). The results therefore indicate the indirect contribution of the Val/Ile switch to the DAT-over-SERT selectivity.

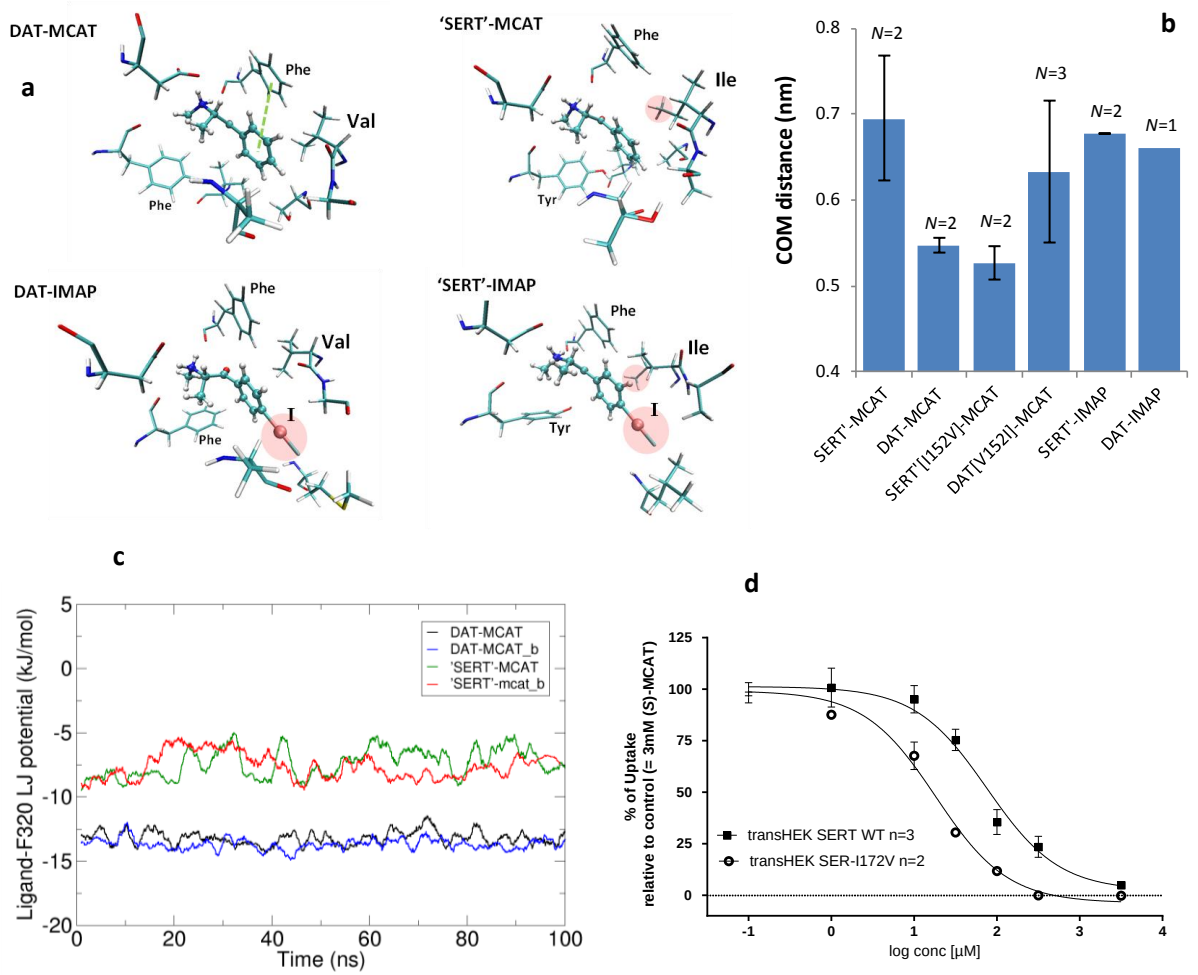

Figure 4 a. *Hypothesis whereby MCAT stacks in DAT with Phe320 due to the lack of a para-substituent and due to Val152. SERT has a Ile at the homologous position preventing such an interaction.* **b.** *Stacking distances between the ligand and Phe320 rings showing differences between Val and Ile containing proteins.* **c.** *MCAT-Phe320 van der Waals potential showing the difference between 'SERT' and DAT.* **d.** *Uptake inhibition curves of (S)-MCAT in the serotonin transporter transiently expressed in HEK-293 cells showing a 4x increase in activity upon mutation to the DAT-like Val172.*

DAT-over-SERT selectivity for unsubstituted amphetamines might be caused by more attractive electrostatic interactions due to pocket volume differences

From the simulation trajectories, the electrostatic component of the potential energy between the ligand and the protein was ca. 20 kJ/mol more favorable in DAT, as compared to in 'SERT' (see Figure 5a). A brute force analysis of the contributions of each residue within the cut-off region of the ligand atoms revealed that a combination of residues contributed to selectivity. This was mostly caused by Ser321 being on average 5.5 kJ/mol more attractive in DAT, whereas Tyr156 was 4.1 kJ/mol more repulsive in 'SERT'. Figure 5b shows a surface representation of the pocket with the color indicating the electrostatic contribution to selectivity. From this perspective, and that on average 3 more water molecules were present in 'SERT' (see Figure 5c), the DAT pocket seems to be packed tighter around the ligand, making the ligand-carbonyl backbone interactions electrostatically more favorable. This was confirmed by measuring the binding site volumes of the complex states, which indicated a 6.2 Å^3 larger 'SERT' pocket on average (see Figure 5d). Additionally, the presence of waters in the pocket indicates a loss in water entropy and enthalpy.

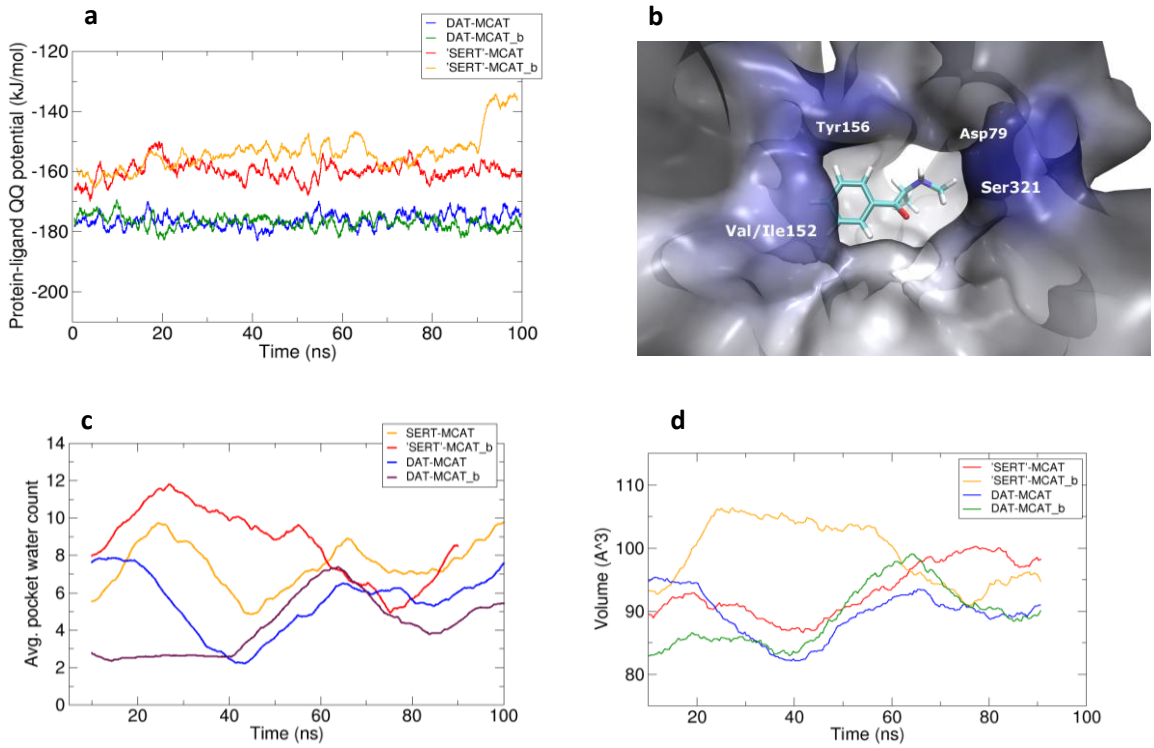

Figure 5 *The differences explained between the 'SERT'- and DAT-MCAT simulation (both in duplicate).* **a.** *Protein-ligand electrostatic potential difference.* **b.** *Surface representation of the substrate binding site. The blue color intensity refers to the difference in the protein-ligand electrostatic potential between 'SERT' and DAT, in the presence of MCAT.* **c.** *Average number of water molecules over a 10 ns running average within a 5 Å radius of the ligand. The average over the whole trajectory is 4.8 in DAT and 7.9 in 'SERT'.* **d.** *Volume of the substrate binding site over a 10 ns running average; the SERT pocket has on average a 6.2 Å^3 larger pocket during the whole trajectory.*

Thermodynamic Integration study on wild-type and mutant DAT in complex with MCAT

The feasibility of the TI method for side chain perturbations was assessed by simulating the DAT-V152I and DAT-F76Y mutants in *apo* form and in complex with the DAT-over-SERT selective (*S*)-MCAT. Estimating the

binding free energy difference between different mutants from experiments is more problematic because the K_D values of the radioligand dopamine (DA) might be different for wild-type and the mutant:

$$\frac{K_{D,mutant}}{K_{D,WT}} \approx \frac{K_{i,mutant}}{K_{i,WT}} = \frac{IC_{50,mutant}}{IC_{50,WT}} \frac{(1+\frac{[DA]}{K_{D,DA:WT}})}{(1+\frac{[DA]}{K_{D,DA:mutant}})}$$

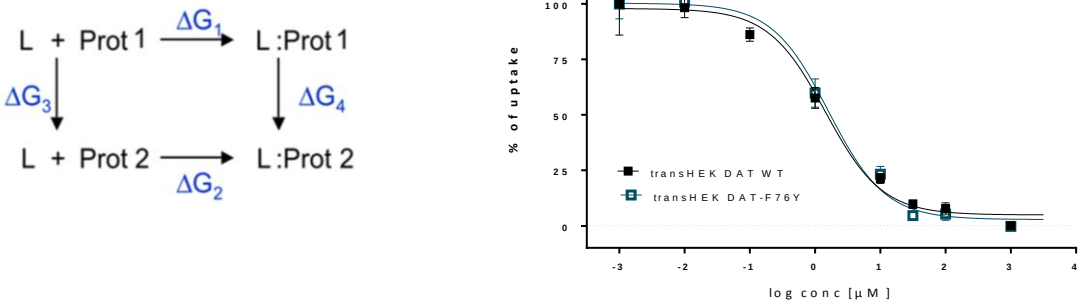

Figure 6 ***Left***: *Thermodynamic cycle employed for the calculation of the relative binding free energy between wild-type and mutant DAT with the methcathinone ligand* ***Right****: Uptake inhibition curves of (S)-MCAT in the dopamine transporter transiently expressed in HEK-293 cells showing no decrease in activity upon mutation to the SERT-like Tyr95. Uptake is relative to the highest inhibitor concentration (1mM (S)-MCAT) and experiments were performed in quadruple.*

The perturbation of DAT-V152I to DAT was trivial to perform; however, the perturbation in complex with the ligand did not reach the expected endstate; the stacking distance was not decreased as in the DAT-MCAT simulations. See supplemental Figure 2. Instead, another binding mode occurred that had not been observed previously, whereby the ligand stacked with Phes326.

The perturbation of DAT-F76Y to and from DAT required more simulation time, in addition to stepwise modifications of the Hamiltonian as postulated previously.[19] The difference in electrostatics seemed to govern the interactions, as can be expected from the relatively large partial charge of the Tyr hydroxyl group. See Supplemental Figure 3. The end states were reached and the relative binding free energy difference from DAT-F76Y to DAT was -9.4 ± 3.4 kJ/mol, hence more favorable. However, experiments did however not show an in increase in IC_{50} upon inserting the mutation, which might indicate that the K_D of the radioligand is substantially different for WT and mutant. See Figure 6.

METHODS

Ligand preparation

The ligand structures were built in Molecular Operating Environment[20] (MOE) as the (*S*)-enantiomer and Topolbuild was used to generate the Gromacs OPLS topology skeleton. Atom types were taken from the OPLS-AA/L[21] force field files in Gromacs, while assigning the α-carbon as a peptidic backbone carbon atom. The sigma hole of the iodine atom in IMAP was represented by a virtual site with parameters described previously.[22] Missing dihedral parameters were taken from the OPLS2005 force field of Schrodinger[23]. Transferability was confirmed by checking the remaining charges, bond lengths, angles and dihedral parameters.

Protein preparation

From the previously published hDAT trajectory of Stockner *et al,*[11] a snapshot with sufficient space for an aromatic ring between Val152 and Ala423 ("B-site")[6,24] was selected for docking (*S*)-4-iodomethcathinone using GOLD 5.2.[25] This corresponded to 17.6 ns of the production run. Distance restraints were imposed to dock the ligand into this site (see Saha *et al* for the procedure[6]). Two different poses were obtained whereby the β-oxo group of the ligand was either pointing to the extracellular space (pose 1) or toward the TM6 (pose 2). Both complexes were placed back in the simulation system, while removing 9 overlapping waters.
Three DAT mutants (V152I, F76Y and the SERT-like octuple V152I, G153A, A423T, M427L, F76Y, S149A, S429G, G425A) were prepared by placing the additional atoms into a void using MOE. Two possible side chain conformations of Thr423 (A423T), depending on the χ1 dihedral angle, in the octuple mutant were simulated. The simulations showed that the hydroxyl group was prone to moving away from the S1 pocket and therefore all simulations with 'SERT' were started with the stable Thr423 conformation, as well as for the TI perturbation on 'SERT'.

MD simulations

All calculations were performed using Gromacs in the OPLS-AA/L force field with settings described previously.[11] The starting systems were energy minimized using the steepest descent method with a maximum force constant of 10 kJ/mol.nm and 0.01 kJ/mol step size. Equilibration was performed by gradually heating in four sessions of 1 ns starting at 100 K with position restraints of 1000 kJ mol^{-1} nm^{-2} on the protein-bound ions and ligand and 100 kJ mol^{-1} nm^{-2} on the backbone atoms, while decreasing the restraints ten times every session and increasing the temperature by 50 K. The systems then underwent a production run at 300 K [11] until stable based on the following criteria: RMSD of the backbone and the residues surrounding the ligand; ligand-Asp79 salt bridge distance, Phe76/Tyr76 χ1 angle, potential energy of the system. This led to 100 ns simulation lengths, while the complexes were run in duplicate or triplicate, depending on the stability, using a different seed for the random starting velocities based on a Maxwell-Boltzmann distribution. Binding site volumes were calculated with POVME.[26]

Thermodynamic Integration

A double topology paradigm was employed whereby atoms were decoupled and coupled simultaneously to or from a dummy atom, respectively. For the MEPH/MCAT perturbation, the thermodynamic cycle in Figure 2 was employed. Every window was simulated for at least 2.5 ns and the equilibration time was kept at 1 ns by default. The simulation windows were run serially, i.e. the same velocities were used for the sequential window, to account for any conformational changes and to assure smooth curves of the LJ component of $\langle dH/d\lambda \rangle$. To accelerate the calculation and assure convergence of $dH/d\lambda$ and its error estimate, a simulation continued to the sequential window as soon as an error of < 2 kJ/mol was achieved and when the slope of the fitted curve to the error as a function of block size was < 0.1 kJ/mol.ns for both the electrostatic and LJ components of $\langle dH/d\lambda \rangle$ (See figure 7). Additionally, the LJ interactions were modified using a soft-core α_{sc} of 0.5. Arrival at the endstate was checked based on the following criteria: Phe76/Tyr76 χ1 angle, stacking distances of ligand with Tyr156, Phe320, Phe326, (ligand-cation)-(Phe/Tyr76-ring) distance.

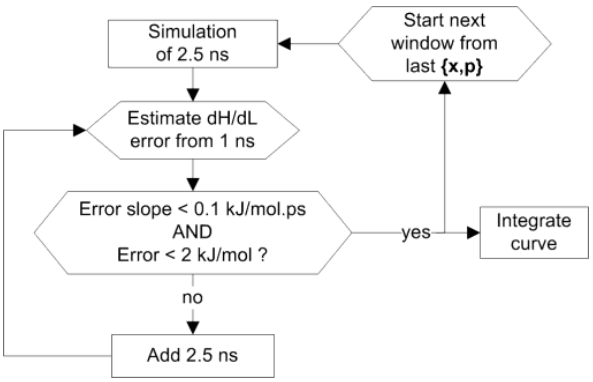

Figure 7 *Applied scheme for the thermodynamic integration (TI) method*

For the perturbation of the DAT-Tyr/Phe76 systems, the run was performed in two separate steps to avoid high fluctuations of the electrostatic potential and to linearly mix these, since the Gromacs code does not support separate hard-core and soft-core interactions.

For the calculation of the ligand in water, a single point charge (SPC) water box was used with a distance of 2 nm to the box edges. Isotropic pressure coupling using the Berendsen barostat was employed and the $dH/d\lambda$ curves were obtained by simulating 10 windows of each 3 ns long, while discarding the first 500 ps as equilibration. The free energy difference between the states was calculated using the trapezoidal rule.

Experimental Methods

Site-directed mutagenesis was performed using the Agilent(R) Quikchange Lightning kit. YFP-synSERT-Ampicillin and CFP-synDAT-Kanamycin wild-type DNA was used as template for the primers obtained from Agilent: DAT-F76Y reverse: 5'-GGTCGACGG**CAT**AGCCGATCACGCTGAGCA-3' and SERT-I172V reverse: 5´-GTGTTGTAGTAGGAAGCA**ACG**TAAAAGGCAATGATGCAG-3´, with the **mutation** indicated. The new plasmids were sequenced and transformed into *Escherichia Coli* XL10 Gold competent bacteria to obtain larger amounts.

HEK293 cells were grown at 37 °C under a 5% CO_2 and humid atmosphere in Dulbecco's Modified Eagle's medium (DMEM) supplemented with 10% fetal calf serum and 1% penicillin. Cells of ca. 80% confluence were transiently transfected using Lipofectamine (Invitrogen) and seeded onto a poly-D-lysine coated 96-well plate while assuring ca. $8 \cdot 10^5$ cells/well for the subsequent day. The (*S*)-MCAT solution series was made by preparing a stock of 100 mM in Krebs-HEPES buffer (KHB) and diluting it stepwise for both the pre-incubation and uptake inhibition solutions. The uptake solution contained 0.2 µM [^{3}H]-5-HT or [^{3}H]-DA for the SERT and DAT measurements, respectively. The buffer solution of the DAT measurement additionally contained 100 µM ascorbic acid and paragyline. After incubating MCAT in triplicate for 5 minutes, the solutions were replaced by 50 µL uptake solution for 60 seconds. The reaction was cooled down to 4 °C and the cells were lysed with 1% SDS solution, followed by liquid scintillation counting. The counts were plotted using SigmaPlot(R) after subtraction of the counts due to unspecific uptake at the highest MCAT concentration.

Author Contributions

We wish to thank N. Cozzi (University of Wisconsin) for providing the activity data of 4-iodomethcathinone and L. Wimmer (Technical University of Vienna) for synthesizing the enantiopure methcathinone and mephedrone.

Supplemental Figure 1

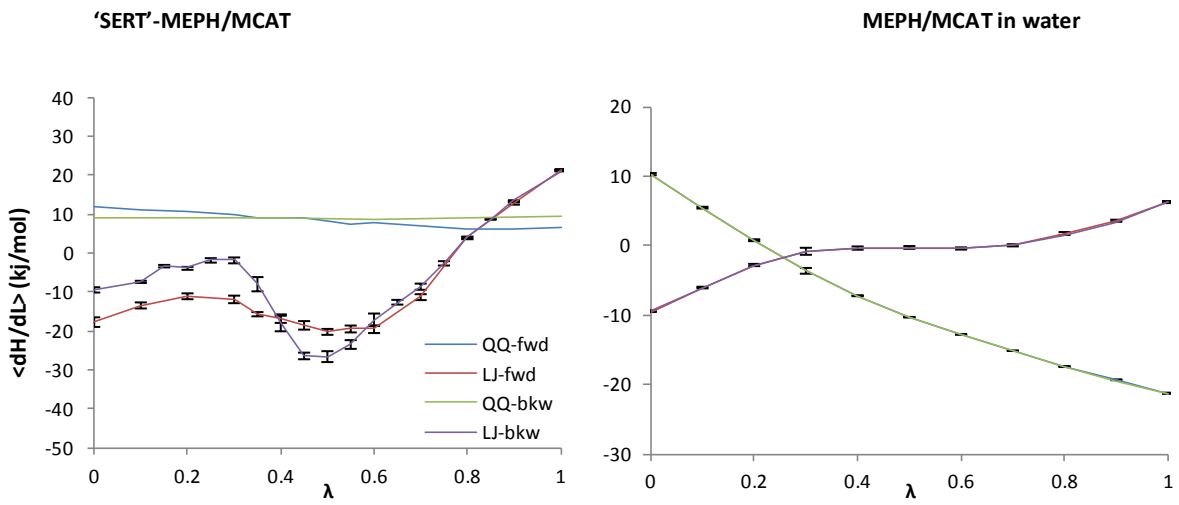

Curves representing the integrand of the TI calculations of the ligands in 'SERT'. **Left:** the forward perturbation (fwd, MEPH to MCAT) was performed by changing the Lennard-Jones (LJ) and Coulombic (QQ) interactions simultaneously using a soft-core, while backwards (bkw) the LJ interactions were changed first using a soft-core, followed by linear modification of the QQ interactions. **Right**: The same calculations performed in SPC water by simultaneous soft-core LJ and QQ perturbation with equidistant windows.

Supplemental Figure 2

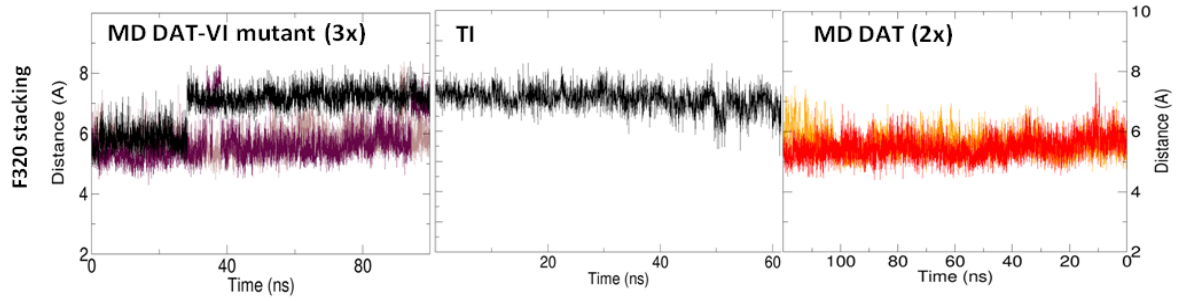

Distance between the centers of mass of MCAT and Phe320 in DAT (right) and DAT-V152I (left). The perturbation (middle) was started from a system with the largest distance between (as seen in the 'SERT'-MCAT simulations, Figure 4b). The distance did not decrease as expected, due to a change of the pocket topology and stacking with another side chain (Phe326).

Supplemental Figure 3

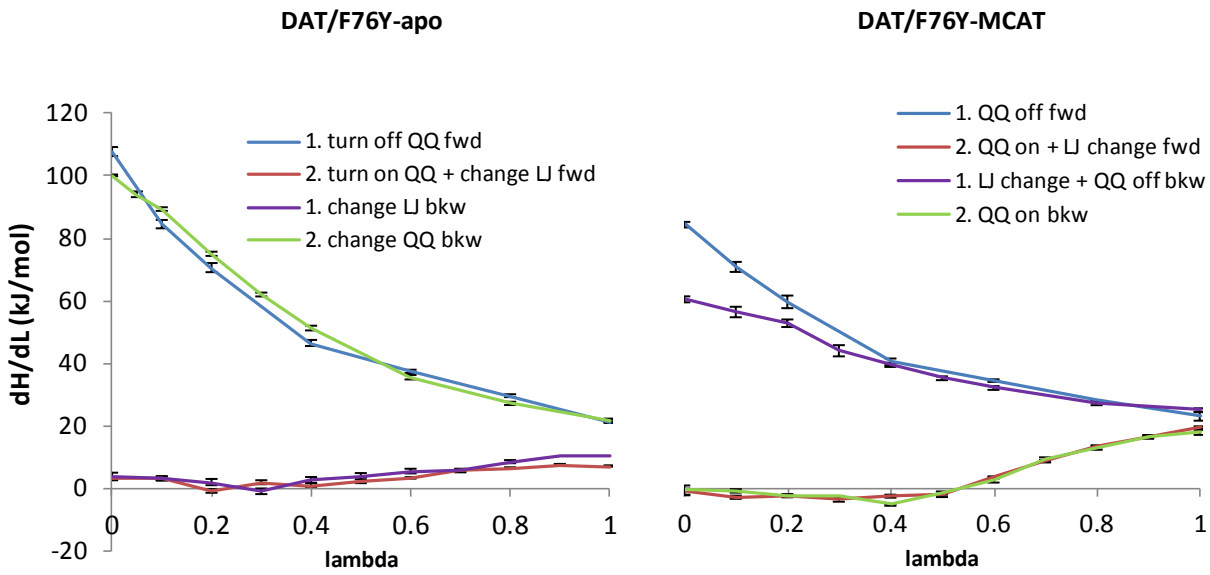

kJ/mol	**ΔG**	**error**	hysteresis
complex	44.3	2.0	4.7
apo	53.7	1.9	-2.0
ΔΔG	**-9.4**	3.4	

Curves representing the integrand of the TI calculations whereby the aromatic side chain in the DAT model was perturbed. **Left:** the forward perturbation (fwd, DAT-F76Y to DAT) was performed by first turning off the charges and then turning them on while changing the LJ interactions using a soft-core. During the backward (bkw) perturbation, the LJ interactions were changed first, followed by linear modification of the QQ interactions. **Right**: The same calculations performed in the presence of MCAT.

REFERENCES

1. Lesch KP, Aulakh CS, Wolozin BL, Murphy DL. Serotonin (5-HT) receptor, 5-HT transporter and G protein-effector expression: implications for depression. Pharmacology & toxicology 1992;71 Suppl 1:49-60.
2. Lesch KP, Bengel D, Heils A, Sabol SZ, Greenberg BD, Petri S, Benjamin J, Muller CR, Hamer DH, Murphy DL. Association of anxiety-related traits with a polymorphism in the serotonin transporter gene regulatory region. Science 1996;274(5292):1527-1531.
3. van der Wee NJ, Stevens H, Hardeman JA, Mandl RC, Denys DA, van Megen HJ, Kahn RS, Westenberg HM. Enhanced dopamine transporter density in psychotropic-naive patients with obsessive-compulsive disorder shown by [123I]{beta}-CIT SPECT. The American journal of psychiatry 2004;161(12):2201-2206.
4. Kent L, Doerry U, Hardy E, Parmar R, Gingell K, Hawi Z, Kirley A, Lowe N, Fitzgerald M, Gill M, Craddock N. Evidence that variation at the serotonin transporter gene influences susceptibility to attention deficit hyperactivity disorder (ADHD): analysis and pooled analysis. Molecular psychiatry 2002;7(8):908-912.
5. Baughman FA, Jr. Dopamine-transporter density in patients with ADHD. Lancet 2000;355(9213):1460-1461; author reply 1461-1462.
6. Saha K, Partilla JS, Lehner KR, Seddik A, Stockner T, Holy M, Sandtner W, Ecker GF, Sitte HH, Baumann MH. 'Second-Generation' Mephedrone Analogs, 4-MEC and 4-MePPP, Differentially Affect Monoamine Transporter Function. Neuropsychopharmacology : official publication of the American College of Neuropsychopharmacology 2014.
7. Agatonovic-Kustrin S, Davies P, Turner JV. Structure-activity relationships for serotonin transporter and dopamine receptor selectivity. Med Chem 2009;5(3):271-278.
8. Greiner E, Boos TL, Prisinzano TE, De Martino MG, Zeglis B, Dersch CM, Marcus J, Partilla JS, Rothman RB, Jacobson AE, Rice KC. Design and synthesis of promiscuous high-affinity monoamine transporter ligands: unraveling transporter selectivity. Journal of medicinal chemistry 2006;49(5):1766-1772.
9. Seddik A, Holy M, Weissensteiner R, Zdrazil B, Sitte HH, Ecker GF. Probing the Selectivity of Monoamine Transporter Substrates by Means of Molecular Modeling. Molecular informatics 2013;32(5-6):409-413.
10. Rothman RB, Baumann MH. Monoamine transporters and psychostimulant drugs. European journal of pharmacology 2003;479(1-3):23-40.
11. Stockner T, Montgomery TR, Kudlacek O, Weissensteiner R, Ecker GF, Freissmuth M, Sitte HH. Mutational analysis of the high-affinity zinc binding site validates a refined human dopamine transporter homology model. PLoS computational biology 2013;9(2):e1002909.
12. Yamashita A, Singh SK, Kawate T, Jin Y, Gouaux E. Crystal structure of a bacterial homologue of Na+/Cl--dependent neurotransmitter transporters. Nature 2005;437(7056):215-223.
13. Beuming T, Kniazeff J, Bergmann ML, Shi L, Gracia L, Raniszewska K, Newman AH, Javitch JA, Weinstein H, Gether U, Loland CJ. The binding sites for cocaine and dopamine in the dopamine transporter overlap. Nature neuroscience 2008;11(7):780-789.
14. Severinsen K, Kraft JF, Koldso H, Vinberg KA, Rothman RB, Partilla JS, Wiborg O, Blough B, Schiott B, Sinning S. Binding of the amphetamine-like 1-phenyl-piperazine to monoamine transporters. ACS chemical neuroscience 2012;3(9):693-705.
15. Koldso H, Christiansen AB, Sinning S, Schiott B. Comparative modeling of the human monoamine transporters: similarities in substrate binding. ACS chemical neuroscience 2013;4(2):295-309.
16. Steinbrecher T, Case DA, Labahn A. Free energy calculations on the binding of novel thiolactomycin derivatives to E. coli fatty acid synthase I. Bioorganic & medicinal chemistry 2012;20(11):3446-3453.
17. Rowley CN, Roux B. A computational study of barium blockades in the KcsA potassium channel based on multi-ion potential of mean force calculations and free energy perturbation. The Journal of general physiology 2013;142(4):451-463.
18. Wales DJ. Intermolecular forces and clusters. Berlin ; New York: Springer.
19. Pan AC, Cuello LG, Perozo E, Roux B. Thermodynamic coupling between activation and inactivation gating in potassium channels revealed by free energy molecular dynamics simulations. The Journal of general physiology 2011;138(6):571-580.
20. Molecular Operating Environment (MOE) CCGI, 1010 Sherbooke St. West, Suite #910, Montreal, QC, Canada, H3A 2R7, 2015.
21. Kaminski GA, Friesner RA, Tirado-Rives J, Jorgensen WL. Evaluation and Reparametrization of the OPLS-AA Force Field for Proteins via Comparison with Accurate Quantum Chemical Calculations on Peptides†. The Journal of Physical Chemistry B 2001;105(28):6474-6487.
22. Jorgensen WL, Schyman P. Treatment of Halogen Bonding in the OPLS-AA Force Field; Application to Potent Anti-HIV Agents. Journal of chemical theory and computation 2012;8(10):3895-3801.
23. Banks JL, Beard HS, Cao Y, Cho AE, Damm W, Farid R, Felts AK, Halgren TA, Mainz DT, Maple JR, Murphy R, Philipp DM, Repasky MP, Zhang LY, Berne BJ, Friesner RA, Gallicchio E, Levy RM. Integrated Modeling Program, Applied Chemical Theory (IMPACT). Journal of computational chemistry 2005;26(16):1752-1780.

24. Andersen J, Olsen L, Hansen KB, Taboureau O, Jorgensen FS, Jorgensen AM, Bang-Andersen B, Egebjerg J, Stromgaard K, Kristensen AS. Mutational mapping and modeling of the binding site for (S)-citalopram in the human serotonin transporter. The Journal of biological chemistry 2010;285(3):2051-2063.
25. Jones G, Willett P, Glen RC, Leach AR, Taylor R. Development and validation of a genetic algorithm for flexible docking. Journal of molecular biology 1997;267(3):727-748.
26. Durrant JD, Votapka L, Sorensen J, Amaro RE. POVME 2.0: An Enhanced Tool for Determining Pocket Shape and Volume Characteristics. Journal of chemical theory and computation 2014;10(11):5047-5056.

D

'Second-Generation' Mephedrone Analogs, 4-MEC and 4-MePPP, Differentially Affect Monoamine Transporter Function

Kusumika Saha, John S Partilla, Kurt R Lehner, Amir Seddik, Thomas Stockner, Marion Holy, Walter Sandtner, Gerhard F Ecker, Harald H Sitte, Michael H Baumann

Published in *Nature Neuropsychopharmacology*, 40, 1321-31, **2014**

My contribution to the following publication was to deliver a structural explanation for the selectivity of the *N*-pyrrolidino-substituted *para*-methylated cathinone (4-MePPP) for the dopamine transporter (DAT) over the serotonin transporter (SERT). Thereby I created homology models based on the recently crystallized *Drosophila* DAT and docked the compounds using distance restraints that are based on previous studies. Due to subtle subpocket differences between the two proteins in the substrate binding site, I noticed that 4-MePPP showed ambiguous docking poses in SERT, indicating a lack of space, whereas in DAT the poses were consistently binding in the favorable “B” subpocket.

Neuropsychopharmacology (2015) 40, 1321–1331

www.neuropsychopharmacology.org

'Second-Generation' Mephedrone Analogs, 4-MEC and 4-MePPP, Differentially Affect Monoamine Transporter Function

Kusumika Saha[1], John S Partilla[2], Kurt R Lehner[2], Amir Seddik[3], Thomas Stockner[1], Marion Holy[1], Walter Sandtner[1], Gerhard F Ecker[3], Harald H Sitte[1,4] and Michael H Baumann*[,2]

[1]Medical University of Vienna, Center for Physiology and Pharmacology, Institute of Pharmacology, Vienna, Austria; [2]Designer Drug Research Unit (DDRU), Intramural Research Program (IRP), NIDA, NIH, Baltimore, MD, USA; [3]Department of Pharmaceutical Sciences, University of Vienna, Vienna, Austria; [4]Medical University of Vienna, Center for Addiction Research and Science, Vienna, Austria

The nonmedical use of synthetic cathinones is increasing on a global scale. 4-Methyl-*N*-methylcathinone (mephedrone) is a popular synthetic cathinone that is now illegal in the United States and other countries. Since the legislative ban on mephedrone, a number of 'second-generation' analogs have appeared in the street drug marketplace, including 4-methyl-*N*-ethylcathinone (4-MEC) and 4′-methyl-α-pyrrolidinopropiophenone (4-MePPP). Here we characterized the interactions of 4-MEC and 4-MePPP with transporters for 5-HT (SERT) and dopamine (DAT) using molecular, cellular, and whole-animal methods. *In vitro* transporter assays revealed that 4-MEC displays unusual 'hybrid' activity as a SERT substrate (ie, 5-HT releaser) and DAT blocker, whereas 4-MePPP is a blocker at both transporters but more potent at DAT. *In vivo* microdialysis experiments in rat brain demonstrated that 4-MEC (1–3 mg/kg, i.v.) produced large increases in extracellular 5-HT, small increases in dopamine, and minimal motor stimulation. In contrast, 4-MePPP (1–3 mg/kg, i.v.) produced selective increases in dopamine and robust motor stimulation. Consistent with its activity as a SERT substrate, 4-MEC evoked inward current in SERT-expressing *Xenopus* oocytes, whereas 4-MePPP was inactive in this regard. To examine drug–transporter interactions at the molecular level, we modeled the fit of 4-MEC and 4-MePPP into the binding pockets for DAT and SERT. Subtle distinctions in ligand–transporter binding were found that account for the differential effects of 4-MEC and 4-MePPP at SERT. Collectively, our results provide key information about the pharmacology of newly emerging mephedrone analogs, and give clues to structural requirements that govern drug selectivity at DAT *vs* SERT.
Neuropsychopharmacology (2015) **40,** 1321–1331; doi:10.1038/npp.2014.325; published online 14 January 2015

INTRODUCTION

In recent years, there has been an alarming increase in the nonmedical use of synthetic psychoactive compounds described as 'designer drugs' or 'legal highs' (Rosenbaum *et al*, 2012). These substances are synthesized by rogue chemists who hijack the medical and patent literature to identify structures that target specific neuronal receptors or transporters known to mediate psychoactive effects (Lewin *et al*, 2014). Synthetic cathinones are designer drugs given innocuous names like 'bath salts', 'plant food', or 'research chemicals' as a ploy to skirt the regulations governing the sale of psychoactive substances (Baumann *et al*, 2013a; De Felice *et al*, 2014). 4-Methyl-*N*-methylcathinone (mephedrone) and 3,4-methylenedioxypyrovalerone (MDPV) are examples of synthetic cathinones that produce stimulant-like subjective effects at low doses, but dangerous side effects after high doses or chronic use (Dargan *et al*, 2011; Spiller *et al*, 2011). Adverse consequences include hypertension, tachycardia, anxiety, hallucinations, psychosis, and even death. Because of public health risks, legislative authorities have banned mephedrone, MDPV, and certain other synthetic cathinones in the United States (Drug Enforcement Administration (DEA), Department of Justice, 2013), and similar legislation has been enacted in European countries. In response to legislative bans, enterprising chemists have synthesized a number of 'second-generation' replacement analogs as a means to evade regulatory control, and this trend is expected to continue (Leffler *et al*, 2014; Marinetti and Antonides, 2013).

Like other stimulant drugs, synthetic cathinones exert their pharmacological effects by disrupting the function of solute carrier SLC6 transporter proteins (ie, monoamine transporters) expressed on nerve cells in the brain and periphery (Baumann *et al*, 2013a; Hadlock *et al*, 2011; Lopez-Arnau *et al*, 2012). Monoamine transporters normally mediate the sodium-dependent reuptake of monoamine neurotransmitters, and there are specific transporter proteins for norepinephrine (NET), dopamine (DAT),

*Correspondence: Dr MH Baumann, Designer Drug Research Unit, IRP, NIDA, NIH, DHHS, 333 Cassell Drive, Suite 4400, Baltimore, MD 21224, USA, Tel: +1 443 740 2660, Fax: +1 443 740 2241, E-mail: mbaumann@mail.nih.gov
Received 5 September 2014; revised 7 November 2014; accepted 9 November 2014; accepted article preview online 15 December 2015

and 5-HT (SERT) (Kristensen *et al*, 2011). Drugs that interact with transporters can be categorized as either amphetamine-like substrates or cocaine-like blockers (Rothman and Baumann, 2003; Sitte and Freissmuth, 2010). Both types of drugs increase extracellular concentrations of monoamines in nervous tissue, but substrates induce transporter-mediated sodium currents (ie, depolarization) and evoke transmitter efflux (ie, release), whereas blockers do not. Importantly, determining the precise molecular mechanism of action for transporter drugs is critical to predict their putative toxic potential (Baumann *et al*, 2014; Steinkellner *et al*, 2011). Previous studies have shown that mephedrone targets monoamine transporters as a nonselective substrate, thereby evoking the release of norepinephrine, dopamine, and 5-HT (Baumann *et al*, 2012; Cameron *et al*, 2013; Eshleman *et al*, 2013; Simmler *et al*, 2013). In contrast, MDPV is a potent blocker at NET and DAT with little influence on SERT. Systemic administration of mephedrone or MDPV to rats increases extracellular concentrations of dopamine in mesolimbic reward pathways, indicating the potential for addiction (Baumann *et al*, 2012, 2013b; Kehr *et al*, 2011; Wright *et al*, 2012). Accordingly, both drugs are readily self-administered and facilitate intracranial self-stimulation in rat models (Aarde *et al*, 2013a; Bonano *et al*, 2014; Hadlock *et al*, 2011; Watterson *et al*, 2014).

As noted above, a number of second-generation analogs of mephedrone and MDPV have recently appeared in the recreational drug marketplace (Leffler *et al*, 2014; Marinetti and Antonides, 2013). We and others have shown that newly emerging analogs of MDPV, like α-pyrrolidinovalerophenone (α-PVP), are potent blockers at DAT and NET (Kolanos *et al*, 2013; Marusich *et al*, 2014). However, little information is available regarding the molecular mechanisms and pharmacological effects of mephedrone analogs (ie, 4-methyl ring-substituted compounds) such as 4-methyl-*N*-ethylcathinone (4-MEC) and 4′-methyl-α-pyrrolidinopropiophenone (4-MePPP). Figure 1 shows the chemical structures of 4-MEC and 4-MePPP as compared with mephedrone; both drugs maintain the 4-methyl ring-substitution of mephedrone, but 4-MEC has an *N*-ethyl group whereas 4-MePPP has an *N*-butyl group that is cyclized to form a pyrrolidine ring. 4-MEC has been identified in products purchased from internet vendors (eg, NRG-2) (Ayres and Bond, 2012), and the drug is associated with adverse medical consequences (Gil *et al*, 2013; Rojek *et al*, 2014). 4-MePPP was available as a recreational stimulant in the late 1990s and was scheduled by the German Controlled Substance Act that prohibited its sale and use. Initial studies with 4-MePPP involved the characterization of its metabolism and development of forensic assays to detect the drug in biological matrices (Springer *et al*, 2003; Springer *et al*, 2002). 4-MePPP has reappeared recently in products containing mixtures of cathinone-related compounds (eg, NRG-3) (Brandt *et al*, 2011). In the present study, we employed molecular, cellular, and whole-animal methods to examine the interactions of 4-MEC and 4-MePPP with monoamine transporters. *In vitro* transporter assays were carried out in rat brain synaptosomes and in cells expressing human transporters. Effects of drugs on *in vivo* neurochemistry were monitored using microdialysis in rat nucleus accumbens. Finally, we analyzed transporter-mediated currents evoked by these drugs in *Xenopus* oocytes expressing SERT. Our results reveal diverse profiles of transporter activity for 4-MEC and 4-MePPP when compared with mephedrone.

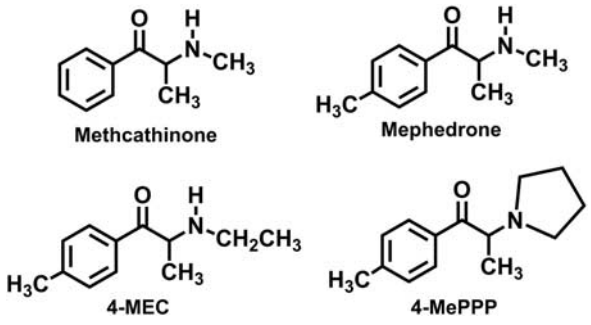

Figure 1 Chemical structure of 4-methyl-*N*-ethylcathinone (4-MEC) and 4′-methyl-α-pyrrolidinopropiophenone (4-MePPP), as compared with *N*-methylcathinone (methcathinone) and 4-methyl-*N*-methylcathinone (mephedrone).

MATERIALS AND METHODS

Drugs and Reagents

For uptake and release assays in synaptosomes, [^{3}H]dopamine, [^{3}H]5-HT, and [^{3}H]1-methyl-4-phenylpyridinium ([^{3}H]MPP+) were purchased from Dupont New England Nuclear (Boston, MA). All reagents, buffer salts, and chemicals were obtained from Sigma Chemical (St Louis, MO) unless otherwise noted. Reagents used in the experiments for uptake and efflux assays in cells were purchased and used according to previous work (Hofmaier *et al*, 2014). Plasmids encoding human SERT were a generous gift of Dr Randy D Blakely.

Animals and Housing

Male Sprague-Dawley rats (Charles River, Wilmington, MA) weighing 250–350 g were housed in standard conditions (lights on 0700–1900 h) with food and water freely available. Rats were maintained in facilities fully accredited by the Association for Assessment and Accreditation of Laboratory Animal Care, and experiments were performed in accordance with the Institutional Care and Use Committee of the NIDA IRP. *Xenopus laevis* frogs (Nasco, Fort Atkinson, WI) were kept in aquaria on a strict 12 h light/dark schedule with food available once weekly.

Uptake and Release Assay in Rat Brain Synaptosomes

Uptake and release assays were carried out in rat brain synaptosomes as previously described (Baumann *et al*, 2013b). Synaptosomes were prepared from rat striatum for DAT assays, whereas synaptosomes were prepared from whole brain minus striatum and cerebellum for SERT assays. For uptake inhibition assays, 5 nM [^{3}H]dopamine and [^{3}H]5-HT were used to assess transport activity at DAT and SERT, respectively. The selectivity of uptake assays was optimized for a single transporter by including unlabeled blockers to prevent uptake of [^{3}H]transmitter by competing transporters. Uptake inhibition assays were initiated by adding

100 µl of tissue suspension to 900 µl Krebs-phosphate buffer containing test drug and [^{3}H]transmitter. Uptake inhibition assays were terminated by rapid vacuum filtration through Whatman GF/B filters, and retained radioactivity was quantified by liquid scintillation counting. For release assays, 9 nM [^{3}H]MPP+ was used as the radiolabeled substrate for DAT, whereas 5 nM [^{3}H]5-HT was used as the radiolabeled substrate for SERT. All buffers used in the release assays contained 1 µM reserpine to block vesicular uptake of substrates. The selectivity of release assays was optimized for a single transporter by including unlabeled blockers to prevent the uptake of [^{3}H]MPP+ or [^{3}H]5-HT by competing transporters. Synaptosomes were preloaded with radiolabeled substrate in Krebs-phosphate buffer for 1 h (steady state). Release assays were initiated by adding 850 µl of preloaded synaptosomes to 150 µl of test drug. Release was terminated by vacuum filtration and retained radioactivity was quantified as described for uptake inhibition.

In Vivo Microdialysis in Rat Nucleus Accumbens

Microdialysis procedures were carried out as previously described (Baumann *et al*, 2012). Male rats were surgically prepared with jugular catheters and intracerebral guide cannulae aimed at the nucleus accumbens (AP +1.6 mm, ML −1.7 mm relative to bregma; −6.2 mm relative to dura). After a 7–10-day recovery period, catheters were attached to extension tubes and 0.5 × 2 mm microdialysis probes (CMA/12, Harvard Apparatus, Holliston, MA) were inserted into guide cannulae. Ringer's solution was perfused through the probe at 0.5 µl/min and dialysate samples were collected at 20 min intervals. Drug treatments were given after three stable baseline samples were obtained. Rats received two i.v. drug injections, 1 mg/kg at time 0 followed by 3 mg/kg 60 min later. Control rats received two i.v. saline injections on the same schedule. Concentrations of 5-HT and dopamine were quantified using high-pressure liquid chromatography coupled to electrochemical detection (HPLC-ECD). Dialysate samples were injected onto a microbore HPLC column coupled to an EC detector with a glassy carbon electrode set at +650 mV relative to Ag/AgCl reference. Mobile phase was pumped at 60 µl/min. Chromatographic data were exported to an Empower software system (Waters, Milford, MA) for peak identification, integration, and analysis.

Uptake and Release Assay in HEK293 Cells

The uptake and release assays in HEK293 cells were carried out as previously described (Hofmaier *et al*, 2014). For uptake assays, cells were washed twice with Krebs HEPES buffer. Test drugs were added to cells for 5 min allowing equilibration with transporters. Subsequently, [^{3}H]5-HT and [^{3}H]dopamine were added, and the reaction was stopped after allowing uptake for 1 min. The uptake was terminated by washing with 500 µl of ice-cold Krebs HEPES buffer, cells were lysed with 500 µl of 1% sodium dodecyl sulfate, and tritium was counted on a Packard 2300 TR TriCarb Liquid Scintillation Analyzer. For release studies, HEK293 cells expressing hSERT or hDAT were grown overnight on round glass coverslips (5-mm diameter, 40 000 cells per coverslip) placed in a 96-well plate and preloaded with 0.4 µM [^{3}H]5HT or 0.03 µM [^{3}H]MPP+ for 20 min at 37 °C in a final volume of 0.1 ml/well. Coverslips were transferred to small chambers (0.2 ml) and superfused with Krebs HEPES buffer (25 °C, 0.7 ml/min). The 40 min baseline for efflux of radioactivity was followed by addition of test drugs and collection of fractions every 2 min. The experiment was terminated by lysis of the cells with 1% sodium dodecyl sulfate and counted.

Electrophysiological Recordings in *X. laevis* Oocytes

Electrophysiology recordings were performed as recently described (Baumann *et al*, 2014). Briefly, the plasmid containing hSERT was linearized and *in vitro* transcription was carried out using a T7 RNA polymerase Kit mMessage mMachine (Ambion, Life Technologies, Grand Island, NY). Stage V–VI oocytes were obtained from *X. laevis* and transferred to calcium-free Ringer's solution. The oocytes were separated into smaller lobes containing 3 to 5 oocytes and defolliculated by enzymatic digestion with collagenase from *Clostridium histolyticum* (1 mg/ml) for 60 min. Oocytes were selected and transferred to Ringer's solution. Oocytes were kept at 18 °C in Ringer's solution containing 2.5 mM sodium pyruvate, 100 µg/ml penicillin, and 100 µg/ml streptomycin. In each oocyte, 10 ng of the prepared hSERT RNA was microinjected. The oocytes were maintained for 7–10 days for functional studies, and solution was changed twice daily. A CA-1B high-performance oocyte clamp was employed for the measurements. The recorded signal was digitized with Digidata 13222A (Axon Instruments, Molecular Devices, Sunnyvale, CA). An Intel PC running pCLAMP 9.2 (Axon Instruments) was used for acquisition. Borosilicate glass capillaries were pulled to a final resistance of 0.4–1.2 MΩ and filled with 3 M KCl. Oocytes were impaled and the membrane potential was clamped to a holding potential of −60 mV. For continuous superfusion with ND100 solution (100 mM NaCl, 2 mM KCl, 1 mM $CaCl_2$, 1 mM $MgCl_2$, 10 mM HEPES, pH adjusted to 7.4 with NaOH), a gravity-driven superfusion system was used. Recordings were started after a stable current baseline was established. The current was sampled with 100 Hz and low pass filtered with 20 Hz.

Ligand and Protein Model Preparation

The ligand structures were built as (*S*)-enantiomers in protonated form using the software MOE (Molecular Operating Environment (MOE), Montreal, QC, Canada). The recently crystallized *Drosophila* DAT, in the outward facing conformation in complex with nortriptyline ($dDAT_{cryst}$), was used as a template for transporter modeling (Penmatsa *et al*, 2013). dDAT displays close to 70% sequence homology with hSERT, hDAT, and hNET in the substrate-binding pocket. Sequence alignment was performed using ClustalX (Thompson *et al*, 2002). Nonstructural waters were removed from the $dDAT_{cryst}$ structure and 250 homology models of each of the human transporters in complex with nortriptyline were created using Modeller 9.11 (Sali *et al*, 1995). Nortriptyline has dissociation constants (K_D) of 18 nM at hSERT, 1140 nM at hDAT, and 4.4 nM at hNET (Tatsumi *et al*, 1997). The models with the highest 'Discrete Optimization of Protein Energy' (DOPE) score showed no

disallowed dihedrals near the central binding site and were protonated at pH 7 using the Protonate3D tool in MOE. Nortriptyline and residues within a radius of 5 Å were energy minimized using a distance-dependent dielectric constant of 2 (Hou *et al*, 2011) to 80 in the OPLS-AA force field (Jorgensen *et al*, 1996).

Docking of 4-MEC and 4-MePPP

In order to determine the influence of the SERT Thr439 conformation on ligand placement, the side chain was rotated by 180° along its C_α–C_β bond. The binding site topology was optimized by energy minimization of nortriptyline (or Thr439 in SERT) as noted above for dDAT (Hou *et al*, 2011; Jorgensen *et al*, 1996). The transporter–ligand complexes were loaded into the docking software GOLD 5.2 (Jones *et al*, 1997) that uses a genetic algorithm to obtain poses nondeterministically. Waters were removed and the binding site was defined as the center of mass of the inhibitor. The cathinone substructure was used for setting restraints, whereby the cationic nitrogen was forced to be within 2–4 Å to the Tyr95/Phe76 (SERT/DAT) backbone carbonyl oxygen. This is in analogy to the positive partial charge density of antidepressant ligands in $dDAT_{cryst}$ and in the humanized leucine transporter structures (Wang *et al*, 2013). Binding modes were generated 50 times per ligand using GoldScore with maximum search efficiency, and the poses retrieved were clustered based on their placement into specific subpockets.

Data Analysis and Statistics

For uptake and release assays, the data from three experiments were fit to a dose–response curve equation, and IC_{50} or EC_{50} values were calculated using GraphPad Prism. For microdialysis experiments, the first three samples collected were considered baseline samples and all subsequent monoamine measures were expressed as a percentage of the mean of this baseline. Effects of drugs on dialysate 5-HT and dopamine were evaluated using two-way ANOVA (treatment × time) followed by Bonferroni *post hoc* tests at specific time points after drug injection. For transporter-mediated currents, the comparison of the maximum currents across drugs was analyzed by one-way ANOVA with Tukey's *post hoc* test. $P<0.05$ was chosen as the minimum criterion for statistical significance.

RESULTS

Effects of 4-MEC and 4-MePPP on DAT and SERT in Synaptosomes

Figure 2 depicts the effects of mephedrone, 4-MEC, and 4-MePPP in transporter assays carried out in rat brain synaptosomes. The ability of test drugs to inhibit uptake of [^{3}H]5-HT and [^{3}H]dopamine is shown in Figure 2a and b, respectively. Mephedrone and 4-MEC displayed nearly equal potency at inhibiting uptake at SERT ($IC_{50}=\sim$500 nM) and at DAT ($IC_{50}=\sim$800 nM). In contrast, 4-MePPP was much more potent as an inhibitor at DAT when compared with SERT, with an $IC_{50}=215\pm13$ nM at DAT *vs* $IC_{50}=>10\,000$ nM at SERT. Thus, mephedrone and

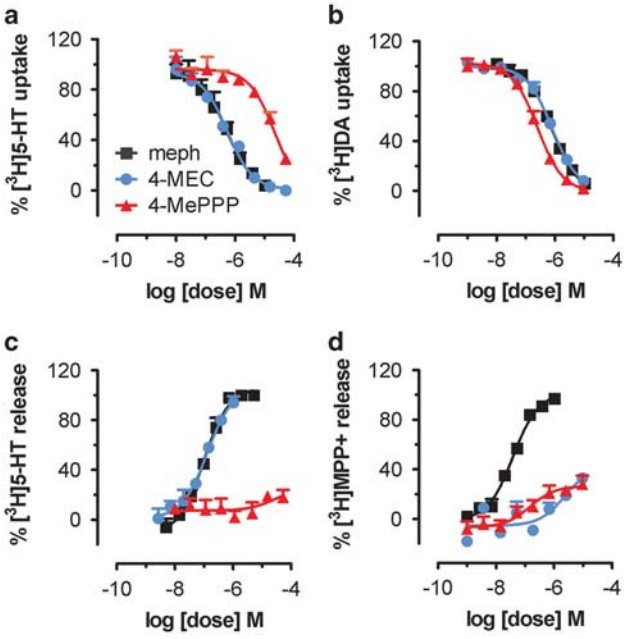

Figure 2 Effects of 4-MEC and 4-MePPP on transporter-mediated uptake and release in rat brain synaptosomes. Inhibition of [^{3}H]5-HT uptake (a) and [^{3}H]DA uptake (b) by 4-MEC, 4-MePPP, and mephedrone. Release of preloaded [^{3}H]5-HT from SERT (c) and [^{3}H]MPP + from DAT (d) evoked by 4-MEC, 4-MePPP, and mephedrone. Data are mean ± SD for $N=3$ separate experiments performed in triplicate.

4-MEC are nonselective uptake blockers, whereas 4-MePPP is 40-fold selective for DAT over SERT. As discussed in previous publications (Baumann *et al*, 2012, 2013a), the effects of drugs in uptake inhibition assays cannot reveal whether drugs are acting as transporter blockers or substrates, and hence we next tested the effects of drugs in the synaptosome release assay. The ability of test drugs to evoke release of preloaded [^{3}H]5-HT and [^{3}H]MPP + is shown in Figure 2c and d, respectively. Mephedrone and 4-MEC displayed similar potency in their ability to evoke [^{3}H]5-HT release from SERT ($EC_{50}=\sim$100 nM), whereas 4-MePPP was inactive as a releaser at SERT. Interestingly, mephedrone was a fully efficacious releaser of [^{3}H]MPP + at DAT ($EC_{50}=39\pm3$ nM), but 4-MEC and 4-MePPP were both inactive in this regard.

Effects of 4-MEC and 4-MePPP on Neurochemistry and Behavior *in vivo*

Figure 3 depicts the effects of i.v. administration of 4-MEC and 4-MePPP on neurochemistry and locomotor activity in rats undergoing microdialysis in the nucleus accumbens. Figure 3a demonstrates a main effect of drug treatment on extracellular 5-HT ($F_{2,16}=34.38$, $p<0.0001$). 4-MEC produced significant dose-related increases in extracellular 5-HT, with 1 mg/kg producing a 3.2-fold elevation above baseline, and 3 mg/kg producing a 6.9-fold elevation. In marked contrast, 4-MePPP had no significant effect on extracellular 5-HT at either dose tested. Figure 3b shows a main effect of drug treatment on extracellular dopamine ($F_{2,16}=27.26$, $p<0.0001$), and the effects of 4-MEC and 4-MePPP on dopamine were opposite to the changes in 5-HT. More specifically, 4-MePPP produced dose-related

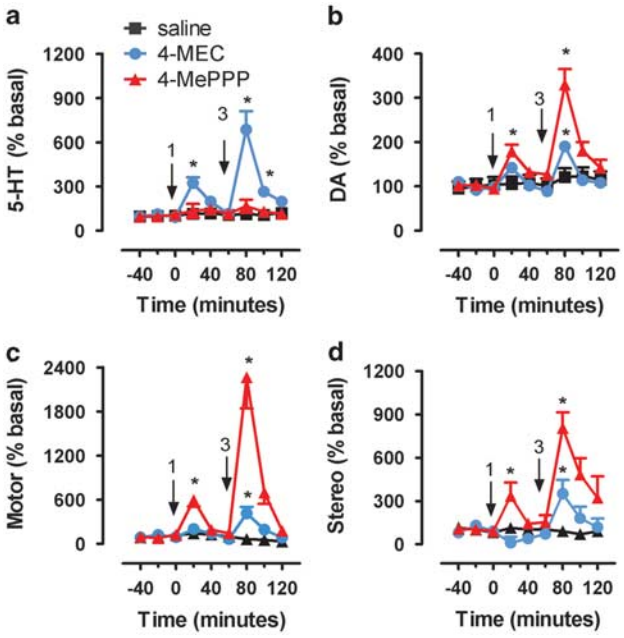

Figure 3 Effects of i.v. administration of saline, 4-MEC, and 4-MePPP on neurochemistry and behavior in rats undergoing microdialysis in nucleus accumbens. Effects of saline, 4-MEC, and 4-MePPP on dialysate 5-HT (a) and dialysate dopamine (DA) (b). Effects of saline, 4-MEC, and 4-MePPP on forward locomotion (Motor) (c) and stereotypic movements (Stereo) (d). Data are mean ± SEM expressed as % baseline for $N = 6$–7 rats/group. Arrows indicate time of injections and numbers indicate i.v. mg/kg doses. *$P < 0.05$ compared with saline-injected control at specific time points.

increases in extracellular dopamine, with 1 mg/kg producing a 1.8-fold elevation above baseline and 3 mg/kg producing a 3.3-fold elevation. 4-MEC, on the other hand, produced no effect on dopamine at 1 mg/kg, but a 1.9-fold increase after the 3 mg/kg dose. Figure 3c and d demonstrate that drug treatment had main effects on forward locomotion ($F_{2,16} = 40.66$, $p < 0.0001$) and stereotypy ($F_{2,16} = 20.98$, $p < 0.0001$). 4-MEC produced small increases in both parameters, but only after the high dose; 4-MePPP produced striking dose-related effects that were much greater than the effects of 4-MEC. Importantly, the motor effects of both drugs were short-lived and quickly returned to baseline values by 60 min after injection.

Effects of 4-MEC and 4-MePPP on Human Transporters Expressed in Cells

Based on the results from rat experiments, we wished to explore the molecular mechanism of action for 4-MEC and 4-MePPP in greater detail, and hence the effects of these drugs were examined in HEK293 cells stably expressing human transporters. Figure 4a and b show the effects of test drugs on uptake inhibition in cells expressing human SERT (hSERT) or human DAT (hDAT), respectively. In agreement with findings from synaptosomes, 4-MEC showed nonselective inhibition of uptake, with IC_{50} values of 10.9 ± 2.2 μM at hSERT and 3.9 ± 0.4 μM at hDAT. In contrast, 4-MePPP displayed much higher potency at inhibiting uptake at hDAT ($IC_{50} = 1.08 \pm 0.1$ μM) when compared with hSERT ($IC_{50} = 126 \pm 36$ μM). Next, we compared the effects of 4-MEC and 4-MePPP on transporter-mediated efflux using superfusion methods. In these experiments, the time-dependent efflux of [^{3}H]5-HT through hSERT and [^{3}H]MPP+ through hDAT was assessed in the presence or absence of monensin (10 μM), an ionophore that dissipates the normal Na+ gradient across cell membranes and selectively enhances the efflux caused by transporter substrates (Baumann *et al*, 2013b; Scholze *et al*, 2000). Thus, monensin can be used to discriminate the effects of transporter substrates *vs* blockers. Figure 4c shows that 4-MEC (10 μM) induced efflux of [^{3}H]5-HT but 4-MePPP did not. Importantly, the efflux of [^{3}H]5-HT produced by 4-MEC was dramatically enhanced in the presence of monensin, confirming that 4-MEC is a substrate at hSERT. Figure 4d demonstrates that 4-MEC and 4-MePPP both induced modest efflux of [^{3}H]MPP+ at hDAT, but in neither case was this response altered by monensin.

Effects of 4-MEC and 4-MePPP on SERT-Mediated Currents

As a final test to confirm that 4-MEC and 4-MePPP display differential effects at SERT, we examined transporter-mediated currents in oocytes expressing hSERT (Baumann *et al*, 2014). For these experiments, the effects of drugs were only evaluated in SERT-expressing cells as neither drug elicited substrate activity at DAT. Figure 5a and b depict the effects of 4-MEC and 4-MePPP on SERT-mediated currents, respectively. 4-MEC evoked robust dose-related inward currents that followed a bell-shaped dose response. The greatest magnitude of current produced by 4-MEC (30 μM) was nearly equivalent to that produced by 10 μM 5-HT. Consistent with the profile of a transporter blocker, 4-MePPP did not elicit any transporter mediated-current at doses up to 100 μM. Figure 5c shows the current-inducing effects of 4-MEC and 4-MePPP when normalized to the effects of 10 μM 5-HT. This figure highlights the bell-shaped dose response for 4-MEC and the lack of effect for 4-MePPP.

Computational Docking with 4-MEC and 4-MePPP

The differential effects of 4-MEC and 4-MePPP at SERT prompted us to employ a molecular docking approach to explore the structural peculiarities between SERT and DAT, and possible differences in the binding modes of the two compounds. The binding modes of the two cathinones in the hSERT and hDAT homology models were analogous to the LeuBAT inhibitor binding mode (Wang *et al*, 2013), whereby the aromatic rings are placed in the previously reported subpocket B (Andersen *et al*, 2010; Seddik *et al*, 2013). 4-MEC and 4-MePPP only differ in their *N*-substitution, with 4-MePPP having a sterically more demanding substituent (pyrrolidine ring *vs* ethyl chain). Remarkably, this difference causes a >100-fold decrease in the affinity of 4-MePPP for SERT *vs* DAT. It seems unlikely that this is solely due to differences in the interaction of the cathinone nitrogen with distinct amino acids, as the only difference in the binding site is F76/Y95 (Table 1). Figure 6 depicts docking poses of 4-MEC and 4-MePPP in hDAT (Figure 6a) and hSERT (Figure 6b and c). Although both compounds show analogous poses in hDAT, which is

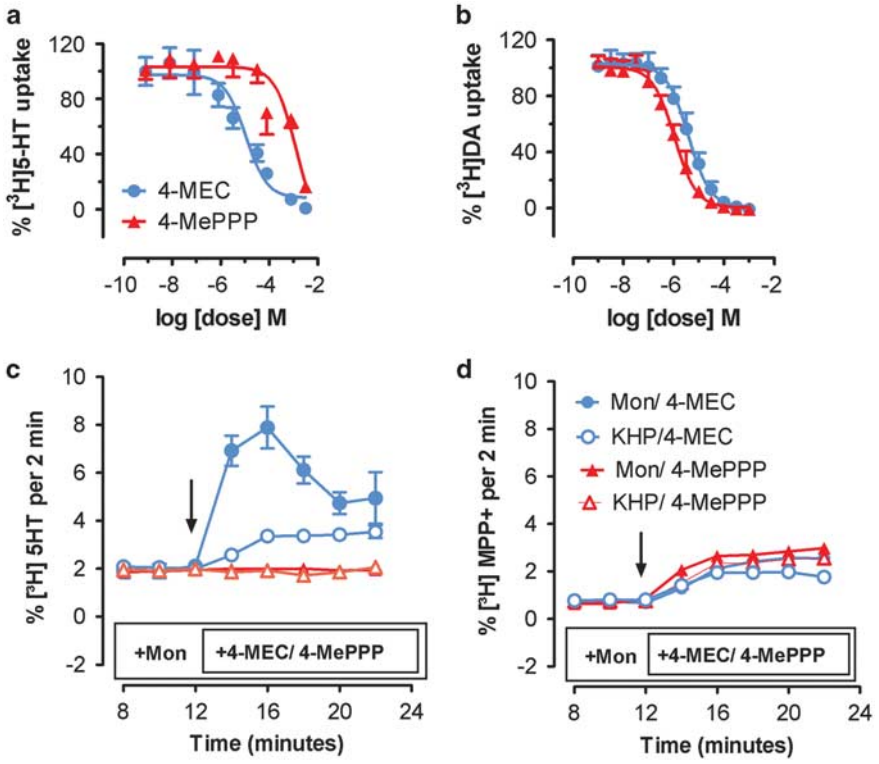

Figure 4 Inhibition of uptake and stimulation of efflux produced by 4-MEC and 4-MePPP in HEK293 cells stably expressing hSERT and hDAT. Inhibition of [^{3}H]5-HT uptake by hSERT (a) and [^{3}H]DA uptake by hDAT (b) in cells. Efflux of [^{3}H]5-HT (c) and [^{3}H]MPP+ (d) via hSERT and hDAT, respectively. Effects of 10 μM 4-MEC and 10 μM 4-MePPP on efflux were carried out in the presence of Krebs HEPES buffer (KHP) or 10 μM monensin. Arrows show the administration of 4-MEC/4-MePPP. Data are mean ± SD for $n = 3$ separate experiments.

supported by their similar effects at inhibiting [^{3}H]dopamine uptake, the placement in hSERT is less consistent. Importantly, this inconsistency only affects 4-MePPP, which shows two clusters, with the aromatic moiety being placed either deeper in subpocket B or in subpocket C. The latter configuration seems unlikely, as no transporter inhibitor was found to occupy this site in LeuBATs. Thus, the ambiguous positioning of 4-MePPP in hSERT might be because of its larger *N*-pyrrolidino substituent that forces a slight shift deeper into subpocket B when compared with the case for 4-MEC. In the case of subpocket B of hDAT, there is sufficient space to accommodate 4-MePPP because of the smaller side chains present (ie, Ala423, Val152, and Gly153); subpocket B in hSERT is formed by bulkier amino-acid side chains (Thr439, Ile172, and Ala173). In particular, Thr439 might be responsible for steric repulsion of 4-MePPP in hSERT, rendering the complex less stable. Thus, two different side chain conformations of Thr439 were probed and similar docking patterns were found (Figure 6b and c), whereby either the polar hydroxyl group or a proximal methyl group repels the positioning of 4-MePPP. In addition, reducing the flexibility of Thr439 upon binding of 4-MePPP also leads to an entropically unfavorable contribution to the binding free energy.

DISCUSSION

A major goal of our study was to determine the mechanism of action and pharmacological effects of the mephedrone analogs, 4-MEC and 4-MePPP. In previous publications, we and others have shown that mephedrone is a nonselective substrate for monoamine transporters, thereby causing the release of 5-HT, dopamine, and norepinephrine (Baumann *et al*, 2012; Eshleman *et al*, 2013; Simmler *et al*, 2013). Once legislation was enacted to render mephedrone illegal, 4-MEC and 4-MePPP began appearing in the recreational drug marketplace (Ayres and Bond, 2012; Brandt *et al*, 2011; Leffler *et al*, 2014), and 4-MEC has been associated with adverse medical consequences leading to death (Gil *et al*, 2013; Rojek *et al*, 2014). The present *in vitro* findings from rat brain synaptosomes show that 4-MEC displays unique activity as a SERT substrate/DAT blocker, whereas 4-MePPP is a DAT blocker with little activity at SERT. Consistent with synaptosome data, i.v. administration of 4-MEC induces predominant elevations in brain extracellular 5-HT, whereas 4-MePPP induces selective elevations in dopamine. Importantly, the effects of 4-MEC and 4-MePPP in cells expressing human transporters agree with the findings in rat brain synaptosomes. Using molecular modeling techniques, we provide evidence that differences in amino-acid composition of the ligand-binding pockets of hDAT and hSERT can explain the ability of 4-MePPP to selectively interact with hDAT. Overall, our findings reinforce the concept that subtle changes in cathinone structure can dramatically alter drug pharmacology.

One of the most interesting findings from our experiments in synaptosomes is the unusual transporter activity of 4-MEC as compared with mephedrone. 4-MEC represents a rare example of a compound that exhibits substrate

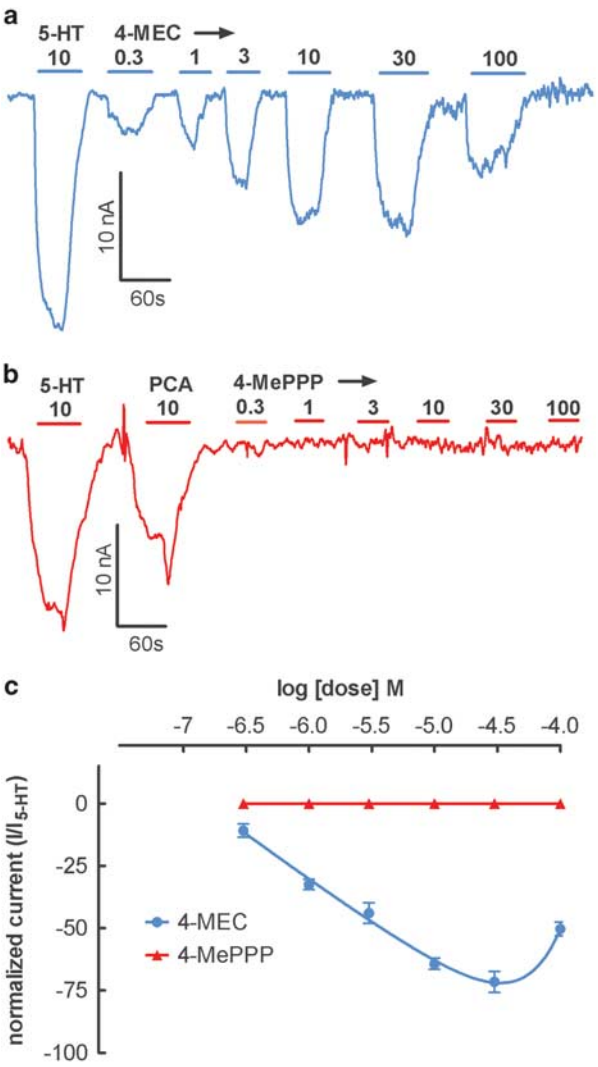

Figure 5 Dose–response effects of 4-MEC and 4-MePPP on SERT-generated currents in *Xenopus* oocytes. Representative electrophysiological traces for 4-MEC (a) and 4-MePPP (b). Concentration–response curves, pooled from different oocytes for 4-MEC and 4-MePPP (c). Data in (c) are mean ± SEM for $n = 8$ oocytes from two independent preparations. Maximal current for 4-MEC was measured at 30 μM and no current was observed for 4-MePPP.

Table 1 Residues Surrounding the Cationic Nitrogen of Cathinone-Type Ligands in Human SERT and DAT

SERT	Y95	A96	D98	F335	S336	G338
DAT	F76	A77	D79	F320	S321	G323

Abbreviations: A, alanine; D, aspartate; F, phenylalanine; G, glycine; S, serine; Y, tyrosine.

activity at SERT and blocker activity at DAT, a profile that we call 'hybrid' transporter activity. Simmler *et al* (2014) reported data consistent with our findings, showing 4-MEC is a 5-HT releaser but a blocker at hDAT and hNET. Although this profile is unusual, it has been reported previously (Blough *et al*, 2014; Simmler *et al*, 2014; Yu *et al*, 2000). Yu *et al* (2000) described SERT substrate/DAT blocker activity for *N*-ethylaminopropiophenone (ie, *N*-ethylcathinone), a bioactive metabolite of the clinically available appetite suppressant diethylpropion. 4-MEC and *N*-ethylcathinone display similar chemical structures, and hence it appears that extension of the *N*-alkyl chain of cathinone compounds, from *N*-methyl to *N*-ethyl, is sufficient to convert activity at DAT from a substrate (eg, mephedrone) to a blocker (eg, 4-MEC). In contrast, mephedrone and 4-MEC display nearly equivalent effects

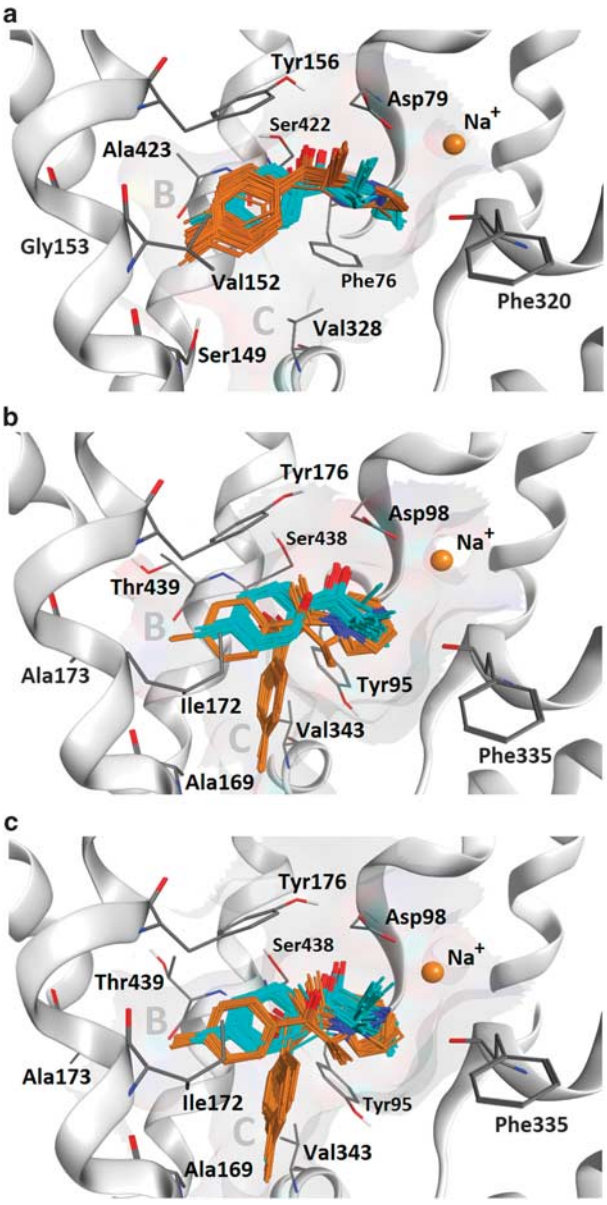

Figure 6 Central binding site of (a) DAT with docking poses of 4-MEC (cyan) and 4-MePPP (orange), (b) SERT with the Thr439 hydroxyl pointing toward the S1 site, and (c) SERT with the Thr439 methyl pointing toward the S1 site. The poses of both ligands in DAT are very consistent whereby the 4-methyl group points into subsite B. The same consistency is found in SERT for 4-MEC, but not for 4-MePPP, presumably because of an unfavorable fit into this subpocket forced by the larger substituent on the nitrogen atom.

as 5-HT releasers, suggesting that minor changes in *N*-alkyl chain length do not alter substrate activity at SERT. The data with 4-MEC and *N*-ethylcathinone illustrate the close structural resemblance among synthetic cathinones in the 'street drug' marketplace and those being prescribed clinically, such as diethylpropion and bupropion (Carroll *et al*, 2014; Cercato *et al*, 2009). Indeed, Blough *et al* (2014) have proposed that hybrid transporter compounds based on the *N*-cyclopropylcathinone structure could have value in the treatment of substance use disorders. Future studies should be carried out to examine the possible therapeutic potential of hybrid transporter ligands.

Extending the *N*-alkyl chain of 4-MEC to form the pyrrolidine ring structure of 4-MePPP has marked effects on pharmacology, converting the compound to a DAT-selective transporter blocker. In fact, the *in vitro* pharmacology of 4-MePPP resembles that of pyrrolidinophenone compounds like pyrovalerone and MDPV rather than mephedrone (Baumann *et al*, 2013b; Cameron *et al*, 2013; Kolanos *et al*, 2013; Marusich *et al*, 2014). Meltzer *et al* (2006) reported that pyrovalerone analogs are potent blockers at DAT and NET with little influence on SERT. More recently, we demonstrated that MDPV, α-PVP, and related pyrrolidinophenones are potent and selective blockers at DAT and NET in rat brain synaptosomes (Baumann *et al*, 2013b; Marusich *et al*, 2014). Kolanos *et al* (2013) examined the effects of MDPV and α-PVP in *Xenopus* oocytes expressing hDAT and found that these compounds do not induce inward DAT-mediated currents, consistent with the present results showing that 4-MePPP does not display DAT substrate activity. Collectively, the *in vitro* data indicate that cathinone analogs that possess a pyrrolidine ring structure, or perhaps other bulky *N*-alkyl substituents, will function as selective uptake blockers at DAT and NET.

The present microdialysis results show that transporter activity of 4-MEC and 4-MePPP strongly influences the *in vivo* neurochemical and behavioral effects of the drugs. Administration of 4-MEC to rats produces predominant increases in extracellular 5-HT with small increases in extracellular dopamine, consistent with its hybrid transporter actions. The *in vivo* neurochemical profile of 4-MEC mimics the effects of mephedrone and methylone (Baumann *et al*, 2012; Kehr *et al*, 2011; Wright *et al*, 2012), but 4-MEC is less potent and has weaker effects on dopamine when compared with other ring-substituted cathinones. Previous studies have shown that 5-HT-releasing actions of amphetamines and cathinones can dampen dopamine-mediated locomotor and reinforcing effects in rats (Baumann *et al*, 2011; Bonano *et al*, 2014), and hence it might be predicted that 4-MEC has weak stimulant properties. In contrast, 4-MePPP produces selective increases in extracellular dopamine and robust locomotor activation. The *in vivo* neurochemical profile of 4-MePPP mimics the effects of MDPV (Baumann *et al*, 2013b), but 4-MePPP is 10-fold less potent and its effects are short-lived. It is well established that elevations in extracellular dopamine in the nucleus accumbens are correlated with the magnitude of locomotor activation produced by stimulant drugs (Baumann *et al*, 2011; Zolkowska *et al*, 2009), and the hyperactivity produced by 4-MePPP agrees with the reported locomotor effects of MDPV and related pyrrolidinophenones (Aarde *et al*, 2013b; Fantegrossi *et al*, 2013; Gatch *et al*, 2013; Marusich *et al*, 2014; Marusich *et al*, 2012). The selective increase in extracellular dopamine produced by 4-MePPP suggests that this drug will be readily self-administered (Aarde *et al*, 2013b; Watterson *et al*, 2014).

Our experiments in synaptosomes provide the advantage of rapid drug screening in native tissue, whereas experiments in cells allow a more detailed assessment of drug–transporter interactions. Here we examined the effects of 4-MEC and 4-MePPP in cells expressing hDAT and hSERT. In uptake inhibition assays, 4-MEC acts as a nonselective transporter blocker whereas 4-MePPP is selective for hDAT, in agreement with the findings in synaptosomes. It is noteworthy that IC_{50} values for 4-MEC and 4-MePPP in transporter-expressing cells are somewhat higher (ie, apparent lower potency) than those determined in synaptosomes. Differences in assay procedures used for synaptosomes *vs* cells could explain these differences. In addition, the complement of accessory membrane proteins present in synaptosomes may not be present in nonneuronal cell systems (Wilhelm *et al*, 2014), and this could influence absolute potency values. In the superfusion assays, 4-MEC evokes 5-HT efflux whereas 4-MePPP does not. The 5-HT efflux produced by 4-MEC is markedly potentiated by monensin, an ionophore that dissipates $Na+$ gradients across cell membranes enhancing intracellular $Na+$ (Hofmaier *et al*, 2014). We have shown previously that monensin augments transporter-mediated efflux caused by substrates but not blockers (Baumann *et al*, 2013b; Hofmaier *et al*, 2014; Scholze *et al*, 2000), and hence the findings with monensin reported here provide decisive evidence that 4-MEC is a SERT substrate. 4-MEC and 4-MePPP also evoke modest efflux from hDAT, but these effects are not altered by monensin, confirming that neither drug is a DAT substrate. Our data from cells expressing human transporters reinforce the findings from rat brain tissue, and serve to validate the translational value of studying cathinone-type drugs in rodent models.

Perhaps the most sophisticated method for examining the interactions of drugs with monoamine transporters involves the measurement of transporter-mediated ionic currents (Sitte *et al*, 1998; Sonders *et al*, 1997). Because the SLC6 transporters co-transport $Na+$ ions along with substrate, inward depolarizing current is generated during translocation of substrate from the outside of the cell to the inside (Kristensen *et al*, 2011). Thus, measuring the electrophysiological signature of transporter ligands can give direct information about the molecular mechanism of action for these substances. We found that 4-MEC, but not 4-MePPP, induces inward current analogous to prototypical SERT substrates like fenfluramine and *p*-chloroamphetamine (Baumann *et al*, 2014; Gobbi *et al*, 2008). Moreover, the current dose–response relationship with 4-MEC appears bell shaped, similar to the effects of other transporter substrates. The decrease in current measured at the highest concentration of 4-MEC (ie, 100 μM) is likely because of the intracellular accumulation of substrate that tends to inhibit SERT-mediated current (Adams and DeFelice, 2003). We have previously shown that the magnitude of inward current produced by SERT substrates may be involved in the persistent 5-HT depletions caused by these drugs in rats

(Baumann *et al*, 2014; Gobbi *et al*, 2008). Our electrophysiological findings with 4-MEC suggest that future studies should examine the potential for this drug to produce long-term serotonergic deficits in rodent models.

Based on the present structure–activity data, a crucial question arises: how does extending the *N*-alkyl chain of mephedrone produce major changes in pharmacology? We carried out molecular modeling studies to address this question, with specific reference to the structural differences between 4-MEC (*N*-ethyl) and 4-MePPP (*N*-containing pyrrolidine ring) that lead to marked loss of activity at SERT for 4-MePPP. Using a computational docking approach based on $dDAT_{cryst}$ (Penmatsa *et al*, 2013), we show that the binding subpocket B of SERT is smaller because of bulkier amino-acid side chains when compared with the binding subpocket of DAT. Therefore, it is tempting to speculate that SERT is less able to accommodate the bulky pyrrolidine ring structure of 4-MePPP when compared with the smaller *N*-ethyl chain of 4-MEC. The present modeling approach may have key predictive value when attempting to understand transporter selectivity of new cathinone analogs as they appear in the recreational drug marketplace.

To summarize, the structure–activity data reported here demonstrate that changing the *N*-alkyl substituent of cathinone drugs can profoundly influence their pharmacology. 4-MEC is a SERT substrate/DAT blocker with predominant 5-HT-releasing effects *in vivo*. The serotonergic actions of 4-MEC may reduce its stimulant properties but enhance its propensity for producing long-term 5-HT deficits. 4-MePPP is a selective DAT blocker with robust locomotor stimulant effects *in vivo*. Although our study focused on the effects of drugs on DAT and SERT, it seems likely that 4-MEC and 4-MePPP interact with NET as well (eg, see Simmler *et al*, 2014). Future studies should examine the neurotoxic potential, abuse liability, and noradrenergic actions of 4-MEC, 4-MePPP, and other newly emerging cathinone derivatives.

FUNDING AND DISCLOSURE

HHS has received honoraria for lectures and consulting from Lundbeck, Ratiopharm, Roche, Sanofi-Aventis, and Serumwerk Bernburg. The other authors declare no conflict of interest.

ACKNOWLEDGEMENTS

This research was supported by the Austrian Research Fund/FWF grants F3506 and W1232 to HHS and the Intramural Research Program of the NIDA, NIH, grant DA000523-07 to MHB.

REFERENCES

Aarde SM, Angrish D, Barlow DJ, Wright MJ Jr, Vandewater SA, Creehan KM *et al* (2013a). Mephedrone (4-methylmethcathinone) supports intravenous self-administration in Sprague-Dawley and Wistar rats. *Addict Biol* **18**: 786–799.

Aarde SM, Huang PK, Creehan KM, Dickerson TJ, Taffe MA (2013b). The novel recreational drug 3,4-methylenedioxypyrovalerone (MDPV) is a potent psychomotor stimulant: self-administration and locomotor activity in rats. *Neuropharmacology* **71**: 130–140.

Adams SV, DeFelice LJ (2003). Ionic currents in the human serotonin transporter reveal inconsistencies in the alternating access hypothesis. *Biophys J* **85**: 1548–1559.

Andersen J, Olsen L, Hansen KB, Taboureau O, Jorgensen FS, Jorgensen AM *et al* (2010). Mutational mapping and modeling of the binding site for (S)-citalopram in the human serotonin transporter. *J Biol Chem* **285**: 2051–2063.

Ayres TC, Bond JW (2012). A chemical analysis examining the pharmacology of novel psychoactive substances freely available over the internet and their impact on public (ill)health. Legal highs or illegal highs? *BMJ Open* **2**: e000977.

Baumann MH, Ayestas MA Jr, Partilla JS, Sink JR, Shulgin AT, Daley PF *et al* (2012). The designer methcathinone analogs, mephedrone and methylone, are substrates for monoamine transporters in brain tissue. *Neuropsychopharmacology* **37**: 1192–1203.

Baumann MH, Bulling S, Benaderet TS, Saha K, Ayestas MA, Partilla JS *et al* (2014). Evidence for a role of transporter-mediated currents in the depletion of brain serotonin induced by serotonin transporter substrates. *Neuropsychopharmacology* **39**: 1355–1365.

Baumann MH, Clark RD, Woolverton WL, Wee S, Blough BE, Rothman RB (2011). *In vivo* effects of amphetamine analogs reveal evidence for serotonergic inhibition of mesolimbic dopamine transmission in the rat. *J Pharmacol Exp Ther* **337**: 218–225.

Baumann MH, Partilla JS, Lehner KR (2013a). Psychoactive "bath salts": not so soothing. *Eur J Pharmacol* **698**: 1–5.

Baumann MH, Partilla JS, Lehner KR, Thorndike EB, Hoffman AF, Holy M *et al* (2013b). Powerful cocaine-like actions of 3,4-methylenedioxypyrovalerone (MDPV), a principal constituent of psychoactive 'bath salts' products. *Neuropsychopharmacology* **38**: 552–562.

Blough BE, Landavazo A, Partilla JS, Baumann MH, Decker AM, Page KM *et al* (2014). Hybrid dopamine uptake blocker-serotonin releaser ligands: a new twist on transporter-focused therapeutics. *ACS Med Chem Lett* **5**: 623–627.

Bonano JS, Glennon RA, De Felice LJ, Banks ML, Negus SS (2014). Abuse-related and abuse-limiting effects of methcathinone and the synthetic "bath salts" cathinone analogs methylenedioxypyrovalerone (MDPV), methylone and mephedrone on intracranial self-stimulation in rats. *Psychopharmacology* **231**: 199–207.

Brandt SD, Freeman S, Sumnall HR, Measham F, Cole J (2011). Analysis of NRG 'legal highs' in the UK: identification and formation of novel cathinones. *Drug Test Anal* **3**: 569–575.

Cameron KN, Kolanos R, Solis E Jr, Glennon RA, De Felice LJ (2013). Bath salts components mephedrone and methylenedioxypyrovalerone (MDPV) act synergistically at the human dopamine transporter. *Br J Pharmacol* **168**: 1750–1757.

Carroll FI, Blough BE, Mascarella SW, Navarro HA, Lukas RJ, Damaj MI (2014). Bupropion and bupropion analogs as treatments for CNS disorders. *Adv Pharmacol* **69**: 177–216.

Cercato C, Roizenblatt VA, Leanca CC, Segal A, Lopes Filho AP, Mancini MC *et al* (2009). A randomized double-blind placebo-controlled study of the long-term efficacy and safety of diethylpropion in the treatment of obese subjects. *Int J Obes* **33**: 857–865.

Dargan PI, Sedefov R, Gallegos A, Wood DM (2011). The pharmacology and toxicology of the synthetic cathinone mephedrone (4-methylmethcathinone). *Drug Test Anal* **3**: 454–463.

De Felice LJ, Glennon RA, Negus SS (2014). Synthetic cathinones: chemical phylogeny, physiology, and neuropharmacology. *Life Sci* **97**: 20–26.

Drug Enforcement Administration (DEA), Department of Justice (2013). Establishment of drug codes for 26 substances. Final rule. *Fed Regist* **78**: 664–666.

Eshleman AJ, Wolfrum KM, Hatfield MG, Johnson RA, Murphy KV, Janowsky A (2013). Substituted methcathinones differ in transporter and receptor interactions. *Biochem Pharmacol* **85**: 1803–1815.

Fantegrossi WE, Gannon BM, Zimmerman SM, Rice KC (2013). *In vivo* effects of abused 'bath salt' constituent 3,4-methylenedioxypyrovalerone (MDPV) in mice: drug discrimination, thermoregulation, and locomotor activity. *Neuropsychopharmacology* **38**: 563–573.

Gatch MB, Taylor CM, Forster MJ (2013). Locomotor stimulant and discriminative stimulus effects of 'bath salt' cathinones. *Behav Pharmacol* **24**: 437–447.

Gil D, Adamowicz P, Skulska A, Tokarczyk B, Stanaszek R (2013). Analysis of 4-MEC in biological and non-biological material–three case reports. *Forensic Sci Int* **228**: e11–e15.

Gobbi M, Funicello M, Gerstbrein K, Holy M, Moya PR, Sotomayor R *et al* (2008). N,N-dimethyl-thioamphetamine and methylthioamphetamine, two non-neurotoxic substrates of 5-HT transporters, have scant *in vitro* efficacy for the induction of transporter-mediated 5-HT release and currents. *J Neurochem* **105**: 1770–1780.

Hadlock GC, Webb KM, McFadden LM, Chu PW, Ellis JD, Allen SC *et al* (2011). 4-Methylmethcathinone (mephedrone): neuropharmacological effects of a designer stimulant of abuse. *J Pharmacol Exp Ther* **339**: 530–536.

Hofmaier T, Luf A, Seddik A, Stockner T, Holy M, Freissmuth M *et al* (2014). Aminorex, a metabolite of the cocaine adulterant levamisole, exerts amphetamine like actions at monoamine transporters. *Neurochem Int* **73**: 32–41.

Hou T, Wang J, Li Y, Wang W (2011). Assessing the performance of the MM/PBSA and MM/GBSA methods. 1. The accuracy of binding free energy calculations based on molecular dynamics simulations. *J Chem Inf Model* **51**: 69–82.

Jones G, Willett P, Glen RC, Leach AR, Taylor R (1997). Development and validation of a genetic algorithm for flexible docking. *J Mol Biol* **267**: 727–748.

Jorgensen WL, Maxwell DS, Tirado Rives J (1996). Development and testing of the OPLS all-atom force field on conformational energetics and properties of organic liquids. *J Am Chem Soc* **118**: 11225–11236.

Kehr J, Ichinose F, Yoshitake S, Goiny M, Sievertsson T, Nyberg F *et al* (2011). Mephedrone, compared with MDMA (ecstasy) and amphetamine, rapidly increases both dopamine and 5-HT levels in nucleus accumbens of awake rats. *Br J Pharmacol* **164**: 1949–1958.

Kolanos R, Solis E Jr, Sakloth F, De Felice LJ, Glennon RA (2013). "Deconstruction" of the abused synthetic cathinone methylenedioxypyrovalerone (MDPV) and an examination of effects at the human dopamine transporter. *ACS Chem Neurosci* **4**: 1524–1529.

Kristensen AS, Andersen J, Jorgensen TN, Sorensen L, Eriksen J, Loland CJ *et al* (2011). SLC6 neurotransmitter transporters: structure, function, and regulation. *Pharmacol Rev* **63**: 585–640.

Leffler AM, Smith PB, de Armas A, Dorman FL (2014). The analytical investigation of synthetic street drugs containing cathinone analogs. *Forensic Sci Int* **234**: 50–56.

Lewin AH, Seltzman HH, Carroll FI, Mascarella SW, Reddy PA (2014). Emergence and properties of spice and bath salts: a medicinal chemistry perspective. *Life Sci* **97**: 9–19.

Lopez-Arnau R, Martinez-Clemente J, Pubill D, Escubedo E, Camarasa J (2012). Comparative neuropharmacology of three psychostimulant cathinone derivatives: butylone, mephedrone and methylone. *Br J Pharmacol* **167**: 407–420.

Marinetti LJ, Antonides HM (2013). Analysis of synthetic cathinones commonly found in bath salts in human performance and postmortem toxicology: method development, drug distribution and interpretation of results. *J Anal Toxicol* **37**: 135–146.

Marusich JA, Antonazzo KR, Wiley JL, Blough BE, Partilla JS, Baumann MH (2014). Pharmacology of novel synthetic stimulants structurally related to the "bath salts" constituent 3,4-methylenedioxypyrovalerone (MDPV). *Neuropharmacology* **87**: 206–213.

Marusich JA, Grant KR, Blough BE, Wiley JL (2012). Effects of synthetic cathinones contained in "bath salts" on motor behavior and a functional observational battery in mice. *Neurotoxicology* **33**: 1305–1313.

Meltzer PC, Butler D, Deschamps JR, Madras BK (2006). 1-(4-Methylphenyl)-2-pyrrolidin-1-yl-pentan-1-one (Pyrovalerone) analogues: a promising class of monoamine uptake inhibitors. *J Med Chem* **49**: 1420–1432.

Penmatsa A, Wang KH, Gouaux E (2013). X-ray structure of dopamine transporter elucidates antidepressant mechanism. *Nature* **503**: 85–90.

Rojek S, Klys M, Maciow-Glab M, Kula K, Strona M (2014). Cathinones derivatives-related deaths as exemplified by two fatal cases involving methcathinone with 4-methylmethcathinone and 4-methylethcathinone. *Drug Test Anal* **6**: 770–777.

Rosenbaum CD, Carreiro SP, Babu KM (2012). Here today, gone tomorrow...and back again? A review of herbal marijuana alternatives (K2, Spice), synthetic cathinones (bath salts), kratom, Salvia divinorum, methoxetamine, and piperazines. *J Med Toxicol* **8**: 15–32.

Rothman RB, Baumann MH (2003). Monoamine transporters and psychostimulant drugs. *Eur J Pharmacol* **479**: 23–40.

Sali A, Potterton L, Yuan F, van Vlijmen H, Karplus M (1995). Evaluation of comparative protein modeling by MODELLER. *Proteins* **23**: 318–326.

Scholze P, Zwach J, Kattinger A, Pifl C, Singer EA, Sitte HH (2000). Transporter-mediated release: a superfusion study on human embryonic kidney cells stably expressing the human serotonin transporter. *J Pharmacol Exp Ther* **293**: 870–878.

Seddik A, Holy M, Weissensteiner R, Zdrazil B, Sitte HH, Ecker GF (2013). Probing the selectivity of monoamine transporter substrates by means of molecular modeling. *Mol Inform* **32**: 409–413.

Simmler LD, Buser TA, Donzelli M, Schramm Y, Dieu LH, Huwyler J *et al* (2013). Pharmacological characterization of designer cathinones in vitro. *Br J Pharmacol* **168**: 458–470.

Simmler LD, Rickli A, Hoener MC, Liechti ME (2014). Monoamine transporter and receptor interaction profiles of a new series of designer cathinones. *Neuropharmacology* **79**: 152–160.

Sitte HH, Freissmuth M (2010). The reverse operation of Na(+)/Cl(-)-coupled neurotransmitter transporters–why amphetamines take two to tango. *J Neurochem* **112**: 340–355.

Sitte HH, Huck S, Reither H, Boehm S, Singer EA, Pifl C (1998). Carrier-mediated release, transport rates, and charge transfer induced by amphetamine, tyramine, and dopamine in mammalian cells transfected with the human dopamine transporter. *J Neurochem* **71**: 1289–1297.

Sonders MS, Zhu SJ, Zahniser NR, Kavanaugh MP, Amara SG (1997). Multiple ionic conductances of the human dopamine transporter: the actions of dopamine and psychostimulants. *J Neurosci* **17**: 960–974.

Spiller HA, Ryan ML, Weston RG, Jansen J (2011). Clinical experience with and analytical confirmation of "bath salts" and "legal highs" (synthetic cathinones) in the United States. *Clin Toxicol* **49**: 499–505.

Springer D, Fritschi G, Maurer HH (2003). Metabolism of the new designer drug alpha-pyrrolidinopropiophenone (PPP) and the toxicological detection of PPP and 4′-methyl-alpha-pyrrolidinopropiophenone (MPPP) studied in rat urine using gas chromatography-mass spectrometry. *J Chromatogr B Analyt Technol Biomed Life Sci* **796**: 253–266.

Springer D, Peters FT, Fritschi G, Maurer HH (2002). Studies on the metabolism and toxicological detection of the new designer

drug 4′-methyl-alpha-pyrrolidinopropiophenone in urine using gas chromatography-mass spectrometry. *J Chromatogr B Analyt Technol Biomed Life Sci* **773**: 25–33.

Steinkellner T, Freissmuth M, Sitte HH, Montgomery T (2011). The ugly side of amphetamines: short- and long-term toxicity of 3,4-methylenedioxymethamphetamine (MDMA, 'Ecstasy'), methamphetamine and D-amphetamine. *Biol Chem* **392**: 103–115.

Tatsumi M, Groshan K, Blakely RD, Richelson E (1997). Pharmacological profile of antidepressants and related compounds at human monoamine transporters. *Eur J Pharmacol* **340**: 249–258.

Thompson JD, Gibson TJ, Higgins DG (2002). Multiple sequence alignment using ClustalW and ClustalX. *Curr Protoc Bioinformatics* **Chapter 2**: Unit 2.3.

Wang H, Goehring A, Wang KH, Penmatsa A, Ressler R, Gouaux E (2013). Structural basis for action by diverse antidepressants on biogenic amine transporters. *Nature* **503**: 141–145.

Watterson LR, Kufahl PR, Nemirovsky NE, Sewalia K, Grabenauer M, Thomas BF *et al* (2014). Potent rewarding and reinforcing effects of the synthetic cathinone 3,4-methylenedioxypyrovalerone (MDPV). *Addict Biol* **19**: 165–174.

Wilhelm BG, Mandad S, Truckenbrodt S, Krohnert K, Schafer C, Rammner B *et al* (2014). Composition of isolated synaptic boutons reveals the amounts of vesicle trafficking proteins. *Science* **344**: 1023–1028.

Wright MJ Jr, Angrish D, Aarde SM, Barlow DJ, Buczynski MW, Creehan KM *et al* (2012). Effect of ambient temperature on the thermoregulatory and locomotor stimulant effects of 4-methylmethcathinone in Wistar and Sprague-Dawley rats. *PLoS One* **7**: e44652.

Yu H, Rothman RB, Dersch CM, Partilla JS, Rice KC (2000). Uptake and release effects of diethylpropion and its metabolites with biogenic amine transporters. *Bioorg Med Chem* **8**: 2689–2692.

Zolkowska D, Jain R, Rothman RB, Partilla JS, Roth BL, Setola V *et al* (2009). Evidence for the involvement of dopamine transporters in behavioral stimulant effects of modafinil. *J Pharmacol Exp Ther* **329**: 738–746.

E

Aminorex, a metabolite of the cocaine adulterant levamisole, exerts amphetamine like actions at monoamine transporters

Tina Hofmaier, Anton Luf, Amir Seddik, Thomas Stockner, Marion Holy, Michael Freissmuth, Gerhard F Ecker, Rainer Schmid, Harald H Sitte, Oliver Kudlacek

Published in *Neurochemistry International*, 73, 32-41, **2014**

My contribution to the following publication was to find out why levamisole shows selectivity for the norepinephrine transporter (NET) over the dopamine and serotonin transporter (DAT, SERT, resp.). I docked the ligands while employing the established salt-bridge restraints. The poses indicated that different aromatic residues, Tyr151 in NET and Phe155 in DAT, lining the S2 pocket could be responsible for NET-over-DAT selectivity, while NET-over-SERT selectivity would be caused by two different residues, Tyr95/Ile172 in SERT and Phe72/Val148 in NET, in the S1 pocket.

Neurochemistry International 73 (2014) 32–41

Contents lists available at ScienceDirect

Neurochemistry International

journal homepage: www.elsevier.com/locate/nci

Aminorex, a metabolite of the cocaine adulterant levamisole, exerts amphetamine like actions at monoamine transporters

Tina Hofmaier [a], Anton Luf [b], Amir Seddik [c], Thomas Stockner [a], Marion Holy [a], Michael Freissmuth [a], Gerhard F. Ecker [c], Rainer Schmid [b], Harald H. Sitte [a,*], Oliver Kudlacek [a]

[a] Institute of Pharmacology, Center for Physiology and Pharmacology, Medical University of Vienna, Waehringerstrasse 13A, 1090 Vienna, Austria
[b] Clinical Department of Laboratory Medicine, Medical University of Vienna, Waehringer Guertel 10-20, 1090 Vienna, Austria
[c] University of Vienna, Department of Medicinal Chemistry, Althanstrasse 14, 1090 Vienna, Austria

ARTICLE INFO

Article history:
Available online 1 December 2013

Keywords:
Levamisole
Aminorex
Neurotransmitter transporter
Cocaine
Adulterant

ABSTRACT

Psychostimulants such as amphetamine and cocaine are illicitly used drugs that act on neurotransmitter transporters for dopamine, serotonin or norepinephrine. These drugs can by themselves already cause severe neurotoxicity. However, an additional health threat arises from adulterant substances which are added to the illicit compound without declaration. One of the most frequently added adulterants in street drugs sold as cocaine is the anthelmintic drug levamisole. We tested the effects of levamisole on neurotransmitter transporters heterologously expressed in HEK293 cells. Levamisole was 100 and 300-fold less potent than cocaine in blocking norepinephrine and dopamine uptake, and had only very low affinity for the serotonin transporter. In addition, levamisole did not trigger any appreciable substrate efflux. Because levamisole and cocaine are frequently co-administered, we searched for possible allosteric effects; at 30 μM, a concentration at which levamisole displayed already mild effects on norepinephrine transport it did not enhance the inhibitory action of cocaine. Levamisole is metabolized to aminorex, a formerly marketed anorectic drug, which is classified as an amphetamine-like substance. We examined the uptake-inhibitory and efflux-eliciting properties of aminorex and found it to exert strong effects on all three neurotransmitter transporters in a manner similar to amphetamine. We therefore conclude that while the adulterant levamisole itself has only moderate effects on neurotransmitter transporters, its metabolite aminorex may exert distinct psychostimulant effects by itself. Given that the half-time of levamisole and aminorex exceeds that of cocaine, it may be safe to conclude that after the cocaine effect "fades out" the levamisole/aminorex effect "kicks in".

1. Introduction

Monoamine transporters for serotonin (SERT), norepinephrine (NET) and dopamine (DAT) belong to the family of Na^+/Cl^--dependent neurotransmitter transporters and remove their substrates to end synaptic transmission (Kristensen et al., 2011). Apart from this physiological role, these transporters are the targets of illicit drugs like cocaine or amphetamines (Rothman and Baumann, 2003). Amphetamines lead to a reverse action of all of these transporters and to a number of other intracellular effects which actively increase the concentration of neurotransmitters in the synaptic cleft (Sitte and Freissmuth, 2010). In contrast, cocaine raises the synaptic concentration of monoamines by inhibiting the activity of these transporters. Both classes of compounds are sold on the street market for illicit drugs at the risk of the users because both the quality and identity of the purchased drugs are without any control. This situation is alleviated by the government-supported Viennese drug prevention project 'checkit! Check your drugs', which offers cost-free and anonymous analyses of drugs. Thereby drug consumers gain information about the contents of their drug as well as possible risks of those compounds. Importantly and often to the great surprise of the user, the purchased drug does not contain the compound under the name it was sold. Recently, a survey of unknown street drugs from the 'checkit!' project revealed that a combination of amphetamine and *m*-chlorophenylpiperazine (*m*CPP) was sold under the name of methylene-dioxymethamphetamine (MDMA, 'ecstasy'; (Rosenauer et al., 2013)). Hence, the combinations of

Abbreviations: SERT, serotonin transporter; NET, norepinephrine transporter; DAT, dopamine transporter; 5-HT, serotonin; DA, dopamine; KHB, Krebs–Ringer–HEPES buffer; HPLC, high performance liquid chromatography; LC–MS, liquid chromatography–mass spectrometry.

* Corresponding author. Tel.: +43 1 40160 31323.
E-mail address: harald.sitte@meduniwien.ac.at (H.H. Sitte).

0197-0186
http://dx.doi.org/10.1016/j.neuint.2013.11.010

two active drugs are common (Schifano et al., 2011). However, drugs are also adulterated with more or less psychoactive active compounds: amphetamines are often mixed with e.g. caffeine (Vanattou-Saifoudine et al., 2012) and cocaine has been found to be mixed with a wide variety of adulterants. One prominent example of these adulterants is levamisole (Fig.1A) which has been found in most of the drug samples sold as cocaine in the past. Levamisole is used by veterinarians as an anthelmintic drug (Martin et al., 2012); its mode of action is the stimulation of ionotropic acetylcholine receptors (AChR) resulting in calcium influx causing paralysis of the worms (Levandoski et al., 2003; Rayes et al., 2004). Under the trade name Ergamisol, levamisole was also used to treat worm infections in humans but had to be withdrawn from the U.S market in 2000 because of its severe side-effects (Renoux, 1980). Most recently, several drug consumers suffered from agranulocytosis after repeated intake of cocaine adulterated ("cut") with levamisole (Muirhead and Eide, 2011; Wolford et al., 2012).

Several plausible explanations exist why levamisole is used as a cocaine-adulterant: (i) levamisole was reported to improve the mood of patients and induced insomnia and hyperalertness (Mutch and Hutson, 1991). (ii) The chemical properties of levamisole are similar to cocaine; for instance, color and melting point render both drugs almost indistinguishable without further chemical analysis (Chang et al., 2010). (iii) The use of levamisole as a drug in veterinary medicine makes it easily available and keeps the costs low (Waller, 2006). (iv) Levamisole was found to be rapidly metabolized in the human body to aminorex and related metabolites (Hess et al., 2013; Reid et al., 1998). Aminorex (Fig.1A) is an amphetamine-like agent that was detected in racehorses after levamisole administration (Barker, 2009). Moreover, aminorex was detected in human urine samples in a multitude of cocaine abusers (Bertol et al., 2011; Karch et al., 2012). Aminorex was marketed as an appetite suppressant in the mid-1960s mainly in Switzerland, Austria, and Germany; it was found to cause pronounced vasoconstriction in the pulmonary vasculature (Byrne-Quinn and Grover, 1972; Stuhlinger et al., 1969; Rothman et al., 1999) and was withdrawn in 1972 due to several cases of fatal and life-threatening pulmonary hypertension (Fishman, 1999a).

In the present work, we examined whether levamisole exerts direct effects on neurotransmitter transporters and compared these to the action of its metabolite, aminorex.

2. Materials and methods

Dulbecco's modified Eagle's medium (DMEM) and trypsin were purchased from PAA Laboratories GmbH (Pasching, Austria). Fetal calf serum was purchased from Invitrogen. [^{3}H]5-HT ([^{3}H]5-hydroxytryptamine; [^{3}H]serotonin; 28.3 μCi/mmol) and [^{3}H]DA ([^{3}H]dihydroxyphenylethylamine, [^{3}H]dopamine; 46 μCi/mmol) were purchased from PerkinElmer, Boston, MA. [^{3}H]1-Methyl-4-phenylpyridinium ([^{3}H]MPP$^+$; 85 μCi/mmol) was supplied by American Radiolabeled Chemicals (St. Louis, MO). Paroxetine was from Santa Cruz Biotechnology, mazindole, serotonin, levamisole, cocaine, aminorex, nisoxetine, D-amphetamine, and monensin were purchased from Sigma–Aldrich Co.

2.1. Sample collection and analysis

The samples used in this study were obtained from drug users participating voluntarily and anonymously in the 'checkit!' drug prevention program. Three to ten milligrams of substance were scraped into a tapered 2 ml test vial and weighed with an analytical balance. The substance was dissolved in 1 mL of methanol and vortex mixed for 1 min. The solution was centrifuged for 3 min at 10,000*g* in an Eppendorf centrifuge. Ten microliters of the supernatant were diluted with 0.4 mL of internal standard solution (trazodone 50 μg/mL dissolved in 10 mM aqueous ammonium formate buffer), 2 μl of the solution was analysed with reversed phase HPLC and LC/mass spectrometry coupling as described in a previous study (Rosenauer et al. 2013).

2.2. Uptake and release assays

The generation of HEK293 cell lines expressing the human isoforms of SERT, NET, or DAT (HEK-SERT, HEK-DAT, or HEK-NET, respectively) was described earlier (Scholze et al., 2002). HEK293 cells stably expressing either neurotransmitter transporter were seeded onto poly-*d*-lysine-coated 96-well plates (40,000 cells/well), 24 h prior to the experiment. For inhibition experiments, the specific activity of the tritiated substrate was kept constant: [^{3}H]DA, 0.1 μM; [^{3}H]MPP+, 0.015 μM; [^{3}H]5-HT, 0.1 μM. Assay conditions were used as outlined earlier (Sucic et al., 2010). In brief, the cells were washed twice with Krebs–Ringer–HEPES buffer (KHB; composition: 25 mM HEPES·NaOH, pH 7.4, 120 mM NaCl, 5 mM KCl, 1.2 mM $CaCl_2$, and 1.2 mM $MgSO_4$ supplemented with 5 mM D-glucose). Then, the diluted reference and sample compounds were added and incubated for 5 min to allow for equilibration with the transporters. Subsequently, the tritiated substrates were added and the reaction was stopped after 1 min (SERT and DAT) and 3 min (NET), respectively. Cells were lysed with 1% SDS and the released radioactivity was quantified by liquid scintillation counting. All determinations were performed in duplicate or triplicate.

For release studies, HEK-SERT, HEK-NET, or HEK-DAT cells were grown overnight on round glass coverslips (5-mm diameter, 40,000 cells per coverslip) placed in a 96-well plate and preloaded with 0.4 μM [^{3}H]dopamine, 0.1 μM [^{3}H]MPP+, or 0.4 μM [^{3}H]5-HT for 20 min at 37 °C in a final volume of 0.1 mL/well. Coverslips were then transferred to small superfusion chambers (0.2 ml) and superfused with KHB (25 °C, 0.7 ml × min^{-1}) as described (Scholze et al., 2002). A washout period of 40 min established a stable baseline for efflux of radioactivity; thereafter, substances were added and the experiment was started with the collection of fractions (2 min). At the end of the experiment, cells were lysed in 1% SDS and the released radioactivity was quantified by liquid scintillation counting.

Table 1
Prevalence of substances traced in 104 samples sold as cocaine.

Substance	Prevalence (%)
4-Methylethcathinone	1
Amphetamine	1
Benzocaine	2
Benzoylecgonine	51
cis-Cinnamoylcocaine	15
Caffeine	35
Hydroxyzine	1
Cocaine	93
Mephedrone	1
Levamisole	63
3,4-Methylenedioxy-*N*-methylamphetamine (MDMA)	2
3′,4′-Methylenedioxy-α-pyrrolidinobutyrophenone (MDPBP)	1
Lidocaine	18
Methylenedioxypyrovalerone (MDV)	2
Paracetamol	7
Phenacetin	43
Procaine	4
Tetracaine	1
trans-Cinnamoylcocaine	13
Unknown substance	14

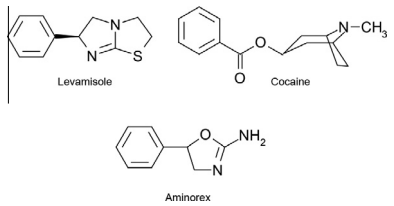

Fig. 1A. Chemical structures of cocaine, levamisole and aminorex.

The release of [^{3}H] labelled substrate was expressed as fractional rate (i.e., the radioactivity released within one fraction was expressed as a percentage of the total radioactivity present in the cells at the beginning of that fraction). Drug-induced release was calculated by subtracting the estimated basal release from total release during the first 8 min of drug exposure and is expressed as a percentage of radioactivity in the cell at the beginning of drug exposure. Data were normalized by using cpm values with no substance present (only solvent) as 100%. IC_{50} values were calculated using non-linear regression fits performed with Prism software (GraphPad 5.0, San Diego, CA, U.S.A.). Data transformed into Dixon plots were fitted by linear regression.

2.3. Homology modelling and docking

Levamisole has a pK_a value of 7. Both the neutral and protonated levamisole structures were built and minimized with QSite (version 5.8, Schrödinger, LLC) using the B3LYP method applying the 6-31G* basis set (Murphy et al., 2000). SERT and NET share over 90% sequence similarity with DAT. Homology models of human SERT and NET were generated with Modeller 9.12 (Sali and Blundell, 1993) using the validated human DAT model in the outward facing conformation (Stockner et al., 2013) as template. The best model out of the 250 generated was used for further studies. The models of SERT, DAT and NET were energy minimized with Molecular Operating Environment (MOE, 2012) applying the CHARMM22 forcefield (Brooks et al., 2009) and using position restrains of 100 kcal/mol on the backbone.

The induced fit docking protocol of the Schrödinger package was used for ligand docking into the central binding site (Glide version 5.8, Schrödinger, LLC, New York) using standard parameter setting (Sherman et al., 2005). The neutral and the protonated form of levamisole were docked as fully flexible molecules. The protonatable nitrogen of levamisole was constrained to interact with the central aspartate in the binding side, because the positive amine functional group of the endogenous substrates of SERT, DAT and NET has been

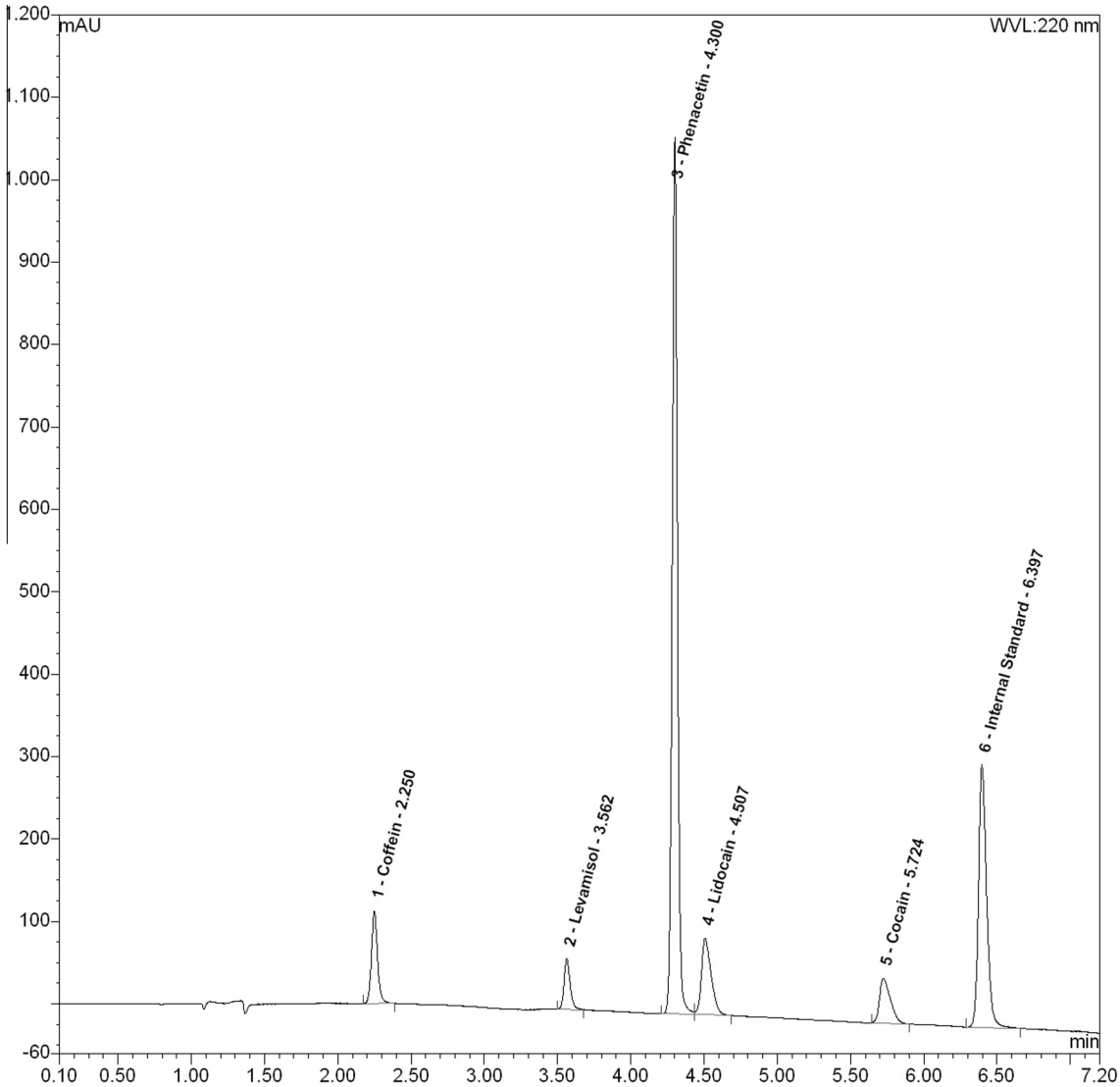

Fig. 1B. HPLC mass spectrometry. Representative HPLC chromatogram (UV detection trace at 220 nm) of a cocaine sample which was anonymously delivered to 'checkit'. Besides cocaine it also contains significant amounts of caffeine, levamisole, phenacetin, and lidocaine.

shown to interact with the respective residue. Conformations of amino acid side chains within 6 Å distance to the ligand were optimized in the OPLS-AA 2005 force field after docking. Default energy levels were employed for selection and filtering of the poses.

The pK_a value of aminorex is 7.4. Both, neutral and protonated form of aminorex were docked using the same methods as for above levamisole.

3. Results and discussion

In 2012, 104 drug samples were obtained from drug users participating voluntarily and anonymously in the 'checkit!' program which were originally purchased as "cocaine". We included all samples in our study and analyzed them by LC–MS. Two samples contained pure cocaine whereas seven samples were completely devoid of cocaine. The remaining 95 samples contained cocaine in varying amounts (Table 1). Importantly, LC–MS revealed a number of different adulterants that were mixed to cocaine: Fig. 1B shows a representative chromatogram. Among others we found paracetamol, benzoylecgonine, levamisole and phenacetin (Table 1); levamisole was present in almost two thirds of all examined samples (66 of 104 samples). The ratio between cocaine and levamisole in these samples was highly variable. While some samples contained less than 1% levamisole, one sample even displayed 20 times more levamisole than cocaine. The mean amount of levamisole was 59 ± 22% relative to cocaine. This highly variable amount of the different drugs also emphasize the risk incurred: people consume the purchased drug until they experience the desired effect (Cole et al., 2010). Hence, they are likely to also consume more of the adulterant.

3.1. Levamisole inhibits NET, DAT and SERT only at high concentrations

Given the fact that in our survey levamisole was the most commonly used adulterant of cocaine, we reasoned that it likely has pharmacological properties that render it especially useful as adulterant. This conjecture is justified, because our findings are in line with other reports: levamisole has been observed to be one of the most predominant adulterants over the past two decades (Buchanan et al., 2010; Chai et al., 2011). Hence, we first explored whether levamisole exerted an action on the three main neurotransmitter transporters SERT, NET and DAT using HEK293 cells stably expressing the individual human isoforms of these transporters. Uptake-inhibition experiments were performed with increasing concentrations of levamisole or cocaine (Fig. 2). Cocaine blocked the uptake at the expected concentrations (Ravna et al., 2003): the observed IC_{50} values were 1.8 ± 1.12 μM (SERT), 1.0 ± 1.07 μM (NET) and 0.56 ± 1.12 μM (DAT). Levamisole also reduced the uptake of substrate but at much higher concentrations. Measured IC_{50} values were 1512 ± 1.09 μM (SERT), 74.5 ± 1.12 μM (NET), 209.9 ± 1.31 μM (DAT). Based on the high IC_{50} values of levamisole, it is unlikely that the compound exerts any significant inhibitory action on the transporters *in vivo*, when administered in therapeutic doses (e.g., as an adjuvant in cancer chemotherapy). Oral administration of 50 mg levamisole gives rise to peak plasma concentrations (c_{max}) of on average 368 μg/L (equivalent to about 1.5 μM) (Gwilt et al., 2000). There is a large intraindividual variation in pharmacokinetics (Gwilt et al., 2000) and some uncertainty about nasal absorption. In addition, levamisole is a highly lipophilic substance that readily permeates the blood–brain barrier (Lin and Tsai, 2006). Therefore levamisole may possibly reach higher concentrations than cocaine in the brain and thereby lead to or support a blockage of NET and DAT, when consumed at excessive levels.

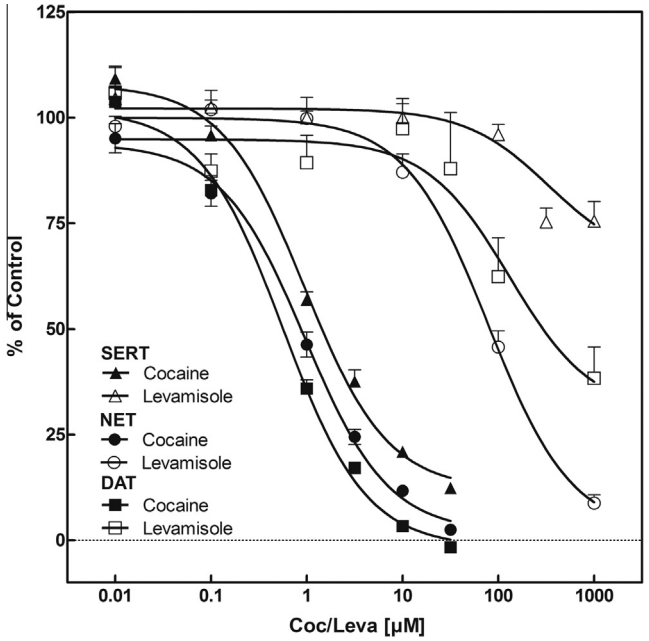

Fig. 2. Uptake inhibition experiments. Uptake inhibitions with levamisole and cocaine were performed using HEK 293 cells stably expressing human DAT, NET or SERT. Therefore cells were incubated with tritiated compounds after a prior incubation for 5 min with test compound. Uptake of substrate (SERT: 5-HT; NET: MPP+; DAT: dopamine) at increasing levamisole, respectively cocaine concentrations is expressed as percentage of the maximum uptake without any inhibitory substance. IC_{50} values for levamisole (SERT: 1512 ± 1.09 μM; NET: 74.53 ± 1.12 μM; DAT: 209.9 ± 1.31 μM) (SERT: 1.8 ± 1.12 μM; NET: 1.1 ± 1.07 μM; DAT: 0.56 ± 1.12 μM). Data are mean ± SEM of four independent experiments.

At the very least, the profile of levamisole is reminiscent of that the action of cocaine at the three transporters, with more prominent inhibition of DAT and NET, and somewhat lower affinity for SERT. Monoamine transporters have at least two binding sites, *i.e.*, the SI-site, which corresponds to the substrate binding site proper, and the SII-site, which resides in the outer vestibule (Chen and Reith, 2004; Kristensen et al., 2011; Sarker et al., 2010). Accordingly, we explored the possibility that levamisole exerts an allosteric effect on the action of cocaine. We performed uptake-inhibition experiments in HEK293 cells expressing all three transporters and used increasing cocaine concentrations at a fixed levamisole concentration or *vice versa*. Representative experiments are shown in Fig. 3 for NET. The observations are consistent with binding of levamisole and cocaine to the same binding site. This can be best appreciated by examining the transformation of the data into Dixon plots (Segel, 1975). For this analysis the reciprocal of uptake velocity is plotted as a function of one inhibitor at a fixed concentration of the second inhibitor. Regardless of whether levamisole was varied at a fixed cocaine concentration (Fig. 3C and D) or – *vice versa* – cocaine was varied at a fixed levamisole concentration (Fig. 3A and B), the transformed data points fell onto parallel lines (Fig. 3B and D). This is indicative of mutually exclusive binding (Segel, 1975); intersecting lines ought to arise, if cocaine and levamisole can bind simultaneously, i.e., at two different sites. Identical experiments were performed for SERT and DAT (Supplementary Figs. S3.1 and S3.2) indicating as well mutually exclusive binding of levamisole and cocaine.

3.2. Is levamisole an inhibitor to NET, DAT and SERT only – or possibly a releaser?

Drugs that interact with neurotransmitter transporters can be either classified as cocaine-like inhibitors, which trap the transporter in the outward facing conformation and thus interrupt the

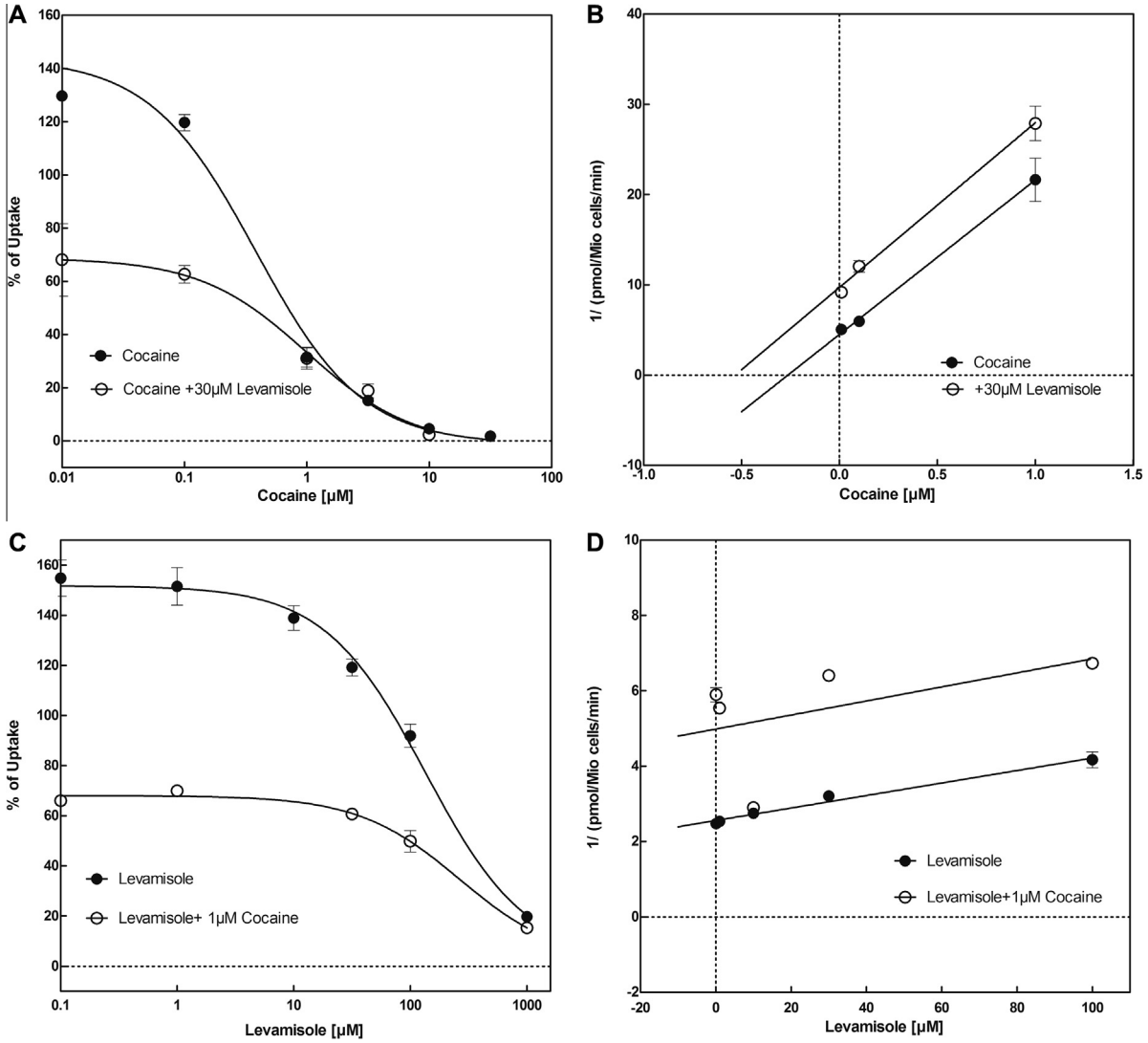

Fig. 3. Determination of allosteric interaction between levamisole and cocaine by using uptake inhibition experiments. Uptake inhibitions with levamisole and cocaine were performed by using HEK 293 cells stably expressing human NET. Uptake of substrate MPP+ at increasing cocaine concentrations at fixed levamisole concentrations (A) is expressed as percentage of the maximum uptake without any inhibitory substance. IC_{50} values for cocaine were 0.80 ± 1.45 µM in the absence and 0.23 ± 1.47 µM in the presence of 30 µM levamisole. Data in (A) were transformed into a Dixon-plot (B) by expressing the reciprocal of MPP+ transported (pmol/million cells/min) as a function of cocaine at fixed concentrations of levamisole. Equally, uptake of MPP+ at increasing levamisole concentrations at fixed cocaine concentrations (C) is expressed as percentage of the maximum uptake without substance. IC_{50} values for levamisole was 521 ± 2.30 µM in the absence and 73 ± 1.47 µM in the presence of 1 µM cocaine. Data in (C) were transformed into a Dixon-plot (D) by expressing the reciprocal of MPP+ transported (pmol/million cells/min) as a function of levamisole at fixed concentrations of cocaine.

transport cycle (Schicker et al., 2012), or amphetamine-like releasers. These raise extracellular monoamine concentrations by triggering substrate efflux (Sitte and Freissmuth, 2010). Levamisole is distantly related in structure to amphetamine. It is therefore conceivable that levamisole has a releasing action. We increased the sensitivity of our analysis by co-incubation of the cells with monensin (Baumann et al., 2013; Scholze et al., 2000; Sitte et al., 2000). Monensin is an ionophore that promotes electroneutral Na^+/H^+ exchange and therefore elevates intracellular Na^+ in cells without altering the membrane potential. Since SERT, NET and DAT couple substrate transport with symport of Na^+ and Cl^-, elevation of intracellular Na^+ accelerates substrate efflux (Sitte and Freissmuth, 2010). Applications of 5–20 µM monensin have been found to raise intracellular Na^+ to 30–50 mM in HEK293 cells (Chen and Reith, 2004). In the absence of monensin, no efflux was observed in SERT (Fig. 4A) or DAT (Fig. 4C) expressing cells at a high levamisole concentration (100 µM); however, there was a slight increase in $[^3H]MPP^+$ in the superfusate collected from HEK293-NET cells (Fig. 4C). Importantly, the addition of monensin did not increase transporter-mediated efflux any further (Fig. 4). This argues for levamisole-mediated inhibition of reuptake of continuously released substrate rather than for a true releasing action. We previously observed similar spurious releasing effects with the selective serotonin reuptake inhibitor paroxetine on HEK293-cells expressing SERT (Scholze et al., 2000). To our knowledge, the experiments show for the first time that levamisole directly inhibits the human NET and to a lesser extent SERT and DAT. This inhibition is mediated by a low-affinity interaction with the same site, to which cocaine is bound and thus the SI site.

3.3. The levamisole-metabolite aminorex modulates NET, SERT and DAT in a different manner

Administration of levamisole to race horses resulted in positive doping tests, because their urine contained aminorex (Barker, 2009). The metabolism of levamisole to the amphetamine-like compound aminorex was later confirmed to also occur in dogs and humans (Bertol et al., 2011; Hess et al., 2013). Hence, for the

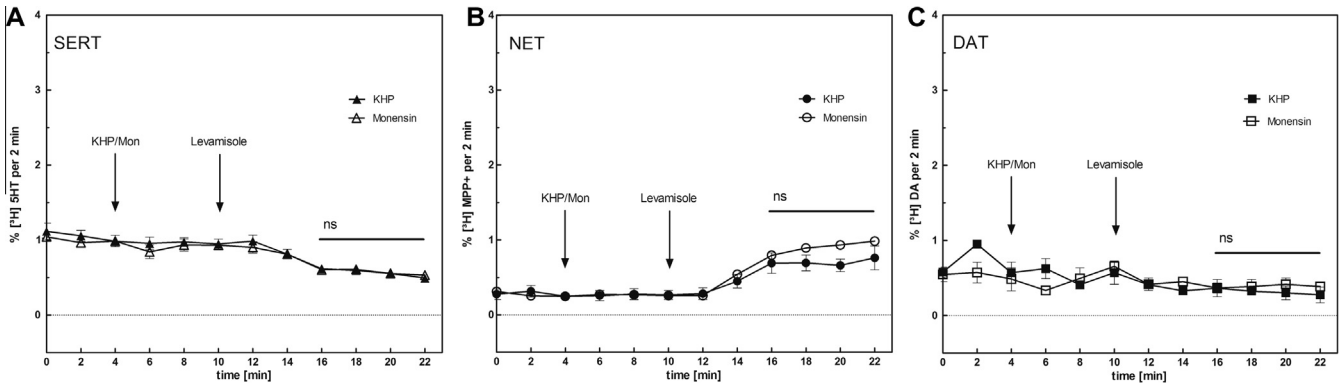

Fig. 4. Releasing effect of levamisole. Substrate efflux after treatment with levamisole was measured for SERT (A), NET (B) and DAT (C). HEK 293 cells stably expressing human SERT, NET or DAT were preloaded with 0.4 μM [3H]5-HT, 0.1 μM [3H]MPP+, or 0.4 μM [3H]dopamine for 20 min at 37 °C in a final volume of 0.1 mL/well, transferred to small superfusion chambers (0.2 ml) and superfused with KRH buffer (25 °C, 0.7 ml × min^{-1}). After a washout period of 40 min to reach stable baseline for efflux, 10 μM monensin or buffer (control) was added after 4 min followed by 100 μM levamisole (10 min). Collection of fractions was carried out in 2 min interval. At the end of the experiment, cells were lysed in 1% SDS. In the absence of monensin we could not detect substrate efflux for SERT (A) or DAT (C). However, we observed a slight increased substrate efflux for NET (B) in presence of levamisole compared to the control. Also, we could not detect an effect of monensine alone for any of the three transporters. Data are shown as mean ± SEM of three independent experiments. Two-way ANOVA (Bonferroni post-test) could not detect significant differences in substrate efflux between levamisole and control neither in NET ($p = 0.945$) nor SERT ($p = 0.989$) nor DAT ($p = 0.678$). IC_{50} values have been calculated using GraphPad Prism 5.04 non-linear regression.

sake of comparison, we quantified the inhibition by aminorex of substrate uptake by NET, SERT or DAT (Fig. 5A). Interestingly, aminorex also preferentially blocked substrate uptake by NET (IC_{50}: 0.33 ± 1.07 μM) and DAT (IC_{50}: 0.85 ± 1.20 μM), while SERT was inhibited only at 20-fold higher concentrations (IC_{50}: 18.39 ± 1.12 μM). Accordingly, the pattern of inhibition (NET > DAT >>> SERT) was reminiscent of the parent compound levamisole, but the inhibitory potency of aminorex was comparable to that of cocaine. To investigate if cocaine has an allosteric modulatory effect on aminorex, we performed uptake-inhibition experiments at increasing concentrations of aminorex in presence of fixed cocaine concentrations (Fig. 6). The resulting Dixon plots indicated that aminorex and cocaine bound in a mutually exclusive manner. In other words, there was not any appreciable allosteric modulatory effect in SERT, NET or DAT.

Aminorex is classified as an amphetamine-like substance, because it is chemically related to amphetamine and it suppresses feeding behavior in a manner similar to amphetamines. However, the neurochemical changes induced by aminorex differ from those of other appetite suppressants (Roszkowski and Kelley, 1963; Zheng et al., 1997). We therefore investigated its effects on substrate efflux by carrying out superfusion experiments in the presence and absence of monensin (10 μM). Interestingly, aminorex induced significant substrate release only in HEK293-SERT cells whereas efflux was completely absent in HEK293-DAT cells. HEK293-NET cells displayed only a slight response (Fig. 5B-D). Importantly, monensin enhanced efflux as predicted for an amphetamine-like releaser (Scholze et al., 2000). Taken together our experimental data showed that aminorex modulates the neurotransmitter transporters in different ways. On the one hand as an uptake inhibitor at NET and DAT with IC_{50} values of less than 1 μM but only weakly at SERT, on the other hand it elicits efflux in SERT without overtly affecting NET or DAT. The observation that aminorex causes significant substrate efflux only in SERT is coherent with the hypothesis that pulmonary hypertension, a major risk of aminorex consumption, is caused by dysregulation of peripheral serotonin transporters (Eddahibi and Adnot, 2002; Pollick, 1999) Hence, it may be assumed that aminorex has the potential to potentiate and/or prolong the effect of cocaine in its blocking propensity. Importantly, it may also prolong the cocaine sensations because it will elicit transporter-mediated substrate efflux owing to its amphetamine-like properties at times when cocaine is not present in the brain anymore (Jatlow, 1988; Moolchan et al., 2000). The pharmacokinetic parameters of levamisole are consistent with this hypothesis (Gwilt et al., 2000). This hypothesis is further supported by a recent analysis of human urine after levamisole administration, which showed that aminorex could be detected for up to 54 h (Hess et al., 2013).

Taken together, we demonstrate for the first time that levamisole directly inhibits the human NET. The metabolite aminorex itself modulates NET, DAT and SERT and results in a strong inhibition of NET and DAT substrate uptake and in substrate efflux at SERT. In addition we could not detect an allosteric modulatory effect of cocaine on aminorex.

3.4. Understanding the levamisole and aminorex–transporter interaction by a ligand-docking approach

DAT, NET and SERT are very closely related (Beuming et al., 2006). The Dixon plots summarized in Fig. 3 provided conclusive evidence that cocaine and levamisole bound to the same site, namely SI, the substrate binding site proper. It is difficult to reconcile the high degree of conversation in the vicinity of the substrate binding site and the large differences in affinity of levamisole. Recently, we validated a ligand-based docking approach to probe the binding pocket of substrates in monoamine transporters (Seddik et al., 2013). Therefore, we used this computational approach to understand the discrimination by levamisole against SERT. The substrate binding sites of DAT and NET are almost identical. They differ only by one residue in helix 3, namely residue F151 in NET that corresponds to residue Y155 in DAT (Fig. 7A). Hence, we investigated, if the phenylalanine – tyrosine substitution explained the threefold difference in uptake inhibition. As levamisole has a pK_a of 7, we docked both the neutral and the protonated form of levamisole into the central substrate binding site of the neurotransmitter transporter. The positively charged amine functional group of serotonin, dopamine and norepinephrine has been found to interact with the sodium coordinating aspartate in the binding site. We made use of this interaction to reduce the search space for docking poses and imposed an interaction of the protonatable nitrogen of levamisole with the conserved aspartate residue (D75 in NET, D79 in DAT and D98 in SERT). Similar docking poses were observed for both protonation states of levamisole in all three transporters. The docking score showed the same ranking for both ligand protonation states. The highest affinity was predicted for NET (charged: −830 kcal/mol; neutral: −820 kcal/mol), followed

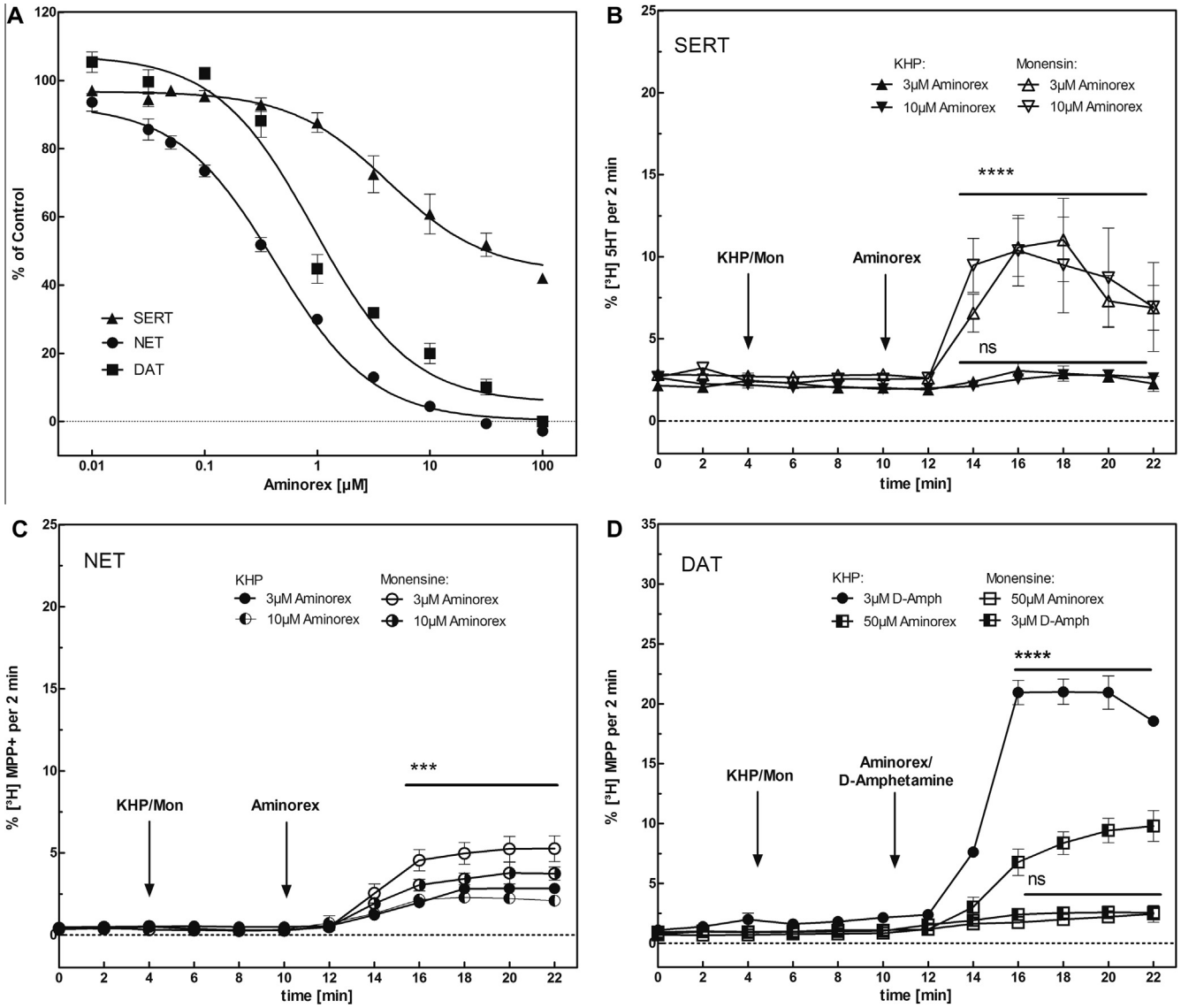

Fig. 5. Inhibitory and releasing effect of aminorex. Uptake of substrate (SERT: 5-HT; NET: MPP+; DAT: dopamine) at increasing aminorex concentrations is shown in (A). IC_{50} values for aminorex (SERT: 18.39 ± 1.12 µM; NET: 0.33 ± 1.07 µM; DAT: 0.855 ± 1.20 µM) are suggesting a comparable inhibitory effect to cocaine for NET and DAT. For SERT the inhibitory effect was more than 10-fold higher compared to cocaine (all experiments were performed three times). Substrate efflux after treatment with aminorex was measured for SERT (B), NET (C) and DAT (D). In brief, HEK 293 cells stably expressing human SERT, NET or DAT were preloaded with 0,4 µM [3H]5-HT or 0,1 µM [3H]MPP+ for 20 min at 37 °C in a final volume of 0.1 mL/well, transferred to small superfusion chambers (0.2 ml) and superfused with KRH buffer (25 °C, 0.7 ml × min^{-1}). After a washout period of 40 min to reach stable baseline for efflux, 10 µM monensin or buffer (control) was added after 4 min followed by 3 or 10 µM aminorex (SERT and NET) and 50 µM aminorex (DAT) respectively for 10 min. In addition we used 3 µM D-amphetamine as an positive control. Collection of fractions was carried out in 2 min interval. At the end of the experiment, cells were lysed in 1% SDS. While levamisole lead to an efflux of substrate via SERT and NET, which was enhanced by addition of monensin, no releasing effect of aminorex was observed at DAT ($p = 0.9981$). A slight increase could be observed in NET ($p = 0.001$) and aminorex could trigger a strong release in SERT ($p < 0.0001$). Data are shown as mean ± SEM of three independent experiments. *p*-values were calculated using a Two-way ANOVA (Bonferroni post-test).

by DAT (charged: −798 kcal/mol neutral: −792 kcal/mol) and SERT (charged: −697 kcal/mol neutral: −683 kcal/mol); nevertheless, scores alone have limited predictive power (Warren et al., 2006) and require confirmation by other means. This limitation, however, is less relevant in our approach, because the same ligand is docked into almost identical binding sites. The observed phenylalanine – tyrosine substitution between NET and DAT is very conservative, but it introduces a polar hydroxyl function by contrast with the hydrophobic phenylalanine side-chain. Importantly, the phenyl ring of levamisole directly contacts residue F151 in NET or residue Y155 in DAT in our docking poses, which is consistent with the experimental data. Our inhibition experiments showed that binding affinities of levamisole for SERT were lower when compared to that for NET and DAT. The binding site differs by five residues between DAT and SERT (residues Y95, G100, I172, Y175 and T497 in SERT) and by four residues between NET and SERT (residue Y95, G100, I172 and T497 in SERT). Levamisole was found to be in direct contact with four of these residues. We only observed that residue T497 was not in direct contact with the inhibitor. In line with our experimental findings, the difference in affinity between SERT and NET or DAT was therefore recapitulated by our computational approach.

The active metabolite of levamisole (aminorex) binds with comparable affinity to DAT and NET, while the affinity to SERT is lower (see Fig. 5). Aminorex is smaller than levamisole. During our docking studies of aminorex, we applied the same protocol as used for levamisole and identified docking poses in the central binding site S1. Both, neutral and positively charged forms of aminorex have

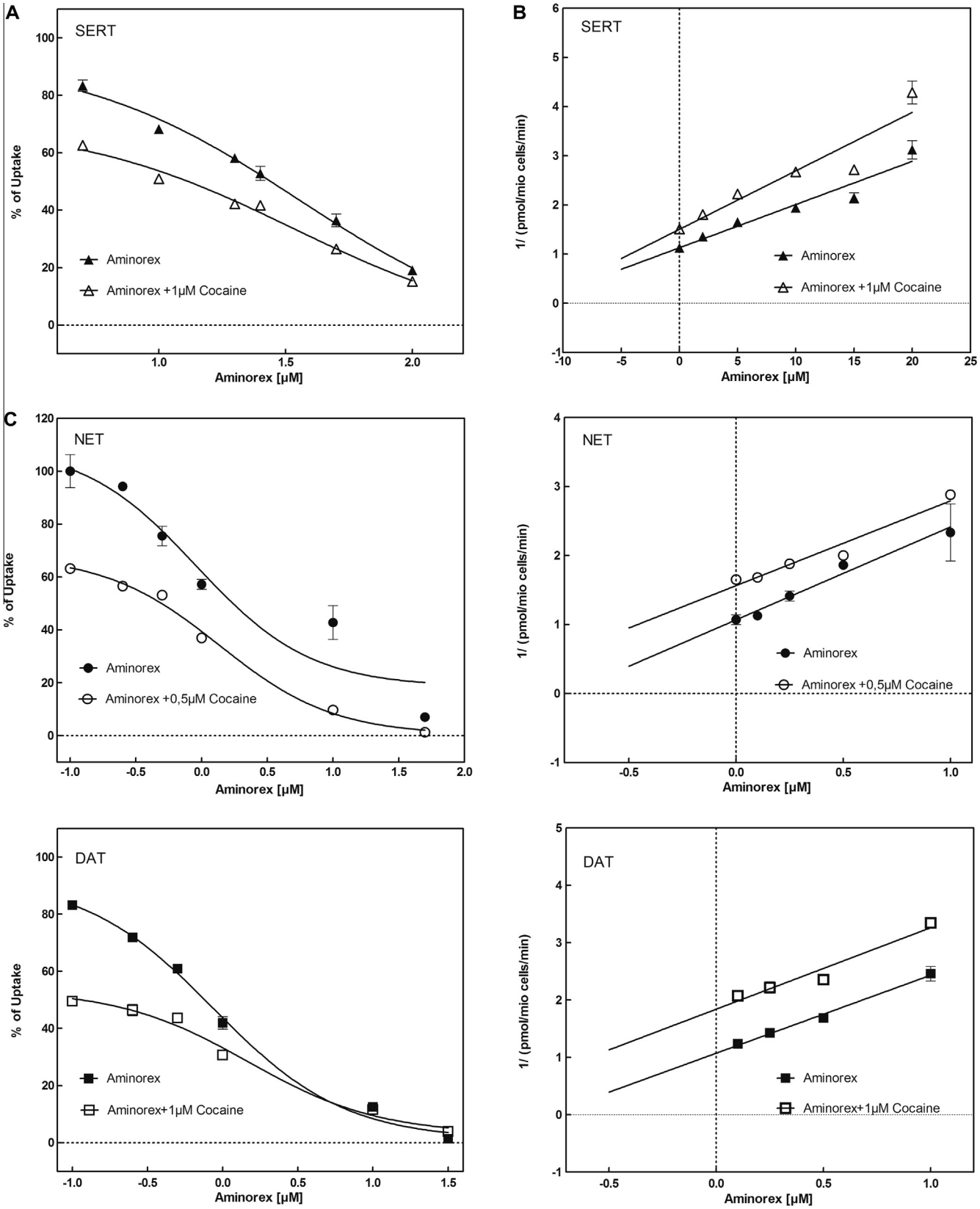

Fig. 6. Determination of allosteric interaction between aminorex and cocaine by using uptake inhibition experiments. Uptake inhibitions with aminorex and cocaine were performed by using HEK cells stably expressing human NET. Uptake of substrate 5-HT, MPP+, and dopamine at increasing cocaine concentrations at fixed aminorex concentrations (A, C, and E) is expressed as percentage of the maximum uptake without substance. IC_{50} values for aminorex were 26.29 ± 1.03 µM for SERT (A), 1.97 ± 1.20 µM for NET (C), and 0.71 ± 1.05 µM for DAT (E) in the absence of cocaine. IC_{50} values in the presence of constant cocaine concentrations were as follows: SERT: 13.22 ± 1.08 µM at 1 µM Cocaine (A); NET: 0.406 ± 1.13 µM at 0.5 µM Cocaine (C); DAT: 0.20 ± 1.19 µM at 0.5 µM Cocaine. Data in (A, C, and E) were transformed into Dixon-plots (B, D, and F). The linear regression lines did not intersect, indicating no allosteric modulation of cocaine on aminorex binding. IC_{50} values have been calculated using GraphPad Prism 5.04 non-linear regression.

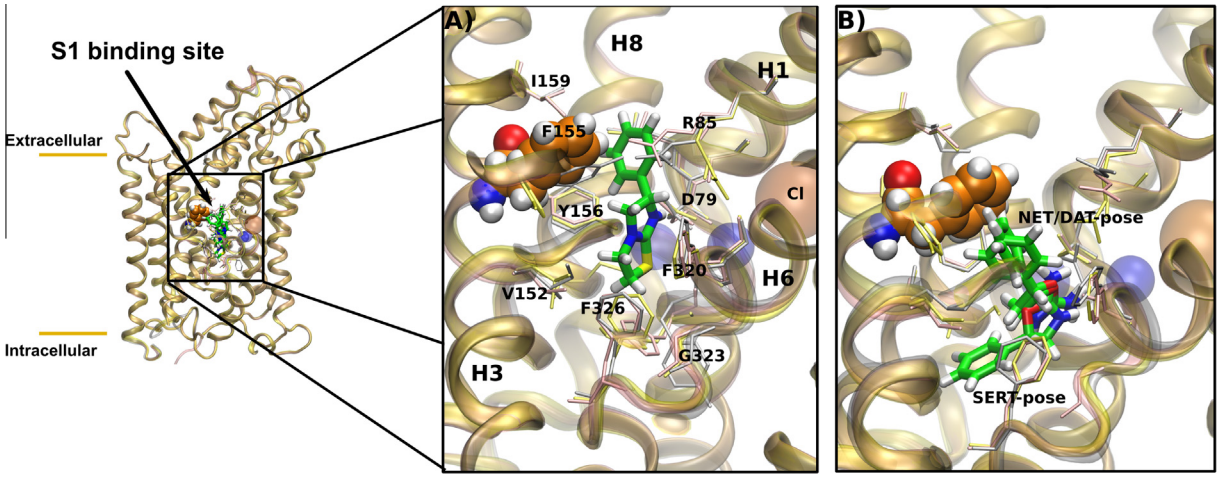

Fig. 7. Docking poses of levamisole. Overlay of the docking poses of levamisole in NET (yellow), DAT (pink) and SERT (grey). The co-transported sodium (blue) and chloride (orange) ions are shown as spheres. Panel A and B show a zoom into the binding site. For clarity, only the docking poses in DAT is shown. The side chains that are within 5 Å from the ligand are shown as sticks Panel A: docking of levamisole into the substrate binding site (S1). The phenyl ring of levamisole directly contacts residue F151 in NET or residue Y155 in DAT. Binding of levamisole in SERT is lower compared to DAT and NET and differs by five residues between DAT and SERT (residues Y95, G100, I172, Y175 and T497 in SERT) and by four residues between NET and SERT (residue Y95, G100, I172 and T497 in SERT). Panel B shows overlaid docking poses of aminorex in the central binding site S1 of SERT, NET and DAT. Aminorex interacts with Y151 in NET and F155 in DAT. Docking pose in SERT showed that aromatic ring of aminorex is not orientated towards Y175, but inserted between I172 and Y95.

been docked, as the pK_a of this psychostimulant is 7.4. We observed similar poses for both protonation states and discuss here the results of the positively charged state, as endogenous substrates are typically transported in their charged form. The positively charged nitrogen of aminorex interacts in a similar way with the aspartate (D75 in NET, D79 in DAT, D98 in SERT) as found for levamisole or nortriptyline in the recently published dDAT structure (Penmatsa et al., 2013).

The rank order of the binding energies scores (IFD score) compares favorably with the experimentally found affinities: NET (−822 kcal/mol), DAT (−789 kcal/mol) and SERT (−693 kcal/mol). Docking poses revealed overlapping geometries for the interaction of aminorex with NET and DAT (see Fig. 7B). Aminorex is in direct contact with Y151 in NET or F155 in DAT which could help to explain the observed differences in affinity. Importantly, the docking pose in SERT is different. We find that the aromatic ring of aminorex is not oriented towards the corresponding residue Y175, but inserted between I172 and Y95. Both residues differ in NET and DAT. We find in the corresponding positions V148 and F72 in NET and V152 and F76 in DAT. These docking results are in line with our experimental observation of the different behavior in the binding of aminorex to SERT compared to NET and DAT.

4. Conclusions

A large part of illicitly sold drugs are marketed in adulterated form; these commercialized preparations often may contain several additional, also pharmacologically active compounds. There are two obvious explanations why certain substances are used to adulterate illicit drugs: substances are added because they are cheap, have similar chemical appearance and taste and therefore increase the profit. Alternatively, the additives enhance the psychoactive effects of the drug by exerting a pharmacological effect *per se*. Accordingly, they contribute to the drug-specific reinforcement, gain more customers and thus increase profits. To our knowledge this work demonstrated for the first time that levamisole as cocaine adulterant itself directly inhibits the neurotransmitter transporters DAT, SERT and NET. Moreover, we found a cocaine-like effect of the levamisole metabolite aminorex at the DAT and the NET and an amphetamine-like effect at SERT. Therefore, it can be assumed that levamisole is used to prolong the effect of cocaine: it is possible that after the cocaine effect "fades out" the aminorex effect "kicks in". However, the physiological consequences of combined cocaine-aminorex administration are still unclear. To our knowledge there are no reports on how the combination of cocaine and aminorex influences drug experience or brain physiology. It can be assumed that massive elevation of extracellular serotonin levels not only by inhibiting uptake (via cocaine) but also increasing efflux (via aminorex) can be the consequence.

The 'checkit!' program offers a glimpse into the epidemiology of the problem:

Two-thirds of the cocaine samples that were analyzed within the past year were contaminated with moderate to exceedingly high concentrations of levamisole. The latter highlight the risk inherent in adulteration of street drugs, namely the occurrence of severe or life-threatening intoxications. Therefore it is important to mention that consumption of cocaine adulterated with levamisole not only provokes severe agranulocytosis (Buchanan and Lavonas, 2012) but also induces the risk of pulmonary hypertension due to aminorex (Fishman, 1999b).

Acknowledgements

The work of HHS, GFE and MF was supported by the Austrian Science Fund/FWF (grant F35). The drug prevention project 'checkit!' is financially supported by the Department of Addiction and Drug Coordination (STW) of the City of Vienna.

Appendix A. Supplementary data

Supplementary data associated with this article can be found, in the online version, at http://dx.doi.org/10.1016/j.neuint.2013.11.010.

References

Barker, S.A., 2009. The formation of aminorex in racehorses following levamisole administration. A quantitative and chiral analysis following synthetic aminorex or levamisole administration vs. aminorex-positive samples from the field: a preliminary report. J. Vet. Pharmacol. Ther. 32, 160–166.

Baumann, M.H., Partilla, J.S., Lehner, K.R., Thorndike, E.B., Hoffman, A.F., Holy, M., Rothman, R.B., Goldberg, S.R., Lupica, C.R., Sitte, H.H., Brandt, S.D., Tella, S.R., Cozzi, N.V., Schindler, C.W., 2013. Powerful cocaine-like actions of 3,4-methylenedioxypyrovalerone (MDPV), a principal constituent of psychoactive 'bath salts' products. Neuropsychopharmacology 38, 552–562.

Bertol, E., Mari, F., Milia, M.G., Politi, L., Furlanetto, S., Karch, S.B., 2011. Determination of aminorex in human urine samples by GC–MS after use of levamisole. J. Pharm. Biomed. Anal. 55, 1186–1189.

Beuming, T., Shi, L., Javitch, J.A., Weinstein, H., 2006. A comprehensive structure-based alignment of prokaryotic and eukaryotic neurotransmitter/Na+ symporters (NSS) aids in the use of the LeuT structure to probe NSS structure and function. Mol. Pharmacol. 70, 1630–1642.

Brooks, B.R., Brooks 3rd, C.L., Mackerell Jr., A.D., Nilsson, L., Petrella, R.J., Roux, B., Won, Y., Archontis, G., Bartels, C., Boresch, S., Caflisch, A., Caves, L., Cui, Q., Dinner, A.R., Feig, M., Fischer, S., Gao, J., Hodoscek, M., Im, W., Kuczera, K., Lazaridis, T., Ma, J., Ovchinnikov, V., Paci, E., Pastor, R.W., Post, C.B., Pu, J.Z., Schaefer, M., Tidor, B., Venable, R.M., Woodcock, H.L., Wu, X., Yang, W., York, D.M., Karplus, M., 2009. CHARMM: the biomolecular simulation program. J. Comput. Chem. 30, 1545–1614.

Buchanan, J.A., Lavonas, E.J., 2012. Agranulocytosis and other consequences due to use of illicit cocaine contaminated with levamisole. Curr. Opin. Hematol. 19, 27–31.

Buchanan, J.A., Oyer, R.J., Patel, N.R., Jacquet, G.A., Bornikova, L., Thienelt, C., Shriver, D.A., Shockley, L.W., Wilson, M.L., Hurlbut, K.M., Lavonas, E.J., 2010. A confirmed case of agranulocytosis after use of cocaine contaminated with levamisole. J. Med. Toxicol. 6, 160–164.

Byrne-Quinn, E., Grover, R.F., 1972. Aminorex (menocil) and amphetamine: acute and chronic effects on pulmonary and systemic haemodynamics in the calf. Thorax 27, 127–131.

Chai, P.R., Bastan, W., Machan, J., Hack, J.B., Babu, K.M., 2011. Levamisole exposure and hematologic indices in cocaine users. Acad. Emerg. Med. 18, 1141–1147.

Chang, A., Osterloh, J., Thomas, J., 2010. Levamisole: a dangerous new cocaine adulterant. Clin. Pharmacol. Ther. 88, 408–411.

Chen, N., Reith, M.E., 2004. Interaction between dopamine and its transporter: role of intracellular sodium ions and membrane potential. J. Neurochem. 89, 750–765.

Cole, C., Jones, L., McVeigh, J., Kicman, A., Syed, Q., Bellis, M., 2010. Cut: A Guide to Adulterants, Bulking Agents and Other Contaminants Found in Illicit Drugs. Centre for Public Health Engagement Liverpool: Liverpool John Moores University.

Eddahibi, S., Adnot, S., 2002. Anorexigen-induced pulmonary hypertension and the serotonin (5-HT) hypothesis: lessons for the future in pathogenesis. Respir. Res. 3, 9.

Fishman, A.P., 1999a. Aminorex to fen/phen: an epidemic foretold. Circulation 99, 156–161.

Fishman, A.P., 1999b. Aminorex to fen/phen: an epidemic foretold. Circulation 99, 156–161.

Gwilt, P., Tempero, M., Kremer, A., Connolly, M., Ding, C., 2000. Pharmacokinetics of levamisole in cancer patients treated with 5-fluorouracil. Cancer Chemother. Pharmacol. 45, 247–251.

Hess, C., Ritke, N., Broecker, S., Madea, B., Musshoff, F., 2013. Metabolism of levamisole and kinetics of levamisole and aminorex in urine by means of LC–QTOF–HRMS and LC–QqQ–MS. Anal. Bioanal. Chem. 405, 4077–4088.

Jatlow, P., 1988. Cocaine: analysis, pharmacokinetics, and metabolic disposition. Yale J. Biol. Med. 61, 105–113.

Karch, S.B., Mari, F., Bartolini, V., Bertol, E., 2012. Aminorex poisoning in cocaine abusers. Int. J. Cardiol. 158, 344–346.

Kristensen, A.S., Andersen, J., Jorgensen, T.N., Sorensen, L., Eriksen, J., Loland, C.J., Stromgaard, K., Gether, U., 2011. SLC6 neurotransmitter transporters: structure, function, and regulation. Pharmacol. Rev. 63, 585–640.

Levandoski, M.M., Piket, B., Chang, J., 2003. The anthelmintic levamisole is an allosteric modulator of human neuronal nicotinic acetylcholine receptors. Eur. J. Pharmacol. 471, 9–20.

Lin, L.-C., Tsai, T.-H., 2006. Pharmacokinetics and brain distribution of unbound levamisole in the anesthetized rats using microdialysis and microbore column liquid chromatography. Anal. Chim. Acta 569, 145–150.

Martin, R.J., Robertson, A.P., Buxton, S.K., Beech, R.N., Charvet, C.L., Neveu, C., 2012. Levamisole receptors: a second awakening. Trends Parasitol. 28, 289–296.

MOE, 2012. Molecular Operating Environment (MOE). Chemical Computing Group Inc., 1010 Sherbooke St. West, Montreal, QC, Canada, H3A 2R7.

Moolchan, E.T., Cone, E.J., Wstadik, A., Huestis, M.A., Preston, K.L., 2000. Cocaine and metabolite elimination patterns in chronic cocaine users during cessation: plasma and saliva analysis. J. Anal. Toxicol. 24, 458–466.

Muirhead, T.T., Eide, M.J., 2011. Images in clinical medicine. Toxic effects of levamisole in a cocaine user. N. Engl. J. Med. 364, e52.

Murphy, R.B., Philipp, D.M., Friesner, R.A., 2000. A mixed quantum mechanics/molecular mechanics (QM/MM) method for large-scale modeling of chemistry in protein environments. J. Comput. Chem. 21, 1442–1457.

Mutch, R.S., Hutson, P.R., 1991. Levamisole in the adjuvant treatment of colon cancer. Clin. Pharmacol. 10, 95–109.

Penmatsa, A., Wang, K.H., Gouaux, E., 2013. X-ray structure of dopamine transporter elucidates antidepressant mechanism. Nature 503, 85–90.

Pollick, C., 1999. Aminorex to Fen/Phen: an epidemic foretold. Circulation 100, e147.

Ravna, A.W., Sylte, I., Dahl, S.G., 2003. Molecular mechanism of citalopram and cocaine interactions with neurotransmitter transporters. J. Pharmacol. Exp. Ther. 307, 34–41.

Rayes, D., De Rosa, M.J., Bartos, M., Bouzat, C., 2004. Molecular basis of the differential sensitivity of nematode and mammalian muscle to the anthelmintic agent levamisole. J. Biol. Chem. 279, 36372–36381.

Reid, J.M., Kovach, J.S., O'Connell, M.J., Bagniewski, P.G., Moertel, C.G., 1998. Clinical and pharmacokinetic studies of high-dose levamisole in combination with 5-fluorouracil in patients with advanced cancer. Cancer Chemother. Pharmacol. 41, 477–484.

Renoux, G., 1980. The general immunopharmacology of levamisole. Drugs 20, 89–99.

Rosenauer, R., Luf, A., Holy, M., Freissmuth, M., Schmid, R., Sitte, H.H., 2013. A combined approach using transporter-flux assays and mass spectrometry to examine psychostimulant street drugs of unknown content. ACS Chem. Neurosci. 4, 182–190.

Roszkowski, A.P., Kelley, N.M., 1963. A rapid method for assessing drug inhibition of feeding behavior. J. Pharmacol. Exp. Ther. 140, 367–374.

Rothman, R.B., Baumann, M.H., 2003. Monoamine transporters and psychostimulant drugs. Eur. J. Pharmacol. 479, 23–40.

Rothman, R.B., Ayestas, M.A., Dersch, C.M., Baumann, M.H., 1999. Aminorex, fenfluramine, and chlorphentermine are serotonin transporter substrates. Implications for primary pulmonary hypertension. Circulation 100, 869–875.

Sali, A., Blundell, T.L., 1993. Comparative protein modelling by satisfaction of spatial restraints. J. Mol. Biol. 234, 779–815.

Sarker, S., Weissensteiner, R., Steiner, I., Sitte, H.H., Ecker, G.F., Freissmuth, M., Sucic, S., 2010. The high-affinity binding site for tricyclic antidepressants resides in the outer vestibule of the serotonin transporter. Mol. Pharmacol. 78, 1026–1035.

Schicker, K., Uzelac, Z., Gesmonde, J., Bulling, S., Stockner, T., Freissmuth, M., Boehm, S., Rudnick, G., Sitte, H.H., Sandtner, W., 2012. Unifying concept of serotonin transporter-associated currents. J. Biol. Chem. 287, 438–445.

Schifano, F., Albanese, A., Fergus, S., Stair, J.L., Deluca, P., Corazza, O., Davey, Z., Corkery, J., Siemann, H., Scherbaum, N., Farre, M., Torrens, M., Demetrovics, Z., Ghodse, A.H., Psychonaut Web, M., Re, D.R.G., 2011. Mephedrone (4-methylmethcathinone; 'meow meow'): chemical, pharmacological and clinical issues. Psychopharmacology 214, 593–602.

Scholze, P., Zwach, J., Kattinger, A., Pifl, C., Singer, E.A., Sitte, H.H., 2000. Transporter-mediated release: a superfusion study on human embryonic kidney cells stably expressing the human serotonin transporter. J. Pharmacol. Exp. Ther. 293, 870–878.

Scholze, P., Norregaard, L., Singer, E.A., Freissmuth, M., Gether, U., Sitte, H.H., 2002. The role of zinc ions in reverse transport mediated by monoamine transporters. J. Biol. Chem. 277, 21505–21513.

Seddik, A., Holy, M., Weissensteiner, R., Zdrazil, B., Sitte, H.H., Ecker, G.F., 2013. Probing the selectivity of monoamine transporter substrates by means of molecular modeling. Mol. Inf. 32, 409–413.

Segel, I., 1975. Steady-state kinetics of multireactant enzymes, Chapter 9, Enzyme kinetics, behavior and analysis of rapid equilibrium and steady-state enzyme systems. John Wiley and Son Inc, New York.

Sherman, W., Day, T., Jacobson, M.P., Friesner, R.A., Farid, R., 2005. Novel procedure for modeling ligand/receptor induced fit effects. J. Med. Chem. 49, 534–553.

Sitte, H.H., Freissmuth, M., 2010. The reverse operation of Na^+/Cl^--coupled neurotransmitter transporters – why amphetamines take two to tango. J. Neurochem. 112, 340–355.

Sitte, H.H., Scholze, P., Schloss, P., Pifl, C., Singer, E.A., 2000. Characterization of carrier-mediated efflux in human embryonic kidney 293 cells stably expressing the rat serotonin transporter: a superfusion study. J. Neurochem. 74, 1317–1324.

Stockner, T., Montgomery, T.R., Kudlacek, O., Weissensteiner, R., Ecker, G.F., Freissmuth, M., Sitte, H.H., 2013. Mutational analysis of the high-affinity zinc binding site validates a refined human dopamine transporter homology model. PLoS Comput. Biol. 9, e1002909.

Stuhlinger, W., Raberger, G., Kraupp, O., 1969. Effect of aminorex (menocil) on pulmonary hemodynamics. Naunyn Schmiedebergs Arch. Pharmakol. 264, 314–315.

Sucic, S., Dallinger, S., Zdrazil, B., Weissensteiner, R., Jorgensen, T.N., Holy, M., Kudlacek, O., Seidel, S., Cha, J.H., Gether, U., Newman, A.H., Ecker, G.F., Freissmuth, M., Sitte, H.H., 2010. The N terminus of monoamine transporters is a lever required for the action of amphetamines. J. Biol. Chem. 285, 10924–10938.

Vanattou-Saifoudine, N., McNamara, R., Harkin, A., 2012. Caffeine provokes adverse interactions with 3,4-methylenedioxymethamphetamine (MDMA, 'ecstasy') and related psychostimulants: mechanisms and mediators. Br. J. Pharmacol. 167, 946–959.

Waller, P.J., 2006. From discovery to development: current industry perspectives for the development of novel methods of helminth control in livestock. Vet. Parasitol. 139, 1–14.

Warren, G.L., Andrews, C.W., Capelli, A.M., Clarke, B., LaLonde, J., Lambert, M.H., Lindvall, M., Nevins, N., Semus, S.F., Senger, S., Tedesco, G., Wall, I.D., Woolven, J.M., Peishoff, C.E., Head, M.S., 2006. A critical assessment of docking programs and scoring functions. J. Med. Chem. 49, 5912–5931.

Wolford, A., McDonald, T.S., Eng, H., Hansel, S., Chen, Y., Bauman, J., Sharma, R., Kalgutkar, A.S., 2012. Immune-mediated agranulocytosis caused by the cocaine adulterant levamisole: a case for reactive metabolite(s) involvement. Drug Metab. Dispos. 40, 1067–1075.

Zheng, Y., Russell, B., Schmierer, D., Laverty, R., 1997. The effects of aminorex and related compounds on brain monoamines and metabolites in CBA mice. J. Pharm. Pharmacol. 49, 89–96.

F

Synthesis and *in Silico* Evaluation of Novel Compounds for PET-Based Investigations of the Norepinephrine Transporter

Catharina Neudorfer, Amir Seddik, Karem Shanab, Andreas Jurik, Christina Rami-Mark, Wolfgang Holzer, Gerhard F Ecker, Markus Mitterhauser, Wolfgang Wadsak, Helmut Spreitzer

Published in *Molecules*, 20, 1712-30, **2015**

My contribution to the following publication was to determine whether fluorination of an existing NET-over-DAT/SERT selective inhibitor would not interfere with binding to NET. To do so, I created an outward-open model of NET and docked a set of fluorinated analogs. Then I performed cluster analysis on the poses based on the common chemical scaffold, which indicated that fluorination does not interfere with the fitting in the pocket. I drew additional hypotheses based on protein-ligand interactions to whether these compounds would have improved selectivity.

Molecules **2015**, *20*, 1712-1730; doi:10.3390/molecules20011712

OPEN ACCESS

molecules

ISSN 1420-3049

www.mdpi.com/journal/molecules

Article

Synthesis and *in Silico* Evaluation of Novel Compounds for PET-Based Investigations of the Norepinephrine Transporter

Catharina Neudorfer [1,2,*], Amir Seddik [3], Karem Shanab [1,2], Andreas Jurik [3], Christina Rami-Mark [1], Wolfgang Holzer [2], Gerhard Ecker [3], Markus Mitterhauser [1], Wolfgang Wadsak [1] and Helmut Spreitzer [2,*]

[1] Department of Biomedical Imaging and Image-guided Therapy, Division of Nuclear Medicine, Medical University of Vienna, Waehringer Guertel 18-20, 1090 Vienna, Austria; E-Mails: karem.shanab@gmail.com (K.S.); christina.rami-mark@meduniwien.ac.at (C.R.-M.); markus.mitterhauser@meduniwien.ac.at (M.M.); wolfgang.wadsak@meduniwien.ac.at (W.W.)

[2] Division of Drug Synthesis, Department of Pharmaceutical Chemistry, Faculty of Life Sciences, University of Vienna, Althanstraße 14, 1090 Vienna, Austria; E-Mail: wolfgang.holzer@univie.ac.at

[3] Division of Drug Design and Medicinal Chemistry, Department of Pharmaceutical Chemistry, Faculty of Life Sciences, University of Vienna, Althanstraße 14, 1090 Vienna, Austria; E-Mails: amir.seddik@univie.ac.at (A.S.); andreas.jurik@univie.ac.at (A.J.); gerhard.f.ecker@univie.ac.at (G.E.)

* Authors to whom correspondence should be addressed; E-Mails: catharina.neudorfer@gmail.com (C.N.); helmut.spreitzer@univie.ac.at (H.S.); Tel.: +43-4277-55629 (C.N.); +43-4277-55621 (H.S.); Fax: +43-4277-855629 (C.N.); +43-4277-855621 (H.S.).

Academic Editor: Svend Borup Jensen

Received: 20 November 2014 / Accepted: 14 January 2015 / Published: 20 January 2015

Abstract: Since the norepinephrine transporter (NET) is involved in a variety of diseases, the investigation of underlying dysregulation-mechanisms of the norepinephrine (NE) system is of major interest. Based on the previously described highly potent and selective NET ligand 1-(3-(methylamino)-1-phenylpropyl)-3-phenyl-1,3-dihydro-2*H*-benzimidaz- ol-2-one (Me@APPI), this paper aims at the development of several fluorinated methylamine-based analogs of this compound. The newly synthesized compounds were computationally

evaluated for their interactions with the monoamine transporters and represent reference compounds for PET-based investigation of the NET.

Keywords: NET; ADHD; cocaine dependence; BAT; PET; FAPPI

1. Introduction

Abnormal regulation of the norepinephrine transporter (NET) or NET dysfunction, respectively, cause either increased or decreased levels of norepinephrine (NE) in the synaptic cleft. Since NE is a fundamental neurochemical messenger, its accurate regulation is of major importance. Thus, the NET, responsible for NE equilibrium in the synaptic cleft, is representing the reuptake site and considered to be involved in a variety of neurological/psychiatric disorders [1,2], but also plays a pivotal role in cardiovascular [1–3] and metabolic diseases [3–5]. Reduced NET levels go along with neurological disorders like major depression [6,7], Parkinson's disease (PD), Alzheimer's disease (AD) [8–18], and cardiovascular diseases such as hypertension, cardiomyopathy, and heart failure [5,13]. Furthermore, a dysfunction of the NE system was reported in Attention Deficit Hyperactivity Disorder (ADHD) [9,17,19], suicide [1,12,20], substance abuse (cocaine dependence) [16], and schizophrenia [10]. A more recent discovery is the involvement of the NET in diseases like diabetes and obesity, due to its presence in brown adipose tissue (BAT) and the proposed activation thereof via NE [4,5,21].

Based on the fact that the NET is involved in such a variety of diseases, the investigation of the underlying dysregulation-mechanism of the NE system is of major interest. For this purpose, information about the transporter abundance and density in healthy and pathological living human brains is required. The most suitable and accurate technique to gain this information is positron emission tomography (PET). As a non-invasive molecular imaging technique, it represents a suitable approach towards the collection of missing data in the living organism and direct quantification of receptor/transporter densities *in vivo*. To fully gain insight in the molecular changes of the noradrenergic system via PET, however, prior development of suitable NET PET radioligands is required.

So far, radiolabeled NET binding reboxetine analogs [^{11}C]MeNER, [^{11}C]MRB, ((*S*,*S*)-2-(α-(2-[^{11}C]-methoxyphenoxy)benzyl)morpholine) and [^{18}F]FMeNER-D$_2$ ((*S*,*S*)-2-(α-(2-[^{18}F]fluoro[^{2}H$_2$]methoxy-phenoxy)benzyl)morpholine) have been described, which however display certain limitations such as metabolic instability, complex radiosyntheses, or late equilibria [22–26].

Recently, Zhang *et al.* [26] evaluated a series of benzimidazolone-based propanamines with *in vitro* inhibitory activity on the human norepinephrine transporter (hNET). The results of these investigations suggested that compounds containing a phenyl moiety directly attached at the benzimidazolone ring (e.g., **1**, Figure 1) were the most potent, representing a half maximal inhibitory concentration (IC_{50}) below 10 nM (IC_{50} < 10 nM). Furthermore, hNET selectivity over human serotonin transporter (hSERT) turned out >300-fold superior to those of reboxetine and atomoxetine (16- and 81-fold) [26]. Fluorination at position 2 of the phenyl moiety attached to the benzimidazolone ring (e.g., **2**, Figure 1), indicated similar hNET potency, comparable to its non-fluorinated analogs (e.g., **1**) and additionally exhibited hNET selectivity over hSERT (80-fold) similar to atomoxetine [26].

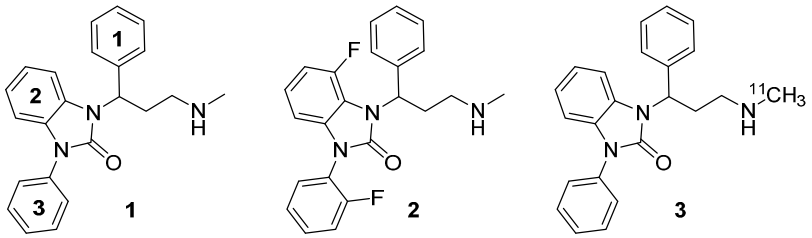

Figure 1. Structures of the highly potent and selective NET ligands 1-(3-(methylamino)- 1-phenylpropyl)-3-phenyl-1,3-dihydro-2*H*-benzimidazol-2-one (Me@APPI, **1**) and 4-fluoro- 1-(2-fluorophenyl)-3-(3-(methylamino)-1-phenylpropyl)-1,3-dihydro-2*H*-benzimidazol-2-one (**2**) as well as radiolabeled analog [^{11}C]Me@APPI (**3**).

Both benzimidazolone derived propanamines with a phenyl moiety (e.g., **1**), as well as a fluorinated phenyl moiety (as in **2**) indicated excellent hNET selectivity over human dopamine transporter (hDAT) with < 50% inhibition of the cocaine analog [^{3}H]WIN-35,428, binding to hDAT at a concentration of 10 μM [26]. Given those findings, both described benzimidazolone-based propanamines **1** and **2** represent excellent candidates for selective and potent NET inhibition with high affinity and low unspecific binding. Thus, on the basis of the results of Zhang *et al.* [26] the methylamino moiety of the core compound **1** has been radiolabeled with ^{11}C and tested by our research group [27]. All investigated preclinical parameters, such as affinity, blood brain barrier penetration, lipophilicity, metabolic degradation, and selectivity showed excellent results, thus suggesting suitability of ^{11}C-radiolabeled 1-(3-(methylamino)-1-phenylpropyl)-3-phenyl-1,3-dihydro-2*H*-benzimidazole-2-one ([^{11}C]Me@APPI) (**3**, Figure 1) as a NET radioligand for use in PET.

Due to successful preclinical testing of [^{11}C]Me@APPI (**3**) and given the excellent *in vitro* results of compound **2**, shown by Zhang *et al.* [26] the aim of this paper is the synthesis and docking studies of several fluorinated analogs **4**–**6** of compound **1** (Figure 2) as reference compounds for their later prepared radioactive analogs. All methylamine-derived benzimidazolone derivatives **4**–**6** will be subjected to affinity, selectivity, and lipophilicity studies towards the NET as well as blood brain barrier penetration experiments at the Medical University of Vienna. The most promising NET ligands will then be selected for the development of new, selective PET tracers for the NET and after radiolabeling with both ^{11}C and ^{18}F, they will be the subject of further experiments.

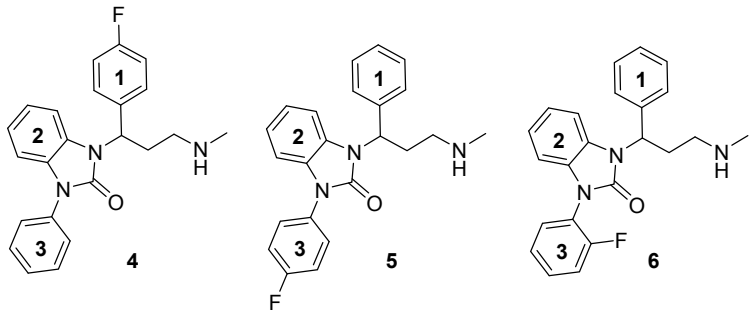

Figure 2. Chemical structure of envisaged reference compounds **4**–**6** (FAPPI:1-3).

2. Results and Discussion

The synthesis of reference compounds **4**–**6** first required the preparation of side chains **11** and **12**, as well as core compounds **16**–**18**. After successful preparation, side chain **11** was merged in a condensation reaction with core compound **16**, whereas side chain **12** was reacted with core compounds **17** and **18**, prior to halogen exchange and substitution with methylamine (Scheme 1).

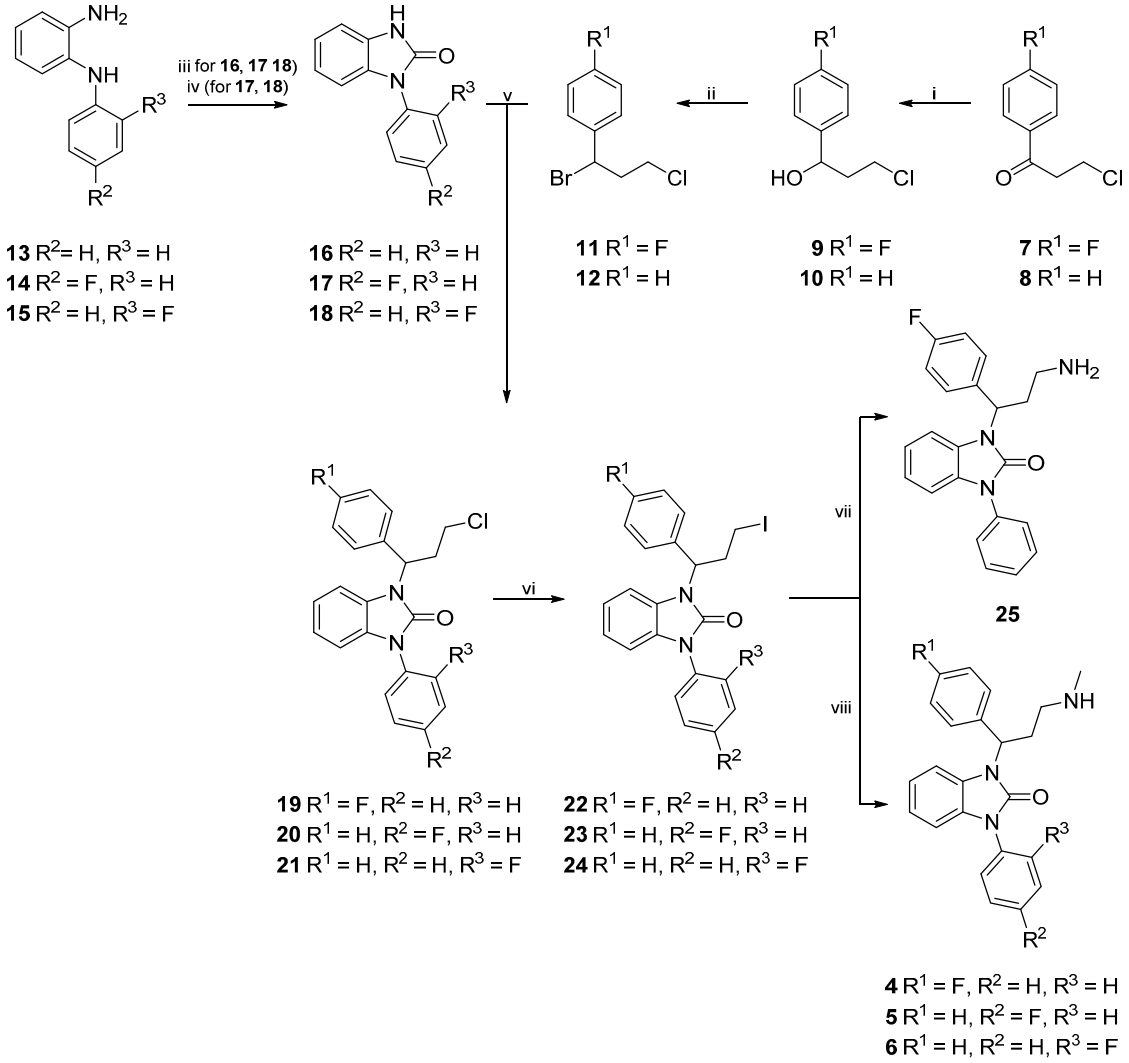

Reagents and conditions: (i) THF, EtOH, $NaBH_4$, −10 °C → −5 °C, 10 min, yields for **9**: 95%, **10**: 100%; (ii) aq. HBr, rt, 3 h, yields for **11**: 64%, **12**: 86%; (iii) 1,1'-carbonyldiimidazole, anhyd. THF, rt, overnight, yields for **16**: 74%, **17**: 61%, **18**: 69%; (iv) 1,1'-carbonyldiimidazole, anhyd. DMF, 90 °C, 2 h, yields for **17**: 80%, **18**: 80%; (v) K_2CO_3, DMF, rt, 30 min → addition of **11** and **12** → rt, 30 min, yields for **19**: 32%, **20**: 63%, **21**: 55%; (vi) NaI, acetone, reflux, 24 h, yields for **22**: 82%, **23**: 76%, **24**: 53%; (vii) NH_3 in isopropanol, 80 °C, 3 h, yield for **25**: 50%; (viii) methylamine in EtOH, 80 °C, 3 h, yields for **4**: 48%, **5**: 29%, **6**: 30%.

Scheme 1. Synthesis of compounds **4**–**6**.

For the synthesis of side chains **11** and **12**, a protocol of Varney *et al.* [28] was adopted and the keto group of commercially available compounds **7** and **8** was reduced with sodium borohydride in order to

obtain intermediate alcohols **9** and **10**. Subsequent bromination of **9** and **10** with aqueous hydrogen bromide led to the formation of products **11** and **12**, respectively.

Core compound **16** was prepared by the reaction of commercially available *N*-phenylbenzene-1,2-diamine (**13**) with 1,1'-carbonyldiimidazole. For the preparation of **17** and **18** however, **14** and **15** first had to be made accessible (Scheme 2). Thus, 1-fluoro-2-nitrobenzene (**26**) reacted with commercially available fluoroanilines **27** and **28**, respectively, to obtain disubstituted amines **29** and **30**. Therefore, two different methods were applied (Scheme 2): The first method (i) was conducted by heating **26** and **27** with anhydrous potassium fluoride and potassium carbonate in a microwave oven [29]. Since the adoption of an alternative method [30]—conventional heating at 180 °C—gave compound **29** in higher yields, this approach (ii) was chosen for the large scale synthesis of **29** as well as for the preparation of **30**.

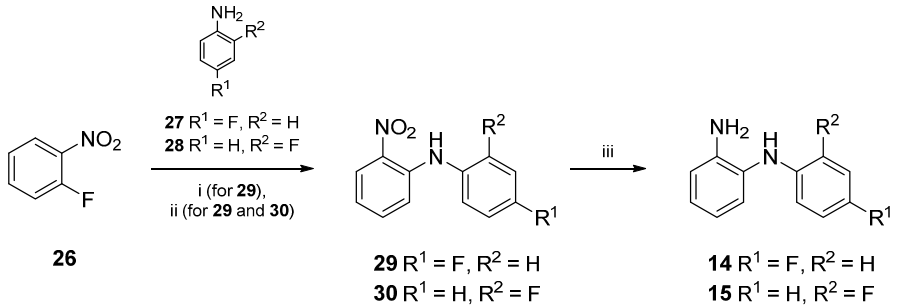

26

29 R^1 = F, R^2 = H
30 R^1 = H, R^2 = F

14 R^1 = F, R^2 = H
15 R^1 = H, R^2 = F

Reagents and conditions: (i) anhyd. KF, K_2CO_3, microwave oven, 900 W, 10 min, yields for **29**: 58%; (ii) anhyd. KF, K_2CO_3, 180 °C, 2 d, yields for **29**: 68%, **30**: 52%; (iii) Zn, AcOH, 0 °C → rt, 2 h, yields for **14**: 93%, **15**: n.d.

Scheme 2. Synthesis of compounds **14**–**15**.

In the next reaction step, the nitro groups of both disubstituted amines **29** and **30** were reduced. For this purpose **29** or **30** were added to a mixture of zinc/acetic acid. The resulting amines **14** or **15** were obtained in excellent yields (Scheme 2) [30].

Freshly prepared intermediates **14** and **15** were then subjected to a cyclization reaction with 1,1'-carbonyldiimidazole in DMF under anhydrous conditions (Scheme 1) by modifying a synthesis protocol according to Zhang *et al.* [26]. DMF was preferred over THF to ensure higher yields and shorter reaction times.

Condensation reactions of benzimidazolones **16**, **17**, and **18** with side chains **11** and **12**, respectively were performed under basic conditions (Scheme 1) by adapting a procedure of Jona *et al.* [31]. After purification, the chloro-substituted derivatives **19**–**21** were converted into the iodo compounds **22**–**24** in a Finkelstein reaction. Target compounds **4**–**6** (FAPPI:1-3) were then obtained by heating derivatives **22**–**24** in a solution of methylamine in ethanol in a sealed tube for 3 h. In addition to reference compounds **4**–**6**, free amine **25** was synthesized by dissolving **22** in a solution of ammonia in isopropanol and heating the resulting mixture in a sealed tube for 3 h. As compound **25** features a free amine moiety, it can be considered a precursor for radiosynthesis.

Since compounds **4** and **5** comprise a novel fluoro substitution, a computational docking study was performed to assess if these compounds still would fit in the binding site of the NET. Furthermore, we aimed at creating a binding mode hypothesis which allows gaining insights into the molecular basis of binding and selectivity towards the monoamine transporters. As the basic scaffold has been shown to act in

an enantioselective manner, the respective (*R*) enantiomers were used throughout the docking studies [26]. The ligands were docked in the substrate binding site (S1) of the outward-open conformation of the transporter models (see Experimental Section for details), since related inhibitors, such as nortriptyline, sertraline, mazindol, *etc.* were also shown to fit in the S1 of the *Drosophila* DAT (dDAT) and the "SERT"-ized leucine transporter ("LeuBAT") in the same protein conformation [32,33]. Interestingly, the co-crystallized ligand in dDAT, nortriptyline (**31**), has the same ranking of human NET, SERT and DAT activity as reference compound **1**, *i.e.*, 4.4, 18 and 1149 nM K_D *vs.* 9, 2995 and >10,000 nM IC_{50}, respectively [26,34]. Additionally, nortriptyline shares important structural features with the benzimidazolones, *i.e.*, two aromatic moieties and an *N*-methyl-ethylenamine side chain. Therefore their binding mode can be expected to be similar.

Common scaffold clustering [35] revealed two binding hypotheses (see Experimental Section) which indicated that compounds **4**–**6** fit in the S1 of all three transporters. Hence, additional fluorination does not seem to cause steric clashes. In both hypotheses, the most prominent protein-ligand interaction was the cationic nitrogen atom placed in the A sub pocket [36], located between the central Asp75/98/79 side chain as a salt-bridge and the Phe72/95/76 side chain as a cation-*pi* interaction in NET/SERT/DAT, respectively. This is well in accordance with the X-ray structures of the templates. Additional *pi-pi* stacking interactions with Phe152/176/156 and Phe323/355/341 further promote the binding in both hypotheses obtained:

Hypothesis 1: the benzimidazolone heterocycle (ring 2) is placed in the B sub pocket and ring 3 in the C pocket, whereas ring 1 is solvent exposed (see figure in Experimental Section).

Hypothesis 2: Ligand ring 1 is placed in the B pocket whereas ring 2 is placed at the same height (measured from the membrane-water interface) and overlap with the rings of nortriptyline (**31**, Figure 3). The solvent exposed Tyr151/Tyr175/Phe155 in NET/SERT/DAT, resp. T-stacks with ring 2 whereas ring 3 points extracellularly (Table 1, Figure 4).

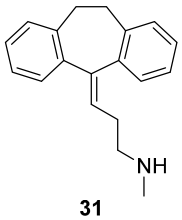

31

Figure 3. Chemical structure of nortriptyline (co-crystallized ligand from the template, PDB code 4M48) [28].

Table 1. Sequence alignment of all distinct monoamine transporter residues located in sub sites (reference [32]) in the vicinity of the docked compounds. Red: hydrophilic side chain, green: lipophilic side chain, bold: bulkier side chain.

	B Site				**C Site**			**Outer Site**	
hNET	S420	M424	G149	V148	A145	F72	D473	Y151	A477
hSERT	T439	L443	A173	I172	A177	Y95	E493	Y175	T497
hDAT	A423	M427	G153	V152	S149	F76	D476	F155	A480

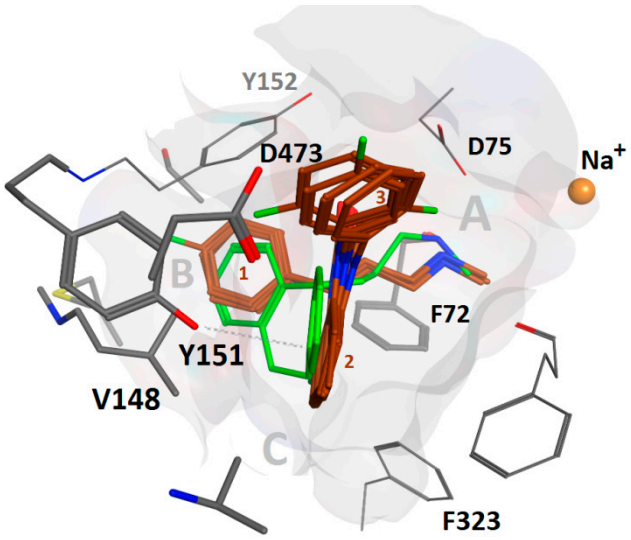

Figure 4. Overlay of compounds **1**, **2**, and **4**–**6** (maroon) in binding hypothesis 2 in hNET showing agreement with the co-crystal pose of nortriptyline (**31**) (green). Val148 and Asp473 allow more space than Ile172 and Glu439 in hSERT, resp., whereas Tyr151 might induce a more potent stacking interaction as compared to Phe155 in hDAT. The angle between ligand ring 2 and 3 is almost 90° in all poses. The extracellular space is located above.

As binding hypothesis 2 is in close agreement with the co-crystallized ligands in dDAT and LeuBAT, we focus further analysis on this proposed binding mode. Binding hypothesis 2 indicates why the investigated compounds (**4**–**6**) show weaker affinity to SERT and DAT than to NET: lower SERT affinity may be due to Ile172 and Glu439, allowing less space for the ligand to be accommodated as compared to in NET, that comprises a valine and an aspartate at the homologous positions, respectively.

Lower DAT affinity could be ascribed to weaker T stacking interactions of Phe155 as compared to Tyr151 in NET, based on previous findings that a Tyr-Phe pair has a stronger binding energy than a Phe-Phe pair [37].

Since the docking studies indicate that fluorinated methyl amines **4**–**6** (FAPPI:1-3) bind in an analogous way to the NET as reference compound **1** [26], compounds **4**–**6** will be employed in future studies and evaluated for affinity and selectivity towards the NET. Additionally, lipophilicity studies and blood brain barrier penetration experiments are planned for compounds **4**–**6** at the Medical University of Vienna. The most promising derivatives regarding their suitability as NET ligands will then be selected for the further development of new and selective PET tracers for the NET, which will comprise either a [^{11}C]methylamine, [^{18}F]fluoroalkyl amine or [^{18}F]fluorobenzene radiolabel, respectively. The results of ongoing studies on affinity, selectivity and lipophilicity of the discussed compounds, will be published in a subsequent paper.

3. Experimental Section

3.1. General

The NMR spectra were recorded from $CDCl_3$ or DMSO-d_6 solutions on a Bruker DPX200 spectrometer (200 MHz for ^{1}H, 50 MHz for ^{13}C) or on a Bruker Avance III 400 spectrometer (400 MHz

for ^{1}H, 100 MHz for ^{13}C, 40 MHz for ^{15}N, 376 MHz for ^{19}F) at 25 °C. The center of the solvent (residual) signal was used as an internal standard which was related to TMS with δ 7.26 ppm (^{1}H in $CDCl_3$), δ 2.49 ppm (^{1}H in DMSO-d_6), δ 77.0 ppm (^{13}C in $CDCl_3$) and δ 39.5 ppm (^{13}C in DMSO-d_6). ^{15}N NMR spectra (gs-HMBC, gs-HSQC) were referenced against neat, external nitromethane, ^{19}F NMR spectra by absolute referencing via Ξ ratio. Digital resolutions were 0.25 Hz/data point in the ^{1}H and 0.3 Hz/data point in the ^{13}C-NMR spectra. Coupling constants (*J*) are quoted in Hz. The following abbreviations were used to show the multiplicities: s: singlet, d: doublet, t: triplet, q: quadruplet, dd: doublet of doublet, m: multiplet. Mass spectra were obtained on a Shimadzu QP 1000 instrument (EI, 70 eV), high-resolution mass spectrometry (HRMS) was carried out on a Finnigan MAT 8230 (EI, 10 eV) or Finnigan MAT 900 S (ESI, 4 kV, 3 μA, CH_3CN/MeOH) electrospray ionization mass spectrometer with a micro-TOF analyzer. Microwave experiments were carried out in a Synthos 3000 microwave oven (SXQ80 rotor, Anton Paar, Graz, Austria) with an internal temperature probe. Compound purity: all compounds synthesized featured a purity of at least 95%.

3.2. Syntheses

3.2.1. General Procedure for the Synthesis of **9** and **10**

Starting materials **7** or **8**, respectively (1 mmol) was dissolved in THF (1 mL) and EtOH (1 mL) was added. The mixture was cooled to −10 °C and $NaBH_4$ (1.05 mmol) was slowly added at this temperature. The solution was stirred at −5 °C for 10 min and thereafter, poured into a mixture of saturated aqueous ammonium chloride (3 mL) in ice (1.5 g). The product was extracted with diethyl ether, dried over Na_2SO_4 and evaporated to dryness. The crude product was employed directly in the subsequent reaction step without further purification.

3-Chloro-1-(4-fluorophenyl)propan-1-ol (**9**). Yield: 4.78 g (95%), pale yellow oil, analytical data are in complete accordance with literature values [38].

3-Chloro-1-phenylpropan-1-ol (**10**). Yield: 4.61 g (99%), light yellow oil, analytical data are in complete accordance with literature values [28].

3.2.2. General Procedure for the Synthesis of **11** and **12**

To starting material **9** or **10**, respectively (1 mmol) was added 48% aqueous HBr (3 mL) and the mixture was stirred for 3h at room temperature. Thereafter, the solution was poured into a mixture of K_2CO_3 (1 g) in ice (5.5 g) and additional solid K_2CO_3 was added for neutralization (pH 7). The crude reaction product was extracted with diethyl ether, the combined organic layers were dried with $MgSO_4$ and evaporated to dryness. The crude product was employed directly in the subsequent reaction step without further purification.

1-(1-Bromo-3-chloropropyl)-4-fluorobenzene (**11**). Yield: 64%, pale yellow oil, analytical data are in complete accordance with literature values [39].

(1-Bromo-3-chloropropyl)benzene (**12**). Yield: 5.64 g (86%), yellow oil, analytical data are in complete accordance with literature values [28].

3.2.3. General Procedure for the Synthesis of **29** and **30**

4-Fluoroaniline or 2-fluoroaniline, respectively (1 mmol), anhydrous KF (1 mmol), and K_2CO_3 (1 mmol) were well powdered with a mortar and a pestle, then 1-fluoro-2-nitrobenzene (1 mmol) was added and the mixture was stirred for 2 days at 180 °C. Thereafter, water (5 mL) and CH_2Cl_2 (5 mL) were added and the organic layer was washed with 10% HCl (5 mL) and brine (5 mL). The combined organic layers were dried over Na_2SO_4 and evaporated to dryness prior to purification by column chromatography.

N-(4-Fluorophenyl)-2-nitroaniline (**29**). Yield: 68%, dark orange crystals, mp. 82–83 °C, purification: silica gel 60, petroleum ether/ethyl acetate 9:1 and RP-18 silica gel, methanol/water 7:3, analytical data are in complete accordance with literature values [29].

2-Fluoro-N-(2-nitrophenyl)aniline (**30**). Yield: 52%, orange crystals, mp. 79–80 °C, purification: silica gel 60, petroleum ether/ethyl acetate 9:1, analytical data are in complete accordance with literature values [40].

3.2.4. Alternative Procedure for the Synthesis of **29**

4-Fluoroaniline (7.89 g, 6.73 mL, 70.87 mmol), anhydrous KF (4.13 g, 70.87 mmol), and K_2CO_3 (9.81 g, 70.87 mmol) were well powdered with a mortar and a pestle, then 1-fluoro-2-nitrobenzene (10.00 g, 7.47 mL, 70.87 mmol) was added and the mixture was irradiated in the microwave (900 W, 10 min). Thereafter, water (8 mL) and CH_2Cl_2 (10 mL) were added and the organic layer was washed with 10% HCl (5 mL) and brine (5 mL). The combined organic layers were dried over Na_2SO_4 and evaporated to dryness prior to purification by column chromatography (silica gel 60, petroleum ether/ethyl acetate 9.5:0.5). Yield: 9.51 g (58%), dark orange crystals, mp. 82 °C–83 °C.

3.2.5. General Procedure for the Synthesis of **14** and **15**

To a solution of Zn^0 (13.8 mmol) in glacial acetic acid (1 mL) was added starting material **28** or **29** (1 mmol) at 0 °C under argon atmosphere. After the addition, the mixture was allowed to warm to room temperature and was stirred for 2 h. Zn^0 was filtered off and the pH of the solution was adjusted to pH 9 with 2N NaOH. Thereafter, the aqueous layer was extracted three times with CH_2Cl_2, the combined organic layers were dried over $MgSO_4$ and evaporated to dryness.

N-(4-Fluorophenyl)benzene-1,2-diamine (**14**). Yield: 93%, dark orange-reddish oil, purification: silica gel 60, petrol ether/ethyl acetate 9:1, analytical data are in complete accordance with literature values [30].

N-(2-Fluorophenyl)benzene-1,2-diamine (**15**). The crude reaction product was subjected to the next reaction step without further purification.

3.2.6. General Procedure for the Synthesis of **16**–**18**

To a solution of starting materials **13**, **14**, or **15** (1 mmol) in THF was added 1,1'-carbonyldiimidazole (1.4 mmol) under argon atmosphere and the mixture was stirred at room temperature overnight. Thereafter, the crude reaction product was purified by column chromatography.

1-Phenyl-1,3-dihydro-2H-benzimidazol-2-one (**16**). Yield: 0.85 g (74%), pink crystals, mp. 201 °C–202 °C, THF: 10 mL, purification: silica gel 60, petroleum ether/ethyl acetate 1:1, analytical data are in complete accordance with literature values [41].

1-(4-Fluorophenyl)-1,3-dihydro-2H-benzimidazol-2-one (**17**). Yield: 61%, brown resin, THF: 25 mL, purification: silica gel 60, petroleum ether/ethyl acetate 9:1, ^{1}H-NMR (200 MHz, $CDCl_3$): δ (ppm) 6.74–6.81 (m, 2H), 6.89–7.11 (m, 2H), 7.14–7.23 (m, 2H), 7.48–7.59 (m, 1H), 7.73–7.78 (m, 1H), 9.03 (br s, 1H), ^{13}C-NMR (50 MHz, $CDCl_3$): δ (ppm) 108.5, 110.0, 116.3, 116.8, 121.4, 121.7, 122.3, 128.0, 128.2, 130.4, 135.1, 155.1, 159.3, 164.2, MS: *m/z* (%) 228 (M^+, 100), 199 (31), 172 (8), 114 (9), 95 (10), 75 (17), 51 (10), HRMS: *m/z* calculated for $C_{13}H_{10}FN_2O$ $[M + H]^+$: 229.0772. Found: 229.0769.

1-(2-Fluorophenyl)-1,3-dihydro-2H-benzimidazol-2-one (**18**). Yield: 69%, brown resin, THF: 20 mL, purification: silica gel 60, petroleum ether/ethyl acetate 9:1, ^{1}H-NMR (200 MHz, $CDCl_3$): δ (ppm) 6.82–6.85 (m, 1H), 7.00–7.19 (m, 3H), 7.26–7.88 (m, 2H), 7.43–7.60 (m, 2H), 10.54 (br s, 1H), ^{13}C-NMR (50 MHz, $CDCl_3$): δ (ppm) 108.9, 110.1, 117.0, 117.4, 121.5, 121.9, 122.4, 124.9, 125.0, 128.2, 129.6, 130.4, 154.8, 155.4, 160.5, MS: *m/z* (%) 228 (M^+, 33), 199 (9), 181 (15), 149 (17), 111 (22), 97 (20), 71 (41), 69 (100), 55 (53), 43 (56), HRMS: *m/z* calculated for $C_{13}H_9FN_2NaO$ $[M + Na]^+$: 251.0597. Found: 251.0592.

3.2.7. Alternative Procedure for the Synthesis of **17** and **18**

A solution of 1,1'-carbonyldiimidazole (1.4 mmol) in DMF (4 mL) was slowly added to a mixture of **14** or **15** (1 mmol) in DMF (4 mL) under argon atmosphere. The resulting solution was stirred at 90 °C for 2 h. After completion of the reaction, the solvent was evaporated *in vacuo*, the slurry was taken up in water, filtered and dried.

1-(4-Fluorophenyl)-1,3-dihydro-2H-benzimidazol-2-one (**17**). Yield: 80%, brown resin.

1-(2-Fluorophenyl)-1,3-dihydro-2H-benzimidazol-2-one (**18**). Yield: 80%, brown resin.

3.2.8. General Procedure for the Synthesis of **19**–**21**

Starting materials **16**–**18** (1 mmol) and K_2CO_3 (2 mmol) were suspended in DMF (1.8 mL) and stirred at 25 °C for 30 min. **11** and **12**, respectively (1.5 mmol) were added after 30 min and the solution was stirred at room temperature overnight. To the mixture was added ethyl acetate (5 mL) and water (5 mL). The aqueous layer was extracted several times with ethyl acetate (10 mL) and the combined organic layers were washed with brine, dried over $MgSO_4$ and evaporated to dryness.

1-(3-Chloro-1-(4-fluorophenyl)propyl)-3-phenyl-1,3-dihydro-2H-benzimidazol-2-one (**19**). Yield: 32%, white oil, purification: silica gel 60, petroleum ether/ethyl acetate 8:2, ^{1}H-NMR (200 MHz, $CDCl_3$): δ (ppm) 2.70–2.87 (m, 1H), 3.12–3.30 (m, 1H), 3.60–3.66 (m, 2H), 5.73 (m, 1H), 7.00–7.11 (m, 6H), 7.38–7.57 (m, 7H), ^{13}C-NMR (50 MHz, $CDCl_3$): δ (ppm) 34.3, 42.0, 53.8, 108.7, 109.0, 115.5, 115.9, 121.7, 122.0, 126.0, 127.8, 129.2, 129.4, 129.5, MS: *m/z* (%) 380 (M^+, 21), 210 (100) (M^+-C_9H_9ClF), 181 (8), 167 (12), 135 (9), 115 (5), 109 (58), 77 (12), HRMS: *m/z* calculated for $C_{22}H_{18}ClFN_2ONa$ $[M + Na]^+$: 403.0989. Found: 403.0989.

1-(3-Chloro-1-phenylpropyl)-3-(4-fluorophenyl)-1,3-dihydro-2H-benzimidazol-2-one (**20**). Yield: 63%, dark orange resin, purification: silica gel 60, petroleum ether/ethyl acetate 9:1 and RP-18 silica gel, methanol, ^{1}H-NMR (400 MHz, $CDCl_3$): δ (ppm) 2.80–2.88 (m, 1H, 2'-C$\underline{H}_2$), 3.17–3.26 (m, 1H, 2'-C$\underline{H}_2$), 3.62–3.70 (m, 2H, 3'-C$\underline{H}_2$), 5.79 (dd, *J* = 10.0 Hz and 5.6 Hz, 1H, 1'-C$\underline{H}$), 7.04–7.09 (m, 4H, benzim 4-C$\underline{H}$, benzim 5-C$\underline{H}$, benzim 6-C$\underline{H}$, benzim 7-C$\underline{H}$), 7.21–7.26 (m, 2H, f-phen 3-C$\underline{H}$, f-phen 5-C$\underline{H}$), 7.31–7.33 (m, 1H, phen 4-C$\underline{H}$), 7.36–7.40 (m, 2H, phen 3-C$\underline{H}$, phen 5-C$\underline{H}$), 7.52–7.56 (m, 4H, f-phen 2-C$\underline{H}$, f-phen 6-C$\underline{H}$, phen 2-C$\underline{H}$, phen 6-C$\underline{H}$), ^{13}C-NMR (100 MHz, $CDCl_3$): δ (ppm) 34.1 (2'-C$\underline{H}_2$), 42.0 (3'-C$\underline{H}_2$), 54.4 (1'-C$\underline{H}$), 108.6 (benzim 4-C$\underline{H}$), 109.0 (benzim 7-C$\underline{H}$), 116.4 (d, *J* = 22.9 Hz, f-phen 3-C$\underline{H}$, 116.4 (d, *J* = 22.9 Hz, f-phen 5-C$\underline{H}$), 121.6 (benzim 5-C$\underline{H}$), 122.1 (benzim 6-C$\underline{H}$), 127.4 (phen 2-C$\underline{H}$), 127.4 (phen 6-C$\underline{H}$), 127.9 (d, *J* = 8.6 Hz, f-phen 2-C$\underline{H}$), 127.9 (d, *J* = 8.6 Hz, f-phen 6-C$\underline{H}$), 128.1 (phen 4-C$\underline{H}$), 128.7 (benzim 7a-C), 128.8 (phen 3-C$\underline{H}$), 128.8 (phen 5-C$\underline{H}$), 129.4 (benzim 3a-C), 130.3 (d, *J* = 3.1 Hz, f-phen 1-C), 138.4 (phen 1-C), 153.2 (benzim 2-C$\underline{O}$), 161.6 (d, *J* = 247.7 Hz, f-phen 4-C$\underline{F}$), ^{19}F-NMR (471 MHz, $CDCl_3$): δ (ppm) -113.31 (m, 5-C$\underline{F}$), MS: *m/z* (%) 380 (M^+, 2), 228 (100) (M^+-$C_9H_{10}Cl$), 199 (11), 185 (16), 153 (6), 117 (14), 91 (73), 75 (8), HRMS: *m/z* calculated for $C_{22}H_{19}ClFN_2O$ $[M + H]^+$: 381.1170. Found: 381.1176.

1-(3-Chloro-1-phenylpropyl)-3-(2-fluorophenyl-1,3-dihydro-2H-benzimidazol-2-one (**21**). Yield: 55%, orange resin, purification: silica gel 60, petroleum ether/ethyl acetate 9:1, ^{1}H-NMR (400 MHz, $CDCl_3$): δ (ppm) 2.78–2.86 (m, 1H, 2'-C$\underline{H}_2$), 3.23 (br s, 1H, 2'-C$\underline{H}_2$), 3.64–3.68 (m, 2H, 3'-C$\underline{H}_2$), 5.79 (br s, 1H, 1'-C$\underline{H}$), 6.85–6.87 (m, 1H, benzim 4-C$\underline{H}$) 7.05–7.06 (m, 3H, benzim 5-C$\underline{H}$, benzim 6-C$\underline{H}$, benzim 7-C$\underline{H}$), 7.28–7.40 (m, 5H, f-phen 3-C$\underline{H}$, f-phen 6-C$\underline{H}$, phen 3-C$\underline{H}$, phen 4-C$\underline{H}$, phen 5-C$\underline{H}$), 7.43–7.48 (m, 1H, f-phen 4-C$\underline{H}$), 7.52–7.56 (m, 3H, f-phen 5-C$\underline{H}$, phen 2-C$\underline{H}$, phen 6-C$\underline{H}$), ^{13}C-NMR (100 MHz, $CDCl_3$): δ (ppm) 34.2 (2'-C$\underline{H}_2$), 41.9 (3'-C$\underline{H}_2$), 54.5 (1'-C$\underline{H}$), 108.8 (d, *J* = 1.7 Hz, benzim 4-C$\underline{H}$), 109.0 (benzim 7-C$\underline{H}$), 117.1 (d, *J* = 19.5 Hz, f-phen 3-C$\underline{H}$), 121.6 (benzim 5-C$\underline{H}$), 121.9 (f-phen 1-C), 122.0 (benzim 6-C$\underline{H}$), 124.8 (d, *J* = 3.9 Hz, f-phen 6-C$\underline{H}$), 127.3 (phen 2-C$\underline{H}$), 127.3 (phen 6-C$\underline{H}$), 128.1 (phen 4-C$\underline{H}$), 128.8 (phen 3-C$\underline{H}$), 128.8 (phen 5-C$\underline{H}$), 129.4 (benzim 3a-C), 129.5 (f-phen 5-C$\underline{H}$), 130.2 (d, *J* = 7.8 Hz, f-phen 4-C$\underline{H}$), 138.4 (phen 1-C), 153.0 (benzim 2-C$\underline{O}$), 157.9 (d, *J* = 253.2 Hz, f-phen 2-C$\underline{F}$), due to limited resolution of the measuring apparatus, quaternary carbon benzim 7a-C could not be detected, ^{19}F-NMR (471 MHz, $CDCl_3$): δ (ppm) -118.39 (m, f-phen 2-C$\underline{F}$), MS: *m/z* (%) 380 (M^+, 12), 228 (100) (M^+-$C_9H_{10}Cl$), 199 (5), 153 (3), 117 (7), 91 (49), 75 (5), HRMS: *m/z* calculated for $C_{22}H_{19}ClFN_2O$ $[M + H]^+$: 381.1170. Found: 381.1164.

3.2.9. General Procedure for the Synthesis of **22**–**24**

A solution of starting materials **19**, **20**, or **21** (1 mmol) and NaI (1.03 g, 6.89 mmol) in acetone (7 mL) was refluxed for 24 h. The precipitate formed was filtered and the solvent was removed *in vacuo*.

1-(1-(4-Fluorophenyl)-3-iodopropyl)-3-phenyl-1,3-dihydro-2H-benzimidazol-2-one (**22**). Yield: 82%, yellow resin, ^{1}H-NMR (200 MHz, $CDCl_3$): δ (ppm) 2.77–2.92 (m, 1H), 3.14–3.31 (m, 3H), 5.63–5.70 (m, 1H), 7.01–7.10 (m, 6H), 7.36–7.56 (m, 7H), ^{13}C-NMR (50 MHz, $CDCl_3$): δ (ppm) 2.3, 35.3, 57.0, 108.8, 108.9, 115.5, 115.9, 121.6, 122.0, 126.0, 127.7, 128.5, 129.1, 129.3, 129.4, 134.0, 134.1, 134.3, 153.0, 159.9, 164.8, MS: *m/z* (%) 472 (M^+, 32), 317 (8), 210 (100) (M^+-C_9H_9F), 181 (11), 167 (23), 140 (3), 135 (43), 115 (8), 109 (34), 77 (15), 51 (7), HRMS: *m/z* calculated for $C_{22}H_{18}FIN_2ONa$ $[M + Na]^+$: 495.0346. Found: 495.0353.

1-(4-Fluorophenyl)-3-(3-iodo-1-phenylpropyl)-1,3-dihydro-2H-benzimidazol-2-one (**23**). Yield: 76%, yellow crystals, mp. 39 °C–41 °C, purification: silica gel 60, petrol ether/ethyl acetate 9:1, ^{1}H-NMR (200 MHz, $CDCl_3$): δ (ppm) 2.81–2.99 (m, 1H, 2'-C$\underline{H}_2$), 3.11–3.35 (m, 3H, 2'-C$\underline{H}_2$, 3'-C$\underline{H}_2$), 5.70 (dd, *J* = 6 Hz and 2 Hz, 1H, 1'-C$\underline{H}$), 7.04–7.09 (m, 4H, benzim 4-C$\underline{H}$, benzim 5-C$\underline{H}$, benzim 6-C$\underline{H}$, benzim 7-C$\underline{H}$), 7.17–7.42 (m, 5H, f-phen 3-C$\underline{H}$, f-phen 5-C$\underline{H}$, phen 4-C$\underline{H}$, phen 2-C$\underline{H}$, phen 5-C$\underline{H}$), 7.51–7.57 (m, 4H, f-phen 2-C$\underline{H}$, f-phen 6-C$\underline{H}$, phen 2-C$\underline{H}$, phen 6-C$\underline{H}$), ^{13}C-NMR (50 MHz, $CDCl_3$): δ (ppm) 2.4 (2'-C$\underline{H}_2$), 35.2 (3'-C$\underline{H}_2$), 57.6 (1'-C$\underline{H}$), 108.6 (benzim 4-C$\underline{H}$), 109.2 (benzim 7-C$\underline{H}$), 116.4 (d, *J* = 23 Hz, f-phen 3-C$\underline{H}$), 116.4 (d, *J* = 23 Hz, f-phen 5-C$\underline{H}$), 121.6 (benzim 5-C$\underline{H}$), 122.1 (benzim 6-C$\underline{H}$), 127.3 (phen 2-C$\underline{H}$), 127.3 (phen 6-C$\underline{H}$), 127.8 (phen 4-C$\underline{H}$), 128.1 (d, *J* = 5 Hz, f-phen 2-C$\underline{H}$), 128.1 (d, *J* = 5 Hz, f-phen 6-C$\underline{H}$), 128.5 (benzim 7a-C), 128.8 (phen 3-C$\underline{H}$), 128.8 (phen 5-C$\underline{H}$), 129.4 (benzim 3a-C), 130.3 (d, *J* = 3Hz, f-phen 1-C), 138.1 (phen 1-C), 153.2 (benzim 2-C$\underline{O}$), 161.6 (d, *J* = 247 Hz, f-phen 4-C$\underline{F}$), MS: *m/z* (%) 472 (M^+, 13), 317 (5), 228 (100) (M^+-$C_9H_{10}I$), 199 (8), 185 (15), 117 (47), 103 (2), 91 (40), 75 (8), 55 (5), HRMS: *m/z* calculated for $C_{22}H_{19}FIN_2O$ $[M + H]^+$: 473.0526. Found: 473.0506.

1-(2-Fluorophenyl)-3-(3-iodo-1-phenylpropyl)-1,3-dihydro-2H-benzimidazol-2-one (**24**). Yield: 53%, yellow crystals, mp. 38 °C–39 °C, purification: silica gel 60, petrol ether/ethyl acetate 9:1, ^{1}H-NMR (200 MHz, $CDCl_3$): δ (ppm) 2.80–2.98 (m, 1H, 2'-C$\underline{H}_2$), 3.13–3.36 (m, 3H, 2'-C$\underline{H}_2$, 3'-C$\underline{H}_2$), 5.67–5.74 (m, 1H, 1'-C$\underline{H}$), 6.85–6.88 (m, 1H, benzim 4-C$\underline{H}$) 6.99–7.07 (m, 3H, benzim 5-C$\underline{H}$, benzim 6-C$\underline{H}$, benzim 7-C$\underline{H}$), 7.26–7.45 (m, 5H, f-phen 3-C$\underline{H}$, f-phen 6-C$\underline{H}$, phen 3-C$\underline{H}$, phen 4-C$\underline{H}$, phen 5-C$\underline{H}$), 7.47–7.58 (m, 4 H, f-phen 4-C$\underline{H}$, f-phen 5-C$\underline{H}$, phen 2-C$\underline{H}$, phen 6-C$\underline{H}$), ^{13}C-NMR (50 MHz, $CDCl_3$): δ (ppm) 2.3 (2'-C$\underline{H}_2$), 35.4 (3'-C$\underline{H}_2$), 57.6 (1'-C$\underline{H}$), 108.9 (d, *J* = 1.5 Hz, benzim 4-C$\underline{H}$), 109.1 (benzim 7-C$\underline{H}$), 117.1 (d, *J* = 19 Hz, f-phen 3-C$\underline{H}$), 121.6 (benzim 5-C$\underline{H}$), 121.9 (f-phen 1-C), 122.0 (benzim 6-C$\underline{H}$), 124.8 (d, *J* = 3.5 Hz, f-phen 6-C$\underline{H}$), 127.3 (phen 2-C$\underline{H}$), 127.3 (phen 6-C$\underline{H}$), 128.1 (phen 4-C$\underline{H}$), 128.8 (phen 3-C$\underline{H}$), 128.8 (phen 5-C$\underline{H}$), 129.5 (f-phen 5-C$\underline{H}$), 130.2 (d, *J* = 8 Hz, f-phen 4-C$\underline{H}$), 138.2 (phen 1-C), 153.0 (benzim 2-C$\underline{O}$), 157.8 (d, *J* = 251.5 Hz, f-phen 2-C$\underline{F}$), MS: *m/z* (%) 472 (M^+, 9), 317 (5), 241 (4), 228 (100) (M^+-$C_9H_{10}I$), 199 (5), 185 (10), 117 (37), 91 (29), 75 (7), HRMS: *m/z* calculated for $C_{22}H_{19}FIN_2O$ $[M + H]^+$: 473.0526. Found: 473.0532.

3.2.10. General procedure for the synthesis of *1-(3-amino-1-(4-fluorophenyl)propyl)-3-phenyl-1,3-dihydro-2H-benzimidazol-2-one* (**25**)

1-(1-(4-fluorophenyl)-3-iodopropyl)-3-phenyl-1,3-dihydro-2*H*-benzimidazol-2-one (0.26 g, 0.55 mmol) and a solution of NH_3 in isopropanol (2 M, 22 mL) were heated in a sealed tube for 3 h at 80 °C. After evaporation of the solvent, the crude product was purified by column chromatography (silica gel 60, CH_2Cl_2/MeOH 9:1). Yield: 0.10 g (50%), light brown crystals, mp. 87–88 °C. ^{1}H-NMR (400 MHz, $CDCl_3$): δ (ppm) 2.74–2.84 (m, 3H, 2'-C$\underline{H}_2$, 3'-C$\underline{H}_2$), 2.98–3.04 (m, 1H, 3'-C$\underline{H}_2$), 5.74–5.78 (m, 1H, 1'-C$\underline{H}$), 6.79–6.81 (m, 1H, benzim 7-C$\underline{H}$), 6.96–7.01 (m, 5H, benzim 4-C$\underline{H}$, benzim 5-C$\underline{H}$, benzim 6-C$\underline{H}$, f-phen 3-C$\underline{H}$, f-phen 5-C$\underline{H}$), 7.30–7.33 (m, 1H, phen 4-C$\underline{H}$), 7.40–7.48 (m, 4H, f-phen 2-C$\underline{H}$, f-phen 6-C$\underline{H}$, phen 3-C$\underline{H}$, phen 5-C$\underline{H}$), 7.52–7.54 (m, 2H, phen 2-C$\underline{H}$, phen 6-C$\underline{H}$), due to limited resolution of the instrumentation, the N$\underline{H}_2$ protons could not be detected, ^{13}C-NMR (100 MHz, $CDCl_3$): δ (ppm) 30.3 (2'-$\underline{C}H_2$), 37.8 (3'-$\underline{C}H_2$), 52.7 (1'-$\underline{C}$H), 109.2 (benzim 4-$\underline{C}$H), 110.0 (benzim 7-$\underline{C}$H), 115.7 (d, *J* = 21.5 Hz, f-phen 3-$\underline{C}$H), 115.7 (d, *J* = 8.2 Hz, f-phen 5-$\underline{C}$H), 122.0 (benzim 5-$\underline{C}$H), 122.3 (benzim 6-$\underline{C}$H), 126.4 (phen 2-$\underline{C}$H), 126.4 (phen 6-$\underline{C}$H), 127.5 (benzim 7a-C), 128.1 (phen 4-$\underline{C}$H), 129.2 (d, *J* = 8.2 Hz, f-phen 2-$\underline{C}$H), 129.2 (d, *J* = 8.2 Hz, f-phen 6-$\underline{C}$H), 129.5 (benzim 3a-C), 129.7 (phen 3-$\underline{C}$H), 129.7 (phen 5-$\underline{C}$H), 133.3 (d, *J* = 3.2 Hz, f-phen 1-C), 134.0 (phen 1-$\underline{C}$H), 153.8 (benzim 2-$\underline{C}$O), 162.3 (d, *J* = 247.4 Hz, f-phen 4-$\underline{C}$F), ^{19}F-NMR (471 MHz, $CDCl_3$): δ (ppm) -113.68 (m, f-phen C$\underline{F}$), MS: *m/z* (%) 361 (M^+, 17), 331 (10), 210 (100) (M^+-$C_9H_{11}FN$), 181 (15), 167 (16), 149 (29), 128 (17), 77 (19), 57 (20), 43 (12), HRMS: *m/z* calculated for $C_{22}H_{21}FN_3O$ $[M + H]^+$: 362.1669. Found: 362.1674.

3.2.11. General Procedure for the Synthesis of **4**–**6**

Starting materials **18**, **19** or **20** (1 mmol) and a solution of methylamine in EtOH (12.5 mL, 8 M) were heated in a sealed tube for 3 h at 80 °C. After evaporation of the solvent, the crude reaction product was purified by column chromatography.

1-(1-(4-Fluorophenyl)-3-(methylamino)propyl)-3-phenyl-1,3-dihydro-2H-benzimidazol-2-one (**4**). Yield: 48%, light orange resin, purification: silica gel 60, dichloromethane/methanol 9:1 and dichloromethane/ethyl acetate/methanol 7:2:1, ^{1}H-NMR (400 MHz, $CDCl_3$): δ (ppm) 2.42 (s, 3H, NHC$\underline{H}_3$), 2.57–2.74 (m, 4H, 2'-C$\underline{H}_2$, 3'-C$\underline{H}_2$), 3.15 (br s, 1H, N$\underline{H}$CH$_3$), 5.76–5.79 (m, 1H, 1'-C$\underline{H}$), 6.88–6.90 (m, 1H, benzim 7-C$\underline{H}$), 6.97–7.05 (m, 4H, benzim 5-C$\underline{H}$, benzim 6-C$\underline{H}$, f-phen 3-C$\underline{H}$, f-phen 5-C$\underline{H}$), 7.07–7.10 (m, 1H, benzim 4-C$\underline{H}$), 7.39–7.43 (m, 1H, phen 4-C$\underline{H}$), 7.46–7.57 (m, 6H, f-phen 2-C$\underline{H}$, f-phen 6-C$\underline{H}$, phen 2-C$\underline{H}$, phen 3-C$\underline{H}$, phen 5-C$\underline{H}$, phen 6-C$\underline{H}$), ^{13}C-NMR (100 MHz, $CDCl_3$): δ (ppm) 30.6 (2'-$\underline{C}H_2$), 35.9 (NH$\underline{C}$H$_3$), 48.3 (3'-$\underline{C}H_2$), 53.1 (1'-$\underline{C}$H), 108.9 (benzim 4-$\underline{C}$H), 109.5 (benzim 7-$\underline{C}$H), 115.5 (d, *J* = 21.5 Hz, f-phen 3-$\underline{C}$H), 115.5 (d, *J* = 21.5 Hz, f-phen 5-$\underline{C}$H) 121.4 (benzim 5-$\underline{C}$H), 121.8 (benzim 6-$\underline{C}$H), 126.0 (phen 2-$\underline{C}$H), 126.0 (phen 6-$\underline{C}$H), 127.7 (phen 4-$\underline{C}$H), 128.0 (benzim 7a-C), 129.0 (d, *J* = 8.1 Hz, f-phen 2-$\underline{C}$H), 129.0 (d, *J* = 8.1 Hz, f-phen 6-$\underline{C}$H), 129.4 (benzim 3a-C), 129.5 (phen 3-C$\underline{H}$), 129.5 (phen 5-C$\underline{H}$), 134.4 (phen 1-$\underline{C}$H), 134.6 (d, *J* = 3.4 Hz, f-phen 1-$\underline{C}$H), 153.5 (benzim 2-$\underline{C}$O), 162.1 (d, *J* = 246.7 Hz, f-phen 4-$\underline{C}$F), ^{19}F-NMR (471 MHz, $CDCl_3$): δ (ppm) -114.36 (m, f-phen 4-C$\underline{F}$), MS: *m/z* (%) 375 (M^+, 16), 210 (57) (M^+-$C_{10}H_{13}FN$), 181 (10), 167 (12), 150 (10), 109 (22), 97 (16), 71 (27), 57 (78), 44 (100), HRMS: *m/z* calculated for $C_{23}H_{23}FN_3O$ $[M + H]^+$: 376.1825. Found: 376.1821.

1-(4-Fluorophenyl)-3-(3-(methylamino)-1-phenylpropyl)-1,3-dihydro-2H-benzimidazol-2-one (**5**). Yield: 29%, light yellow crystals, mp. 100 °C–102 °C, purification: silica gel 60, dichloromethane/methanol 9:1 and RP-18 silica gel methanol/water 9:1 and 7:3, ^{1}H-NMR (200 MHz, $CDCl_3$): δ (ppm) 2.53 (s, 3H, NHC$\underline{H}_3$), 3.13 (br s, 4H, 2'-C$\underline{H}_2$, 3'-C$\underline{H}_2$), 5.77–5.81 (m, 1H, 1'-C$\underline{H}$), 6.96–7.03 (m, 4H, benzim 4-C$\underline{H}$, benzim 5-C$\underline{H}$, benzim 6-C$\underline{H}$, benzim 7-C$\underline{H}$), 7.16–7.34 (5H, f-phen 3-C$\underline{H}$, f-phen 5-C$\underline{H}$, phen 4-C$\underline{H}$, phen 2-C$\underline{H}$, phen 5-C$\underline{H}$), 7.49–7.56 (m, 4H, f-phen 2-C$\underline{H}$, f-phen 6-C$\underline{H}$, phen 2-C$\underline{H}$, phen 6-C$\underline{H}$), due to limited resolution of the instrumentation, the N$\underline{H}$ proton could not be detected, ^{13}C-NMR (50 MHz, $CDCl_3$): δ (ppm) 27.6 (2'-$\underline{C}H_2$), 33.1 (NH$\underline{C}H_3$), 47.0 (3'-$\underline{C}H_2$), 54.2 (1'-$\underline{C}$H), 108.8 (benzim 4-$\underline{C}$H), 109.9 (benzim 7-$\underline{C}$H), 116.6 (d, *J* = 23 Hz, f-phen 3-$\underline{C}$H), 116.6 (d, *J* = 23 Hz, f-phen 5-$\underline{C}$H), 122.1 (benzim 5-$\underline{C}$H), 122.6 (benzim 6-$\underline{C}$H), 127.2 (phen 2-$\underline{C}$H), 127.2 (phen 6-$\underline{C}$H), 127.7 (phen 4-$\underline{C}$H), 128.3 (d, *J* = 6 Hz, f-phen 2-$\underline{C}$H), 128.3 (d, *J* = 6 Hz, f-phen 6-$\underline{C}$H), 128.4 (benzim 7a-C), 128.9 (phen 3-$\underline{C}$H), 128.9 (phen 5-$\underline{C}$H), 129.2 (benzim 3a-C), 129.7 (d, *J* = 3 Hz, f-phen 1-C), 136.9 (phen 1-C), 153.4 (benzim 2-$\underline{C}$O), 161.7 (d, *J* = 248 Hz, f-phen 4-$\underline{C}$F), MS: *m/z* (%) 375 (M^+, 11), 330 (7), 228 (50) (M^+-$C_{10}H_{14}N$), 199 (7), 185 (9), 147 (17), 128 (26), 117 (8), 91 (13), 58 (34), 44 (100), HRMS: *m/z* calculated for $C_{23}H_{23}FN_3O$ $[M + H]^+$: 376.1825. Found: 376.1828.

1-(2-Fluorophenyl)-3-(3-(methylamino)-1-phenylpropyl)-1,3-dihydro-2H-benzimidazol-2-one (**6**). Yield: 30%, yellow crystals, mp. 92 °C–93 °C, purification: silica gel 60, dichloromethane/methanol 9:1 and RP-18 silica gel methanol/water 9:1 and 7:3, ^{1}H-NMR (200 MHz, $CDCl_3$): δ (ppm) 2.57 (s, 3H, NHC$\underline{H}_3$), 3.01–3.15 (m, 4H, 2'-C$\underline{H}_2$, 3'-C$\underline{H}_2$), 5.75–5.86 (m, 1H, 1'-C$\underline{H}$), 6.83–6.87 (m, 1H, benzim 4-C$\underline{H}$) 6.98–7.05 (m, 3H, benzim 5-C$\underline{H}$, benzim 6-C$\underline{H}$, benzim 7-C$\underline{H}$), 7.25–7.42 (m, 5H, f-phen 3-C$\underline{H}$, f-phen 6-C$\underline{H}$, phen 3-C$\underline{H}$, phen 4-C$\underline{H}$, phen 5-C$\underline{H}$), 7.48–7.61 (m, 4 H, f-phen 4-C$\underline{H}$, f-phen 5-C$\underline{H}$, phen 2-C$\underline{H}$, phen 6-C$\underline{H}$), due to limited resolution of the instrumentation, the N$\underline{H}CH_3$ proton could not be detected, ^{13}C-NMR (50 MHz, $CDCl_3$): δ (ppm) 27.7 (2'-$\underline{C}H_2$), 33.2 (NH$\underline{C}$H3), 46.9 (3'-$\underline{C}H_2$), 53.5 (1'-$\underline{C}$H), 109.0 (benzim 4-$\underline{C}$H), 110.1 (benzim 7-$\underline{C}$H), 117.1 (d, *J* = 19.5 Hz, f-phen 3-$\underline{C}$H), 122.2 (benzim 5-$\underline{C}$H), 122.7 (benzim 6-$\underline{C}$H), 125.1 (d, *J* = 3.0 Hz, f-phen 6-$\underline{C}$H), 127.3 (phen 2-$\underline{C}$H), 127.1 (phen 6-$\underline{C}$H), 128.3 (phen 4-$\underline{C}$H), 128.9 (phen 3-$\underline{C}$H), 128.9 (phen 5-$\underline{C}$H), 129.5 (f-phen 5-$\underline{C}$H), 130.7 (d, *J* = 4.5 Hz, f-phen 4-$\underline{C}$H), 136.5 (phen 1-C), 153.6 (benzim 2-$\underline{C}$O), 157.6 (d, *J* = 250.5 Hz, f-phen 2-$\underline{C}$F), due to limited resolution of the measuring apparatus, quaternary carbon f-phen 1-C could not be detected, MS: *m/z* (%) 375 (M^+, 17), 318 (10), 228 (82) (M^+-$C_{10}H_{14}N$), 199 (9), 185 (9), 147 (16), 128 (35), 117 (9), 91 (20), 58 (43), 44 (100), HRMS: *m/z* calculated for $C_{23}H_{23}FN_3O$ $[M + H]^+$: 376.1825. Found: 376.1822.

3.3. Computational Methods

The ligand structures were built in the protonated form using Molecular Operating Environment (MOE) 2013 [42]. Homology models of human NET, SERT and DAT were obtained from the *Drosophila* dopamine transporter template ($dDAT_{cryst}$, PDB id 4M48 [32]), by selecting the model with the most favorable Discrete Optimized Protein Energy (DOPE) of 250 generated by Modeller 9.11 [43]. The co-crystallized inhibitor nortriptyline was retained during model generation and the compounds were docked in the same site using Genetic Optimization for Ligand Docking (GOLD) 5.2 [44]. One hundred poses per ligand (*i.e.*, five hundred poses per protein target) were generated based on the GoldScore scoring function, while keeping the ligand flexible and the protein rigid.

The common chemical scaffold, *i.e.*, the reference compound, was extracted from the resulting poses, analogous to the methods of our previous study [35]. Cluster analysis was performed based on Euclidian distance and complete linkage of the root-mean square deviation of the ligand's heavy atoms matrix using XLStat [45]. The dendrogram was cut at eight clusters and the ones containing all five ligands were selected (Figure 5).

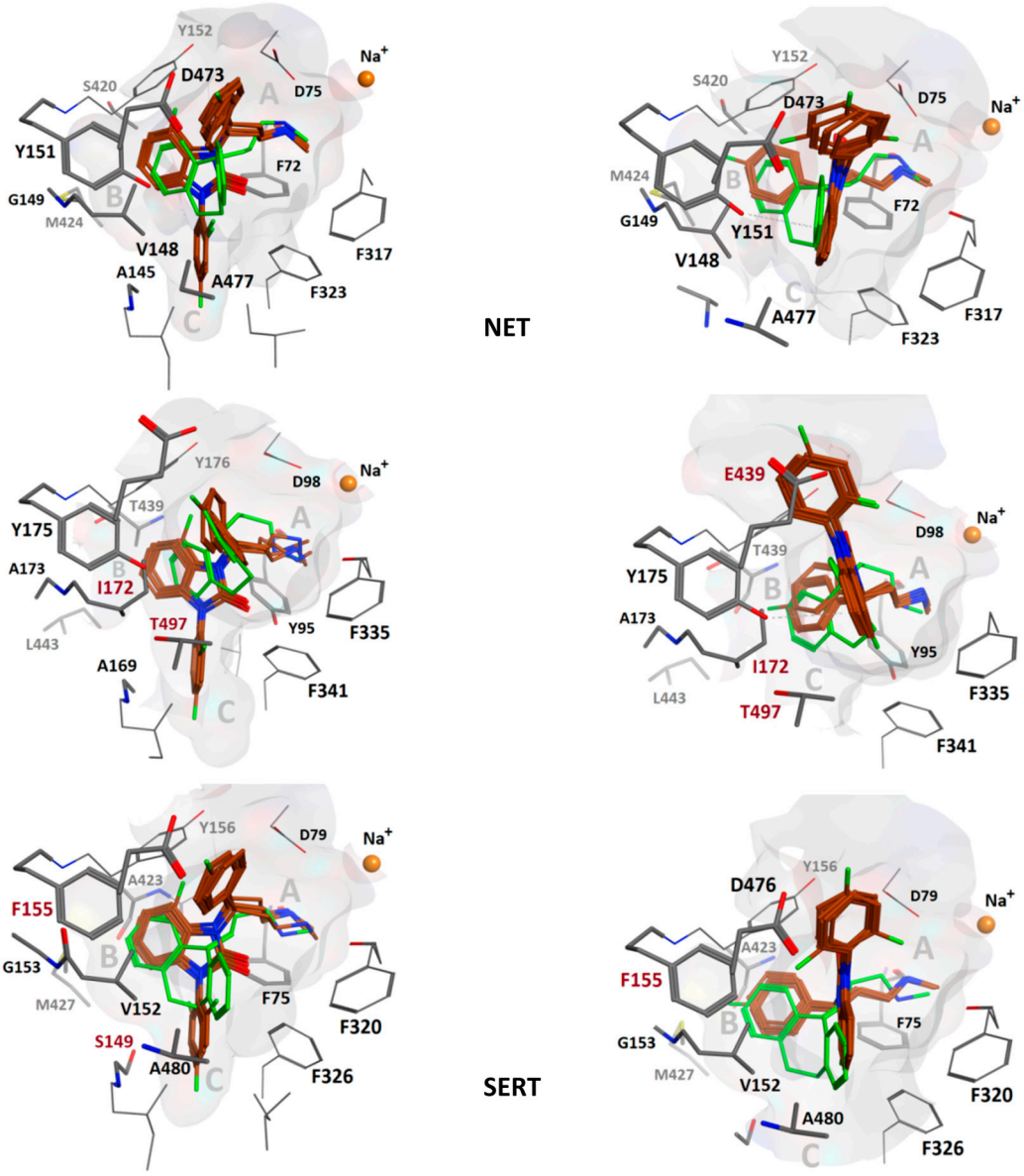

Figure 5. *Left column*: Overlay of compounds **1**, **2**, and **4**–**6** (maroon) in binding hypothesis 1 and comparison with the co-crystal pose of nortriptyline (**31**) (green). In NET, V148 allows more space than I172 in SERT. The angle between ligand ring 2 and 3 is *ca.* 60° in all poses. *Right column*: Overlay of compounds **1**, **2**, and **4**–**6** (maroon) in binding hypothesis 2. In NET, V148 still allows more space than in hSERT, whereas E439 might disrupt ligand ring 3. DAT lacks a more potent stacking interaction due to F155 as compared to NET[Y151] and SERT[Y175]. Binding mode 2 poses are more in agreement with the co-crystal pose. The angle between ligand ring 2 and 3 is almost 90° in all poses. The extracellular space is located above in all figures.

4. Conclusions

In conclusion, ten new compounds have been synthesized within the scope of this work, which aimed at the development of new, selective, high affinity references for the imaging of the NET system via PET. Four of these new compounds (**4**–**6** and **25**) will be employed in future studies. Whilst methylamines **4**–**6** (FAPPI:1-3) represent reference compounds for their later prepared radioactive analogs, additionally prepared free amine **25** (APPI:1) will serve as precursor for radiolabeling. Since docking studies indicate that fluorinated methyl amines **4**–**6** (FAPPI:1-3) bind in an analogous way to the NET as reference compound **1**, these compounds **4**–**6** are promising candidates for biological evaluation.

Acknowledgments

AS, AJ, and GFE acknowledge financial support provided by the Austrian Science Fund, grants AW/0123221 and F3502. This article was supported by the Open Access Publishing Fund of the University of Vienna.

Author Contributions

Catharina Neudorfer: Responsible for the performance of the syntheses and writing; Amir Seddik: Structure activity relationships calculations; Karem Shanab: Contributions to syntheses and experimental procedures; Andreas Jurik: Structure activity relationships calculations; Christina Rami-Mark: Participated in design and performance of the experiments; Wolfgang Holzer: Performance of the NMR analyses; Gerhard Ecker: Conceived and supervised the SAR experiments; Markus Mitterhauser: Designed parts of the research and proofread the manuscript; Wolfgang Wadsak: Designed parts of the research and proofread the manuscript; Helmut Spreitzer: Conceived and supervised the syntheses.

Conflicts of Interest

The authors declare no conflict of interest.

References

1. Sung, U.; Apparsundram, S.; Galli, A.; Kahlig, K.M.; Savchenko, V.; Schroeter, S.; Quick, M.W.; Blakely, R.D. A regulated interaction of syntaxin 1A with the antidepressant-sensitive norepinephrine transporter establishes catecholamine clearance capacity. *J. Neurosci.* **2003**, *23*, 1697–1709.
2. Kim, C.H.; Hahn, M.K.; Joung, Y.; Anderson, S.L.; Steele, A.H.; Mazei-Robinson, M.S.; Gizer, I.; Teicher, M.H.; Cohen, B.M.; Robertson, D.; *et al*. A polymorphism in the norepinephrine transporter gene alters promoter activity and is associated with attention-deficit hyperactivity disorder. *Proc. Natl. Acad. Sci. USA* **2006**, *103*, 19164–19169.
3. Hahn, M.K.; Robertson, D.; Blakely, R.D. A mutation in the human norepinephrine transporter gene (SLC6A2) associated with orthostatic intolerance disrupts surface expression of mutant and wild-type transporters. *J. Neurosci*. **2003**, *23*, 4470–4478.

4. Mirbolooki, M.R.; Upadhyay, S.K.; Constantinescu, C.C.; Pan, M.L.; Mukherjee, J. Adrenergic pathway activation enhances brown adipose tissue metabolism: A [^{18}F]FDG PET/CT study in mice. *Nucl. Med. Biol.* **2014**, *41*, 10–16.
5. Lin, S.L.; Fan, X.; Yeckel, C.W.; Weinzimmer, D.; Mulnix, T.; Gallezot, J.D.; Carson, R.E.; Sherwin, R.S.; Ding, Y.S. *Ex vivo* and *in vivo* Evaluation of the Norepinephrine Transporter Ligand [^{11}C]MRB for Brown Adipose Tissue Imaging. *Nucl. Med. Biol.* **2012**, *39*, 1081–1086.
6. Stöber, G.; Nöthen, M.M.; Pörzgen, P.; Brüss, M.; Bönisch, H.; Knapp, M.; Beckmann, H.; Propping, P. Systematic search for variation in the human norepinephrine transporter gene: Identification of five naturally occurring missense mutations and study of association with major psychiatric disorders. *Am. J. Med. Genet. (Neuropsychiatr. Genet.)* ***1996***, 67, 523–532.
7. Young, J.B.; Landsberg, L. Catecholamines and the adrenal medulla. In *Williams Textbook of Endocrinology*, 9th ed.; Wilson, J.D., Foster, D.W., Eds.; W.B. Saunders Co.: Philadelphia, PA, USA, 1998; p. 680.
8. Tellioglu, T.; Robertson, D. Genetic or acquired deficits in the norepinephrine transporter: Current understanding of clinical implications. *Exp. Rev. Mol. Med*. **2001**, 1–10.
9. Blakely, R.D.; Bauman, A.L. Biogenic amine transporters: regulation in flux. *Curr. Opin. Neurobiol*. **2000**, *10*, 328–336.
10. Zhu, M.Y.; Shamburger, S.; Li, J.; Ordway, G.A. Regulation of the Human Norepinephrine Transporter by Cocaine and Amphetamine. *J. Pharmacol. Exp. Ther.* **2000**, *295*, 951–959.
11. Moron, J.A.; Brockington, A.; Wise, R.A.; Rocha, B.A.; Hope, B.T. Dopamine Uptake through the Norepinephrine Transporter in Brain Regions with Low Levels of the Dopamine Transporter: Evidence from Knock-Out Mouse Lines. *J. Neurosci*. **2002**, *22*, 386–395.
12. Schroeter, S.; Apparsundaram, S.; Wiley, R.G.; Miner, L.H.; Sesack, S.R.; Blakely, R.D. Immunolocalization of the cocaine- and antidepressant-sensitive l-norepinephrine transporter. *J. Comp. Neurol.* **2000**, *420*, 211–232.
13. Torres, G.E.; Gainetdinov, R.R.; Caron, M.G. Plasma membrane monoamine transporters: Structure, regulation and function. *Nat. Rev. Neurosci.* **2003**, *4*, 13–25.
14. Ordway, G.A.; Stockmeier, C.A.; Cason, G.W.; Klimek, V. Pharmacology and Distribution of Norepinephrine Transporters in the Human Locus Coeruleus and Raphe Nuclei. *J. Neurosci*. **1997**, *17*, 1710–1719.
15. Smith, H.R.; Beveridge, T.J. R.; Porrino, L.J. Distribution of norepinephrine transporters in the non-human primate brain. *Neuroscience* **2006**, *138*, 703–714.
16. Zhou, J. Norepinephrine transporter inhibitors and their therapeutic potential. *Drugs Future* **2004**, *29*, 1235–1244.
17. Curatolo, P.; D'Agati, E.; Moavero, R. The neurobiological basis of ADHD. *Ital. J. Pediatr*. **2010**, *36*, 79.
18. Mash, D.C.; Ouyang, Q.; Qin, Y.; Pablo, J. Norepinephrine transporter immunoblotting and radioligand binding in cocaine abusers. *Neurosci. Methods* **2005**, *143*, 79–85.
19. Barr, C.L.; Kroft, J.; Feng, Y.; Wigg, K.; Roberts, W.; Malone, M.; Ickowicz, A.; Schachar, R.; Tannock, R.; Kennedy, J.L. The Norepinephrine Transporter Gene and Attention-Deficit Hyperactivity Disorder. *Am. J. Med. Genet. (Neuropsychiatr. Genet.)* **2002**, *114*, 255–229.

20. Klimek, V.; Stockmeier, C.; Overholser, J.; Meltzer, H.Y.; Kalka, S.; Dilley, G.; Ordway, G.A. Reduced Levels of Norepinephrine Transporters in the Locus Coeruleus in Major Depression. *J. Neurosci.* **1997**, *17*, 8451–8458.
21. Nedergaard, J.; Cannon, B. The changed metabolic world with human brown adipose tissue: Therapeutic visions. *Cell Metab.* **2010**, *11*, 268–272.
22. Gulyas, B.; Brockschnieder, D.; Nag, S.; Pavlova, E.; Kasa, P.; Beliczai, Z.; Legradi, A.; Gulya, K.; Thiele, A.; Dyrks, T.; *et al*. The norepinephrine transporter radioligand [18F]FD2MeNER shows significant decreases in NET density in the locus coeruleus and the thalamus in Alzheimer's disease: A post-mortem autoradiographic study in human brains. *Neurochem. Int.* **2010**, *56*, 789–798.
23. Wilson, A.A.; Johnson, D.P.; Mozley, D.; Hussey, D.; Ginovart, N.; Nobrega, J.; Garcia, A.; Meyer, J.; Houle, S. Synthesis and *in vivo* evaluation of novel radiotracers for the *in vivo* imaging of the norepinephrine transporter. *Nucl. Med. Biol.* **2003**, *30*, 85–92.
24. Takano, A.; Gulyas, B.; Varrone, A.; Halldin, C. Saturated norepinephrine transporter occupancy by atomoxetine relevant to clinical doses: a rhesus monkey study with (S,S)-[(18)F]FMeNER-D (2). *Eur. J. Nucl. Med. Mol. Imaging* **2009**, *36*, 1308–1314.
25. Schou, M.; Zoghbi, S.S.; Shetty, H.U.; Shchukin, E.; Liow, J.S.; Hong, J.; Andrée, B.A.; Gulyás, B.; Farde, L.; Innis, R.B.; *et al*. Investigation of the metabolites of [^{11}C](S,S)-MeNER in humans, monkeys and rats. *Mol. Imaging Biol.* **2009**, *11*, 23–30.
26. Zhang, P.; Terefenko, E.A.; McComas, C.C.; Mahaney, P.E.; Vu, A.; Trybulski, E.; Koury, E.; Johnston, G.; Bray, J.; Deecher, D. Synthesis and activity of novel 1- or 3-(3-amino-1-phenyl propyl)-1,3-dihydro-2*H*-benzimidazol-2-ones as selective norepinephrine reuptake inhibitors. *Bioorg. Med. Chem. Lett.* **2008**, *18*, 6067–6070.
27. Mark, C.; Bornatowicz, B.; Mitterhauser, M.; Hendl, M.; Nics, L.; Haeusler, D.; Lanzenberger, R.; Berger, M.L.; Spreitzer, H.; Wadsak, W. Development and automation of a novel NET-PET tracer: [C-11]Me@APPI. *Nucl. Med. Biol.* **2013**, *40*, 295–303.
28. Varney, M.D.; Romines, W.H.; Boritzki, T.; Margosiak, S.A.; Barlett, C.; Howland, E.J. Synthesis and biological evaluation of -n[4-(2-trans-[([2,6-diamino-4(3H)-oxopyrimidin-5-yl]methyl)thio]cyclobutyl)benzoyl] -l-glutamic acid a novel 5-thiapyrimidinone inhibitor of dihydrofolate reductase. *J. Heterocycl. Chem.* **1995**, *32*, 1493–1498.
29. Xu, Z.B.; Lu, Y.; Guo, Z.R. An Efficient and Fast Procedure for the Preparation of 2-Nitrophenylamines under Microwave Conditions. *Synlett* **2003**, *4*, 564–566.
30. Wang, X.J.; Xi, M.Y.; Fu, J.H.; Zhang, F.R.; Cheng, G.F.; Yin, D.L.; You, Q.D. Synthesis, biological evaluation and SAR studies of benzimidazole derivatives as H_1-antihistamine agents. *Chin. Chem. Lett.* **2012**, *23*, 707–710.
31. Jona, H.; Shibata, J.; Asai, M.; Goto, Y.; Arai, S.; Nakajima, S.; Okamoto, O.; Kawamoto, H.; Iwasawa, Y. Efficient and practical asymmetric synthesis of 1-tert-butyl 3-methyl (3*R*,4*R*)-4-(2-oxo-2,3-dihydro-1*H*-benzimidazol-1-yl)piperidine-1,3-dicarboxylate, a useful intermediate for the synthesis of nociceptin antagonists. *Tetrahedron: Asymmetry* **2009**, *20*, 2439–2446.
32. Penmatsa, A.; Wang, K.H.; Gouaux, E. X-ray structure of dopamine transporter elucidates antidepressant mechanism. *Nature* **2013**, *503*, 85–90.
33. Wang, H.; Goehring, A.; Wang, K.H.; Penmatsa, A.; Ressler, R.; Gouaux, E. Structural basis for action by diverse antidepressants on biogenic amine transporters. *Nature* **2013**, *503*, 141–145.

34. Tatsumi, M.; Groshan, K.; Blakely, R.D.; Richelson, E. Pharmacological profile of antidepressants and related compounds at human monoamine transporters. *Eur. J. Pharmacol.* **1997**, *340*, 249–258.
35. Richter, L.; de Graaf, C.; Sieghart, W.; Varagic, Z.; Morzinger, M.; de Esch, I.J.; Ecker, G.F.; Ernst, M. Diazepam-bound GABAA receptor models identify new benzodiazepine binding-site ligands. *Nat. Chem. Biol.* **2012**, *8*, 455–464.
36. Andersen, J.; Olsen, L.; Hansen, K.B.; Taboureau, O.; Jorgensen, F.S.; Jorgensen, A.M.; Bang-Andersen, B.; Egebjerg, J.; Stromgaard, K.; Kristensen, A.S. Mutational Mapping and Modeling of the Binding Site for (*S*)-Citalopram in the Human Serotonin Transporter. *J. Biol. Chem.* **2010**, *285*, 2051–2063.
37. Chelli, R.; Gervasio, F.L.; Procacci, P.; Schettino, V. Stacking and T-shape Competition in Aromatic–Aromatic Amino Acid Interactions. *J. Am. Chem. Soc.* **2002**, *124*, 6133–6143.
38. Yu, F.; Zhou, J.N.; Zhang, X.C.; Sui, Y.Z.; Wu, F.F.; Xie, L.J.; Chan, A.S.C.; Wu, J. Copper(II)-Catalyzed Hydrosilylation of Ketones Using Chiral Dipyridylphosphane Ligands: Highly Enantioselective Synthesis of Valuable Alcohols. *Chemistry* **2011**, *17*, 14234–14240.
39. La Regina, G.; Diodata D'Auria, F.; Tafi, A.; Piscitelli, F.; Olla, S.; Caporuscio, F.; Nencioni, L.; Cirilli, R.; La Torre, F.; Rodrigues De Melo, N.; *et al*. 1-[(3-Aryloxy-3-aryl)propyl]-1H-imidazoles, new imidazoles with potent activity against Candida albicans and dermatophytes. Synthesis, structure-activity relationship, and molecular modeling studies. *J. Med. Chem.* **2008**, *51*, 3841–3855.
40. Panagopoulos, A.M.; Steinman, D.; Goncharenko, A.; Geary, K.; Schleisman, C.; Spaargaren, E.; Zeller, M.; Becker, D.P. Apparent Alkyl Transfer and Phenazine Formation via an Aryne Intermediate. *J. Org. Chem.* **2013**, *78*, 3532–3540.
41. Liu, P.; Wang, Z.; Hu, X. Highly Efficient Synthesis of Ureas and Carbamates from Amides by Iodosylbenzene-Induced Hofmann Rearrangement. *Eur. J. Org. Chem.* **2012**, *10*, 1994–2000.
42. *Molecular Operating Environment (MOE)*; Chemical Computing Group Inc.: Montreal, QC, Canada, 2013.
43. Sali, A.; Potterton, L.; Yuan, F.; van Vlijmen, H.; Karplus, M. Evaluation of comparative protein modeling by MODELLER. *Proteins* **1995**, *23*, 318–326.
44. Jones, G.; Willett, P.; Glen, R.C.; Leach, A.R.; Taylor, R. Development and validation of a genetic algorithm for flexible docking. *J. Mol. Biol.* **1997**, *267*, 727–748.
45. *XLStat*; Addinsoft Inc.: New York, NY, USA, 2009.

Sample Availability: Samples of the compounds **4**–**6**, **9**–**25**, and **29** and **30** are available from the authors.

Concluding Remarks

The thesis was focused on elucidating the selectivity of substrates for the monoamine transporters, whereby most attention has been given to DAT and SERT. Since substrates are relatively small, their affinity is rather low and therefore they are not commonly applied as therapeutic drugs. The interest for the pharmaceutical industry is therefore minimal and this explains the low number of literature data present for these compounds. Nonetheless, academic institutions exploit the activity of these compounds to gain a more fundamental understanding of the MAT selectivity and selectivity for biomolecules in general.

At the start of thesis, a summary was given of the substrate activity data available in the literature. Based on uptake inhibitory activities of amphetamines on the rat and human transporter, it was found that chirality of α-methylene atom does not influence selectivity, that the (*S*)-enantiomer is most active in DAT and SERT and that DAT- and NET-selective substrates are smaller than SERT substrates. A docking study of the SERT-selective (*S*)-fenfluramine indicated that certain residues present in SERT, but not in DAT, are accountable for this (section II.A).

The ligand-based Hansch analysis applied on the cathinone dataset (section II.B), indicated that a lipophilic or polarizable *para*-substituent positively influences SERT binding, which was in agreement with the docking studies of section II.A, where the SERT pocket contains lipophilic side chains Ile172, Ala173 and depending on the conformation, Thr439. The subsequent molecular dynamics (MD) study on 'SERT'-ized DAT indicated that the Thr439 conformation with the methyl group towards the binding pocket is energetically more favorable both in presence and absence of MCAT and IMAP. This indicated that the SERT pocket is indeed highly lipophilic.

The Hansch analysis on the amphetamine and cathinone dataset (section II.B) led to a comparable model, which indicated that the aromatic ring of both molecule types bind with the same topology in the substrate binding pocket of SERT. Hence the presence of a 2-oxo group on the beta-position seems not to induce a different conformation in the binding pocket.

The MD simulations on the transporter systems dramatically increased the understanding of the protein-ligand interactions and the flexibility of the protein pockets. The MCAT and IMAP ligands were simulated in an occluded model of DAT and 'SERT'-ized DAT, which indicated that the ligand's conformation with the carbonyl group toward TM6 was enthalpically more favorable. Additionally, more stable hydrogen bonding was observed in agreement with previous studies with dopamine and MDMA (section II.C).

The DAT-over-SERT selectivity of small amphetamines has been explained by differences in stacking interactions and suggested by differences in electrostatic interactions. The stacking was more favorable in DAT presumably, due to a less bulky Val152 compared to Ile172 in SERT which would disrupt such an interaction. This was validated by uptake inhibitory assays where an increase in affinity was observed for the DAT-like SERT-I172V mutant (section II.C). The more attractive

electrostatic interactions in DAT were caused by a slightly tighter binding pocket as compared to in the SERT-like DAT. The results are very supportive; however, a more conclusive result would be obtained by simulating the complete SERT model, since the packing of the 'SERT'-like model might not be fully representative.

The study on SERT selectivity of the ligand pair 4-MePPP and 4-MEC, with a difference in the bulkiness of their *N*-substituent, was explained by docking. The placement of 4-MePPP in SERT was more ambiguous than in DAT, whereas the docking poses of 4-MEC were similar in both protein pockets. This might have been caused by the larger *N*-substituent of 4-MePPP that causes a steric repulsion of the ligand's aromatic ring in subpocket B of SERT, unlike in the slightly more spacious B subpocket in DAT (section II.D).

The docking studies on levamisole (section II.E) and the Me@PPI compounds (section II.F) gained insight into the NET-over-DAT/SERT selectivity. Docking poses indicated that selectivity lies in the different aromatic residues between NET and DAT residing in the S2 pocket, i.e. Tyr151 in NET and Phe155 in DAT. NET-over-SERT selectivity would be caused by two different residues, Ile172 and Glu439 in SERT, that supposedly allow less space for the ligand to be accommodated, in contrast to NET that bears a Val and an Asp at the homologous positions.

Hence, conclusive results are summarized as follows:

1. A lipophilic or polarizable *para*-substituent positively influences amphetamine binding in SERT
2. The DAT-over-SERT selectivity of small amphetamines seems to be caused by differences in aromatic stacking and attractive electrostatic interactions
3. DAT-over-SERT selectivity cathinones with a bulky nitrogen substituent seems caused by steric repulsion of the ligand's aromatic ring in the SERT B subpocket, unlike in the more spacious pocket in DAT

The results have improved our understanding of the molecular determinants of monoamine transporter selectivity for substrates. This knowledge may assist in the development of more selective therapeutic drugs. The applied methods have proven the predictive power of computational methods and can stimulate other researchers to tackle selectivity phenomena of other (membrane) proteins.

Appendix

A1 Plotting heatmaps for interatomic distances

```
#!/bin/env python

# Script to plot the ligand-protein distances on a heatmap in a browser
# Make sure Plotly is installed on your linux system, www.plot.ly

import plotly.plotly as py
from plotly.graph_objs import *
import matplotlib.pyplot as plt
import os

# global vars
models=["sert", "dat"]
ligands=["H","Me","Et"]
name="protein_name"           # change to e.g. SERT
ligands=[1,2,3]               # you can also use range()

num_bins = 20                 # number of bins horizontally in heatmap
min=3                         # minimum distance
max=5                         # maximum distance

# functions
def make_bins(a, b, step):
    lijst=[]
    iter=a-step
    while iter<=b:
        iter+=step
        lijst.append(str(iter))
    return lijst

xlist=make_bins(min,max,0.1)

os.chdir("/home/amir/distances")   # change to folder files containing distance files

zlist=[]
for l in ligands:
    file=name+"-dists-lig-"+l
    f=open(file, "r")
    list=[]
    for i in f:
        j=i[0:4]
        k=float(j)
        list.append(k)
    f.close()

    n_l, bins_l, patches = plt.hist(list, num_bins, normed=0, range=[min,max])
    zlist.append(n_l.tolist())

layout= Layout(
    title="ligand cation - D98 distance", font=Font( family='PT Sans Narrow, sans-serif',
size=14 ), autosize=False, height=300, width=500, margin=Margin(l=130),
    xaxis=XAxis(title='Salt bridge distance (A)', type='linear', autotick=False, dtick=1 ,
tick0=1 ), yaxis=YAxis(title='Ligand')     )

data = 0
data = Data( [ Heatmap( zauto=False, zmax=60, z=zlist, colorbar = ColorBar(
title='Occurrences', thickness=25,  autotick=True, ticks='outside' ),
   x=xlist ,  y=['ligand_1', 'ligand_2', 'ligand_3']   )   ])

fig = Figure(data=data, layout=layout)

plot_url = py.plot(fig, filename=name)
```

A2 Derivation of TI formula

Canonical partition function: $Z\,(N, V, T, \lambda) = c \iint e^{-\beta E\,(\mathbf{r},\mathbf{p},\lambda)} \mathrm{d}\mathbf{r}\,\mathrm{d}\mathbf{p}$

Probability of finding a certain state: $P\,(\mathbf{r},\mathbf{p}) = \frac{e^{-\beta E\,(\mathbf{r},\mathbf{p})}}{\iint e^{-\beta E\,(\mathbf{r},\mathbf{p})} \mathrm{d}\mathbf{r}\,\mathrm{d}\mathbf{p}}$

Ensemble average of a quantity Q: $\langle Q \rangle = P\,(\mathbf{r},\mathbf{p}) \iint Q\,(\mathbf{r},\mathbf{p})\,\mathrm{d}\mathbf{r}\,\mathrm{d}\mathbf{p}$

Helmholtz Free energy: $\Delta A\,(N, V, T, \lambda) = -\frac{1}{\beta} \ln \mathrm{Z}\,(N, V, T, \lambda)$

$$\Delta A\,(N,V,T,\lambda) = \int_{\lambda=0}^{1} \frac{\partial A}{\partial \lambda} \partial\lambda$$

$$\frac{\partial A}{\partial \lambda} = \frac{\partial(-\frac{1}{\beta}\ln\,(c \iint e^{-\beta E\,(\mathbf{r},\mathbf{p},\lambda)}\,\mathrm{d}\mathbf{r}\,\mathrm{d}\mathbf{p})\,)}{\partial\lambda} = -\frac{1}{\beta}\frac{\partial}{\partial\lambda}(c \iint e^{-\beta E\,(\mathbf{r},\mathbf{p},\lambda)}\,\mathrm{d}\mathbf{r}\,\mathrm{d}\mathbf{p})$$

$$= \frac{1}{\beta}\frac{\iint \beta \frac{\partial E\,(\mathbf{r},\mathbf{p},\lambda)}{\partial\lambda} e^{-\beta E\,(\mathbf{r},\mathbf{p},\lambda)}\,\mathrm{d}\mathbf{r}\,\mathrm{d}\mathbf{p})}{\iint e^{-\beta E\,(\mathbf{r},\mathbf{p},\lambda)}\,\mathrm{d}\mathbf{r}\,\mathrm{d}\mathbf{p}} = \frac{e^{-\beta E\,(\mathbf{r},\mathbf{p},\lambda)}}{\iint e^{-\beta E\,(\mathbf{r},\mathbf{p},\lambda)}\,\mathrm{d}\mathbf{r}\,\mathrm{d}\mathbf{p}} \iint \frac{\partial E\,(\mathbf{r},\mathbf{p},\lambda)}{\partial\lambda}\mathrm{d}\mathbf{r}\,\mathrm{d}\mathbf{p}$$

$$= P\,(\mathbf{r},\mathbf{p}) \iint \frac{\partial E\,(\mathbf{r},\mathbf{p},\lambda)}{\partial\lambda}\mathrm{d}\mathbf{r}\,\mathrm{d}\mathbf{p} = \left\langle \frac{\partial E\,(\lambda)}{\partial\lambda} \right\rangle$$

Hence: $\Delta A\,(N,V,T,\lambda) = \int_{\lambda=0}^{1} \frac{\partial A}{\partial\lambda}\partial\lambda = \int_{\lambda=0}^{1} \left\langle \frac{\partial E\,(\mathbf{r},\mathbf{p},\lambda)}{\partial\lambda} \right\rangle \partial\lambda$

A3 OPLS-AAx charges for 4-iodo-methcathinone

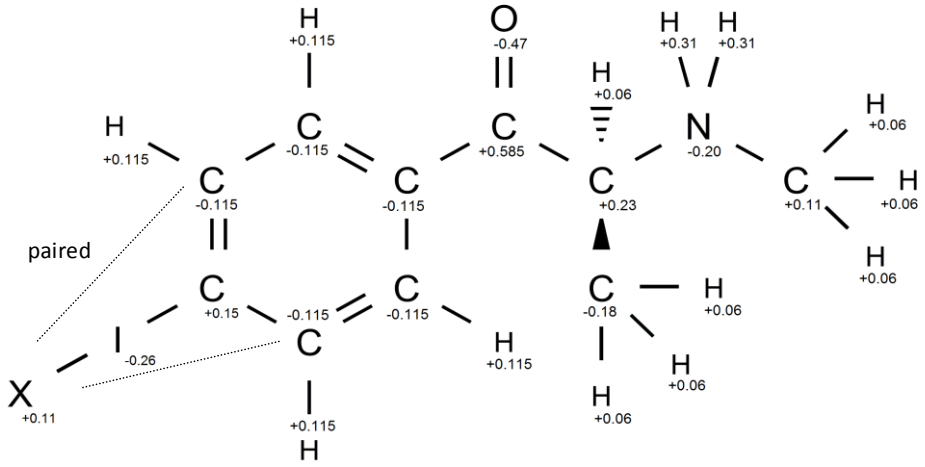

A4 MD Simulation parameter input file

```
; Run parameters
integrator      = md
nsteps          = 10000000
dt              = 0.002

; Bond parameters
constraint_algorithm = lincs
constraints     = all-bonds
lincs_iter      = 1
lincs_order     = 4

; Neighborsearching
ns_type         = grid
nstlist         = 10
rlist           = 1.0          ; short-range neighborlist cutoff (in nm)
rcoulomb        = 1.0          ; short-range electrostatic cutoff (in nm)
rvdw            = 1.0          ; short-range van der Waals cutoff (in nm)
vdw-type        = Cut-off

; Electrostatics
coulombtype     = PME          ; Particle Mesh Ewald for long-range electrostatics
pme_order       = 4            ; cubic interpolation
fourierspacing = 0.14          ; grid spacing for FFT

; Temperature coupling
tcoupl          = v-rescale
tc-grps         = around stuff POP
tau_t           = 0.5   0.5     0.5          ; time constant, in ps
ref_t           = 300   300     300          ; reference temperature in K

; Pressure coupling
pcoupl          = Berendsen
pcoupltype      = semiisotropic
tau_p           = 1.0   1.0                    ; time constant, in ps
ref_p           = 1.0   1.0                    ; reference pressure, x-y, z (in bar)
compressibility = 4.5e-5       4.5e-5         ; in bar^-1

pbc             = xyz
DispCorr        = EnerPres
gen_vel         = no
continuation    = yes

; COM motion removal
nstcomm          = 1
comm-mode        = Linear
comm-grps        = system
```

Nederlandse samenvatting

De serotonine, dopamine en norepinephrine transporter (respectievelijk SERT, DAT, NET) worden samen aangeduid als de monoamine transporter eiwitten (MATs) en zijn betrokken bij verscheidene psychiatrische aandoeningen zoals depressie, angst, verslaving en *attention-deficit hyperactivity disorder* (ADHD). De hoge *sequence identity* en onderlinge structurele gelijkenis, tezamen met hun relatie tot verschillende gedragspatronen en -aandoeningen, hebben de oorzaak van hun selectiviteit een centraal thema in het levenswetenschappelijk onderzoek tijdens de afgelopen decennia gemaakt. De selectiviteit van MAT substraten, die in tegenstelling tot remmers getransporteerd worden, zijn in het kader van dit proefschrift grondig bestudeerd met behulp van computermodellen en biochemische methoden.

De bindingsmodi van endogene substraten zoals dopamine, norepinephrine en serotonine zijn in voorgaande onderzoeken gesuggereerd, maar de modi en selectiviteit van exogene verbindingen niet extensief. Cathinonen zijn amfetaminederivaten met toenemend recreatief gebruik en worden ook door de MATs getransporteerd, afhankelijk van hun fysisch-chemische eigenschappen. Hun opname-remmende werking op de MATs is in dit onderzoek gebruikt om het selectiviteitsfenomeen van de MATs beter te begrijpen.

Het moleculair docken van een reeks cathinonen in een homologiemodel van SERT in de naar buiten gekeerde conformatie, heeft een bindingmodus opgeleverd in de *substrate binding site* en gesuggereerd dat hun chemische basisstructuur overlapt. Daarnaast is de bindingsactiviteit verklaard op basis van de interactie tussen de chemische substituenten en de omringende eiwitresiduen. Aanvullende validatie werd verkregen door middel van Hansch analyse, een kwantitatieve structuur-activiteitsrelatie (QSAR) methode, waarbij chemische substituenten worden beschreven door hun electronenzuigende, lipofiele, sterische of polariseerbare eigenschappen. Deze ligand-gebaseerde analyse heeft aangegeven dat een polariseerbare of lipofiele *para*-substituent de SERT affiniteit verhoogt, terwijl een substituent op het kationische stikstofatoom met groter volume ongunstig zou zijn.

De DAT-over-SERT selectiviteit is echter niet verklaard met behulp van docken en QSAR. Datasets gaven aan dat het ontbreken van substituenten op de aromatische ring de verbindingen DAT-over-SERT-selectief maakt. Aan de hand hiervan is een moleculaire dynamica (MD) en thermodynamische integratie (TI) studie uitgevoerd, waarbij de *substrate binding site* aangeduid werd als de voor affiniteit meest bepalende bindingsplaats van deze verbindingen. De DAT-over-SERT selectiviteit werd verklaard door een verschil in aromatische stacking en attractieve elektrostatische interacties. De stacking interacties worden in DAT vermoedelijk veroorzaakt door een kleinere Val152, in tegenstelling tot Ile172 in SERT dat deze interactie zou verstoren. Dit werd bevestigd door uptake inhibitory assays op mutanten van de transporters. De sterkere elektrostatische interacties in DAT werden veroorzaakt door een iets nauwere DAT pocket, vergeleken met SERT.

Résumé Français

Les transporteurs membranaires de la sérotonine, dopamine et noradrénaline (respectivement SERT, DAT, NET) sont collectivement désignés comme les transporteurs à monoamine (TMA) et sont impliqués dans une variété de maladies psychiatriques tels que la dépression, l'anxiété, la toxicomanie et le trouble de déficit de l'attention / hyperactivité (TDAH). Ces transporteurs se caractérisent par une très grande similarité de séquence et fonctionnelle, tandis que leur implication dans des comportements et troubles est différente. Cette particularité les ont fait un thème central dans la recherche en neuroscience au cours des dernières décennies. Les petites molécules qui se lient aux TMA peuvent être classés entre inhibiteurs ou substrats, dont la sélectivité pour le ce dernier a été étudiée en profondeur au cours de cette thèse, en utilisant des méthodes de calcul et biochimiques.

Les modes de liaison des substrats endogènes comme la dopamine, norépinephrine et sérotonine ont été suggérés précédemment, mais peu d'information est disponible concernant la liaison et la sélectivité des composes exogènes. Les cathinones dérivés d'amphétamines qui gagnent de plus en plus de popularité dans le milieu festif pour leurs effets psychostimulants, sont également transportés par les TMA. Leur activité inhibitrice de la recapture des neurotransmetteurs a été exploitée afin de mieux comprendre le phénomène de sélectivité.

L'amarrage moléculaire d'un ensemble de ces cathinones dans les modèles d'homologie du transporteur de la sérotonine (SERT) dans la conformation tournée vers l'extérieur a permis de valider leur mode de liaison dans le site de substrat et indiqué que leurs squelettes chimiques se chevauchent. En outre, leur activité de liaison a été rationalisée sur la base des interactions entre les substituants du squelette et des aminoacides du site de liaison. Une validation supplémentaire a été obtenue par l'approche de Hansch, un type de relation quantitative de structure à activité (QSAR). Cette approche, basée uniquement sur la structure des ligands, a indiqué qu'un substituant en position *para* sera polarisable ou lipophile pour augmenter l'affinité a SERT, tandis qu'un substituant volumineux sur l'atome d'azote serait défavorable.

La sélectivité pour DAT n'a cependant pas été saisie par l'amarrage et la technique basée sur la structure des ligands. Des bases données différents ont indiqué que l'absence de substituants sur le cycle aromatique rend les composés sélectifs pour DAT. Par conséquent, une étude de dynamique moléculaire et d'intégration thermodynamique a été menée, ces qui indiques le site de liaison au substrat sera le site de reconnaissance primaire pour ces composés. La sélectivité pour DAT a été attribuée à des interactions d'empilement aromatique et des interactions électrostatiques attractives plus favorables. Les interactions d'empilement semblent plus favorables pour DAT probablement en raison d'un volume réduit de Val152, par rapport au résidu équivalent Ile172 dans SERT, ce qui perturberait une telle interaction. Les hypothèses ont été validées par des tests d'inhibition de la capture sur des mutants des transporteurs. Les interactions électrostatiques plus favorables dans DAT sont été causées par une poche de liaison plus serrée avec un plus petit nombre molécules d'eau entrant en moyenne, par rapport à SERT.

Curriculum vitae

Personal information

Name	Amir Seddik
Address	Schreygasse 8/12 1020 Vienna (Austria)
Email	amir.seddik@univie.ac.at
Place of Birth	Algiers (Algeria)
Date of Birth	26 December 1983
Nationality	Dutch

Education and Training

2011	Started **PhD** study in Computational Chemistry, University of Vienna (Austria) Title: *Substrate Selectivity Profiling of the human Monoamine Transporters* under supervision of Prof. Gerhard F. Ecker
2007 – 2010	**Master** in Drug Innovation, Utrecht University (the Netherlands)
2003 - 2007	**Bachelor** in Chemistry, Utrecht University

Internships and jobs

01-03.2015	**Visiting PhD student** under H.H. Sitte, Institute of Pharmacology, Medical Univ. of Vienna *Performing site-directed mutagenesis and uptake inhibitory assays on transiently transfected HEK cells for validating molecular dynamics hypotheses*
03-06.2014	**Visiting PhD student** under supervision of D.P. Geerke at AIMMS Division of Molecular and Computational Toxicology, VU Amsterdam *MD studies on (4-iodo)-methcathinone binding to DAT and 'SERT'-ized DAT:* *Learned to parametrize, equilibrate and run molecular dynamics simulations, conduct relative binding free energy calculations on transmembrane transporter systems.*
08.2013	**Visiting PhD student** under T. Stockner, Inst. of Pharmacology, Medical Univ. of Vienna *Docking of levamisole and aminorex in the Monoamine Transporters*
08.2012	**Visiting PhD student** under M. Ernst, Center for Brain Research, Medical Univ. of Vienna *Homology Modelling of the Norepinephrine Transporter*
05-08.2011	**Trainee Analyst** at Syncom b.v., Groningen (Netherlands) *GC and HPLC/MS analysis of drug leads for pharmaceutical companies.*

01-08.2009 **Research Student** under P.F. Alewood, Institute for Molecular Bioscience, University of Queensland, Brisbane (Australia)

Fluorescent tagging of Bv8 - Novel methods to screen Bioactive Peptides:
Synthesized a fluorescent BODIPY dye and a bioactive peptide on solid phase and ligated them together. Conducted HPLC, ESI- and MALDI-ToF MS, 1H/13C-NMR

11.2007–09.2008 **Research Student** under M. Kas, Rudolf Magnus Institute for Neuroscience, University Medical Centre, Utrecht

Neurochemical and Pharmacological Validation of a Mouse Model for Obsessive-Compulsive Disorder (OCD):
Set up an open-field test for two different strains of mice injected with varying concentrations of the D2 agonist quinpirole to validate a model for OCD.

Modelling Software knowledge

CCDC GOLD:	Docking, by setting up a ligand backbone molecule for distance restraints, applying flexible side chains, soft potentials, post-processing final complexes.
Schrodinger:	Preparing proteins, Glide docking, Induced-Fit docking, MM/GBSA, QM minimization and obtaining partial charges with QSite, MD with Desmond.
CCG MOE	Preparing ligands, proteins and databases; conformational analyses, creating pharmacophores. Energy minimization of complexes by svl scripting. QSAR analyses.
Gromacs:	Performing classical MD simulations, modifying forcefield for virtual sites, setting up dummy atoms on ligands and side chains for thermodynamic integration, analyzing HBs, RMSD, RMSF, distances, angles, area per lipid, DSSP, Schlitter entropy and enthalpy.
POVME:	Measuring binding site volumes.
Modeller:	Creating homology models.
VMD:	Processing MD trajectories, creating figures with tcl/tk scripting.
FLAP:	Creating ligand conformers, making 3D-QSAR models
XLStat:	Performing Agglomerative Hierarchical Clustering.
Weka:	Creating ligand-based models with random forest and linear regression.
LigandScout:	Creating pharmacophores, decoy set validation.

Programming languages

Bash:	Making scripts using seq, grep, sed, while, for, awk, tr, cut, getopts, defining functions.
Python:	Defining functions, file operations, using packages: Matplotlib, Plotly, numpy, scipy.

Other jobs and activities

01-06.2013 **Student Representative** of Teaching Committee of MolTag PhD program, Vienna, Austria
Discussing financial plans for the Science Day and PhD retreats

2002 - 2008 **Working Student** at Communication Service Centre, Utrecht University (Netherlands)
Organizing open days for upcoming students

06-2007 **Department Assistant** at Diakonessen Hospital, Utrecht

06-2006 **Department Assistant** at University Medical Centre, Utrecht

Languages

Dutch, English, German, French, Portuguese

Hobbies

Football, Biking, Nike tweaking, Photography, Squash

Publication list

- Neudorfer et al, "Synthesis and in Silico Evaluation of Novel Compounds for PET-Based Investigations of the Norepinephrine Transporter", Molecules, **2015**, 20, 1712-30
- Saha K *et al*, "'Second-Generation' Mephedrone Analogs, 4-MEC and 4-MePPP, Differentially Affect Monoamine Transporter Function", *Neuropsychopharmacology*, **2014**
- Hofmaier T *et al*, "Aminorex, a metabolite of the cocaine adulterant levamisole, exerts amphetamine like actions at monoamine transporters", *Neurochem Int*, **2014**, 73, 32-41
- Seddik A *et al,* "Probing the Selectivity of Monoamine Transporter Substrates by Means of Molecular Modeling" *Mol Inform*, **2013**, 32, 409-413
- de Haas *et al,* "Marked inbred mouse strain difference in the expression of quinpirole induced compulsive like behavior based on behavioral pattern analysis", *Eur Neuropsychopharmacol*, **2012**, 22, 657-63

Manuscripts in preparation

- Seddik A *et al*, "Combined Hansch analysis and Docking suggest Binding Mode of Cathinone Designer Drug Analogs in the Serotonin Transporter"
- Seddik A *et al*, "Stacking interactions confer selectivity in the Dopamine Transporter for unsubstituted Amphetamine-like Cathinones"

Conference talks

2014

Amir Seddik, Thomas Steinkellner, Thomas Stockner, Walter Sandtner, Michael Freissmuth, Harald H. Sitte, Gerhard F Ecker, *Interaction type differences as proposed determinants of monoamine transporter selectivity for amphetamines.* American Chemical Society, San Francisco, USA

Awards

04.2013 CINF Scholarship for Scientific Excellence, American Chemical Society, New Orleans (USA)

Poster presentations

2014

Amir Seddik, Daan P. Geerke, Nicholas V. Cozzi, Thomas Stockner, Harald H. Sitte, Gerhard F. Ecker, *Molecular dynamics and docking studies on DAT and 'SERT'-ized DAT suggest induced fit effects upon cathinone binding*, SFB symposium, Vienna, Austria

Amir Seddik, Marion Holy, Barbara Zdrazil, Harald H. Sitte, Gerhard F. Ecker, *Docking of fenfluramine in Monoamine Transporter models indicates basis for substrate selectivity*, Amsterdam Institute for Molecules, Medicines and Systems, Netherlands

2013

Amir Seddik, Barbara Zdrazil, Thomas Stockner, Simon Bulling, Andreas Tulzer, Thomas Steinkellner, Walter Sandtner, Michael Freissmuth, Harald H. Sitte , Gerhard F. Ecker, *Prediction of high-affinity SERT substrates by 2D-QSAR*, SFB symposium, Vienna, Austria

Amir Seddik, Barbara Zdrazil, Harald H. Sitte, Gerhard F. Ecker, *Combining ligand- and Structure based methods to probe Monoamine Transporter Substrate Selectivity*, 9th European Workshop in Drug Design, Siena, Italy

Amir Seddik, Marion Holy, Barbara Zdrazil, Harald H. Sitte, Gerhard F Ecker, *Probing the Substrate Selectivity of Monoamine Transporters,* American Chemical Society, New Orleans, USA

2012

Amir Seddik, René Weissensteiner, Barbara Zdrazil, Harald H. Sitte, Gerhard F. Ecker, *Interaction profiling of Mephedrone at the Human Serotonin and Dopamine transporter,* EFMC-ISMC Berlin, Germany

Amir Seddik, Barbara Zdrazil, Simon Bulling, Andreas Tulzer, Thomas Stockner, Walter Sandtner, Harald H. Sitte, Gerhard F. Ecker, *Exhaustive docking suggests equivalent orientation of Mephedrone in the human Serotonin and Dopamine transporter*, SFB symposium, Vienna, Austria

Amir Seddik, Barbara Zdrazil, Harald H. Sitte, Gerhard F. Ecker, Probing the Substrate Selectivity of the Serotonin and Dopamine Transporter by Structure-Based Design, EuroQSAR, Vienna, Austria

Amir Seddik, Simon Bulling, Barbara Zdrazil, Harald H. Sitte, Gerhard F. Ecker, *Common Scaffold Clustering as a Versatile Tool for Prioritizing Docking Poses of Amphetamine Derivatives*, Chemoinformatics Summer School, Strasbourg, France

Amir Seddik, Barbara Zdrazil, René Weissensteiner, Harald H. Sitte, Gerhard F. Ecker, *Prioritization of Docking poses in human Serotonin and Dopamine transporters by the use of Common Scaffold Clustering*, American Chemical Society, Philadelphia, USA